

No d'ordre : 41468

Université Lille 1 – Sciences et Technologies

Ecole Doctorale 104 – Sciences de la Matière, du Rayonnement et de l'Environnement

Thèse de Doctorat en Cotutelle

par

Bogdan MAREKHA

pour l'obtention du titre de

Docteur de l'Université Lille 1

Discipline : Optique, Lasers, Physico-Chimie et Atmosphère

Structure et dynamique microscopiques dans les mélanges de liquides ioniques à base d'imidazolium et de solvants polaires aprotiques : RMN, spectroscopie Raman et modélisation moléculaire

Soutenue le 19 septembre 2014 devant le jury :

Toshiyuki	TAKAMUKU <i>Professeur, Université de Saga (Japon)</i>	Rapporteur
Thierry	TASSAING <i>Directeur de recherche, ISM, Université de Bordeaux I</i>	Rapporteur
Abdenacer	IDRISSI <i>Professeur, Université Lille 1</i>	Directeur de thèse
Oleg	KALUGIN <i>Professeur, Université nationale de Kharkiv V.N. KARAZINE (UKRAINE)</i>	Co-directeur de thèse
Pál	JEDLOVSZKY <i>Professeur, Université Loránd Eötvös (Hongrie)</i>	Examineur
Ari	SEITSONEN <i>Chercheur, Université de Zurich (Suisse)</i>	Examineur
Guy	BUNTINX <i>Directeur de recherche, Université Lille 1</i>	Président

No of order: 41468

Lille 1 University – Science and Technology

Doctoral School 104 – Science of the Matter, of the Radiation, and of the Environment

Doctoral Thesis under cosupervision

by

Bogdan MAREKHA

to obtain the degree of

Doctor of Lille 1 University

Discipline: Optics, Lasers, Physical Chemistry and Atmosphere

Microscopic Structure and Dynamics in Mixtures of Imidazolium-Based Ionic Liquids with Polar Aprotic Solvents: NMR, Raman Spectroscopy and Molecular Modeling

Defended on 19 september 2014 in front of the jury:

Toshiyuki	TAKAMUKU <i>Professor, Saga University (Japan)</i>	Referee
Thierry	TASSAING <i>Director of research, ISM, University of Bordeaux I</i>	Referee
Abdenacer	IDRISSI <i>Professor, Lille 1 University</i>	Supervisor
Oleg	KALUGIN <i>Professor, V.N. Karazin Kharkiv National University (UKRAINE)</i>	Co-supervisor
Pál	JEDLOVSZKY <i>Professor, Loránd Eötvös University (Hungary)</i>	Examiner
Ari	SEITSONEN <i>Researcher, University of Zurich (Switzerland)</i>	Examiner
Guy	BUNTINX <i>Director of research, Lille 1 University</i>	President

ACKNOWLEDGEMENTS

This thesis was prepared in the framework of co-tutorial agreement between Lille 1 University and V. N. Karazin Kharkiv National University and I hereby thank to these institutions and the respecting hosting laboratories LASIR, headed by Dr. Guy BUNTINX, and the Department of Inorganic Chemistry, headed by Prof. Ivan Vyunnik, for provision with chance to pursue my doctoral studies. I thank to all the sources of financial support that contributed, namely, French and Ukrainian governments for the basic doctoral scholarships, as well as for grant support from Lille 1 Doctoral School ED SMRE, Marie Curie 'Biosol' research program and French-Bavarian Center for University Cooperation (CCUFB) for visiting conferences (EUCHEM 2014 in Talinn, Estonia and ICSC 2013 in Kyoto, Japan) and for short-term research visits to Regensburg University (Germany) and Institute of Solution Chemistry in Ivanovo (Russian Federation).

I express my sincere gratitude to my co-supervisors, Profs. Abdenacer IDRISSE and Oleg KALUGIN, for doing their best in creating favorable scientific environment and wise counseling and guidance that have been vital for me in order to complete this thesis. They have different styles but I appreciate and try to learn best from both of them.

The referees of this thesis, Profs. Toshiyuki TAKAMUKU and Thierry TASSAING, are gratefully acknowledged for their time and efforts to examine my research.

A special thank is given to scientific and instrument staff who helped me a lot to master different experimental techniques, namely Marc BRIA from CCM RMN in Lille 1, Myriam MOREAU from LASIR, Prof. Richard BUCHNER and his students Andreas NAZET and Thomas SONNLEITNER from Regensburg University and every person who helped even with a little piece of advice.

It is impossible not to mention all my colleagues and office-mates that have been creating extremely friendly and supportive atmosphere throughout these three years of my doctorate in Khakiv, namely Dr. Vira AGIEIENKO, Dr. Elena LUKINOVA, Anastasiia RYABCHUNOVA, Roman KULYK, and in Lille – Fatima LAFRAD, Dr. Thomas GUILLON, Dr. Bruno DEBUS, Dr. Mateusz REBARZ, Maya ABOU FADEL and others.

And, of course, I thank my dear mother for all her love and support.

RESUME

Les mélanges de liquides ioniques à base d'imidazolium (LI) possédant des anions perfluorés et de solvants aprotiques polaires sont des candidats prometteurs comme électrolytes utilisables dans les différents dispositifs électrochimiques. L'état actuel de la technologie dans ce domaine nécessite des informations détaillées sur l'influence de la nature des constituants et de la composition du mélange sur la structure et la dynamique au niveau microscopique de ces mélanges d'électrolytes.

Cette thèse présente une approche multi-technique pour l'analyse de la structure et la dynamique de mélanges d'une part de LIs à base du cation 1-butyl-3-méthylimidazolium (Bmim^+) couplés à des anions perfluorés (BF_4^- , PF_6^- , CF_3SO_3^- , $(\text{CF}_3\text{SO}_2)_2\text{N}^-$), et d'autre part de solvants aprotiques polaires tels que l'acétonitrile (AN), la γ -butyrolactone (γ -BL), le carbonate de propylène (PC).

La spectroscopie Raman et la RMN (mesures de déplacements chimiques) ont été utilisées pour sonder les changements de densité électronique au niveau des sites d'interactions spécifiques des LIs et des molécules de solvant en fonction de la composition du mélange. Des calculs de chimie quantique de configurations représentatives du LI-solvant couplés à des méthodes avancées d'analyse de la distribution de densité électroniques ont été réalisés pour compléter l'interprétation des observations spectrales. Les variations de la structure microscopique en fonction de la composition du mélange ont été analysées en termes de compétition entre les processus d'association et de solvation des ions. Des changements importants dans la structure de la solution ont été observés uniquement à faible teneur en LI ($x_{\text{LI}} < 0,2$). Il a été établi que les phénomènes de solvation des ions l'emportent sur l'association ionique pour les solvants à haute donicité (γ -BL, PC) et pour les LIs dont les anions sont volumineux et ont une distribution de charge diffuse (PF_6^- , $(\text{CF}_3\text{SO}_2)_2\text{N}^-$). Par ailleurs, les plus importants changements dans les spectres Raman et RMN concernent principalement les hydrogènes du cycle de l'imidazolium.

Les coefficients de diffusion des constituants du mélange ont été déterminés par RMN. Les coefficients de diffusion relatives des molécules de solvant par rapport aux cations en fonction de la concentration dépendent de la nature du solvant et non de celle de l'anion. Dans tous les cas, ces coefficients présentent des valeurs constantes à faible teneur en LI ($x_{\text{LI}} < 0,2$), puis croissant fortement (AN), modérément (γ -BL), ou négligeablement (PC) à des concentrations plus élevées de LI. Ce comportement est lié aux différents schémas de solvation en fonction des solvants utilisés. Dans les systèmes à base de BmimPF_6 , la diffusion des anions a été suivie par la RMN des noyaux ^{31}P . A basses x_{LI} , cette diffusion est plus élevée que celle des cations. Elle est plus faible à hautes x_{LI} . Le point d'inversion entre les deux régimes de la diffusion a été trouvé autour de la composition équimolaire et ne dépend pas du solvant. A ce point, un changement notable dans le mécanisme de diffusion des ions semble avoir lieu.

Mots clés : liquides ioniques, solvants polaires aprotiques, solvation d'ions, association d'ions, spectroscopie Raman, RMN, déplacement chimique, coefficient de diffusion

ABSTRACT

Mixtures of imidazolium ionic liquids (ILs) with perfluorinated anions and polar aprotic solvents are promising candidates for electrolytic components used in different electrochemical devices. Current state of technologies requires detailed information on the influence of the nature of the constituents and of the mixture composition on the microscopic level structure and dynamics.

This thesis presents a multitechnique approach to this issue on example of 1-butyl-3-methylimidazolium (Bmim⁺) ILs with perfluorinated anions (BF₄⁻, PF₆⁻, CF₃SO₃⁻, (CF₃SO₂)₂N⁻) mixed together with polar aprotic solvents such as acetonitrile (AN), γ -butyrolactone (γ -BL), propylene carbonate (PC).

Variations in microscopic structure as a function of mixture composition were addressed in terms of competition between ion pairing (or ion association in general) and ion solvation processes. Raman spectroscopy and NMR chemical shift measurements were employed to probe electron density changes at the representative interaction sites of IL and solvent molecules over the entire range of compositions. Quantum chemical calculations of representative configurations of IL-solvent clusters and advanced methods of analysis of electron density distribution were used to complement the interpretation of the spectral observations. Significant changes in solution structure are observed only at low IL content ($x_{\text{IL}} < 0.2$). It was established that ion solvation phenomena prevail over ionic association for solvents with high donicity (γ -BL, PC) and for ILs whose anions are large and have diffusive charge distribution (PF₆⁻, (CF₃SO₂)₂N⁻). Multiple intermolecular weak non-covalent interactions preferentially localized at imidazolium ring hydrogens stand for molecular-level picture determining the observed variations in Raman and NMR spectra.

NMR was also used to follow self-diffusion coefficients of cations and solvent molecules. The relative diffusivities of solvent molecules to cations as a function of concentration were found to depend on the solvent but not on the anion (*i.e.*, IL). In all cases the values exhibit a plateau at low IL content ($x_{\text{IL}} < 0.2$) and then increase steeply (AN), moderately (γ -BL), or negligibly (PC) at higher IL concentrations. This behavior was related to the different solvation patterns in the employed solvents. In BmimPF₆-based systems, anionic diffusivities were followed via ³¹P nuclei and found to be higher than the corresponding cation values in IL-poor systems and lower in the IL-rich region. The inversion point of relative ionic diffusivities was found around equimolar composition and does not depend on the solvent. At this point, a distinct change in the ion-diffusion mechanism appears to take place.

Keywords: ionic liquids, polar aprotic solvents, solvation of ions, association of ions, Raman spectroscopy, NMR, chemical shift, diffusion coefficient.

TABLE OF CONTENTS

LIST OF ABBREVIATIONS.....	13
CHAPTER 1. GENERAL INTRODUCTION	15
1.1. Towards the intermolecular interactions in mixtures of ILs with molecular solvents	20
1.2. Organization of the thesis.....	24
1.3. References for Chapter 1	26
CHAPTER 2. EXPERIMENTAL AND COMPUTATIONAL DETAILS	31
2.1. Objects of investigation. Sample preparation and handling.....	32
2.2. Raman measurements	36
2.3. NMR measurements	37
2.3.1 Diffusion measurements.....	38
2.4. Quantum chemical calculations	40
2.4.1 General aspects	40
2.4.2 Level of theory validation.....	41
2.4.3 Quantum theory of atoms in molecules	47
2.4.4 Noncovalent interactions	55
2.5. References for Chapter 2	60
CHAPTER 3. QUANTUM CHEMICAL INTERPRETATION OF THE INTERACTIONS IN IL-MOLECULAR SOLVENT MIXTURES.....	67
3.1. Introduction.....	68
3.2. IL ion pairs and ion pair dimers.....	68
3.2.1 Main structural features of the ion pairs	68
3.2.2 Weak noncovalent interactions in the IL ion pairs	78
3.2.3 The effect of implicit solvation	82
3.2.4 Ion pair dimers.....	87
3.3. IL-solvent complexes	93
3.3.1 Explicit solvation in AN	94
3.3.2 Explicit solvation in γ -BL.....	100
3.3.3 Explicit solvation in PC	105
3.4. Conclusions	111
3.5. References for Chapter 3	113
3.6. Chapter 3 appendix	117
CHAPTER 4. CHEMICAL SHIFT VARIATION IN IL-MOLECULAR SOLVENT MIXTURES.....	121
4.1. Introduction.....	122
4.2. Problems of chemical shift referencing.....	125

4.3.	Results and discussion	137
4.3.1	Relative chemical shift variation in AN	137
4.3.2	Relative chemical shift variation in γ -BL and PC	141
4.3.3	^{13}C relative chemical shift variations of anions in mixtures containing BmimTfO and BmimTFSI	145
4.4.	Conclusions	148
4.5.	References for Chapter 4	150
CHAPTER 5. TRANSLATIONAL DIFFUSION IN IL-MOLECULAR SOLVENT MIXTURES		155
5.1.	Introduction	156
5.2.	Results and Discussion	157
5.2.1	Absolute self-diffusion coefficients as a function of mixture composition	157
5.2.2	Relative self-diffusion coefficients solvent-cation as a function of mixture composition.....	160
5.2.3	Relative self-diffusion coefficients as a function of mixture composition	168
5.3.	Conclusions	170
5.4.	References for Chapter 5	172
5.5.	Chapter 5 Appendix	175
CHAPTER 6. INTERMOLECULAR INTERACTIONS IN A REPRESENTATIVE SYSTEM IL-MOLECULAR SOLVENT AS SEEN FROM RAMAN SPECTROSCOPY		181
6.1.	Introduction	182
6.2.	Advanced methods of Raman spectra analysis	184
6.2.1	Two-dimensional correlation spectroscopy (2DCoS).....	184
6.2.2	Perturbation-correlation moving window 2DCoS	187
6.3.	Results and Discussion	189
6.3.1	Selecting bands for analysis.....	189
6.3.2	Model molecular clusters structures	190
6.3.3	Experimental Raman spectra of BmimPF ₆ - γ -BL mixtures	200
6.4.	Conclusions	217
6.5.	References for Chapter 6	218
6.6.	Chapter 6 Appendix	224
CONCLUSIONS AND PERSPECTIVES		227

LIST OF ABBREVIATIONS

AN	acetonitrile
γ-BL	γ -butyrolactone, dihydro-2(3H)-furanone
PC	propylene carbonate, 4-methyl-1,3-dioxolan-2-one
IL	ionic liquid
Bmim⁺	1- <i>n</i> -butyl-3-methylimidazolium
TfO⁻	trifluoromethylsulfonate, triflate, CF ₃ SO ₃ ⁻
TFSI⁻	bis(trifluoromethanesulfonyl)imide, triflimide, Tf ₂ N ⁻ , (CF ₃ SO ₂) ₂ N ⁻
NMR	nuclear magnetic resonance
ATR	attenuated total reflectance
IR	infrared
2DCoS	two-dimensional correlation spectroscopy
PCMW 2DCoS	perturbation correlation moving window two-dimensional correlation spectroscopy
DFT	density functional theory
PCM	polarized continuum model
QTAIM	quantum theory of atoms in molecules
BCP	bond critical point
RCP	ring critical point
CCP	cage critical point
NCI	noncovalent interactions
RDG	reduced density gradient
MD	molecular dynamics
ppm	parts per million
a.u.	atomic units (Bohr for length, Hartree for energy, elementary charge for electric charge <i>etc.</i>)

Chapter 1. General Introduction

Ionic liquids (ILs) constitute a large class of substances which present a considerable scientific interest due to their number of advantageous properties. In many applications ILs are used in mixtures with molecular solvents of different nature. It still remains to be an unresolved task of creating a comprehensive microscopic picture on the structure and dynamics in such systems as a function of mixture composition and nature of the constituents.

This chapter gives a brief introduction to ILs, as well as an overview of the problem and possible strategies to study mixtures of ILs with molecular solvents.

During the last decade ionic liquids (ILs), which are low-temperature molten salts, have turned from promising functional materials into objects that are routinely used both in laboratory practice and at large industrial chemical enterprises.¹⁻⁵ Despite the booming research activity in the field of ILs,⁶ they still constitute a considerable interest for physical chemists.⁷ One should also mention a vast variety of application fields of ILs: from solvents for carrying out organic reactions^{1,8-9} and biopolymer dissolution,¹⁰⁻¹¹ up to functional materials based on magnetic ILs.¹² Such progress in the scale and in the range of applications of ILs is determined by the unique set of properties of these substances (negligibly low vapor pressure, wide liquidus range, thermal and electrochemical stability, high dissolving capability towards both organic and inorganic matter *etc.*) and also by enormous number of possible counterion combinations¹³⁻¹⁴ which allow one to select an IL fitting almost any requested set of properties.

Molecular structures of commonly employed cations and anions of ILs are shown in Figure 1.1. Among the cations, it is the family of dialkylimidazolium-based ILs which is the most investigated, particularly the ILs containing 1-alkyl-3-methylimidazolium cations. The selection of anion depends more on the field of application, *e.g.*, acetates are popular for cellulose dissolution, while perfluorinated anions like BF_4^- or $(\text{CF}_3\text{SO}_2)_2\text{N}^-$ are common for electrochemical applications.

However, the effective usage of ILs is partly hindered by several disadvantages of which the very high viscosity is the primary one, while difficulties in purification and rather high cost should also be mentioned.

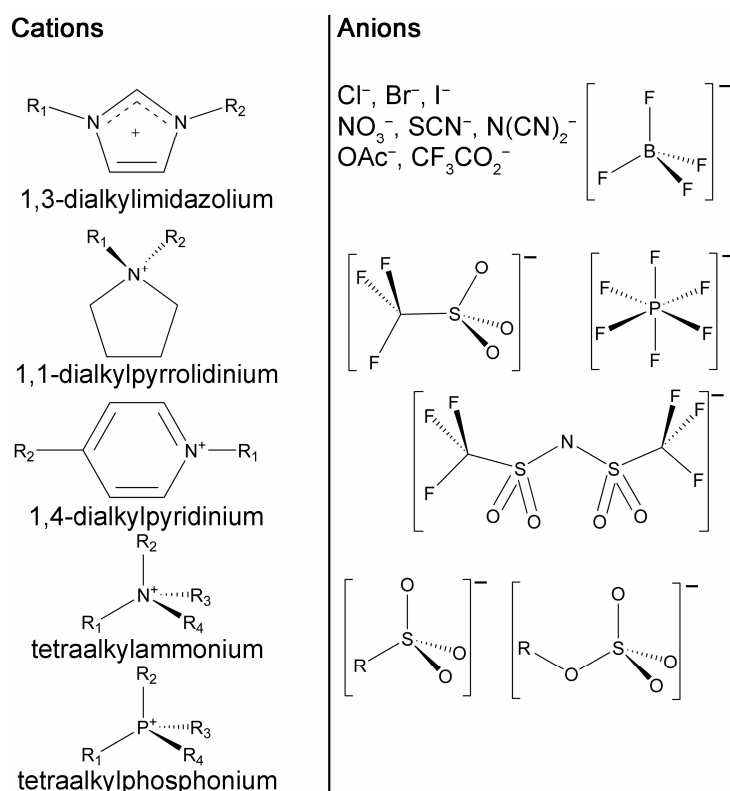


Figure 1.1. Chemical structures of the representative ions composing ILs.

In particular, in the field of electrochemical applications the family of 1-alkyl-3-methylimidazolium (Rmim^+) ILs with perfluorinated anions (PF_6^- , BF_4^- , CF_3SO_3^- , $(\text{CF}_3\text{SO}_2)_2\text{N}^-$) has proven to be good candidates for conducting components of various electrochemical devices such as supercapacitors or electrochemical actuators.¹⁵⁻²¹ Among the key factors which determine successful performance of these ILs in electrochemical devices, it is the mobility of ions which is limited by the inherent high viscosity of ILs stemming from strong long range Coulomb interactions between the ions.²²

Possibly feasible temperature variations (*ca.* by less than 50 K) would only lead to reduction in viscosity by less than one order of magnitude.²³ However, this point can be overcome by combining the ILs with low-weight molecular solvents, which leads to an exponential decay of the viscosity as a function of molar fraction,²⁴⁻²⁶ and, then, opens new application areas and a wider range of operating

conditions. Reduced consumption of ILs should be also mentioned in this perspective, keeping in mind their high cost.

In this regard, polar aprotic solvents, such as acetonitrile (AN) and cyclic organic esters and carbonates, *e.g.*, γ -butyrolactone (γ -BL) and propylene carbonate (PC), seem to be a good choice since they are well known for their good performance in conventional electrochemical systems for Li-ion battery technology and organic electrolyte-based supercapacitors.²⁷⁻²⁹ Moreover, cyclic organic esters, like γ -BL, and carbonates, like PC, are very promising in various fields of chemical technology due to their low volatility and flammability, as well as environmental friendliness coupled with high polarity and low viscosity.³⁰⁻³¹ Thus, mixtures of ionic liquids with this kind of solvents can be also regarded as advantageous in the ‘green chemistry’ perspective.

For a broad selection of mixtures of imidazolium ILs with polar aprotic solvents showing virtually full miscibility it was found that electrical conductivity has a maximum at IL mole fraction, x_{IL} , between 0.1 and 0.2.³²⁻³⁴ (See Figure 1.2) This phenomenon is traditionally explained via the interplay between concentration and ionic association effects from one side and viscosity variation from the other.³⁵ The former determine the effective number of charge carriers while the latter influences their mobility.³⁵

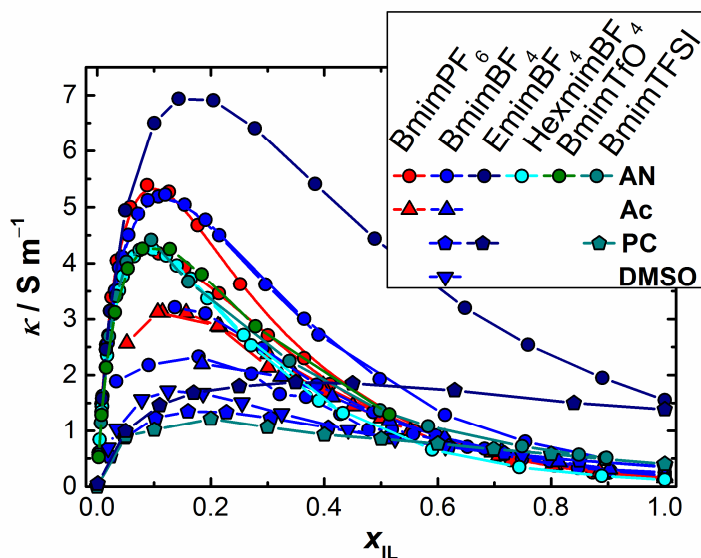


Figure 1.2. Experimental electrical conductivity, κ , as a function of IL mole fraction in different mixtures of imidazolium-based ILs with polar aprotic solvents. Data are taken from refs. ^{25,32} for BmimPF₆ – AN, refs. ^{25,36} for BmimPF₆ – Ac, refs. 25,32,34,36 for BmimBF₄ – AN, ref. 25 for BmimBF₄ – Ac, ref. 32 for BmimBF₄ – PC, BmimBF₄ – DMSO; refs. 32,34 for HexmimBF₄ – AN, ref. 37 for BmimTFSI-PC, ref. 24 for BmimTFSI-AN, ref. 32 for EmimBF₄ – AN, ref. 38 for EmimBF₄ – PC, ref. 34 for BmimTfO – AN.

Indeed, admixing molecular solvent to IL should, in general, influence not only the viscosity but modulate the overall microscopic structure and dynamics as a result of concentration modulation of the interactions between the components. Depending on the propensity of each neat component to give up its inherent interaction pattern (*i.e.*, ion-ion interactions giving rise to network structure in ILs and dipole-dipole interactions in polar aprotic solvents leading to their self-association) in favor of solvation one could anticipate different concentration regimes over the entire range of compositions.³⁹ At present, there exists no well-established predictive approach that would take into account such system-specific peculiarities and allow selecting a combination ‘IL+molecular solvent’ as well as its proper composition to suite for a particular set of properties (conductivity, electrochemical stability, thermophysical behavior etc.). As a result, modern approach still implies exhaustive empirical search of optimal systems to be used in practice.^{29,40-43} Thus, a comprehensive picture on the influence of the nature of

constituents as well as of the concentration on the structural and dynamical properties of the mixtures of ILs with molecular solvents over the entire range of compositions at the microscopic level is of high importance. It is a crucial element for successful development of the above mentioned predictive approach which is still lacking

1.1. Towards the intermolecular interactions in mixtures of ILs with molecular solvents

Mixtures of ILs with molecular solvents can be considered as electrolyte solutions for which their structure and properties are determined by the balance of such types of interactions as 'cation-anion', 'cation-cation' and 'anion-anion' that govern the existence of ionic associates and high order aggregates like $[\text{Cat}_n\text{An}_m]^{-/0/+}$, and also by interactions 'cation-solvent', 'anion-solvent', and 'solvent-solvent'. In this context the peculiarity of binary systems based on ILs is that the composing ions are multiatomic and, in general, asymmetric, as a result, the mentioned above interactions should be regarded as anisotropic ones, having preferential localization around some molecular fragment (interaction center or site). Another prominent feature of these systems, in comparison with conventional electrolyte solutions, is the full miscibility of ILs with many molecular solvents that allows obtaining mixtures corresponding to either a solution of IL in molecular solvent or a solution of molecular solvent in IL.

Intermolecular interactions in mixtures of two liquids of different nature at different compositions of these mixtures can be represented as a gradual transition from one pure liquid through solution of the second liquid in the first one, then through solution of the first liquid in the second one, and to pure second liquid. In this type of representation the problem converges to the following question: which composition ranges correspond to the mentioned above regions and which intermolecular interactions are determinative.

In pure dipolar aprotic liquids the main structure motif is the anti-parallel orientation of molecular dipoles and dipole-dipole interactions are considered to be the key ones.⁴⁴⁻⁴⁷

For pure ILs, at the present moment, there is no commonly agreed picture of their structure due to indirect nature of the applied techniques. It is widely considered that, in the liquid state, the structure of imidazolium ILs is determined by the strong interionic Coulombic interactions which are relatively efficiently screened moving away from the central ion (*i.e.*, they are rather local).⁴⁸⁻⁴⁹ A significant contribution is also supposed to arise from three-dimensional network of hydrogen bonds between the counterions. The strength and structure of this network are determined by the nature (polarizability, polarizing action, size *etc.*) of anion.⁵⁰⁻⁵² Triolo and his colleagues have established a substantial degree of microheterogeneity in various ILs by means of a set of scattering techniques complemented with simulations.⁵³⁻⁵⁶ The effect is more pronounced for ILs with longer alkyl chains and it is attributed to the microscopic segregation of the polar (ionic) and nonpolar (alkyl chain) domains.

The mentioned above considerations on the structure of pure components suggest for the corresponding mixtures two main phenomena, in which redistribution of the balance between possible ion-ion, ion-molecular, and intermolecular interactions upon the composition change can be manifested. They are ionic association/aggregation and ionic solvation. Going from pure IL to pure solvent, these phenomena can be understood as a gradual destruction of large ionic aggregates (basic structure units of pure ILs) into smaller ones up to ion pairs, followed by complete dissociation into 'free' ions in very dilute solutions as a result of interaction with solvent.³⁹ The interaction with the solvent can be both specific (localized ion-molecular interactions) and non-specific (effect of accumulation of significant amount of solvent which is capable of forming a medium, which is similar to the pure solvent).

The phenomena of ionic association and solvation manifest themselves at the microscopic level in the redistribution of electron density at the corresponding interaction sites and, consequently, in changes of the corresponding force constants. Among the currently known experimental methods that can reveal such effects, NMR and vibrational (IR and Raman) spectroscopy should be highlighted. The former can bring out information on the change of the electronic microenvironment of every chemically non-equivalent nucleus and on the relative arrangement for some nuclei, whereas the latter probes the changes of dipole moment/polarizability/force constants, *i.e.*, the changes in the microenvironment of the atoms involved in a studied vibrational mode.

The two phenomena being considered (association and solvation) are also reflected in 'statistical' microstructure of such binary mixtures, especially in the microstructure of ionic subsystem. Thus, a certain ordering of mutual distribution of counterions at low distances can be expected in case of pronounced ionic association as well as a certain ordering of distribution of the solvent molecules relative to ions in case of specific solvation. Nowadays experimental evidence on 'statistical' microstructure at different temporal and dimensional scales can only be provided by diffraction techniques (various methods of diffraction of X-rays and neutrons). These methods are rather expensive and not easily accessible, as well as complicated in terms of raw data treatment. At the same time they are the only 'direct' methods of investigation of microstructure of condensed matter. Most of the studies in this field deal with a single representative system IL-molecular solvent,⁵⁷⁻⁵⁹ so the generalized and systematic picture is still to be established.

Important information about the change of character of intermolecular interactions upon the change in composition of binary mixtures can be extracted via methods that study microscopic dynamics and transport coefficients (electrical conductivity, diffusion coefficient etc.). Most of the methods mentioned above can be classified as 'structural' ones since they do not take into account in an explicit

manner the motion of particles that form the observed signal. However, information about the relative speed of motion of different molecules and ions along with idea of which supramolecular entities are composed of which particles can be a sufficient basis to build a model of determinative interactions and the corresponding microstructure. Among the modern methods for investigation of diffusion in condensed matter at the microscopic level, NMR-diffusometry (DOSY)⁶⁰ and quasi-elastic neutron scattering should be noted.⁶¹ The two methods are coupled with both difficulties in experimental data treatment and problems of methodological character in setting up the experiment.

Despite the broad set of experimental approaches targeted at the discovery of peculiarities of intermolecular interactions in binary systems of ILs with molecular solvents, as mentioned above, most of them are indirect methods which are typically challenging in interpretation. Modern methods of molecular modeling can help to solve these problems and they also can complete the picture with information which is inaccessible from experiment. In view of the phenomena, effects and objects of interest, methods that would be definitely complementary to the proposed experimental techniques are quantum chemical calculations joined with modern methods of analysis of electron density distribution as well as the methods of molecular dynamics simulation.⁶²⁻⁶³

Quantum chemical calculations can describe electron density distribution in stationary states (normally in energy minima) of molecular systems with high accuracy. The results obtained in this way can be interpreted in terms of various theories among which the quantum theory of atoms in molecules (QTAIM)⁶⁴⁻⁶⁵ deserves particular attention, being widely applied to study weak noncovalent interactions and having rather clear and obvious foundations. The limitations of static quantum chemical calculations are external conditions (usually zero point temperature and without consideration of any effects of medium) as well as the size of a system that can be investigated. With modern accessible computational

resources routine calculations are limited to molecular and small supramolecular entities.

Methods of molecular dynamics simulations allow one to study systems of larger size (thousands of atoms and more) and at a finite temperature explicitly taking into account thermal motion during the ‘observation’ period (hundreds of picoseconds up to tens of nanoseconds) thus enabling accumulation of information that has been averaged among ensemble of particles. In case of quantum molecular dynamics simulation it is even possible to include all interaction effects in the best theoretically based way. However, very high computational cost of this method leads to significant limitations for the size of the studied systems and affordable simulation times (hundreds of atoms and tens of picoseconds, respectively). In classical MD simulation, simplification of the description of the interactions does not always make possible to extend simulation times up to the experimental observation times.

As mentioned above, the methods of quantum molecular dynamics are enormously resource demanding which makes them practically inapplicable to these systems given their very slow relaxation.⁶⁶ Unfortunately, the problem of the force-field development for classical MD simulation of ILs remains an open issue and a subject to discussion.⁶² In particular, it was found that dynamical properties of neat ILs are properly reproduced only when the polarization effects are taken into account.⁶⁷⁻⁷³ However, the way of treating the polarization effects^{69-70,72,74-76} as well as their implementation in simulations of binary mixtures with molecular solvents is far away from being well justified.

1.2. Organization of the thesis

This thesis presents a multitechnique investigation of the microscopic structure and dynamics in mixtures of imidazolium based ILs with polar aprotic molecular solvents relevant for electrochemistry. It is organized as follows.

Chapter 2 presents the details of experimental procedures and computational approaches used in the study. Particular attention is paid to the selection of the computational level of theory and to the advanced methods of analysis of electron density distribution.

The main results of quantum chemical calculations of the representative model molecular clusters of ILs and their adducts with the solvent molecules are discussed in details in Chapter 3. Electron density distribution and the nature of weak noncovalent interactions are assessed in order to help with the interpretation of the NMR chemical shift data, presented in Chapter 4. Preferential location and relative strength of the specific interactions as a function of mixture composition and of the nature of IL and molecular solvent are established.

Translational dynamics in the studied mixtures IL-molecular solvent is assessed by means of NMR diffusometry and the results are set forth in Chapter 5.

Chapter 6 is devoted to Raman spectroscopic investigation of a representative mixture by following the characteristic bands of the constituents. Spectral variations were deciphered with the help of advanced two-dimensional correlation techniques and interpreted in view of the results of calculations.

Finally, conclusions, summarizing the key findings of the work, and future perspectives are outlined.

1.3. References for Chapter 1

- (1) Hallett, J. P.; Welton, T., Room-Temperature Ionic Liquids: Solvents for Synthesis and Catalysis. 2. *Chem. Rev.* **2011**, *111*, 3508-3576.
- (2) Torimoto, T.; Tsuda, T.; Okazaki, K. I.; Kuwabata, S., New Frontiers in Materials Science Opened by Ionic Liquids. *Adv. Mater.* **2010**, *22*, 1196-1221.
- (3) Olivier-Bourbigou, H.; Magna, L.; Morvan, D., Ionic liquids and catalysis: recent progress from knowledge to applications. *Appl. Catal., A* **2010**, *373*, 1-56.
- (4) Giernoth, R., Task-Specific Ionic Liquids. *Angew. Chem., Int. Ed.* **2010**, *49*, 2834-2839.
- (5) Patel, D. D.; Lee, J.-M., Applications of Ionic Liquids. *Chem. Rec.* **2012**, *12*, 329-355.
- (6) Wasserscheid, P.; Schröer, W., Towards a better fundamental understanding of ionic liquids. *J. Mol. Liq.* **2014**, *192*, 1-2.
- (7) Endres, F.; Zein El Abedin, S., Air and Water Stable Ionic Liquids in Physical Chemistry. *Phys. Chem. Chem. Phys.* **2006**, *8*, 2101-2116.
- (8) Welton, T., Room-Temperature Ionic Liquids. Solvents for Synthesis and Catalysis. *Chem. Rev.* **1999**, *99*, 2071-2084.
- (9) Reichardt, C.; Welton, T. *Solvents and Solvent Effects in Organic Chemistry*; Fourth, Updated and Enlarged Edition ed.; Wiley-VCH Verlag GmbH & Co. KGaA: Weinheim, 2011; 718 p.
- (10) Huo, F.; Liu, Z.; Wang, W., Cosolvent or Antisolvent? A Molecular View of the Interface between Ionic Liquids and Cellulose upon Addition of Another Molecular Solvent. *J. Phys. Chem. B* **2013**, *117*, 11780-11792.
- (11) Gericke, M.; Liebert, T.; Seoud, O. A. E.; Heinze, T., Tailored Media for Homogeneous Cellulose Chemistry: Ionic Liquid/Co-Solvent Mixtures. *Macromolecular Materials and Engineering* **2011**, *296*, 483-493.
- (12) Wang, J.; Yao, H.; Nie, Y.; Zhang, X.; Li, J., Synthesis and characterization of the iron-containing magnetic ionic liquids. *J. Mol. Liq.* **2012**, *169*, 152-155.
- (13) Plechkova, N. V.; Seddon, K. R., Applications of ionic liquids in the chemical industry. *Chem. Soc. Rev.* **2008**, *37*, 123-150.
- (14) Rogers, R. D.; Seddon, K. R., Ionic Liquids--Solvents of the Future? *Science* **2003**, *302*, 792-793.
- (15) MacFarlane, D. R.; Forsyth, M.; Howlett, P. C.; Pringle, J. M.; Sun, J.; Annat, G.; Neil, W.; Izgorodina, E. I., Ionic Liquids in Electrochemical Devices and Processes: Managing Interfacial Electrochemistry. *Acc. Chem. Res.* **2007**, *40*, 1165-1173.
- (16) MacFarlane, D. R.; Tachikawa, N.; Forsyth, M.; Pringle, J. M.; Howlett, P. C.; Elliott, G. D.; Davis, J. H.; Watanabe, M.; Simon, P.; Angell, C. A., Energy applications of ionic liquids. *Energy & Environmental Science* **2014**, *7*, 232-250.
- (17) Lu, W.; Qu, L.; Henry, K.; Dai, L., High performance electrochemical capacitors from aligned carbon nanotube electrodes and ionic liquid electrolytes. *J. Power Sources* **2009**, *189*, 1270-1277.
- (18) Fedorov, M. V.; Kornyshev, A. A., Ionic Liquids at Electrified Interfaces. *Chem. Rev.* **2014**, *114*, 2978-3036.
- (19) Merlet, C.; Rotenberg, B.; Madden, P. A.; Taberna, P.-L.; Simon, P.; Gogotsi, Y.; Salanne, M., On the molecular origin of supercapacitance in nanoporous carbon electrodes. *Nat. Mater.* **2012**, *11*, 306-310.
- (20) Lewandowski, A.; Galiński, M., Carbon-ionic liquid double-layer capacitors. *Journal of Physics and Chemistry of Solids* **2004**, *65*, 281-286.

- (21) Liu, S.; Liu, W.; Liu, Y.; Lin, J.-H.; Zhou, X.; Janik, M. J.; Colby, R. H.; Zhang, Q., Influence of imidazolium-based ionic liquids on the performance of ionic polymer conductor network composite actuators. *Polymer International* **2010**, *59*, 321-328.
- (22) Fumino, K.; Wulf, A.; Ludwig, R., Strong, Localized, and Directional Hydrogen Bonds Fluidize Ionic Liquids. *Angew. Chem., Int. Ed.* **2008**, *47*, 8731-8734.
- (23) Tokuda, H.; Hayamizu, K.; Ishii, K.; Susan, M. A. B. H.; Watanabe, M., Physicochemical Properties and Structures of Room Temperature Ionic Liquids. 1. Variation of Anionic Species. *J. Phys. Chem. B* **2004**, *108*, 16593-16600.
- (24) Canongia Lopes, J. N.; Costa Gomes, M. F.; Husson, P.; Pádua, A. I. A. H.; Rebelo, L. P. N.; Sarraute, S.; Tariq, M., Polarity, Viscosity, and Ionic Conductivity of Liquid Mixtures Containing [C₄C₁im][Ntf₂] and a Molecular Component. *J. Phys. Chem. B* **2011**, *115*, 6088-6099.
- (25) Li, W.; Zhang, Z.; Han, B.; Hu, S.; Xie, Y.; Yang, G., Effect of water and organic solvents on the ionic dissociation of ionic liquids. *J. Phys. Chem. B* **2007**, *111*, 6452-6456.
- (26) Wang, J.; Tian, Y.; Zhao, Y.; Zhuo, K., A volumetric and viscosity study for the mixtures of 1-n-butyl-3-methylimidazolium tetrafluoroborate ionic liquid with acetonitrile, dichloromethane, 2-butanone and N, N - dimethylformamide. *Green Chem.* **2003**, *5*, 618-622.
- (27) Rizzuto, A. M.; Pennington, R. L.; Sienerth, K. D., Study of the BMIM-PF₆: acetonitrile binary mixture as a solvent for electrochemical studies involving CO₂. *Electrochim. Acta* **2011**, *56*, 5003-5009.
- (28) Trivedi, S.; Sarkar, A.; Pandey, S., Solvatochromic absorbance probe behavior within 1-butyl-3-methylimidazolium hexafluorophosphate + propylene carbonate: preferential solvation or solvent-solvent interaction? *Chem. Eng. J.* **2009**, *147*, 36-42.
- (29) Chagnes, A.; Diaw, M.; Carré, B.; Willmann, P.; Lemordant, D., Imidazolium-Organic Solvent Mixtures as Electrolytes for Lithium Batteries. *J. Power Sources* **2005**, *145*, 82-88.
- (30) Kollipost, F.; Hesse, S.; Lee, J. J.; Suhm, M. A., Dimers of cyclic carbonates: chirality recognition in battery solvents and energy storage. *Phys. Chem. Chem. Phys.* **2011**, *13*, 14176-14182.
- (31) Hesse, S.; Suhm, M. A., On the low volatility of cyclic esters: an infrared spectroscopy comparison between dimers of γ -butyrolactone and methyl propionate. *Phys. Chem. Chem. Phys.* **2009**, *11*, 11157-11170.
- (32) Stoppa, A.; Hunger, J.; Buchner, R., Conductivities of binary mixtures of ionic liquids with polar solvents. *J. Chem. Eng. Data.* **2009**, *54*, 472-479.
- (33) Nishida, T.; Tashiro, Y.; Yamamoto, M., Physical and electrochemical properties of 1-alkyl-3-methylimidazolium tetrafluoroborate for electrolyte. *J. Fluorine Chem.* **2003**, *120*, 135-141.
- (34) Kalugin, O. N.; Voroshylova, I. V.; Riabchunova, A. V.; Lukinova, E. V.; Chaban, V. V., Conductometric Study of Binary Systems Based on Ionic Liquids and Acetonitrile in a wide Concentration Range. *Electrochim. Acta* **2013**, *105*, 188-199.
- (35) Marcus, Y.; Hefter, G., Ion Pairing. *Chem. Rev.* **2006**, *106*, 4585-4621.
- (36) Zhu, A.; Wang, J.; Han, L.; Fan, M., Measurements and correlation of viscosities and conductivities for the mixtures of imidazolium ionic liquids with molecular solutes. *Chem. Eng. J.* **2009**, *147*, 27-35.
- (37) Vraneš, M.; Zec, N.; Tot, A.; Papović, S.; Dožić, S.; Gadžurić, S., Density, electrical conductivity, viscosity and excess properties of 1-butyl-3-methylimidazolium bis(trifluoromethylsulfonyl)imide + propylene carbonate binary mixtures. *J. Chem. Thermodyn.* **2014**, *68*, 98-108.
- (38) Jarosik, A.; Krajewski, S. R.; Lewandowski, A.; Radzimski, P., Conductivity of ionic liquids in mixtures. *J. Mol. Liq.* **2006**, *123*, 43-50.

- (39) Dupont, J., On the solid, liquid and solution structural organization of imidazolium ionic liquids. *J. Braz. Chem. Soc.* **2004**, *15*, 341-350.
- (40) Palm, R.; Kurig, H.; Tõnurist, K.; Jänes, A.; Lust, E., Electrical double layer capacitors based on 1-ethyl-3-methylimidazolium tetrafluoroborate with small addition of acetonitrile. *Electrochim. Acta* **2012**, *85*, 139-144.
- (41) Diaw, M.; Chagnes, A.; Carré, B.; Willmann, P.; Lemordant, D., Mixed ionic liquid as electrolyte for lithium batteries. *J. Power Sources* **2005**, *146*, 682-684.
- (42) Zhu, Q.; Song, Y.; Zhu, X.; Wang, X., Ionic Liquid-Based Electrolytes for Capacitor Applications. *J. Electroanal. Chem.* **2007**, *601*, 229-236.
- (43) Coadou, E.; Timperman, L.; Jacquemin, J.; Galiano, H.; Hardacre, C.; Anouti, M., Comparative Study on Performances of Trimethyl-Sulfonium and Trimethyl-Ammonium Based Ionic Liquids in Molecular Solvents as Electrolyte for Electrochemical Double Layer Capacitors. *J. Phys. Chem. C* **2013**, *117*, 10315-10325.
- (44) Wright, D.; El-Shall, M. S., Monte Carlo simulation of acetonitrile clusters $[\text{CH}_3\text{CN}]_N$, $N=2-256$: melting transitions and even/odd character of small clusters ($N=2-9$), heat capacities, density profiles, fractal dimension, intracluster dimerization, and dipole orientation. *J. Chem. Phys.* **1994**, *100*, 3791-3802.
- (45) Cabaleiro-Lago, E. M.; Hermida-Ramón, J. M.; Peña-Gallego, A.; Martínez-Núñez, E.; Fernández-Ramos, A., Intermolecular interactions and cooperative effects in acetonitrile clusters. An ab initio molecular orbital study. *J. Mol. Struct.: THEOCHEM* **2000**, *498*, 21-28.
- (46) Mennucci, B.; da Silva, C. O., A quantum mechanical strategy to investigate the structure of liquids: the cases of acetonitrile, formamide, and their mixture. *J. Phys. Chem. B* **2008**, *112*, 6803-3813.
- (47) Nigam, S.; Majumder, C., Growth pattern and electronic properties of acetonitrile clusters: a density functional study. *J. Chem. Phys.* **2008**, *128*, 214307.
- (48) Angenendt, K.; Johansson, P., Ionic liquid structures from large density functional theory calculations using mindless configurations. *J. Phys. Chem. C* **2010**, *114*, 20577-20582.
- (49) Tokuda, H.; Tsuzuki, S.; Susan, M. A. B. H.; Hayamizu, K.; Watanabe, M., How ionic are room-temperature ionic liquids? An indicator of the physicochemical properties. *J. Phys. Chem. B* **2006**, *110*, 19593-19600.
- (50) Avent, A. G.; Chaloner, P. A.; Day, M. P.; Seddon, K. R.; Welton, T., Evidence for hydrogen bonding in solutions of 1-ethyl-3-methylimidazolium halides, and its implications for room-temperature halogenoaluminate(III) ionic liquids. *J. Chem. Soc., Dalton Trans.* **1994**, 3405-3413.
- (51) Bonhôte, P.; Dias, A.-P.; Papageorgiou, N.; Kalyanasundaram, K.; Grätzel, M., Hydrophobic, highly conductive ambient-temperature molten salts. *Inorg. Chem.* **1996**, *35*, 1168-1178.
- (52) Consorti, C. S.; Suarez, P. A. Z.; de Souza, R. F.; Burrow, R. A.; Farrar, D. H.; Lough, A. J.; Loh, W.; da Silva, L. H. M.; Dupont, J., Identification of 1,3-dialkylimidazolium salt supramolecular aggregates in solution. *J. Phys. Chem. B* **2005**, *109*, 4341-4349.
- (53) Russina, O.; Lo Celso, F.; Di Michiel, M.; Passerini, S.; Appetecchi, G. B.; Castiglione, F.; Mele, A.; Caminiti, R.; Triolo, A., Mesoscopic structural organization in triphilic room temperature ionic liquids. *Faraday Discuss.* **2013**, *167*, 499-513.
- (54) Fazio, B.; Triolo, A.; Di Marco, G., Local organization of water and its effect on the structural heterogeneities in room-temperature ionic liquid/ H_2O mixtures. *J. Raman. Spectrosc.* **2008**, *39*, 233-237.
- (55) Macchiagodena, M.; Gontrani, L.; Ramondo, F.; Triolo, A.; Caminiti, R., Liquid structure of 1-alkyl-3-methylimidazolium-hexafluorophosphates by wide angle x-ray and neutron scattering and molecular dynamics. *J. Chem. Phys.* **2011**, *134*, 114521.

- (56) Zheng, W.; Mohammed, A.; Hines, L. G.; Xiao, D.; Martinez, O. J.; Bartsch, R. A.; Simon, S. L.; Russina, O.; Triolo, A.; Quitevis, E. L., Effect of Cation Symmetry on the Morphology and Physicochemical Properties of Imidazolium Ionic Liquids. *J. Phys. Chem. B* **2011**, *115*, 6572-6584.
- (57) Russina, O.; Sferrazza, A.; Caminiti, R.; Triolo, A., Amphiphile Meets Amphiphile: Beyond the Polar–Apolar Dualism in Ionic Liquid/Alcohol Mixtures. *J. Phys. Chem. Lett.* **2014**, *5*, 1738-1742.
- (58) Takamuku, T.; Honda, Y.; Fujii, K.; Kittaka, S., Aggregation of imidazolium ionic liquids in molecular liquids studied by small-angle neutron scattering and NMR. *Anal. Sci.* **2008**, *24*, 1285-1290.
- (59) Shimomura, T.; Takamuku, T.; Yamaguchi, T., Clusters of Imidazolium-Based Ionic Liquid in Benzene Solutions. *J. Phys. Chem. B* **2011**, *115*, 8518-8527.
- (60) Price, W. S., NMR Diffusometry. *Mod. Magn. Reson.* **2006**, *Part 1*, 109-115.
- (61) Triolo, A.; Russina, O.; Arrighi, V.; Juranyi, F.; Janssen, S.; Gordon, C. M., Quasielastic neutron scattering characterization of the relaxation processes in a room temperature ionic liquid. *J. Chem. Phys.* **2003**, *119*, 8549-8557.
- (62) Kirchner, B., Ionic liquids from theoretical investigations. In *Ionic Liquids*, Kirchner, B., Ed. Springer-Verlag: Berlin/Heidelberg, 2010; Vol. 290, pp 213-262.
- (63) Zahn, S.; Brehm, M.; Brüssel, M.; Hollóczki, O.; Kohagen, M.; Lehmann, S.; Malberg, F.; Pensado, A. S.; Schöppke, M.; Weber, H.; Kirchner, B., Understanding ionic liquids from theoretical methods. *J. Mol. Liq.* **2014**, *192*, 71-76.
- (64) Bader, R. F. W., A quantum theory of molecular structure and its applications. *Chem. Rev.* **1991**, *91*, 893-928.
- (65) Bader, R. F. W., Atoms in molecules. *Acc. Chem. Res.* **1985**, *18*, 9-15.
- (66) Spickermann, C.; Thar, J.; Lehmann, S. B. C.; Zahn, S.; Hunger, J.; Buchner, R.; Hunt, P. A.; Welton, T.; Kirchner, B., Why are ionic liquid ions mainly associated in water? A Car-Parrinello study of 1-ethyl-3-methyl-imidazolium chloride water mixture. *J. Chem. Phys.* **2008**, *129*, 104505.
- (67) Maginn, E. J., Atomistic simulation of the thermodynamic and transport properties of ionic liquids. *Acc. Chem. Res.* **2007**, *40*, 1200-1207.
- (68) Wu, X.; Liu, Z.; Huang, S.; Wang, W., Molecular dynamics simulation of room-temperature ionic liquid mixture of [bmim][BF₄] and acetonitrile by a refined force field. *Phys. Chem. Chem. Phys.* **2005**, *7*, 2771-2779.
- (69) Chaban, V., Polarizability versus mobility: atomistic force field for ionic liquids. *Phys. Chem. Chem. Phys.* **2011**, *13*, 16055-16062.
- (70) Chaban, V. V.; Prezhdo, O. V., A new force field model of 1-butyl-3-methylimidazolium tetrafluoroborate ionic liquid and acetonitrile mixtures. *Phys. Chem. Chem. Phys.* **2011**, *13*, 19345-19354.
- (71) Chaban, V. V.; Voroshylova, I. V.; Kalugin, O. N., A new force field model for the simulation of transport properties of imidazolium-based ionic liquids. *Phys. Chem. Chem. Phys.* **2011**, *13*, 7910-7920.
- (72) Chaban, V. V.; Voroshylova, I. V.; Kalugin, O. N.; Prezhdo, O. V., Acetonitrile boosts conductivity of imidazolium ionic liquids. *J. Phys. Chem. B* **2012**, *116*, 7719-7727.
- (73) Chaban, V.; Voroshylova, I. V.; Kalugin, O., The phenomenological account for electronic polarization in ionic liquid. *ECS Trans.* **2011**, *33*, 43-55.
- (74) Mondal, A.; Balasubramanian, S., Quantitative Prediction of Physical Properties of Imidazolium Based Room Temperature Ionic Liquids through Determination of Condensed Phase Site Charges: A Refined Force Field. *J. Phys. Chem. B* **2014**.

- (75) Holloczki, O.; Malberg, F.; Welton, T.; Kirchner, B., On the origin of ionicity in ionic liquids. Ion pairing versus charge transfer. *Phys. Chem. Chem. Phys.* **2014**, *16*, 16880-16890.
- (76) Borodin, O.; Henderson, W. A.; Fox, E. T.; Berman, M.; Gobet, M.; Greenbaum, S., Influence of Solvent on Ion Aggregation and Transport in PY15TFSI Ionic Liquid–Aprotic Solvent Mixtures. *J. Phys. Chem. B* **2013**, *117*, 10581-10588.

Chapter 2. Experimental and Computational Details

2.1. Objects of investigation. Sample preparation and handling

In this study, mixtures of four imidazolium ILs with three polar aprotic molecular solvents have been investigated. The ILs contain a common cation 1-*n*-butyl-3-methylimidazolium (Bmim⁺). It is combined with perfluorinated anions of different, size, shape, symmetry, and electronic structure, namely, tetrafluoroborate (BF₄⁻), hexafluorophosphate (PF₆⁻), trifluoromethylsulfonate (TfO⁻), and bis(trifluoromethanesulfonyl)imide (TFSI⁻). Molecular structures of the ions composing the investigated ILs are shown in the top panel of Figure 2.1.

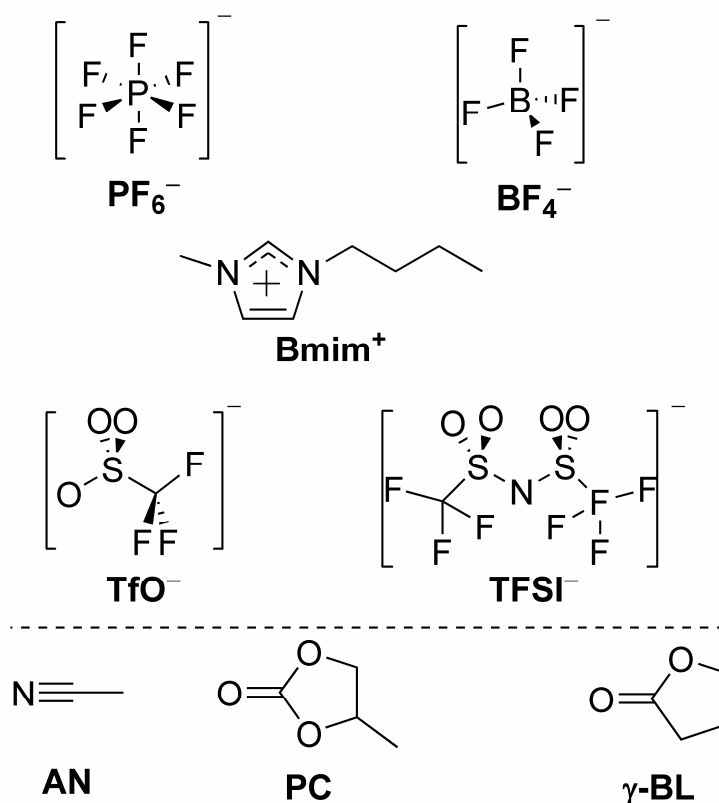


Figure 2.1. Chemical structures of the ions composing the four employed ILs BmimBF₄, BmimPF₆, BmimTfO, BmimTFSI (*top*) and the three molecular solvents used in this study (*bottom*).

All the ILs investigated in the present study were supplied by Solvionic (France) with a stated purity of 99.5%. According to the supplier major impurities were not higher than 500 ppm for water, 10 ppm for halides and 50 ppm for

methylimidazole. It is well known that overall purity and even traces of some particular impurities (namely, water and halides) can severely influence many properties of ILs. Especially transport properties like viscosity¹ and, as shown by Umecky and colleagues, particle diffusivities,²⁻³ are very sensitive.

To minimize the effects of absorbed moisture, all ILs were vacuum ($p < 10^{-6}$ bar) dried at 60 °C for at least 4 hours prior to the preparation of solutions as this procedure is known to lower the water content below 200–500 ppm. In the framework of a parallel project performed in Regensburg University, a Karl Fisher titration analysis of BmimPF₆ from the same supplier and of the same stated purity revealed the content of water to be *ca.* 60 ppm. Given the negligible halide content, no additional purification procedures were performed with the ILs.

The main physicochemical properties of the studied ILs are collected in Table 2.1. One can see that the neat ILs differ significantly in their transport properties, *i.e.*, viscosity and conductivity. At same time, they have rather close polarity (slightly higher value of the relative static dielectric permittivity of BmimTfO is related to significant contribution of its polar anion).

Table 2.1 Selected properties of ILs used in the present study: molar mass, M , density, d , dynamic viscosity, η , relative static dielectric permittivity, ϵ_r , electrical conductivity, κ , at 298.15 K

Property	BmimBF ₄	BmimPF ₆	BmimTfO	BmimTFSI
$M / \text{g mol}^{-1}$	226.02	284.18	288.29	419.36
$d / \text{g cm}^{-3}$	1.20164 ^a	1.36832 ^a	1.29963 ^b	1.43430 ^c
$\eta / \text{mPa s}$	90-219 ^d	207-450 ^d	75-93 ^d	49-69 ^d
ϵ_r	11.7 ^e	11.4 ^e	13.2 ^e	11.6 ^e
$\kappa / \text{mS cm}^{-1}$	3.53 ^a	1.469 ^a	2.90 ^f	3.90 ^f

^aRef. 4, ^bref. 5, ^cref. 6; ^ddata scatter a lot depending on the origin and purity of the sample and on the method, extreme values are given in refs. 7 and 8 for BmimBF₄, refs. 9 and 10 for BmimPF₆, refs. 11 and 10 for BmimTfO, refs. 7 and 8 for BmimTFSI; ^eref. 12, ^fref. 13.

As it was mentioned above, even minor impurities can significantly influence the viscosity of ILs. This can be illustrated by the enormous scattering of the

reported literature viscosity data, as shown in Figure 2.2, which originates from different degrees of purification.

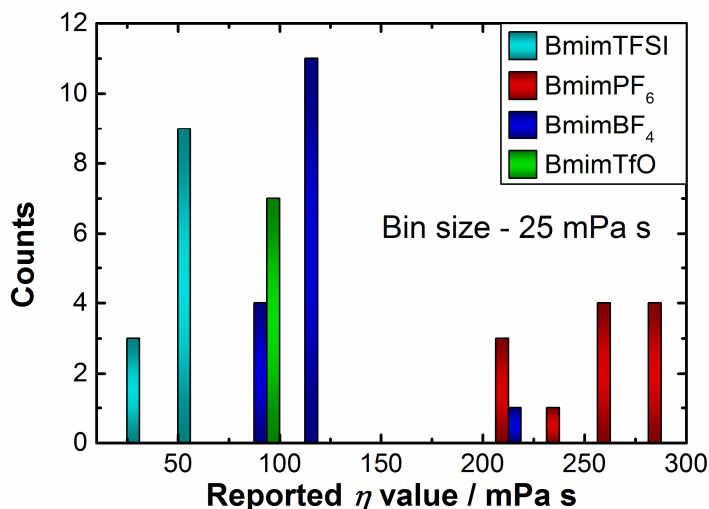


Figure 2.2. Histogram of distribution of the reported in literature values of dynamic viscosity, η , for the studied ILs.

Polar aprotic molecular solvents employed in this study are those common in electrochemistry of electrolyte solutions:¹⁴ acetonitrile (AN), γ -butyrolactone (γ -BL), and propylene carbonate (PC). Their molecular structures are depicted in the bottom panel of Figure 1.1

PC (anhydrous, 99.7%, ≤ 20 ppm of H₂O) and γ -BL (ReagentPlus, 99.0%, ≤ 1000 ppm of H₂O) were supplied by Sigma-Aldrich (France), AN (Rotisolv, 99.9%, UV-IR grade, ≤ 100 ppm of H₂O) was supplied by Carl Roth (Germany). γ -BL and AN were additionally dried with activated 4 Å molecular sieves while PC was used without further purification.

Main physicochemical properties of the solvents are given in Table 2.2. They differ in terms polarity both on macro- and microscopic scales as quantified by relative static dielectric permittivity and molecular dipole moment values, respectively. They follow the sequence AN < γ -BL < PC. However, their solvating capabilities towards cations, described by their electron donating or nucleophilic properties in the framework of Gutmann's donor numbers,¹⁵⁻¹⁶ follow a slightly

different trend AN << PC < γ -BL. Note that donor numbers of other common polar aprotic organic solvents like acetone or dimethyl sulfoxide are 17 and 29.8, respectively.¹⁵ In terms of electrophilic properties as quantified by Gutmann's acceptor numbers, which indirectly characterize solvent's capability of anion solvation all the solvents show comparable values which are typical for this class of polar aprotic molecular solvents.¹⁵

Table 2.2 Selected properties of molecular solvents used in the present study: molar mass, M , density, d , dynamic viscosity, η , relative static dielectric permittivity, ϵ_r , molecular dipole moment, μ , Gutmann's donor and acceptor numbers at 298.15 K

Property	AN	γ -BL	PC
$M / \text{g mol}^{-1}$	41.05	86.09	102.09
$d / \text{g cm}^{-3}$	0.776565 ^a	1.124210 ^b	1.19993 ^c
$\eta / \text{mPa s}$	0.339 ^a	1.76 ^d	2.5120 ^c
ϵ_r	35.96 ^e	41.7 ^f	64.96 ^c
μ / Debye	3.90 ^g	4.19 ^h	4.95 ^g
<i>Donor number</i>	14.1 ^g	18.0 ⁱ	15.1 ^g
<i>Acceptor number</i>	18.9 ^g	17.3 ^g	18.3 ^g

^aRef. 17, ^bref. 18, ^cref. 19, ^dref. 20, ^eref. 21, ^fref. 22, ^gref. 15, ^href. 23, ⁱref. 16.

All solutions were prepared in glass vials by weight in an Ar-filled glovebox, where the H₂O and O₂ content were kept below 2.5 ppm (volume / volume). To accelerate mixing the solutions were sonicated for 30 minutes. For NMR measurements solutions were afterwards transferred, in the glove-box as well, into 5-mm o.d. NMR tubes (supplied by Wilmad-LabGlass) fitted with a coaxial insert containing D₂O as NMR-lock solvent and parafilm. We employed a non-uniform concentration grid with more points taken around the composition corresponding to maximum conductivity in such mixtures, *i.e.*, $x_{\text{IL}} \sim 0.15$.

2.2. Raman measurements

Raman spectrometric study was conducted for a representative system BmimPF₆ – γ -BL. Particular interest to this system will be discussed in detail in Chapter 6.

Raman spectra of the bulk samples (contained in sealed 2 ml glass vials used for preparation of solutions) were acquired at room temperature (24±1 °C) using LabRam HR visible micro-Raman spectrometer (produced by HORIBA Jobin Yvon, France), equipped with confocal microscope (10x magnifying objective was used), in back-scattering geometry in the spectral range 50-3500 cm⁻¹. He-Ne laser ($\lambda = 632.81$ nm) was used for excitation. Raman signal was collected with a CCD-detector (1024×256 pixels) placed after a diffraction grating (1800 grooves/mm) giving the final spectral resolution of about 0.3 cm⁻¹. The wavenumber scale was calibrated prior to every measurement series with a standard Si sample (520.7 cm⁻¹). Spectra were accumulated in a single scan with exposure time of 300 s per each orientation of the grating which assured sufficient use of sensitivity of the detector and reducing the background noise. Band fitting in the spectral regions selected for analysis $y(\tilde{\nu})$ (see Chapter 6) was performed with OriginPro software (OriginLab, Northampton, MA) using Voigt profiles

$$y(\tilde{\nu}) = \sum_i A_i \frac{2 \ln 2}{\pi^{3/2}} \frac{w_{iL}}{w_{iG}^2} \int_{-\infty}^{\infty} \frac{e^{-t^2}}{\left(\sqrt{\ln 2} \frac{w_{iL}}{w_{iG}} \right)^2 + \left(\sqrt{4 \ln 2} \frac{\tilde{\nu} - \tilde{\nu}_i}{w_{iG}} - t \right)^2} dt \quad (2.1)$$

parametrized via peak areas, A_i , peak positions, $\tilde{\nu}_i$, and Lorentzian, w_{iL} , and Gaussian full width at half maximum (FWHM), w_{iG} . FWHM of a peak can be estimated as

$$\text{FWHM}_i = 0.5346 \cdot w_{iL} + \sqrt{0.2166 \cdot w_{iL}^2 + w_{iG}^2} \quad (2.2)$$

2.3. NMR measurements

All NMR measurements were performed on a Bruker Avance-II 400 spectrometer equipped with a 5-mm BBI probe with z-gradient, operating at 400.33 MHz, 100.66 MHz, and 162.04 MHz for ^1H , ^{13}C , and ^{31}P nuclei, respectively. Sample temperature was kept constant at 300.0 ± 0.1 K by means of VT-2000 Bruker variable temperature unit which was calibrated with standard samples of 4% MeOH in MeOH- d_4 and 80% ethylene glycol in DMSO- d_6 ²⁴. Prior to measurements, each sample was thermally equilibrated in the probe's acquisition zone for at least 15 min. Chemical shifts were referenced to the residual signal of the internal-lock solvent for ^1H and to external 85% H_3PO_4 for ^{31}P . For subsequent analysis the ^1H and ^{13}C NMR spectra were referenced to the signal of terminal methyl carbon of the butyl chain of IL cation (see Chapter 4 for discussion). An example of ^1H -NMR spectra of the neat ILs referenced in this way is shown in.

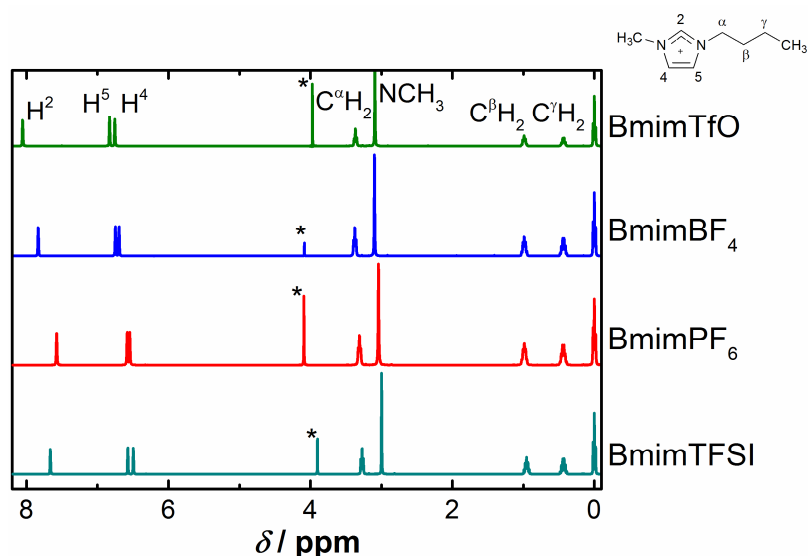


Figure 2.3. ^1H -NMR spectra of the neat ILs studied in this work. The spectra are referenced to the peak of the terminal methyl group of butyl chain. Peak assignment is given for the top spectrum. The signal of residual H₂O in the capillary insert which was used for primary referencing by the instrument is marked with an asterisk.

2.3.1 Diffusion measurements

Diffusion coefficients were measured by means of pulsed-field gradient (PFG) NMR method with the standard Bruker `ledbpgp2s` pulse sequence originally developed by Wu *et al.*²⁵ Measurements with this pulse sequence were shown to be free of artifacts from thermal convection when used with sample rotation,²⁶⁻²⁷ as done in our experiments. The `ledbpgp2s` pulse sequence is of stimulated-echo type and, hence, also satisfies recommendations from Annat *et al.*²⁸

Gradients were separately calibrated using known diffusion coefficient of residual HDO in D₂O.²⁹ Typical NMR-diffusion experiments employed 16 acquisition scans with a gradient pulse length (δ) of 1.2–5 ms and a diffusion delay (Δ) of 100–200 ms. These parameters were adjusted to achieve ~ 95% attenuation of the signal at the highest gradient strength. The latter was varied in 16 steps up to ~50 G cm⁻¹ in a way that its squared value changed in equal increments. Gradient pulses were of squared sine shape, gradient recovery and longitudinal eddy-current delays equaled to 0.2 and 5 ms, respectively. According to the literature, radiofrequency pulse length and relaxation delay do not severely influence reliability of the results.²⁷ Nevertheless, rough estimations of these parameters were performed for each sample. As these characteristic times were found to depend significantly on concentration, they were optimized to ensure accurate results.

Selected samples were tested at different diffusion delays to ensure the absence of thermal convection effects.²⁶ The data was analyzed with the standard TopSpin T₁/T₂ relaxation utility by fitting the decay of the integral intensity of the corresponding signal to the Stejskal-Tanner equation³⁰ (eq (2.3))

$$A = A_0 \exp\left(-\gamma^2 \delta^2 g^2 D \left(\Delta - \frac{\delta}{3}\right)\right) \quad (2.3)$$

which relates the attenuated signal amplitude, A , with its nonperturbed value, A_0 , using the gyromagnetic ratio of the probe nucleus, γ , gradient strength, g , gradient

pulse length, δ , diffusion delay time, Δ , and self-diffusion coefficient of the diffusing particle, D .

The accuracy of our data can be judged by comparing our results for the pure components with literature values (Table 2.3). Generally, rather good agreement was achieved for the pure ILs despite calibrating the gradient strength with a standard having a 2 orders-of-magnitude higher self-diffusion constant.

Table 2.3 Experimental self-diffusion coefficients, D , of the neat components measured at 300 K and the corresponding literature values obtained with different methods^a

$D, 10^{-9} \text{ m}^2 \text{ s}^{-1}$			
component	this work	literature	
		value	method
AN	5.1	4.85 (298.15 K) ^b	NMR
		4.31 (298.2 K) ^c	NMR, high-pressure diaphragm cell with trace [¹⁴ C]H ₃ CN
γ -BL	0.83	4.37 (298.15 K) ^d	NMR
		4.34 (298.15 K) ^e	open-end-capillary
		0.83 (303.15 K) ^f	NMR
		0.9 (303.15 K) ^g	NMR
PC	0.62	0.83 (295 K) ^h	NMR
		0.55 (303.15 K) ^f	NMR
		0.58 (303.15 K) ^g	NMR
		0.57 (298.15 K) ⁱ	NMR
		0.49 (298.15 K) ^j	NMR
		0.52 (298.15 K) ^k	NMR
Bmim ⁺ /TfO ⁻	0.018 / –	0.019 / 0.014 (300 K) ^l	NMR
Bmim ⁺ /PF ₆ ⁻	0.0078 0.0066	/ 0.0080 / 0.0059 (300 K) ^l	NMR
			0.0071 / 0.0054 (300 K) ^m
Bmim ⁺ /BF ₄ ⁻	0.017 / –	0.016 / 0.015 (300 K) ^l	NMR
		0.0158 / 0.0146 (300 K) ^m	NMR
		0.01301 / 0.01292 (300 K) ⁿ	NMR
		0.016 / – (298.15 K) ^b	NMR
Bmim ⁺ /TFSI ⁻	0.036 / –	0.0299 / 0.0238 (300 K) ^l	NMR
		0.0282 / 0.0216 (300 K) ^m	NMR

^aExperimental temperatures are given in parentheses. ^bRef. 31. ^cRef. 32. ^dRef. 33. ^eRef. 34. ^fRef. 35, estimated from a digitized graph. ^gRef. 36. ^hRef. 37. ⁱRef. 38. ^jRef. 39. ^kRef. 40. ^lInterpolated using equations from ref. 13. ^mRef. 41. ⁿRef. 42.

2.4. Quantum chemical calculations

2.4.1 General aspects

Most of the quantum chemical calculations reported in this work were conducted using density functional theory (DFT) with the help of GAUSSIAN 09 program suite.⁴³ Ultrafine integration grid and the default convergence criteria were used throughout. Second order Møller-Plesset perturbation theory (MP2) was employed as a reference method for benchmarking purposes.

Geometry optimizations were followed by harmonic frequency analysis to ensure that the obtained structures were true minima by the absence of imaginary wavenumbers.

Quantum chemical calculations of optimal structures followed by harmonic vibrational analysis were performed in order to rationalize experimental results in terms of optimized configurations of ILs (isolated ions, ion pair and ion pair dimer), solvent molecules, and IL-solvent complex (cation-solvent, anion-solvent, ion pair-solvent). The revealed lowest energy structures were obtained both in vacuum and in polar solvent medium treated via implicit solvation approach.

Binding energies were estimated in supramolecular approximation (*i.e.*, as a difference between energy of a given complex and a sum of energies of isolated molecules and/or ions constituting it) taking into account zero-point vibrational energies of the species. Basis set superposition error correction was shown to be insignificant for DFT calculations of IL ion pairs and larger clusters⁴⁴ performed with triple-zeta valence split basis set and thus it was not taken into account in the present study. Calculations involving polar medium were performed for the most stable representative structures in the framework of polarizable continuum model (PCM)⁴⁵ using the defaults in the software. Since γ -BL and PC are not on the list of default solvents in GAUSSIAN 09, their static relative dielectric permittivity values

of 41.7²² and 64.96¹⁹, respectively, were manually entered. PCM calculations on ion pair dimers were not feasible due to limited computational resources.

2.4.2 Level of theory validation

Dispersion plays significant role in ILs and, hence, acquiring reliable results from computational studies requires a good enough level of theory to capture such effects.⁴⁶⁻⁴⁹ Hydrogen bonding in ILs also remains a rather open question and special care needs to be taken in theoretical calculations as well as in interpretation of experimental results.⁵⁰ At present, the highest employed level of theory for geometry optimizations of imidazolium IL ion pairs is MP2/aug-cc-pvtz^{44,51} and MP2/aug-cc-pvdz for larger aggregates.⁴⁴ Single point energy estimations were feasible even with CCSD(T)/complete basis set extrapolation.⁵² However, these front-end calculation studies already require enormous amount of time and memory resources on modern supercomputers for the model systems with small 1,3-dimethylimidazolium (Mmim⁺) cation and/or monoatomic anions. This is definitely unaffordable for routine studies where it is not the ultrahigh precision, particularly in the energy values, which is needed, but rather reliable geometries and other properties, which capture all the key peculiarities of a given system.

In pursuit of quality to cost ratio, the overwhelming majority of published to date computational studies on imidazolium IL ion pairs and other representative systems has been performed by means of density functional theory calculations.⁵³⁻⁵⁴ Unfortunately, most of these reports are based on the results obtained with the popular B3LYP functional,⁵³⁻⁵⁴ which is known to be one of the worst performing ones for systems where dispersion plays role, including ILs.^{52,55-58} Thus, many conclusions drawn from these calculations may turn out to be an artifact of poor description of dispersion interactions. For example, as it was shown by Matthews *et al.*,⁴⁴ B3LYP gives wrong energy ordering of the most stable ion pair structures of MmimCl when benchmarked against MP2 and CCSD(T).

At present, there are two mainstream approaches to overcome this issue at little increase of computational cost. One deals with the addition of an empirical atom pairwise correction term, which scales as inverse sixth power of interatomic separation distance, as introduced by Grimme⁵⁹ to account for dispersion interactions and it is known as Grimme's D-correction or DFT-D. Another approach benefits from implicit parametrization of novel functionals in order to better describe medium-range dispersion effects.⁶⁰ Truhlar's Minnesota family of functionals, particularly the M06-2X,⁶¹ are the most popular in the field. Both approaches have been found to bring about considerable improvement of accuracy benchmarked against high-level calculations on test datasets of systems with dispersion and hydrogen bonding,⁵⁶⁻⁵⁸ and those including IL ion pairs and larger structures.^{48,52,55,62}

In order to select a reasonable level of theory for our calculations, we performed a small benchmark study on MmimBF₄ ion pair in vacuum (see Figure 2.4). This model ion pair was selected as the smallest one to have the main features of our systems of interest, namely, dialkylimidazolium cation and multiatomic perfluorinated anion. Anion is located symmetrically on top of the C²-H² fragment, which is essentially the most positively charged in the dialkylimidazolium cations⁶³, and establishes a number of short noncovalent contacts between its fluorine atoms and the C²-H² fragment as all as with the adjacent alkyl groups.

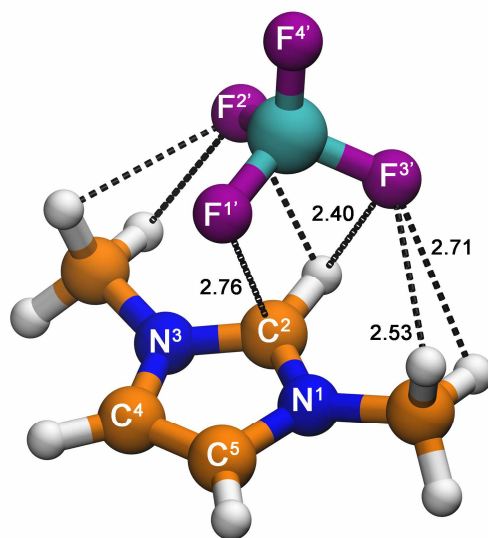


Figure 2.4. Geometry of MmimBF₄ ion pair obtained at MP2/6-311++g(d,p) level of theory. Key interionic short contacts are indicated with dashed black lines. Symmetry unique distances are given in Å. Color coding of the elements: white – H, orange – C, blue – N, purple – F, cyan – B.

We compared the DFT-D approach applied to such functionals as B3LYP, B97, and wB97x, which are notated as B3LYP-D3, B97D, and wB97xD, as implemented in the software,⁴³ with the M06-2X functional. Recently, Grimme even proposed parameters for the dispersion correction for the M06-2X functional, notated as M06-2X-D3⁵⁶ which was also tested here. As a reference method, we employed MP2, classical B3LYP was also taken for comparison. Most of the tests were performed using Pople-type triple-zeta split-valence basis set with diffuse and polarization functions on both hydrogens and heavy elements 6-311++g(d,p). The influence of the basis set was studied for the M06-2X functional coupled with 6-31+g(d), 6-311+g(d,p), 6-311++g(d,p), and aug-cc-pvdz. Generally, at least triple-zeta basis sets are recommended for the Minnesota family of functional⁶⁰, however, some benchmark studies claim that M06-2X is better coupled with Dunning's type double-zeta basis set aug-cc-pvdz.⁶⁴ The reference methods MP2 and B3LYP were additionally tested with heavier aug-cc-pvtz and lighter 6-31+g(d) basis sets, respectively.

The geometries, which define the interaction energies, electron density distribution and other subsequently derived properties of interest, obtained at the various levels of theory tested are compared in Figure 2.5. We note that the common B3LYP method with a very moderate basis set 6-31+g(d) erroneously predicts the anion to be asymmetrically tilted and positioned more towards the in-plane orientation, *i.e.*, more in front of the C²-H² fragment, rather than on top of it (Figure 2.5, B). Moreover, larger basis set 6-311++g(d,p) does not fix the problem. Neither the B97D, nor the wB97xD functional do. They only shift the anion closer to the on-top of the C²-H² fragment, but it is still asymmetrically tilted. It is only, when the B3LYP-D3 was used, that we could obtain a symmetrical structure compatible with the reference one. We stress, that this is an inherent problem of these functionals, but it is not of a bad choice of the initial configuration. It was impossible for us to reach the symmetrical structure with the B3LYP, B97D, and wB97xD functionals even when the MP2 structure was the starting one and very strict convergence thresholds were employed.

In contrast, M06-2X shows impressively good results already with the moderate 6-31+g(d) basis set (Figure 2.5, B). It is also noteworthy that either the basis set variation or inclusion of the empirical dispersion correction do not appreciably alter the optimized geometry. Aiming at higher computational efficiency without using too moderate basis sets, we have picked up the slightly smaller triple-zeta basis set 6-311++g(d,p) to the heavier double-zeta aug-cc-pvdz as the main basis set for our calculations.

General comparison between the best representatives of each of the two families, *i.e.*, M06-2X and B3LYP-D3 along with the reference results obtained with MP2 and B3LYP is presented in the panel D of Figure 2.5. It is apparent, that even though B3LYP-D3 significantly corrects the main erroneous features of the B3LYP structure, it still performs slightly worse than the M06-2X functional. The latter was thus selected for our main calculations.

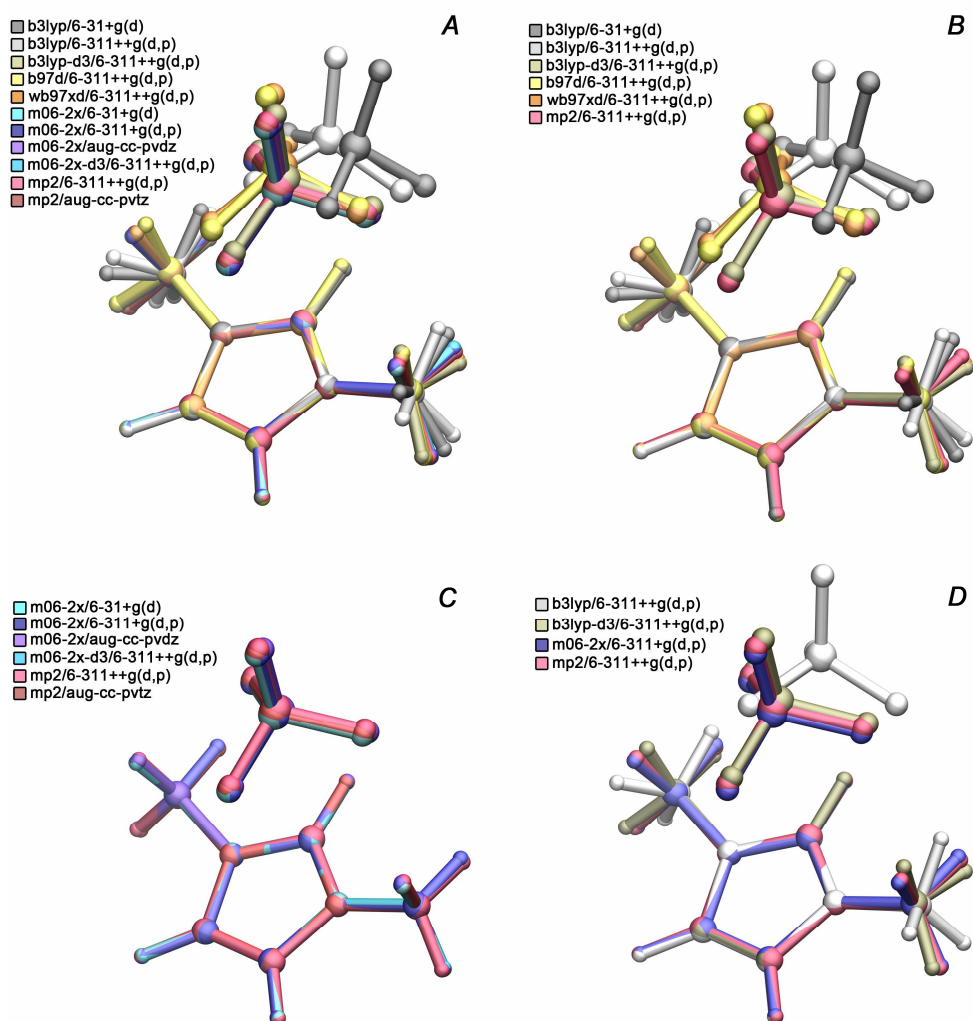


Figure 2.5. Overlaid by the imidazolium ring optimized in vacuum structures of MmimBF₄ ion pair as obtained at different levels of theory. *A* – overall comparison of all the tested approaches. *B* – assessment of the DFT-D style correction. *C* – assessment of the basis set dependence for the M06-2X functional. *D* – comparison of B3LYP, B3LYP-D3, and M06-2X functionals coupled with the 6-311++g(d,p) basis set. The reference structure obtained at the MP2/6-311++g(d,p) level of theory is shown in all the panels for comparison.

Quantitative comparison of the structures presented in the panel D of Figure 2.5 is given in Table 2.4. The main geometrical parameter of the corresponding isolated ions are also given and it is evident that the main differences are observed for the ion pairs, *i.e.*, for the relative arrangement of the counterions, but not for the ions themselves.

Table 2.4. Comparison of the main geometrical and energetic properties for MmimBF₄ ion pair and its isolated ions calculated at different levels of theory in vacuum.

	B3LYP/6-31+g(d)	B3LYP/6-311++g(d,p)	B3LYP-D3/6-311++g(d,p)	B97D/6-311++g(d,p)	wB97xD/6-311++g(d,p)	M06-2X/6-31+g(d)	M06-2X/6-311++g(d,p)	M06-2X-D3/6-311++g(d,p)	M06-2X/aug-cc-pVDZ	MP2/6-311++g(d,p)	MP2/aug-cc-pvtz
BF₄⁻											
d(B-F) / Å	1.418	1.417	1.419	1.432	1.414	1.409	1.409	1.409	1.415	1.415	1.409
Mmim⁺											
d(C ⁴⁻⁵ -H) / Å	1.080	1.077	1.077	1.081	1.077	1.080	1.077	1.077	1.083	1.080	1.076
d(C ² -H) / Å	1.080	1.078	1.077	1.081	1.078	1.081	1.079	1.079	1.083	1.080	1.076
∠NC ² N / deg.	108.958	108.858	108.770	108.609	108.887	108.823	108.833	108.837	108.760	108.381	108.309
∠HCNC ² / deg.	-0.003	1.141	1.154	0.046	1.126	0.976	1.237	0.025	-0.003	1.229	1.110
MmimBF₄											
max d(B-F) / Å	1.440	1.439	1.431	1.446	1.431	1.422	1.422	1.422	1.427	1.427	1.422
min d(B-F) / Å	1.377	1.374	1.377	1.389	1.374	1.373	1.370	1.370	1.378	1.377	1.374
d(C ⁴⁻⁵ -H) / Å	1.079	1.076	1.076	1.080	1.076	1.079	1.076	1.076	1.081	1.079	1.075
d(C ² -H) / Å	1.082	1.078	1.076	1.079	1.078	1.080	1.077	1.077	1.082	1.077	1.074
∠NC ² N / deg.	108.810	108.811	108.747	108.577	108.874	108.803	108.837	108.837	108.747	108.420	108.244
∠HCN ^{1/3} C ² / deg.	0.839/25.577	7.761/23.917	38.025	36.451/37.730	25.988/32.211	22.107	22.464	22.464	24.228	25.770	21.863
d(C···B) / Å	3.129	3.103	3.018	3.071	3.030	2.926	2.924	2.924	2.908	2.983	2.959
∠C ⁴ N ³ C ² B / deg.	130.459	127.869	104.349	108.882	110.421	101.602	101.714	101.714	103.542	102.276	101.969
-E ^{int} / kJ mol ⁻¹	347.9	353.8	375.3	369.4	369.2	380.7	387.3	388.7	388.1	376.8	377.7
No of basis functions	246	327	327	327	327	246	327	327	357	327	759

One can also see from Table 2.4 that in the tilted structures obtained with the B3LYP, B97D, and wB97xD functionals the anion is not only shifted towards the in-plane configuration (note the higher values of the $C^4N^3C^2B$ dihedral angle, *i.e.*, the angle between the C^2 -B vector and the imidazolium ring plane; the value of 180 degrees would correspond to the perfect in-plane arrangement of the anion, while for anion located exactly above the C^2 carbon a value of 90 degrees is expected) but it is also further apart from the center of positive charge of the cation (note the higher values of the $C^2\cdots B$ distances). The latter observation is logically reflected in reduced values of the interaction energy which is dominated by the Coulomb attraction.⁶⁵⁻⁶⁶

The effect of the level of theory on the electronic properties in terms of electron density distribution and weak noncovalent interactions will be discussed in the subsequent sections of this chapter.

2.4.3 Quantum theory of atoms in molecules

As it was noted for the structure of the model ion pair $MmimBF_4$, shown in Figure 2.4, there are multiple short contacts between the counterions which can be attributed to weak noncovalent interactions and even to hydrogen bonds. These contacts are bifurcated as the same hydrogen/fluorine atom can participate in several interactions. The characterization based on the information on angles and distances is rather poor with respect to the explanation of the nature of such interactions. A well-justified approach to quantitatively describe such phenomena in molecular systems is Bader's 'quantum theory of atoms in molecules' (QTAIM).⁶⁷

In a molecular structure, electron density is inhomogeneously distributed: it is accumulated around the atomic nuclei and vanishes at infinite separation. The phenomenon of 'chemical bonding' is considered as a local accumulation of electron density in the internuclear space of the interacting, *i.e.*, chemically bonded

atoms. This electron density, however, is far less than at the corresponding nuclear sites and, thus, it goes through a minimum along the bonding direction.

In his works,⁶⁷⁻⁷⁰ Bader showed that the structure of a molecular system is uniquely determined by the type of the electron density (ρ) critical points (CPs) where the gradient of the electron density equals zero ($\nabla\rho=0$). Eigenvalues λ_i (of the matrix of second derivatives of the electron density (electron density Hessian) define the type of a critical point which is usually notated as (ω, λ) , where ω is the rank of the electron density Hessian (*i.e.*, the number of non-zero eigenvalues), and λ is its signature (*i.e.*, algebraic sum of signs of the eigenvalues). Typically for minima on potential energy surfaces there are three non-zero λ_i values ($\lambda_1 < \lambda_2 < \lambda_3$)

Subsequently, in a stable molecular systems there can be the following types of CPs in the spatial distribution of the electron density:

- (3, -3) – nuclear attractor which corresponds to a local electron density maximum in all the directions ($\lambda_1, \lambda_2, \lambda_3 < 0$);
- (3, +3) – cage CP (CCP) which is a local minimum in the electron density in all the directions ($\lambda_1, \lambda_2, \lambda_3 < 0$);
- (3, +1) – ring CP (RCP) where the electron density is a minimum in the ring plane, but it is a maximum along the normal to the ring plane ($\lambda_1 < 0, \lambda_2, \lambda_3 > 0$);
- (3, -1) – bond CP (BCP). A point where the electron density is minimal along the interaction path between two atoms and it is maximum in the plane perpendicular to the pathline ($\lambda_1, \lambda_2 < 0, \lambda_3 > 0$).

Bonding pattern of a molecular system can be described as a system of nuclear attractors connected via bond paths. A bond path is a line of maximum electron density connecting two interacting atoms and BCP is the point of lowest electron density on this line (see Figure 2.6). Typically, bond paths are straight lines between the nuclei, but sometimes they can be rather curved.

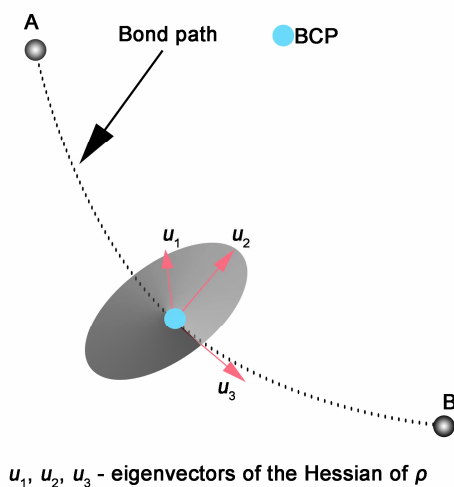


Figure 2.6. Schematic representation of the bonding between two interacting atoms A and B. Shaded area indicates the plane perpendicular to the bond path at the BCP. Directions of the \mathbf{u}_1 , \mathbf{u}_2 , and \mathbf{u}_3 eigenvectors of the Hessian of ρ at the BCP are also shown. Their eigenvalues are λ_1 , λ_2 , and λ_3 , respectively.

In view of characterization of the weak noncovalent interactions, including hydrogen bonds, the properties of electron density at the corresponding BCPs are typically considered. The following descriptors are commonly used for their quantitative characterization in the QTAIM framework:

- 1) electron density (ρ) at the BCP;
- 2) electron density Laplacian ($\Delta\rho$) at the BCP which is the sum of the eigenvalues of the electron density Hessian:

$$\Delta\rho = \nabla^2\rho = \frac{\partial^2\rho}{\partial x^2} + \frac{\partial^2\rho}{\partial y^2} + \frac{\partial^2\rho}{\partial z^2} = \sum_{i=1}^3 \lambda_i \quad (2.4)$$

Its positive value indicates that the corresponding BCP is located in the region of electron density depletion, which is typical for weak, noncovalent, mainly electrostatic interactions;⁷¹

- 3) local total electron energy density (H) at the BCP which is the sum of the corresponding kinetic (G) and potential (V) energy densities. G values are positive and those of V are negative:

$$H = G + V \quad (2.5)$$

The local kinetic and potential energy densities are related to the electron density Laplacian via:

$$\frac{1}{4}\Delta\rho = 2G + V \quad (2.6)$$

One can see, that for the positive Laplacian value ($\Delta\rho > 0$) there can be situations where the local potential energy density still outweighs the local kinetic energy density, i.e. $|V| > |G|$ and, hence, $H < 0$. This is a case of electrostatic interactions ($\Delta\rho > 0$) with some degree of covalency, since the negative value of the electron density localization at a given BCP has a stabilizing effect on the system. It is typical for strong hydrogen bonds and noncovalent interactions. Weak and medium strength noncovalent interactions typically show positive values for both $\Delta\rho$ and H .

- 4) ellipticity ($\varepsilon = \lambda_1/\lambda_2 - 1$) characterizes the uniformity of the electron density accumulation in the plane which is orthogonal to the bond path. For a perfectly cylindrically symmetric distribution of the electron density along the bond path the ellipticity value is zero. Values higher than *ca.* 0.5 are considered to be indicative of significant nonuniformity of the electron density distribution at the BCP.

Koch and Popelier proposed several practical criteria for hydrogen bonding on the basis of extensive QTAIM studies on presumably hydrogen bonded systems.⁷² They can be summarized as follows.

A hydrogen atom can be considered as forming a hydrogen bond with an acceptor if the following three necessary conditions are satisfied:

- 1) there is a BCP between the hydrogen atom and the hydrogen bond acceptor and of the corresponding bond path which connects the hydrogen and acceptor atoms;
- 2) low value of the electron density (ρ) in the BCP – 0.002-0.034 a.u..

3) low positive value of the Laplacian of the electron density ($\Delta\rho$) – 0.024-0.139 a.u.

Apart from the analysis of bonding pattern in molecular systems, QTAIM also provides tools to partition the molecular space into distinct atomic compartments, which are called ‘atomic basins’, based on the electron density topology. An atomic basin is a locus in space for which all the gradient paths terminate at a given nuclear attractor. In other words, within an atomic basin, the electron density always increases when approaching the nuclear attractor. Atomic basins are separated by so-called zero-flux surfaces where the electron density gradient normal to this surface equals zero. Having established these topological boundaries between the atomic basins, any property can be integrated within these boundaries to determine atomic contribution into the overall molecular property. In particular, atomic charges are defined within QTAIM as the electron density integrated over the given atomic basin after subsequent subtraction of the corresponding nuclear charges. QTAIM charges are known to be robust and reliable for determining the atomic charges of the inner atoms in bulky molecular structures, they also capture the symmetry of charge distribution, where it is relevant, in contrast to other charge calculation protocols based on the electrostatic potential fitting.⁷³

Formation of a hydrogen bond is also accompanied with an increase of charge on the hydrogen atom.

In the present study, all the QTAIM calculations were performed with the MultiWFN software using its default parameters.⁷⁴

Basic QTAIM properties of the model ion pair MmimBF_4 calculated for the structures presented in the panel D of Figure 2.5 are collected in Table 2.5. As it was mentioned above for the structural properties, major differences are observed for the ion pairs rather than for the isolated counterions. Since the electron density distribution is determined by the underlying molecular geometry, the discrepancies

noted for the geometries are also reflected in the parameters of the interionic BCPs and in the atomic charges of the relevant atomic sites.

We note that, indeed, as it was anticipated from the geometry of the ion pair, QTAIM analysis reveals several types of weak noncovalent interactions between the counterions. They have intermediate values of the electron density at the BCPs ρ^{BCP} (0.010-0.013 a.u.) and should be classified as weak and electrostatic, since the corresponding values of the Laplacian $\Delta\rho^{\text{BCP}}$ and of the total electron energy density H^{BCP} are slightly positive. In all the structures compared here there is a particular contact with the C² carbon atom which is a consequence of its direct contact with one of the fluorine atoms of the anion. This contact shows an appreciable ellipticity at the BCP which might originate from the peculiarities of the electron density distribution in the imidazolium ring.

Table 2.5. Comparison of the main QTAIM parameters for MmimBF₄ ion pair and its isolated ions calculated at different levels of theory in vacuum.

	B3LYP/6-311++g(d,p)	B3LYP-D3/6-311++g(d,p)	M06-2X/6-311++g(d,p)	MP2/6-311++g(d,p)
BF₄⁻				
$q(\text{F}) / e$	-0.839	-0.839	-0.853	-0.856
Mmim⁺				
$q(\text{C}^2) / e$	0.995	0.995	1.070	0.997
$q(\text{H}^2) / e$	0.149	0.150	0.154	0.159
MmimBF₄				
$q(\text{BF}_4^-) / e$	-0.969	-0.977	-0.986	-0.987
$q(\text{C}^2) / e$	1.018	1.029	1.110	1.044
$q(\text{H}^2) / e$	0.231	0.191	0.191	0.195
BCPs				
$\rho^{\text{BCP}}(\text{C}^2 \cdots \text{F}^1) / \text{a.u.}$	0.0109	0.0121	0.0140	0.0133
$\Delta\rho^{\text{BCP}}(\text{C}^2 \cdots \text{F}^1) / \text{a.u.}$	0.0429	0.0477	0.0569	0.0528
$H^{\text{BCP}}(\text{C}^2 \cdots \text{F}^1) / \text{a.u.}$	0.0014	0.0012	0.0011	0.0010
$\varepsilon^{\text{BCP}}(\text{C}^2 \cdots \text{F}^1) / \text{a.u.}$	0.77	0.37	0.62	0.42
$\rho^{\text{BCP}}(\text{H}^2 \cdots \text{F}^{2-3}) / \text{a.u.}$	0.0136/0.0192	0.0126	-	-
$\Delta\rho^{\text{BCP}}(\text{H}^2 \cdots \text{F}^{2-3}) / \text{a.u.}$	0.0744/0.0558	0.0518	-	-
$H^{\text{BCP}}(\text{H}^2 \cdots \text{F}^{2-3}) / \text{a.u.}$	0.0021/0.0020	0.0018	-	-
$\varepsilon(\text{H}^2 \cdots \text{F}^{2-3}) / \text{a.u.}$	0.05/0.36	0.43	-	-
$\rho^{\text{BCP}}(\text{C}^2 \cdots \text{F}^{2-3}) / \text{a.u.}$	-	-	0.0146	0.0130
$\Delta\rho^{\text{BCP}}(\text{C}^2 \cdots \text{F}^{2-3}) / \text{a.u.}$	-	-	0.0609	0.0547
$H^{\text{BCP}}(\text{C}^2 \cdots \text{F}^{2-3}) / \text{a.u.}$	-	-	0.0017	0.0016
$\varepsilon^{\text{BCP}}(\text{C}^2 \cdots \text{F}^{2-3}) / \text{a.u.}$	-	-	0.65	0.60
$\rho^{\text{BCP}}(\text{H}^{\text{Me}} \cdots \text{F}^{2-3}) / \text{a.u.}$	0.0125/0.0115	0.0117	-	0.0102
$\Delta\rho^{\text{BCP}}(\text{H}^{\text{Me}} \cdots \text{F}^{2-3}) / \text{a.u.}$	0.0461/0.0407	0.0453	-	0.0431
$H^{\text{BCP}}(\text{H}^{\text{Me}} \cdots \text{F}^{2-3}) / \text{a.u.}$	0.0014/0.012	0.0014	-	0.0010
$\varepsilon^{\text{BCP}}(\text{H}^{\text{Me}} \cdots \text{F}^{2-3}) / \text{a.u.}$	0.01/0.07	0.35	-	0.76
$\rho^{\text{BCP}}(\text{C}^{\text{Me}} \cdots \text{F}^{2-3}) / \text{a.u.}$	-	-	0.0115	-
$\Delta\rho^{\text{BCP}}(\text{C}^{\text{Me}} \cdots \text{F}^{2-3}) / \text{a.u.}$	-	-	0.0500	-
$H^{\text{BCP}}(\text{C}^{\text{Me}} \cdots \text{F}^{2-3}) / \text{a.u.}$	-	-	0.0015	-
$\varepsilon^{\text{BCP}}(\text{C}^{\text{Me}} \cdots \text{F}^{2-3}) / \text{a.u.}$	-	-	1.02	-
RCPs				
$\rho^{\text{RCP}}(\text{imidazolium}) / \text{a.u.}$	0.0545	0.0547	0.0570	0.0551
$\rho^{\text{RCP}}(\text{interionic}) / \text{a.u.}$	0.0065-0.0128	0.0074-0.0101	0.0094-0.0116	0.0079-0.0105
CCPs				
$\rho^{\text{CCP}} / \text{a.u.}$	-	0.0092	0.0108	0.0100

Another prominent feature to mention is that the arrangement of the anion roughly on-top of the C²-H² fragment is not really favorable for directional hydrogen bonding. As a result, the numerical QTAIM algorithm sometimes reveals

the corresponding bond paths terminating not at the hydrogen atoms but to the adjacent carbon atoms. This results in rather curved bond paths which can be judged by rather high values of ellipticity (Table 2.5) and visually in the corresponding molecular graph, *i.e.*, a set of CPs connected via bond paths and BCP-to-RCP paths, shown in Figure 2.7 (note the bondpaths $F^{3-2}\cdots C^2$ curved when approaching the carbon site).

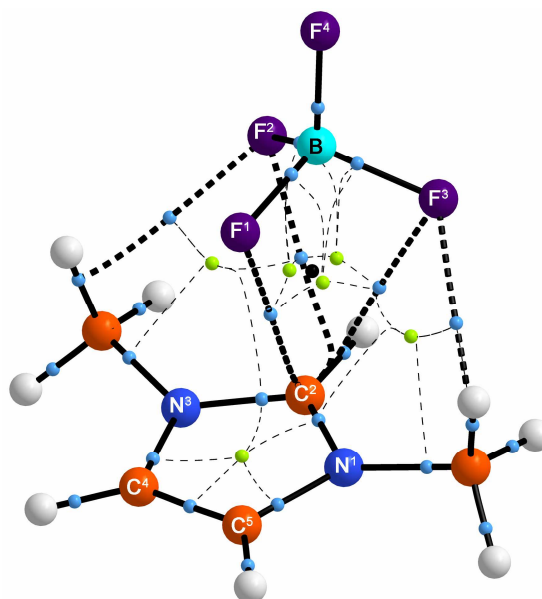


Figure 2.7. Molecular graph of the $MmimBF_4$ ion pair obtained by means QTAIM analysis of its optimal structure at the MP2/6-311++g(d,p) level of theory. Bond paths for covalent interactions are shown as solid thick black lines, those of the weak noncovalent ones are thick dashed black lines. Thin dashed black lines show the RCP-to-BCP paths. CCP is shown as a black sphere, BCPs are light-blue, and RCPs are green. Color coding of the elements: white – H, orange – C, blue – N, purple – F, cyan – B.

From Figure 2.7 it is also apparent that within the interionic space in addition to the BCPs there is a number of RCPs and a CCP in the region on top of the C^2-H^2 fragment which is in accordance with the recent results of Matthews *et al.*⁷⁵ These give some hints that the weak noncovalent interactions in such systems are more than a set of short interionic contacts. It was shown in the literature for systems, where hydrogen bonds are a part of a cyclic structure, that the RCP densities correlate well with other BCP descriptors of intramolecular hydrogen bonds.⁷⁶⁻⁷⁸ CCPs were found to be a characteristic feature of ion adducts with aromatic π -

substrates. The corresponding densities correlate with the interaction energies, as it was shown for complexes with anions⁷⁹⁻⁸⁰ and with cations.⁸¹⁻⁸³ Moreover electron density properties at CCPs are also quite important to understand interaction in stacked aromatic systems.⁸⁴

As can be seen from Table 2.5 the electron density values at the interionic BCPs and CCPs are slightly lower than at the corresponding BCPs (ca. 0.008-0.011 a.u.). This proves that there are multiple weak noncovalent interactions in the model MmimBF₄ ion pair.

2.4.4 Noncovalent interactions

One of the drawbacks of the QTAIM approach is that the whole analysis, which starts with location of the CPs, relies on a numerical differentiation procedure which can fail to locate the CPs, particularly the BCPs corresponding to weak noncovalent interactions in the regions of low electron density.⁸⁵ In fact, there are situations described in the literature, where everything points to the existence of a weak attractive noncovalent interaction, like the intramolecular hydrogen bond in ethylene glycol,⁸⁵ but QTAIM does not reveal the corresponding BCP. The problem is that the electron density gradient in the vicinity of the anticipated BCP location approaches zero, but does not reach it, in terms of numerical accuracy of the QTAIM algorithm.

An approach that is capable of overcoming this problem has been recently developed by Cotreras García and Johnson.⁸⁶⁻⁸⁹ It is called ‘noncovalent interactions’, or NCI, and it deals with analysis of the electron density distribution in molecular systems in the regions of low electron density and low gradient values. This approach is also often referred to as ‘reduced density gradient’ (RDG) analysis.⁷⁴

$$\text{RDG} = \frac{1}{2(3\pi^2)^{1/3}} \frac{|\nabla\rho|}{\rho^{4/3}} \quad (2.7)$$

When the RDG is plotted as a function of the electron density (see Figure 2.8) several peculiar features become apparent. At nuclear sites, where the electron density is high, the gradient reaches the zero value leading to low values of the RDG at high ρ values (beyond the bottom right edge of the top left panel in Figure 2.8). At infinite separation from the nuclei, the electron density vanishes and this corresponds to the region of high RDG values as $\rho \rightarrow 0$ (beyond the top left edge of the top left panel in Figure 2.8). The decay of electron density between these two limiting cases is roughly exponential. As a result, the main trend in the dependence of the RDG on the electron density value is of a general form $\rho^{-1/3}$.⁸⁸ However, as it is implied in QTAIM, the bonding pattern in a molecular structure is determined by a set of CPs where the electron density gradient is zero. The BCPs for covalent bonds appear as spikes of zero RDG value at the electron density values corresponding to ρ^{BCP} . For systems with weak noncovalent interactions, whether hydrogen bonding, dispersion, or steric repulsion, the corresponding plots reveal similar spikes, but at much lower values of the electron density (typically, below 0.05 a.u.).

As it was mentioned before, it happens that the electron density gradient itself does not reach the zero value for the weak noncovalent interactions, however, the characteristic spike-like pattern is still observed. It reflects the electron density distribution in the vicinity of the anticipated density CP. To distinguish between the attractive and repulsive interactions, it was proposed to use the sign of the second eigenvalue of the electron density Hessian λ_2 .⁸⁸ For a case of two interacting atoms, as shown in Figure 2.6, the λ_3 value is positive at the BCP, since it is a minimum of the electron density along the bond path. The λ_2 value characterizes the distribution of the electron density in the plane which is orthogonal to the bond path. For bonding interactions where the electron density is accumulated in the vicinity of the BCP, the λ_2 value is negative, while for the nonbonding and repulsive interactions $\lambda_2 > 0$. The corresponding graphical representation, often called as NCI plots, is a

graph of the RDG value as a function of $\text{sign}(\lambda_2)\rho$, which is shown in the top right panel in Figure 2.6. The covalent bonds, characterized by spikes reaching zero at rather high values of ρ , appear at the left (negative) side of the NCI plot. The RCP which corresponds to the imidazolium ring gives a spike at the positive side of the NCI plot for MmimBF₄ ion pair at *ca.* 0.05 a.u. which perfectly corresponds with the results of QTAIM analysis (Table 2.5).

The region of weak noncovalent interactions between the counterions, which constitutes the main point of interest for us in the present study, is shown in the bottom panel of Figure 2.8. The spikes reaching zero RDG values at the negative side of the NCI plot at around *ca.* 0.012-0.015 a.u. correspond to the interionic BCPs revealed by the QTAIM analysis (Table 2.5). Similarly, the spikes at the positive side of the NCI plot in this region correspond to the interionic CCP and RCPs with ρ values of about 0.01 a.u.

A spike at the negative side of the NCI plot which does not reach zero RDG value is an example of a bonding, *i.e.*, stabilizing weak noncovalent interaction which is not captured by the QTAIM analysis. In order to assign this interaction a visualization method is required. Within the NCI approach, this is performed by plotting an isosurface of the RDG which encloses the regions of space where the RDG values are below a given isovalue.⁸⁷⁻⁸⁸ The strength of interaction in the regions of noncovalent interactions highlighted by the isosurfaces can be visualized by coloring the surfaces in accordance with the corresponding $\text{sign}(\lambda_2)\rho$ values. A conventional palette for this color mapping of NCI is blue-green-red,⁸⁷⁻⁸⁸ that is the regions of bonding interactions with $\text{sign}(\lambda_2)\rho < 0$ are in blue, repulsive interactions and steric clashes where $\text{sign}(\lambda_2)\rho > 0$ are in red, and the weak dispersive interactions of low electron density appear as green isosurfaces. The latter type of interactions is characterized by the electron density values below *ca.* 0.01 a.u. However, despite rather low values of ρ they are usually rather delocalized and can significantly contribute to the overall pattern of noncovalent interactions.⁸⁹⁻⁹⁰

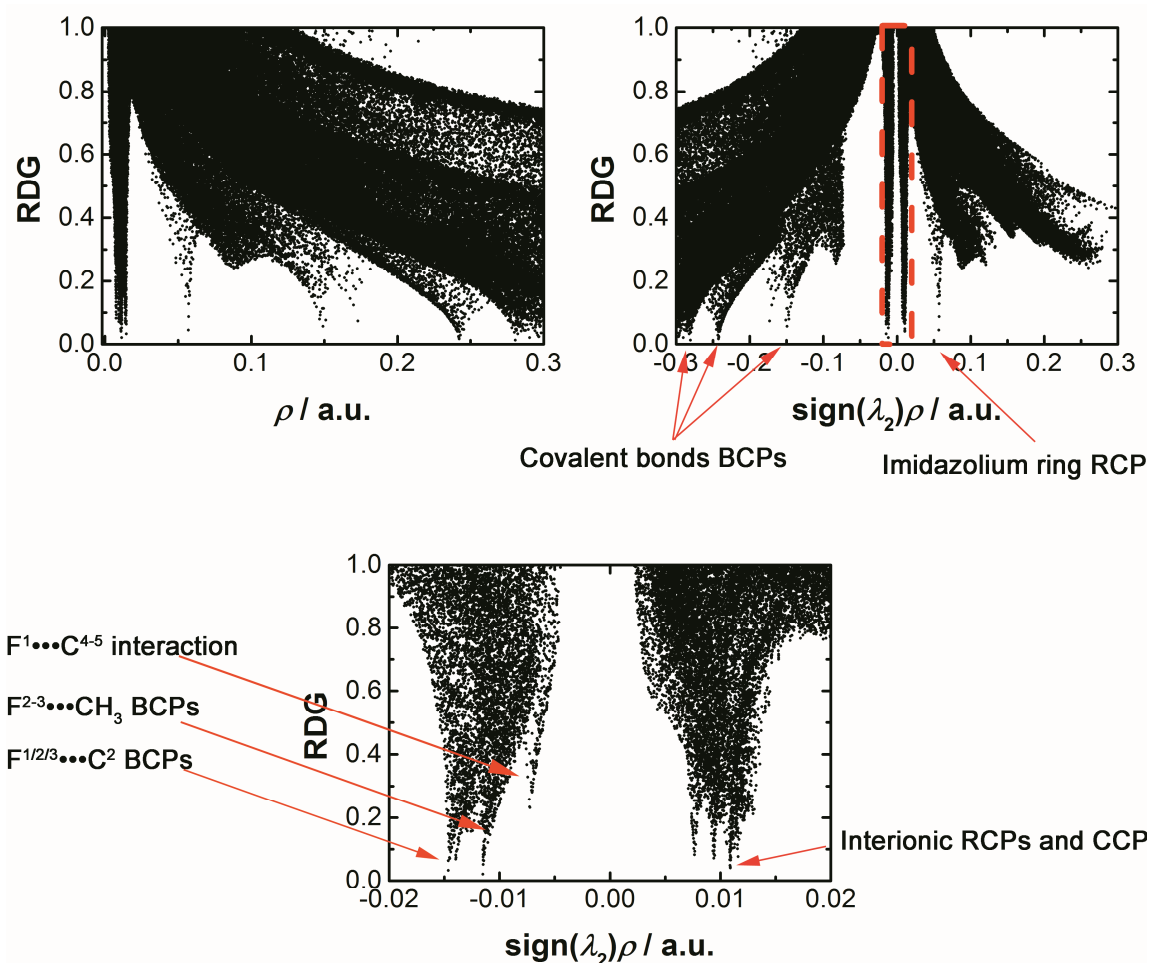


Figure 2.8. Reduced density gradient as a function of the electron density in MmimBF₄ ion pair structure, which was obtained at the MP2/6-311++g(d,p) level of theory (*top left panel*). Reduced density gradient of the same system as a function of the electron density multiplied by the sign of the second eigenvalue of the electron density Hessian (*top right panel*) – NCI plot. Enlarged portion of the NCI plot marked in red, which corresponds to the region of weak noncovalent interactions, is shown in the *bottom panel*.

The NCI isosurfaces for the model MmimBF₄ ion pair are shown in Figure 2.9 along with the noncovalent BCPs, RCPs and the CCP revealed by the QTAIM analysis. One can see an illustrated connection between the results of QTAIM and NCI analyses. The BCPs are located in the center of blueish regions of the NCI isosurfaces, the RCPs and CCP in the region between the counterions correspond to green-yellow parts of the surfaces (weak van der Waals interactions). The imidazolium ring RCP is in between the two distinctly red colored NCI region

which is indicative of destabilizing crowding of the electron density due to the ring closure.

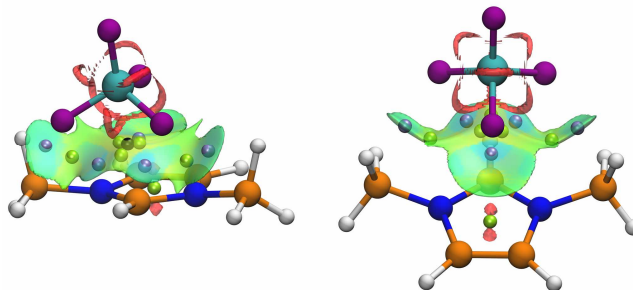


Figure 2.9. NCI isosurfaces for the MmimBF₄ ion pair structure, which was obtained at the MP2/6-311++g(d,p) level of theory. The reduced density gradient cut-off value is 0.6. The $\text{sign}(\lambda_2)\rho$ value is colormapped onto the isosurfaces in the region from -0.03 a.u. to $+0.03$ a.u. in the blue-green-red palette. CPs revealed by the QTAIM analysis are shown for comparison: BCPs as light blue spheres, RCPs as green spheres, and CCP is shown in black. Color coding of the elements: white – H, orange – C, blue – N, purple – F, cyan – B. The two images represent different points of view.

The only blueish-green part of the NCI isosurface in the space between the counter ions, which does not contain a BCP, is the one between the F¹ atom and the C⁴⁻⁵ site. This corresponds to the feature noted in the NCI plot (Figure 2.8) as a spike at low negative $\text{sign}(\lambda_2)\rho$ values that does not reach zero RDG values.

The red traces around the B-F bonds in the anion are due to steric clashes between the electron shells of the electron-rich fluorine atoms.

From this brief analysis of the electron density distribution in the model ion pair MmimBF₄, it is apparent that due to the multiatomic nature of the counterions a broad and delocalized surface of weak noncovalent interactions is established in the interionic space. Their relative strength between selected fragments can be estimated via the NCI surfaces and plots. The results are not only compatible with the QTAIM analysis of CPs, but can also reveal stabilizing interactions which cannot be captured within the QTAIM approach.

In order to assess the influence of the level of theory on the results of NCI analysis, as it was done for QTAIM in the previous section, the NCI plots for the

model ion pair obtained with different methods and the 6-311++g(d,p) basis set are compared in Figure 2.10.

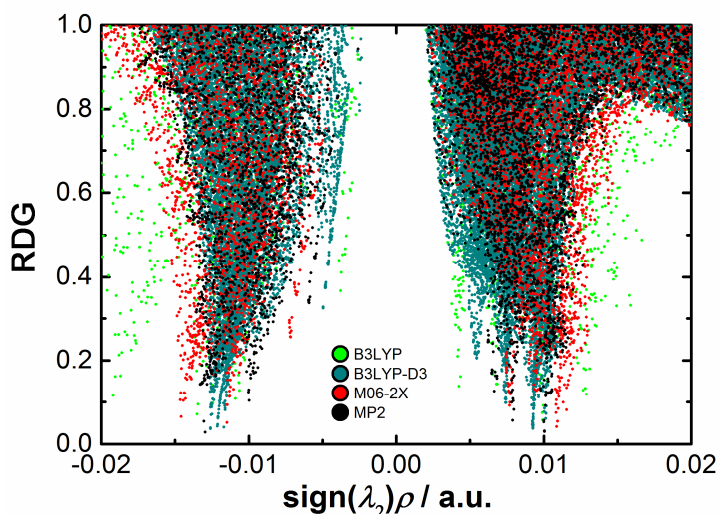


Figure 2.10. NCI plot for the MmimBF₄ ion pair structures which were obtained with different methods coupled with the 6-311++g(d,p) basis set.

Similarly to structural and QTAIM analyses, B3LYP is an outlier due to too poor geometry. M06-2X, which was selected as the working functional for the present study, slightly overestimates the electron densities in the region of bonded interactions, but performs well in the region of weak repulsive and van der Waals interactions, when referenced to MP2.

All the NCI calculations were performed with the MultiWFN software⁷⁴ utilizing a uniform spatial grid with a step of 0.1 a.u. In order to focus on the weak noncovalent interactions, only the regions of $\rho < 0.05$ a.u. were analyzed. All the NCI isosurfaces were plotted with VMD.⁹¹

2.5. References for Chapter 2

- (1) Seddon, K. R.; Stark, A.; Torres, M.-J., Influence of Chloride, Water, and Organic Solvents on the Physical Properties of Ionic Liquids. *Pure Appl. Chem.* **2000**, *72*, 2275-2287.
- (2) Umecky, T.; Kanakubo, M.; Ikushima, Y., Self-Diffusion Coefficients of 1-Butyl-3-Methylimidazolium Hexafluorophosphate with Pulsed-Field Gradient Spin-Echo NMR Technique. *Fluid Phase Equilib.* **2005**, *228-229*, 329-333.
- (3) Umecky, T.; Takamuku, T.; Matsumoto, T.; Kawai, E.; Takagi, M.; Funazukuri, T., Effects of Dissolved Water on Li⁺ Solvation in 1-Ethyl-3-methylimidazolium

Bis(trifluoromethanesulfonyl)amide Ionic Liquid Studied by NMR. *J. Phys. Chem. B* **2013**, *117*, 16219-16226.

(4) Stoppa, A.; Hunger, J.; Buchner, R., Conductivities of binary mixtures of ionic liquids with polar solvents. *J. Chem. Eng. Data*. **2009**, *54*, 472-479.

(5) Seoane, R. G.; Corderí, S.; Gómez, E.; Calvar, N.; González, E. J.; Macedo, E. A.; Domínguez, Á., Temperature Dependence and Structural Influence on the Thermophysical Properties of Eleven Commercial Ionic Liquids. *Ind. Eng. Chem. Res.* **2012**, *51*, 2492-2504.

(6) Vraneš, M.; Zec, N.; Tot, A.; Papović, S.; Dožić, S.; Gadžurić, S., Density, electrical conductivity, viscosity and excess properties of 1-butyl-3-methylimidazolium bis(trifluoromethylsulfonyl)imide + propylene carbonate binary mixtures. *J. Chem. Thermodyn.* **2014**, *68*, 98-108.

(7) Jacquemin, J.; Husson, P.; Padua, A. A. H.; Majer, V., Density and viscosity of several pure and water-saturated ionic liquids. *Green Chem.* **2006**, *8*, 172-180.

(8) Huddleston, J. G.; Visser, A. E.; Reichert, W. M.; Willauer, H. D.; Broker, G. A.; Rogers, R. D., Characterization and comparison of hydrophilic and hydrophobic room temperature ionic liquids incorporating the imidazolium cation. *Green Chem.* **2001**, *3*, 156-164.

(9) Baker, S. N.; Baker, G. A.; Kane, M. A.; Bright, F. V., The Cybotactic Region Surrounding Fluorescent Probes Dissolved in 1-Butyl-3-methylimidazolium Hexafluorophosphate: Effects of Temperature and Added Carbon Dioxide. *J. Phys. Chem. B* **2001**, *105*, 9663-9668.

(10) Kitaoka, S.; Nobuoka, K.; Ishikawa, Y., Ionic liquids for tetraarylporphyrin preparation. *Tetrahedron* **2005**, *61*, 7678-7685.

(11) Ge, M.-L.; Zhao, R.-S.; Yi, Y.-F.; Zhang, Q.; Wang, L.-S., Densities and Viscosities of 1-Butyl-3-methylimidazolium Trifluoromethanesulfonate + H₂O Binary Mixtures at T = (303.15 to 343.15) K. *J. Chem. Eng. Data*. **2008**, *53*, 2408-2411.

(12) Weingärtner, H., The Static Dielectric Constant of Ionic Liquids. *Z. Phys. Chem.* **2006**, *220*, 1395-1405.

(13) Tokuda, H.; Hayamizu, K.; Ishii, K.; Susan, M. A. B. H.; Watanabe, M., Physicochemical Properties and Structures of Room Temperature Ionic Liquids. 1. Variation of Anionic Species. *J. Phys. Chem. B* **2004**, *108*, 16593-16600.

(14) Izutsu, K. *Electrochemistry in Nonaqueous Solutions*; John Wiley & Sons: Weinheim, 2010; 432 p.

(15) Reichardt, C.; Welton, T. *Solvents and Solvent Effects in Organic Chemistry*; Fourth, Updated and Enlarged Edition ed.; Wiley-VCH Verlag GmbH & Co. KGaA: Weinheim, 2011; 718 p.

(16) Wu, J.; Lan, Z.; Lin, J.; Huang, M.; Hao, S.; Fang, L., Influence of solvent on the poly (acrylic acid)-oligo-(ethylene glycol) polymer gel electrolyte and the performance of quasi-solid-state dye-sensitized solar cells. *Electrochim. Acta* **2007**, *52*, 7128-7135.

(17) Zafarani-Moattar, M. T.; Majdan-Cegincara, R., Viscosity, density, speed of sound, and refractive index of binary mixtures of organic solvent + ionic liquid, 1-butyl-3-methylimidazolium hexafluorophosphate at 298.15 K. *J. Chem. Eng. Data*. **2007**, *52*, 2359-2364.

(18) Awwad, A. M.; Salman, M. A.; Hassan, F. A., Liquid-liquid equilibria for the ternary systems .gamma.-butyrolactone-n-heptane-benzene, .gamma.-butyrolactone-n-heptane-toluene, and .gamma.-butyrolactone-n-heptane-p-xylene. *J. Chem. Eng. Data*. **1988**, *33*, 263-265.

(19) Barthel, J.; Neueder, R.; Roch, H., Density, Relative Permittivity, and Viscosity of Propylene Carbonate + Dimethoxyethane Mixtures from 25 °C to 125 °C. *J. Chem. Eng. Data*. **2000**, *45*, 1007-1011.

(20) Aparicio, S.; Alcalde, R., Characterization of two lactones in liquid phase: an experimental and computational approach. *Phys. Chem. Chem. Phys.* **2009**, *11*, 6455-6467.

- (21) Barthel, J.; Bachhuber, K.; Buchner, R.; Gill, J. B.; Kleebauer, M., Dielectric spectra of some common solvents in the microwave region. Dipolar aprotic solvents and amides. *Chem. Phys. Lett.* **1990**, *167*, 62-66.
- (22) Mialkowski, C.; Chagnes, A.; Carré, B.; Lemordant, D.; Willmann, P., Excess thermodynamic properties of binary liquid mixtures containing dimethylcarbonate and γ -butyrolactone. *J. Chem. Thermodyn.* **2002**, *34*, 1847-1856.
- (23) Fornefeld-Schwarz, U. M.; Svejda, P., Refractive Indices and Relative Permittivities of Liquid Mixtures of γ -Butyrolactone, γ -Valerolactone, δ -Valerolactone, or ϵ -Caprolactone + Benzene, + Toluene, or + Ethylbenzene at 293.15 K and 313.15 K and Atmospheric Pressure. *J. Chem. Eng. Data.* **1999**, *44*, 597-604.
- (24) Yangzhong, L. NMR temperature calibration. http://staff.ustc.edu.cn/~liuyz/methods/NMR_VT_calibration.htm (accessed Jan 30, 2014).
- (25) Wu, D. H.; Chen, A. D.; Johnson, C. S., An Improved Diffusion-Ordered Spectroscopy Experiment Incorporating Bipolar-Gradient Pulses. *J. Magn. Reson., Ser. A* **1995**, *115*, 260-264.
- (26) Esturau, N.; Sánchez-Ferrando, F.; Gavin, J. A.; Roumestand, C.; Delsuc, M.-A.; Parella, T., The Use of Sample Rotation for Minimizing Convection Effects in Self-Diffusion NMR Measurements. *J. Magn. Reson.* **2001**, *153*, 48-55.
- (27) Augé, S.; Amblard-Blondel, B.; Delsuc, M.-A., Investigation of the Diffusion Measurement Using PFG and Test of Robustness against Experimental Conditions and Parameters. *J. Chim. Phys.* **1999**, *96*, 1559-1565.
- (28) Annat, G.; MacFarlane, D. R.; Forsyth, M., Transport Properties in Ionic Liquids and Ionic Liquid Mixtures: The Challenges of NMR Pulsed Field Gradient Diffusion Measurements. *J. Phys. Chem. B* **2007**, *111*, 9018-9024.
- (29) Longworth, L. G., The Mutual Diffusion of Light and Heavy Water. *J. Phys. Chem.* **1960**, *64*, 1914-1917.
- (30) Tanner, J. E.; Stejskal, E. O., Restricted Self-Diffusion of Protons in Colloidal Systems by the Pulsed-Gradient, Spin-Echo Method. *J. Chem. Phys.* **1968**, *49*, 1768-1777.
- (31) Liang, M.; Zhang, X.-X.; Kaintz, A.; Ernsting, N. P.; Maroncelli, M., Solvation Dynamics in a Prototypical Ionic Liquid + Dipolar Aprotic Liquid Mixture: 1-Butyl-3-methylimidazolium Tetrafluoroborate + Acetonitrile. *J. Phys. Chem. B* **2014**, *118*, 1340-1352.
- (32) Hurle, R. L.; Woolf, L. A., Self-diffusion in liquid acetonitrile under pressure. *J. Chem. Soc., Faraday Trans. 1* **1982**, *78*, 2233-2238.
- (33) Holz, M.; Mao, X.-a.; Seiferling, D.; Sacco, A., Experimental study of dynamic isotope effects in molecular liquids: Detection of translation-rotation coupling. *J. Chem. Phys.* **1996**, *104*, 669-679.
- (34) Hawlicka, E.; Grabowski, R., Solvation of Ions in Acetonitrile-Methanol Solutions of Sodium Iodide. *Ber. Bunsenges. Phys. Chem.* **1990**, *94*, 486-489.
- (35) Aihara, Y.; Sugimoto, K.; Price, W. S.; Hayamizu, K., Ionic Conduction and Self-Diffusion Near Infinitesimal Concentration in Lithium Salt-Organic Solvent Electrolytes. *J. Chem. Phys.* **2000**, *113*, 1981-1991.
- (36) Hayamizu, K.; Aihara, Y.; Arai, S.; Garcia, Pulse-Gradient Spin-Echo ^1H , ^7Li , and ^{19}F NMR Diffusion and Ionic Conductivity Measurements of 14 Organic Electrolytes Containing $\text{LiN}(\text{SO}_2\text{CF}_3)_2$. *J. Phys. Chem. B* **1999**, *103*, 519-524.
- (37) Hayamizu, K.; Aihara, Y.; Arai, S.; Price, W. S., Diffusion, conductivity and DSC studies of a polymer gel electrolyte composed of cross-linked PEO, γ -butyrolactone and LiBF_4 . *Solid State Ionics* **1998**, *107*, 1-12.
- (38) Takeuchi, M.; Kameda, Y.; Umabayashi, Y.; Ogawa, S.; Sonoda, T.; Ishiguro, S.-i.; Fujita, M.; Sano, M., Ion-ion interactions of LiPF_6 and LiBF_4 in propylene carbonate solutions. *J. Mol. Liq.* **2009**, *148*, 99-108.

- (39) Kondo, K.; Sano, M.; Hiwara, A.; Omi, T.; Fujita, M.; Kuwae, A.; Iida, M.; Mogi, K.; Yokoyama, H., Conductivity and Solvation of Li⁺ Ions of LiPF₆ in Propylene Carbonate Solutions. *J. Phys. Chem. B* **2000**, *104*, 5040-5044.
- (40) Tsunekawa, H.; Narumi, A.; Sano, M.; Hiwara, A.; Fujita, M.; Yokoyama, H., Solvation and Ion Association Studies of LiBF₄-Propylenecarbonate and LiBF₄-Propylenecarbonate-Trimethyl Phosphate Solutions. *J. Phys. Chem. B* **2003**, *107*, 10962-10966.
- (41) Nama, D.; Kumar, P.; Pregosin, P.; Geldbach, T.; Dyson, P., ¹H, ¹⁹F-HOESY and PGSE diffusion studies on ionic liquids: The effect of co-solvent on structure. *Inorg. Chim. Acta* **2006**, *359*, 1907-1911.
- (42) Wu, T.-Y.; Wang, H.-C.; Su, S.-G.; Gung, S.-T.; Lin, M.-W.; Lin, C.-B., Aggregation Influence of Polyethyleneglycol Organic Solvents with Ionic Liquids BMIMBF₄ and BMIMPF₆. *Journal of the Chinese Chemical Society* **2010**, *57*, 44-55.
- (43) Frisch, M. J.; Trucks, G. W.; Schlegel, H. B.; Scuseria, G. E.; Robb, M. A.; Cheeseman, J. R.; Scalmani, G.; Barone, V.; Mennucci, B.; Petersson, G. A.; Nakatsuji, H.; Caricato, M.; Li, X.; Hratchian, H. P.; Izmaylov, A. F.; Bloino, J.; Zheng, G.; Sonnenberg, J. L.; Hada, M.; Ehara, M.; Toyota, K.; Fukuda, R.; Hasegawa, J.; Ishida, M.; Nakajima, T.; Honda, Y.; Kitao, O.; Nakai, H.; Vreven, T.; Montgomery, J. A. J.; Peralta, J. E.; Ogliaro, F.; Bearpark, M.; Heyd, J. J.; Brothers, E.; Kudin, K. N.; Staroverov, V. N.; Keith, T.; Kobayashi, R.; Normand, J.; Raghavachari, K.; Rendell, A.; Burant, J. C.; Iyengar, S. S.; Tomasi, J.; Cossi, M.; Rega, N.; Millam, J. M.; Klene, M.; Knox, J. E.; Cross, J. B.; Bakken, V.; Adamo, C.; Jaramillo, J.; Gomperts, R.; Stratmann, R. E.; Yazyev, O.; Austin, A. J.; Cammi, R.; Pomelli, C.; Ochterski, J. W.; Martin, R. L.; Morokuma, K.; Zakrzewski, V. G.; Voth, G. A.; Salvador, P.; Dannenberg, J. J.; Dapprich, S.; Daniels, A. D.; Farkas, O.; Foresman, J. B.; Ortiz, J. V.; Cioslowski, J.; Fox, D. J. *Gaussian 09, Revision D.01*, Gaussian, Inc.: Wallingford CT, 2013.
- (44) Matthews, R. P.; Welton, T.; Hunt, P. A., Competitive pi interactions and hydrogen bonding within imidazolium ionic liquids. *Phys. Chem. Chem. Phys.* **2014**, *16*, 3238-3253.
- (45) Tomasi, J.; Mennucci, B.; Cammi, R., Quantum Mechanical Continuum Solvation Models. *Chem. Rev.* **2005**, *105*, 2999-3094.
- (46) Izgorodina, E. I.; MacFarlane, D. R., Nature of Hydrogen Bonding in Charged Hydrogen-Bonded Complexes and Imidazolium-Based Ionic Liquids. *J. Phys. Chem. B* **2011**, *115*, 14659-14667.
- (47) Zahn, S.; Uhlig, F.; Thar, J.; Spickermann, C.; Kirchner, B., Intermolecular Forces in an Ionic Liquid ([Mmim][Cl]) versus Those in a Typical Salt (NaCl). *Angew. Chem., Int. Ed.* **2008**, *47*, 3639-3641.
- (48) Izgorodina, E. I.; Rigby, J.; MacFarlane, D. R., Large-scale ab initio calculations of archetypical ionic liquids. *Chem. Commun.* **2012**, *48*, 1493-1495.
- (49) Izgorodina, E. I.; Golze, D.; Maganti, R.; Armel, V.; Taige, M.; Schubert, T. J. S.; MacFarlane, D. R., Importance of dispersion forces for prediction of thermodynamic and transport properties of some common ionic liquids. *Phys. Chem. Chem. Phys.* **2013**.
- (50) Kempter, V.; Kirchner, B., The role of hydrogen atoms in interactions involving imidazolium-based ionic liquids. *J. Mol. Struct.* **2010**, *972*, 22-34.
- (51) Zahn, S.; MacFarlane, D. R.; Izgorodina, E. I., Assessment of Kohn-Sham density functional theory and Moller-Plesset perturbation theory for ionic liquids. *Phys. Chem. Chem. Phys.* **2013**, *15*, 13664-13675.
- (52) Fong-Padrón, C.; Cabaleiro-Lago, E. M.; Rodríguez-Otero, J., Water interaction with ion pairs from ionic liquids. Computational study and performance assessment of several common functionals. *Chem. Phys. Lett.* **2014**, *593*, 181-188.

- (53) Zahn, S.; Brehm, M.; Brüssel, M.; Hollóczki, O.; Kohagen, M.; Lehmann, S.; Malberg, F.; Pensado, A. S.; Schöppke, M.; Weber, H.; Kirchner, B., Understanding ionic liquids from theoretical methods. *J. Mol. Liq.* **2014**, *192*, 71-76.
- (54) Kirchner, B., Ionic liquids from theoretical investigations. In *Ionic Liquids*, Kirchner, B., Ed. Springer-Verlag: Berlin/Heidelberg, 2010; Vol. 290, pp 213-262.
- (55) Chen, S.; Vijayaraghavan, R.; MacFarlane, D. R.; Izgorodina, E. I., Ab Initio Prediction of Proton NMR Chemical Shifts in Imidazolium Ionic Liquids. *J. Phys. Chem. B* **2013**, *117*, 3186-3197.
- (56) Goerigk, L.; Grimme, S., A thorough benchmark of density functional methods for general main group thermochemistry, kinetics, and noncovalent interactions. *Phys. Chem. Chem. Phys.* **2011**, *13*, 6670-6688.
- (57) Goerigk, L.; Kruse, H.; Grimme, S., Benchmarking Density Functional Methods against the S66 and S66x8 Datasets for Non-Covalent Interactions. *ChemPhysChem* **2011**, *12*, 3421-3433.
- (58) Li, A.; Muddana, H. S.; Gilson, M. K., Quantum Mechanical Calculation of Noncovalent Interactions: A Large-Scale Evaluation of PMx, DFT, and SAPT Approaches. *J. Chem. Theory Comput.* **2014**, *10*, 1563-1575.
- (59) Grimme, S., Density functional theory with London dispersion corrections. *Wiley Interdisciplinary Reviews: Computational Molecular Science* **2011**, *1*, 211-228.
- (60) Peverati, R.; Truhlar, D. G., Quest for a universal density functional: the accuracy of density functionals across a broad spectrum of databases in chemistry and physics. *Philosophical Transactions of the Royal Society A: Mathematical, Physical and Engineering Sciences* **2014**, 372.
- (61) Hohenstein, E. G.; Chill, S. T.; Sherrill, C. D., Assessment of the Performance of the M05-2X and M06-2X Exchange-Correlation Functionals for Noncovalent Interactions in Biomolecules. *J. Chem. Theory Comput.* **2008**, *4*, 1996-2000.
- (62) Addicoat, M. A.; Fukuoka, S.; Page, A. J.; Irle, S., Stochastic structure determination for conformationally flexible heterogenous molecular clusters: Application to ionic liquids. *J. Comput. Chem.* **2013**, *34*, 2591-2600.
- (63) Hunt, P. A.; Kirchner, B.; Welton, T., Characterising the electronic structure of ionic liquids: an examination of the 1-butyl-3-methylimidazolium chloride ion pair. *Chem. – Eur. J.* **2006**, *12*, 6762-6775.
- (64) Plumley, J. A.; Dannenberg, J. J., A comparison of the behavior of functional/basis set combinations for hydrogen-bonding in the water dimer with emphasis on basis set superposition error. *J. Comput. Chem.* **2011**, *32*, 1519-1527.
- (65) Tsuzuki, S.; Tokuda, H.; Hayamizu, K.; Watanabe, M., Magnitude and Directionality of Interaction in Ion Pairs of Ionic Liquids: Relationship with Ionic Conductivity. *J. Phys. Chem. B* **2005**, *109*, 16474-16481.
- (66) Tsuzuki, S.; Tokuda, H.; Mikami, M., Theoretical analysis of the hydrogen bond of imidazolium C2-H with anions. *Phys. Chem. Chem. Phys.* **2007**, *9*, 4780.
- (67) Bader, R. F. W., A quantum theory of molecular structure and its applications. *Chem. Rev.* **1991**, *91*, 893-928.
- (68) Bader, R. F. W., The Quantum Mechanical Basis of Conceptual Chemistry. *Monatsh. Chem.* **2005**, *136*, 819-854.
- (69) Bader, R. F. W., From Schrodinger to atoms in molecules. *Pure Appl. Chem.* **1988**, *60*, 145-155.
- (70) Matta, C. F.; Bader, R. F. W., An Experimentalist's Reply to "What Is an Atom in a Molecule?". *J. Phys. Chem. A* **2006**, *110*, 6365-6371.

- (71) Grabowski, S. J., What Is the Covalency of Hydrogen Bonding? *Chem. Rev.* **2011**, *111*, 2597-2625.
- (72) Koch, U.; Popelier, P. L. A., Characterization of C-H-O hydrogen bonds on the basis of the charge density. *J. Phys. Chem.* **1995**, *99*, 9747-9754.
- (73) Rigby, J.; Izgorodina, E. I., Assessment of atomic partial charge schemes for polarisation and charge transfer effects in ionic liquids. *Phys. Chem. Chem. Phys.* **2013**, *15*, 1632-1646.
- (74) Lu, T.; Chen, F., Multiwfn: A multifunctional wavefunction analyzer. *J. Comput. Chem.* **2012**, *33*, 580-592.
- (75) Matthews, R. P.; Ashworth, C.; Tom, W.; Patricia, A. H., The impact of anion electronic structure: similarities and differences in imidazolium based ionic liquids. *J. Phys.: Condens. Matter* **2014**, *26*, 284112.
- (76) Grabowski, S. J., Properties of a Ring Critical Point as Measures of Intramolecular H-Bond Strength. *Monatshefte für Chemie / Chemical Monthly* **2002**, *133*, 1373-1380.
- (77) Grabowski, S. J.; Małecka, M., Intramolecular H-Bonds: DFT and QTAIM Studies on 3-(Aminomethylene)pyran-2,4-dione and Its Derivatives. *J. Phys. Chem. A* **2006**, *110*, 11847-11854.
- (78) Rybarczyk-Pirek, A. J.; Grabowski, S. J.; Małecka, M.; Nawrot-Modranka, J., Crystal and Molecular Structures of New Chromone Derivatives as Empirical Evidence of Intramolecular Proton Transfer Reaction; Ab Initio Studies on Intramolecular H-Bonds in Enaminones. *J. Phys. Chem. A* **2002**, *106*, 11956-11962.
- (79) Garau, C.; Frontera, A.; Quiñero, D.; Ballester, P.; Costa, A.; Deyà, P. M., A Topological Analysis of the Electron Density in Anion- π Interactions. *ChemPhysChem* **2003**, *4*, 1344-1348.
- (80) Estarellas, C.; Frontera, A.; Quiñero, D.; Deyà, P. M., Unexpected Nonadditivity Effects in Anion- π Complexes. *J. Phys. Chem. A* **2011**, *115*, 7849-7857.
- (81) Mohajeri, A.; Karimi, E., AIM and NBO analyses of cation- π interaction. *J. Mol. Struct.: THEOCHEM* **2006**, *774*, 71-76.
- (82) Rao, J. S.; Zipse, H.; Sastry, G. N., Explicit Solvent Effect on Cation- π Interactions: A First Principle Investigation. *J. Phys. Chem. B* **2009**, *113*, 7225-7236.
- (83) Vijay, D.; Sastry, G. N., The cooperativity of cation- π and π - π interactions. *Chem. Phys. Lett.* **2010**, *485*, 235-242.
- (84) Zhikol, O. A.; Shishkin, O. V.; Lyssenko, K. A.; Leszczynski, J., Electron density distribution in stacked benzene dimers: A new approach towards the estimation of stacking interaction energies. *J. Chem. Phys.* **2005**, *122*, -.
- (85) Lane, J. R.; Contreras-García, J.; Piquemal, J.-P.; Miller, B. J.; Kjaergaard, H. G., Are Bond Critical Points Really Critical for Hydrogen Bonding? *J. Chem. Theory Comput.* **2013**, *9*, 3263-3266.
- (86) Contreras-García, J.; Calatayud, M.; Piquemal, J.-P.; Recio, J. M., Ionic interactions: Comparative topological approach. *Comput. Theor. Chem.* **2012**, *998*, 193-201.
- (87) Contreras-García, J.; Johnson, E. R.; Keinan, S.; Chaudret, R.; Piquemal, J.-P.; Beratan, D. N.; Yang, W., NCIPLOT: A Program for Plotting Noncovalent Interaction Regions. *J. Chem. Theory Comput.* **2011**, *7*, 625-632.
- (88) Johnson, E. R.; Keinan, S.; Mori-Sánchez, P.; Contreras-García, J.; Cohen, A. J.; Yang, W., Revealing Noncovalent Interactions. *J. Am. Chem. Soc.* **2010**, *132*, 6498-6506.
- (89) Otero-de-la-Roza, A.; Johnson, E. R.; Contreras-García, J., Revealing non-covalent interactions in solids: NCI plots revisited. *Phys. Chem. Chem. Phys.* **2012**, *14*, 12165-12172.
- (90) Chaudret, R.; de Courcy, B.; Contreras-García, J.; Gloaguen, E.; Zehnacker-Rentien, A.; Mons, M.; Piquemal, J. P., Unraveling non-covalent interactions within flexible biomolecules:

from electron density topology to gas phase spectroscopy. *Phys. Chem. Chem. Phys.* **2014**, *16*, 9876-9891.

(91) Humphrey, W.; Dalke, A.; Schulten, K., VMD: Visual molecular dynamics. *Journal of Molecular Graphics* **1996**, *14*, 33-38.

Chapter 3. Quantum Chemical Interpretation of the Interactions in IL-Molecular Solvent Mixtures

In order to establish the main peculiarities of the intermolecular interactions in IL-molecular solvent mixtures, quantum chemical calculations have been performed for a set of representative model molecular clusters. These calculations were coupled with the advanced methods of analysis of the electron density distribution aimed at deciphering of weak noncovalent interactions in molecular systems, namely the quantum theory of atoms in molecules (QTAIM) and the noncovalent interactions (NCI) approaches.

Model systems were constructed in order to simulate different environments at the lowest computational cost. IL ion pairs and ion pair dimers were considered as model structures for the neat ILs and large aggregates. Complexes between the solvent molecules and the ion pairs or individual cations were studied with respect to specific solvation effects. Implicit solvation effects were modeled within the PCM approach.

Weak electrostatic hydrogen bonding has been found in the structure of ILs between the anions and the imidazolium ring hydrogen atoms of cations. Weaker but still appreciable hydrogen bonding has been also noted for hydrogen atoms of the adjacent to the imidazolium ring alkyl groups. The relative strength of the hydrogen bonding is higher for BmimTfO and BmimBF₄ ILs than for BmimPF₆ and BmimTFSI. BmimTfO and BmimTFSI, in turn, reveal higher sensitivity of hydrogen bonding at the hydrogen atom at position 2 of the imidazolium ring compared to those at positions 4-5.

Taking into account the solvent effect, the native structure of ILs is perturbed and the new hydrogen bonding interactions are established. The strength of hydrogen bonding between cation and different solvent molecules follows the order AN < PC < γ -BL. BmimPF₆ and BmimTFSI ILs are more prone to the perturbing effect of the solvent.

3.1. Introduction

Quantum chemical calculations have been routinely used to study various properties of the IL-based systems and to help with the analysis of experimental results, including those obtained from NMR and vibrational spectroscopy.¹⁻² One should always be cautious when trying to connect the results obtained from calculations on model systems of the size of tens of atoms, often performed for the gas phase, to some subtle peculiarities of the macroscopic samples. It is exactly the case of the IL-molecular solvent mixtures. As it was mentioned in Chapter 1, it is only very recently that MD simulations of the IL-based mixtures of relevant size and trajectory length have become feasible. Nevertheless, there is still a severe lack of proper force field models suitable to be applied over the entire concentration range.³ At present, quantum chemical calculations of small model systems are affordable methods for the routine use in order to reveal their electronic properties in details.

In this chapter we study several types of model systems, *e.g.*, IL ion pairs and ion pair dimers to reveal the features that could be characteristic for the neat ILs and large aggregates; ion pair-solvent and ion-solvent complexes to simulate local microenvironments in the mixtures. Given the limited size of these model systems, the results obtained in this approach should be treated rather as a hint to interpret the experimental data than solid evidence.

3.2. IL ion pairs and ion pair dimers

3.2.1 Main structural features of the ion pairs

Ion pairs are often taken as the smallest unit to represent the main features of the neat ILs.^{1,4} Ion pair structures for the studies set of imidazolium ILs obtained from gas-phase calculations are shown in Figure 3.1. Most of the literature studies on quantum-chemical calculations of the imidazolium IL ion pairs containing BF_4^-

and PF_6^- anions suggest that the configuration where the anion sits on top of the $\text{C}^2\text{-H}^2$ fragment is the most stable one.⁵⁻¹⁸ When referencing to ‘above’ or ‘on-top’ of the imidazolium ring plane, it means at the same side as the alkyl chain with respect to the ring. This configuration was found in our optimizations even when other initial structures revealed by some previous investigations^{7,9-11,13,16,19} were employed, *e.g.*, with anion positioned in front of the $\text{C}^2\text{-H}^2$ fragment or at the $\text{C}^5\text{-H}^5\text{-C}^6\text{H}_2$ site in the plane of the imidazolium ring. This can be explained as a result of poor performance of the B3LYP functional that was used in most of the previously cited studies. We also note rather rare usage of triple-zeta basis sets in these investigations which could lead to improper description of the potential energy surface. The on-top of $\text{C}^2\text{-H}^2$ arrangement of the PF_6^- anion with its three fluorine atoms pointing towards the cation was also established by Hardacre *et al.* in neutron scattering studies on RmimPF_6 coupled with MD simulations.²⁰⁻²¹

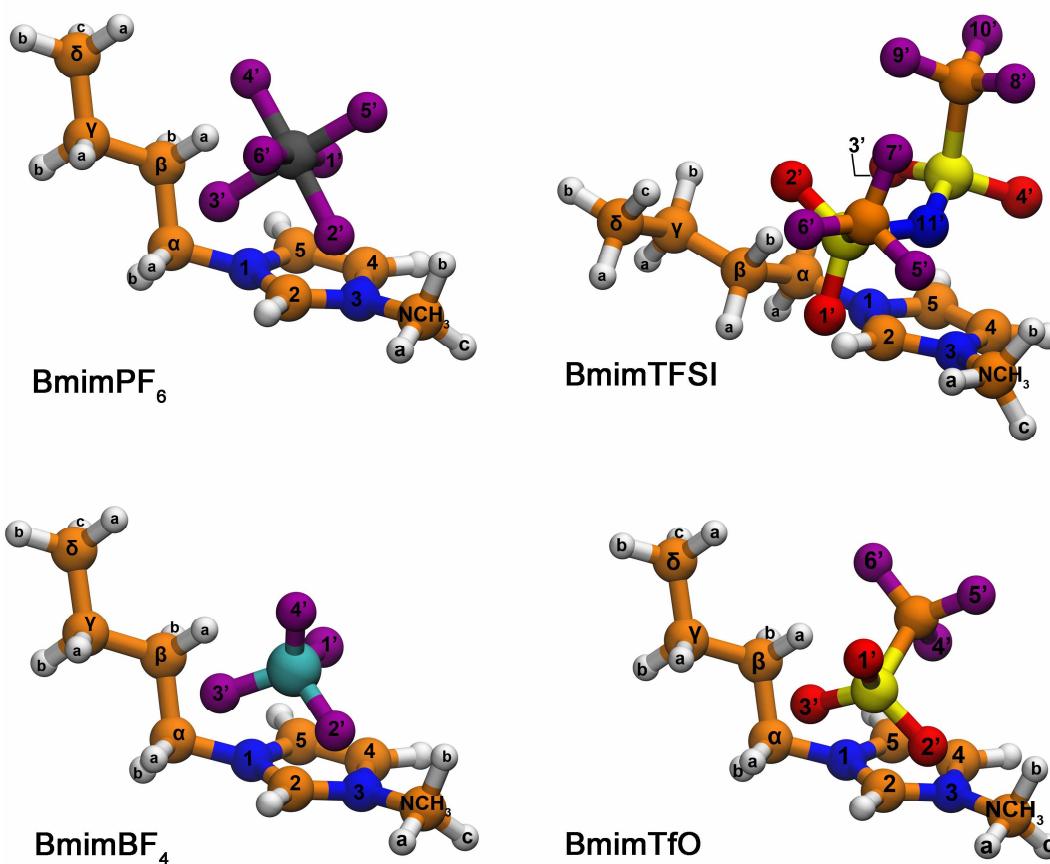


Figure 3.1. Optimized in vacuum at the M06-2X/6-311++g(d,p) level of theory structures of the studied ion pairs. Color coding of the elements: white – H, orange – C, blue – N, purple – F, cyan – B, gray – P, yellow – S.

Calculations on the TFSI⁻ containing imidazolium ILs reveal two kinds of results. B3LYP and Hartree-Fock based studies employing rather moderate basis sets^{10,22-24} predict the anion to be in front of the C²-H² fragment in the plane of the imidazolium ring. In these structures the anion was found in the trans-conformation with respect to its C-S-N-S-C fragment and strong directional hydrogen bonds were observed between the C²-H² hydrogen and anion's nitrogen and/or oxygen atoms.²² On the other hand, more recent studies on EmimTFSI ion pair, employing MP2/aug-cc-pvtz²⁵ and M06/6-311++g(d,p)²⁶ levels of theory, revealed the TFSI⁻ anion to be in the cis-configuration in all the stable low-energy minima and located on top of the C²-H² fragment with one of its SO₂ moieties. This exactly corresponds

to the structure found as the lowest energy minimum for the BmimTFSI ion pair Figure 3.1. A remarkable point in this structure is that due to the bulkiness of the anion the butyl chain is pushed towards the in-plane orientation. Similar feature was also observed for the BmimTFSI ion pair by Hunt *et al.* using B3LYP/6-311++g(d,p) level of theory.¹¹ Such orientation of the anion also agrees with the results of Hardacre *et al.*²⁰ that for the TFSI⁻ anion the position above/below the imidazolium ring is even more favored than for PF₆⁻.

Raman²⁷⁻²⁸ and MD²⁹ studies suggest a comparable population of the cis- and trans-conformations of the TFSI⁻ anion in neat ILs. This contradiction can be resolved if one assumes that the trans-conformations, which are thermodynamically more stable, are more frequently found for ‘free’, or less bound configurations of the anion, while in tightly bound structures, like the ion pairs, the cis-conformation is stabilized by multiple bonding contacts with the counterions.

Theoretical studies on the ion pair structures of imidazolium ILs with TfO⁻ anions are far less ubiquitous.^{10,30-32} Our calculated optimal structure is in accordance with these reports. The strongly negatively charged SO₃ group of the anion is positioned on top of the C²-H² fragment with two oxygen atoms being in the vicinity of C²-H² and of the NCH₃ and C^αH₂ hydrogen atoms. Trifluoromethyl group CF₃ of the anion is located exactly above the imidazolium ring center and the fluorine atoms are in close contact with the hydrogen atoms of the butyl group.

The common property of all the revealed optimal ion pair structures is presented in Figure 3.2. One can easily see that the central atom of the negatively charged group of every anion (B for BF₄⁻, P for PF₆⁻, and S for TfO⁻ and TFSI⁻) is positioned roughly on top of the C²-H² fragment (the most positively charged part of the cation³³) and its electronegative atoms are at hydrogen bonding distance away from the C²-H² hydrogen and allegedly from the alkyl ones adjacent to the imidazolium ring.

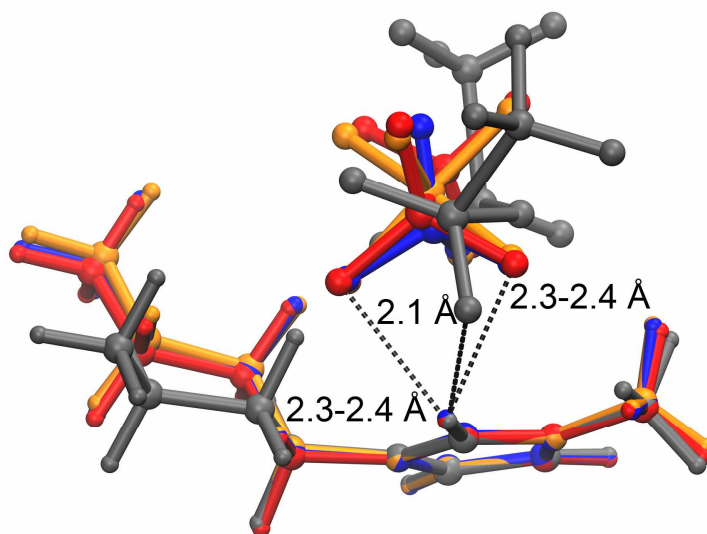


Figure 3.2. Optimized in vacuum structures of the studied ion pairs, superimposed by the imidazolium ring carbon atoms. Red – BmimTfO, blue – BmimBF₄, yellow – BmimPF₆, gray – BmimTFSI. Dashed lines indicate short contacts between the C²H² hydrogen atoms and the nearest electronegative atoms of anion.

The general stability of the ion pairs in vacuum can be estimated with the binding energies which are shown in Figure 3.3. The relatively large values of *ca.* –360 - –380 kJ mol⁻¹ stem from the fact that the dominant interaction in such systems is Coulomb attraction.¹⁰ In the studied set of ILs, absolute values of the ion pair binding energy follow the order BmimPF₆ < BmimTFSI < BmimTfO < BmimBF₄, which is in agreement with the literature results.¹⁰

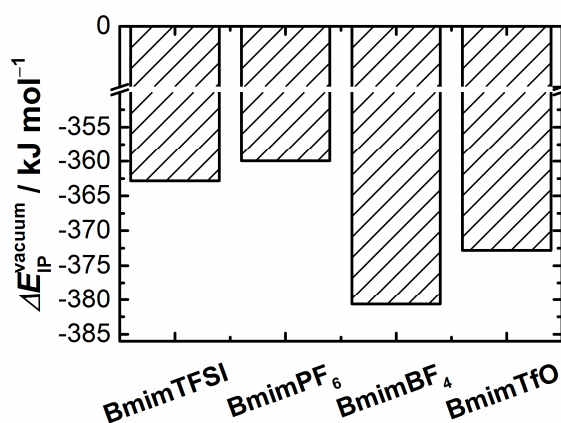


Figure 3.3. Binding energies of the studied ion pairs in vacuum obtained at the M06-2X/6-311++g(d,p) level of theory.

In order to estimate the stability of the revealed configurations with respect to the position of the anion around the imidazolium ring plane and to the rotation of the butyl chain. The dihedral angles which were scanned/monitored are shown in Figure 3.4. We performed relaxed potential energy scans along the selected dihedral angles with a step of ten degrees. A slightly smaller basis set 6-31+g(d) coupled with the M06-2X functional was used in these calculations.

Position of the anion relative to the imidazolium ring plane was characterized via a dihedral angle φ , which is the angle between the vector connecting C² carbon with the central atom of the negatively charged group of anion X and the imidazolium ring plane. Perfect on-top-of-C² arrangement would correspond to the values of φ equal 90 degrees, an inplane arrangement is characterized by zero value of φ , and the configurations where anion is below the imidazolium ring plane are found at negative values of φ .

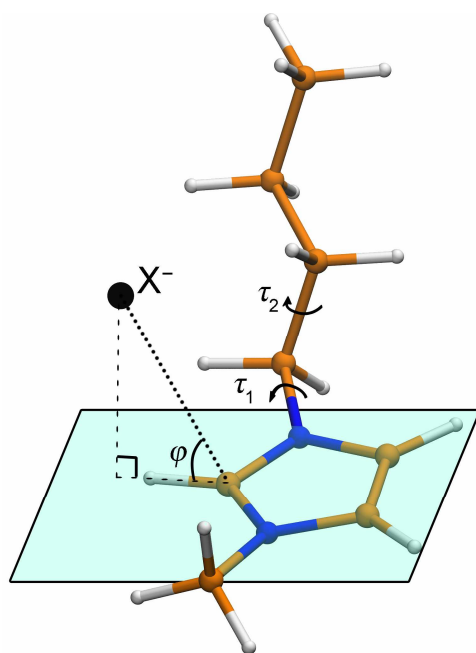


Figure 3.4. Schematic representation of the main dihedral angles defining the geometry of a BmimX ion pair. τ_1 and τ_2 determine the orientation of the butyl chain while the φ dihedral describes the position of anion X^- relative to the imidazolium ring plane. Color coding of the elements: white – H, orange – C, blue – N, black – X.

Such scan along the φ dihedral was performed for BmimBF₄ ion pair and for MmimCl and BmimCl ion pairs. For the chloride containing ion pairs, the in-plane configuration was found to be one of the most stable in many previous computational studies.^{11,13,17,19,33-36} The results of these potential energy scan calculations are shown in Figure 3.5.

It is apparent that, indeed, both MmimCl and BmimCl reveal a minimum at the in-plane configuration in contrast to BmimBF₄ for which it is a maximum. The global maximum for all three ion pairs is the on-top configuration with φ equal *ca.* 80 degrees. We note that the asymmetry of Bmim⁺ cation is reflected in the asymmetry of the potential energy profile, *i.e.*, the on-top minimum structure is more stable than the one below the C²-H² fragment. This effect is more pronounced for BmimBF₄ than for BmimCl, since in the case of chloride anion, it stabilizes the below-the-ring arrangement by forcing the butyl chain to be in the plane of the ring

and maintaining short contacts with the alkyl hydrogen atoms of the butyl chain (see below).

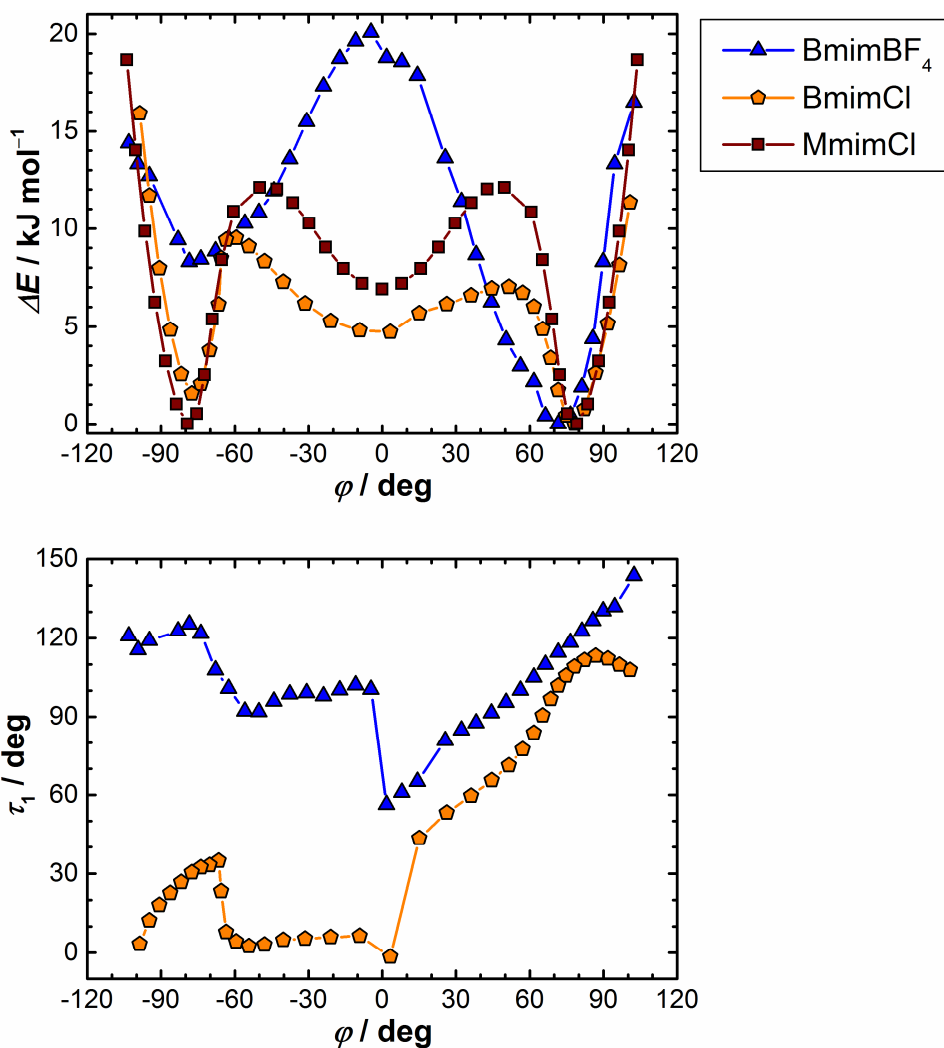


Figure 3.5. The results of relaxed potential energy scan along the ϕ dihedral for BmimBF₄, BmimCl, and MmimCl ion pairs obtained in vacuum at the M06-2X/6-31+g(d) level of theory. Top panel shows the energy variation relative to the lowest energy structures. Bottom panel shows how the τ_1 dihedral changes as the ϕ is varied.

While scanning the ϕ dihedral, we also monitored the τ_1 dihedral angle which describes the position of the butyl chain with respect to the imidazolium ring plane. From the bottom panel in Figure 3.5, one can see that in both cases, when going from the ontop configuration to the in-plane arrangement, anion pulls the butyl chain to lower τ_1 values, *i.e.*, towards the in-plane orientation. After flipping of anion below the imidazolium ring plane, the butyl chain ultimately switches to the

in-plane orientation ($\tau_1 < 0$) in the case of BmimCl, but for BmimBF₄ it stays around its equilibrium out-of-plane position above the imidazolium ring.

This potential energy scan allowed us to claim that the on-top of C²-H² arrangement of a multiatomic anion in the structure of imidazolium IL ion pairs is rather stable and the corresponding structures obtained in our geometry optimizations can be considered as global minima.

The second set of potential energy scan calculations was undertaken in order to find out the influence of the butyl chain rotation on the stability of the ion pair structure. Rotation around the τ_1 dihedral was studied in detail by Hunt and Gould.³⁴ They showed for BmimCl ion pair that the butyl chain strongly prefers to be oriented out of plane of the imidazolium ring regardless of its conformation and the position of anion. However, the range of values for the τ_1 dihedral was found to be rather broad.³⁴ Here we study the rotation along the τ_2 dihedral for the optimal configurations of the ion pairs and of the isolated Bmim⁺ cation (Figure 3.6).

The potential energy profiles, which are shown in the top left panel in Figure 3.6, are similar between the ion pairs and the isolated cation in terms of position of the extrema and the barrier heights. For the isolated cation, gauche-conformation of the butyl chain ($\tau_2 \approx 300$ degrees) corresponds to the global minimum, while in all the ion pairs the trans-conformation ($\tau_2 \approx 180$ degrees) is the most stable. This result is in accordance with the literature.^{34,37-39} Variations of τ_2 do not alter significantly the τ_1 value for the isolated cation and all the ion pairs except for the BmimTFSI (bottom right panel in Figure 3.6). As it was mentioned before, due to the bulkiness of the TFSI⁻ anion, the butyl chain is close to the in-plane orientation, however, rotation about the τ_2 dihedral forces it to deviate significantly from the equilibrium orientation.

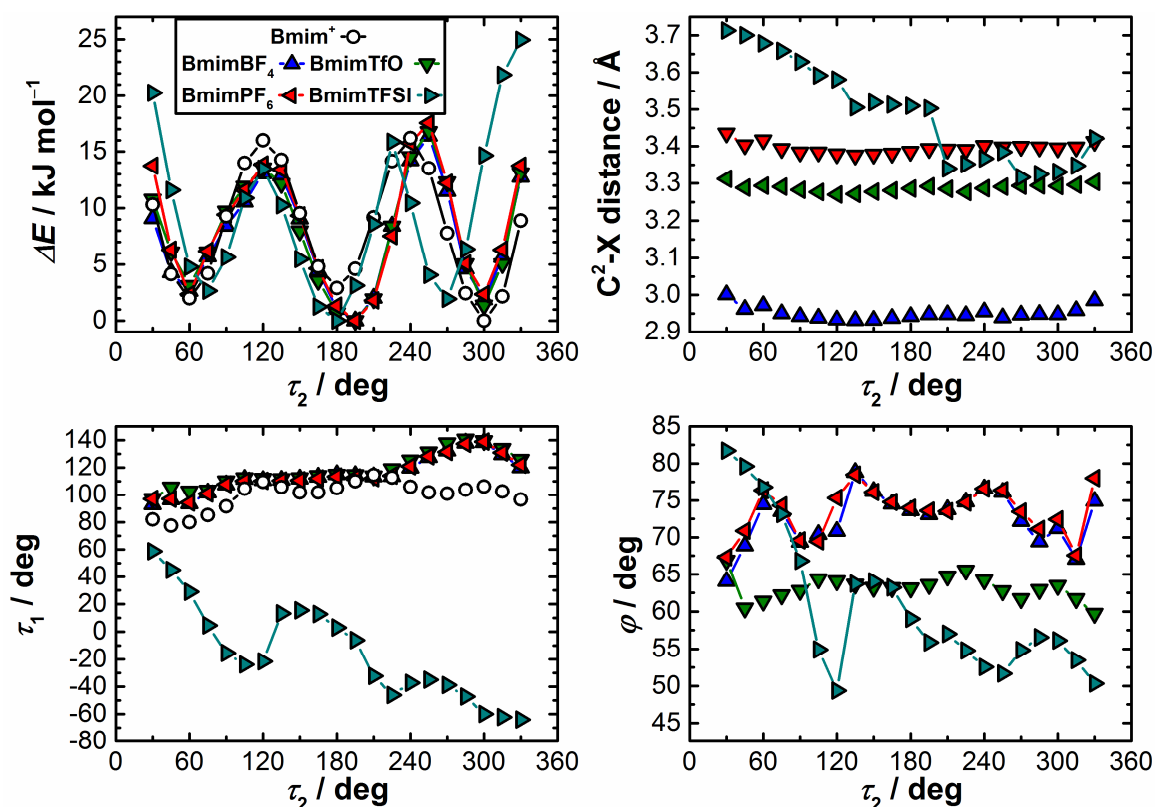


Figure 3.6. The results of relaxed potential energy scan along the τ_2 dihedral for Bmim^+ cation and the studied ion pairs obtained in vacuum at the M06-2X/6-31+g(d) level of theory. Top left panel shows the energy variation relative to the lowest energy structure. The variations of the distance $\text{C}^2\text{-X}$ ($\text{X}=\text{B}$ for BF_4^- , P for PF_6^- , S for TfO^- , and the nearest S for TFSI^-) as a function of the scanned variable are given in the top right panel. Bottom right panel shows how the τ_1 dihedral changes as the τ_2 is varied. Bottom right panel present the ϕ dihedral as a function the scanned variable.

Similar observations can be made for the interionic separation characterized as the distance between the cation C^2 carbon atom and the central atom of the negatively charged group of anion, X (top right panel in Figure 3.6). The variations in the scanned variable do not induce changes in the interionic separation higher than 0.05 \AA for BmimBF_4 , BmimPF_6 and BmimTfO ion pairs. The distance $\text{C}^2\text{-S}$ in the BmimTFSI ion pair can vary by as much as 0.4 \AA .

Relative position of anion with respect to the imidazolium ring plane, in terms of the ϕ dihedral values (bottom right panel in Figure 3.6), follows the same trends as the interionic separation. In BmimBF_4 , BmimPF_6 and BmimTfO anions remain on top of the $\text{C}^2\text{-H}^2$ fragment during the rotation of the butyl chain around

the C^α-C^β bond, the corresponding dihedral variations do not exceed 10 degrees. In contrast, the TFSI⁻ shows rather broad distribution of the φ dihedral values. Numerous Raman investigations⁴⁰⁻⁴⁴ claim the coexistence of different conformers stemming from the rotation around the τ₂ dihedral in the neat Bmim⁺ based ILs. Our results show that the corresponding rotation of the butyl chain has almost the same energy profile for the studied ILs and, hence, does not depend markedly on the anion. Moreover, the principal position of anion on top of the C²-H² fragment of anion is hardly influenced by the rotation of the butyl chain around the C^α-C^β bond for all the IL ion pairs except BmimTFSI. The latter exhibits particular behavior which reflects that its structure is rather labile and the anion is evidently mobile and it can change its position around the equilibrium one to a considerable extent already as a consequence of the butyl chain rotation.

Altogether, these findings justify our selection of the on-top configurations of the ion pairs with cations in trans-conformations as the representative structures for subsequent analysis of weak noncovalent interionic interactions and for investigation of larger aggregates like ion pair dimers. Some literature reports also suggest that the butyl chain conformation does not influence the interionic interactions in analogous ion pairs, since they are mainly localized at the imidazolium ring.^{9,34} The results on the BmimTFSI ion pair should be interpreted cautiously though.

3.2.2 Weak noncovalent interactions in the IL ion pairs

Having established the most stable representative ion pair configurations and their main structural features, we now proceed to the analysis of the weak noncovalent interactions in these systems by means of the QTAIM and NCI approaches which were introduced in the previous chapter.

Figure 3.7 shows the NCI surfaces and the CPs, revealed by the QTAIM analysis, for the studied ion pairs. Just as in the case of MmimBF₄ ion pair (see

Chapter 2), there are broad surfaces of weak noncovalent contacts in the interionic space.

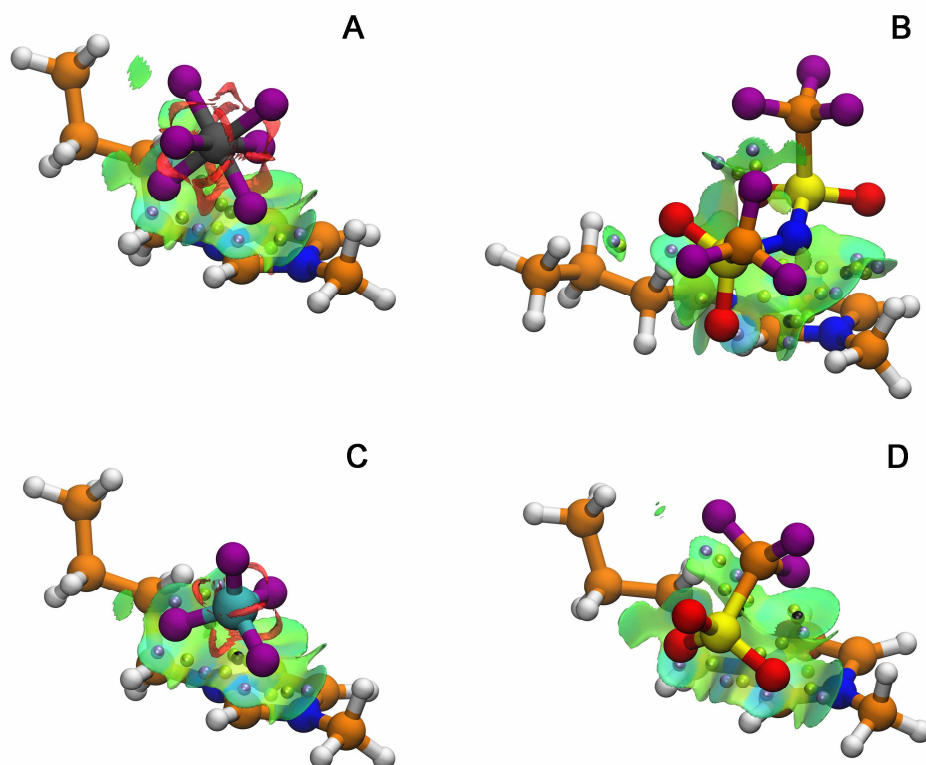


Figure 3.7. NCI isosurfaces for the BmimPF₆ (A), BmimTFSI (B), BmimBF₄ (C), and BmimTfO (D) ion pair structures obtained at the M06-2X/6-311++g(d,p) level of theory in vacuum. The RDG isovalue is 0.6. The $\text{sign}(\lambda_2)\rho$ value is colormapped onto the isosurfaces in the region from -0.03 a.u. to $+0.03$ a.u. in the blue-green-red palette. QTAIM revealed CPs are depicted as light blue (BCPs), green (RCPs), and black (CCPs) spheres. Color coding of the elements: white – H, orange – C, blue – N, purple – F, cyan – B, gray – P, yellow – S.

In all the ion pairs, the most blueish regions and the corresponding BCPs are observed in the zones of multiple contacts between the most electronegative atoms of anions (F in BF₄⁻ and PF₆⁻, and O in TfO⁻ and TFSI⁻) and the C²-H² fragment. Less intense interactions, which appear as cyan or blue-green regions of the NCI surfaces, are observed for the contacts between anions and the alkyl hydrogen atoms of the NCH₃ and C^αH² groups.

The general extent of the NCI surfaces corresponding to the same RDG isovalue for all the ion pairs presented in Figure 3.7, *i.e.*, the area of noncovalent contacts, is higher for larger anions. For example, for the region of interaction

between the anion and the C⁴⁻⁵ site, in the case of small BF₄⁻ anion and the slightly larger PF₆⁻, there is only a small part of green NCI isosurface typical for van der Waals like weak interaction, while for the larger TfO⁻, the isosurface extends closer to the C⁴⁻⁵ side of the imidazolium ring and even several CPs are found. For the largest anion studied here, TFSI⁻, the NCI isosurfaces covers the entire imidazolium ring and the corresponding BCPs with the C⁴⁻⁵ fragment are in the light blue region of the surface, indicating a weak attractive bonding interaction.

We also note that in the NCI isosurfaces, that build up between the butyl chain and anions, the regions of weak dispersive contacts, where there are no CPs, are found.

Quantitative results of the QTAIM analysis of the weak noncovalent interactions between the counterions in the studied IL ion pairs are collected in Table A 3.1. The main BCP characteristics, such as the electron density (ρ^{BCP}), the electron density Laplacian ($\Delta\rho^{\text{BCP}}$), and the total electronic energy density (H^{BCP}) values are plotted as a function of interatomic distance in Figure 3.8.

Two types of BCPs are observed. The first is between the electronegative atoms of the anions and the hydrogen atoms of the cation. The second corresponds to the distortions of the bondpaths of the first type where the BCP connects anion not with a hydrogen atom, but with the adjacent carbon atoms. Direct bonding noncovalent contacts between nonhydrogen atoms, *e.g.*, F^{1'}-C² in BmimBF₄, fall in this category as well.

The BCPs of the second type are logically found at slightly higher interatomic distances (Figure 3.8). Almost linear correlations between the selected BCP descriptors and the corresponding distances are observed for both types of contacts (somewhat worse for H^{BCP}).

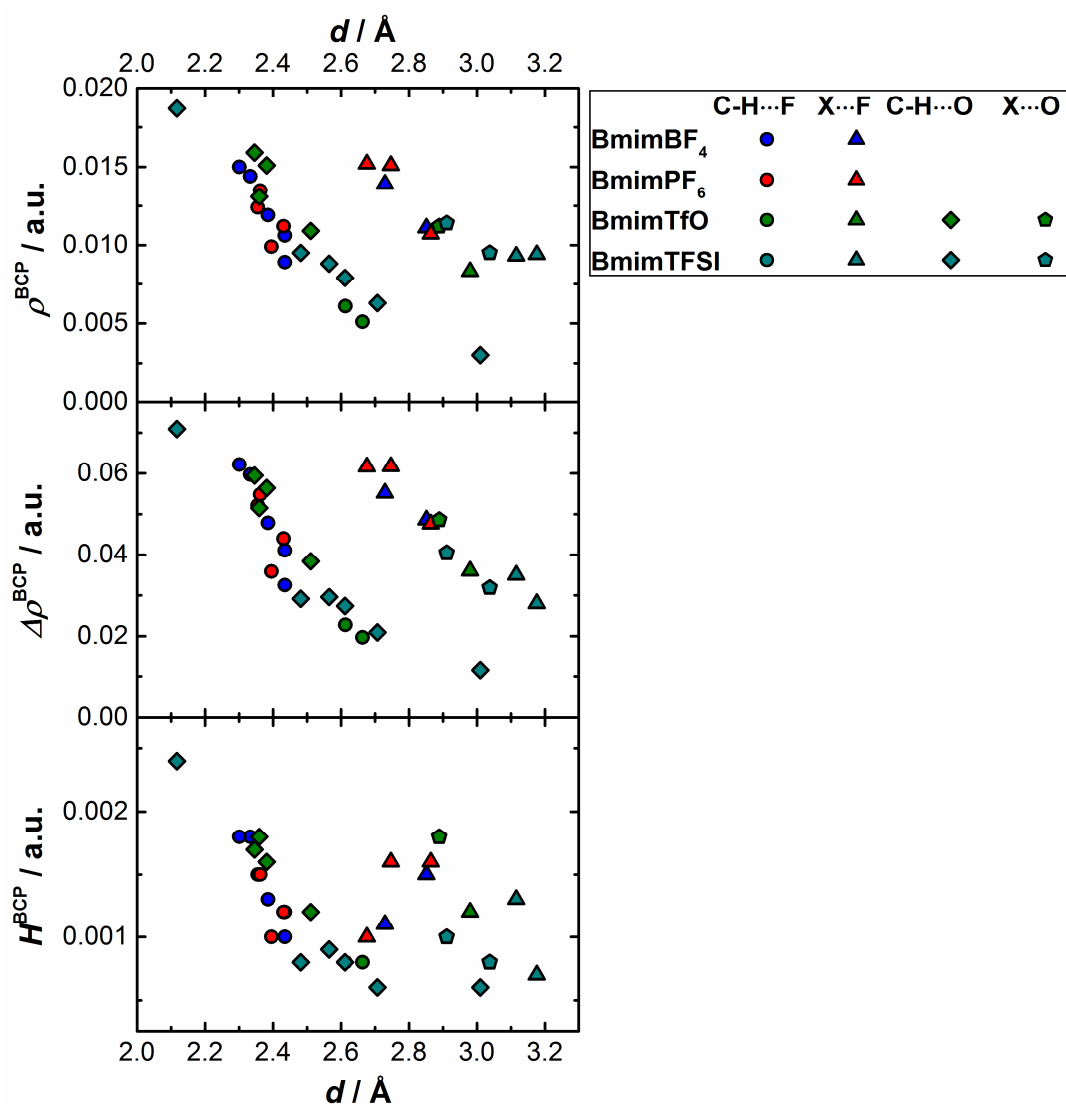


Figure 3.8. The BCP electron density (*top panel*), electron density Laplacian (*middle panel*), and total electron energy density (*bottom panel*) values for the weak noncovalent interactions as a function of distance between the interacting atoms, as revealed in the structures of the studied ion pairs by means of QTAIM analysis.

Also, both types of contacts have very close range of the electron density values at the BCPs, though somewhat higher for the contacts with hydrogen atoms. Given the values of ρ^{BCP} , as well as the signs of $\Delta\rho^{\text{BCP}}$ and H^{BCP} , these contacts should be classified as weak bonding contacts of electrostatic nature. The contacts with the hydrogen atoms can thus be classified as weak hydrogen bonds.⁴⁵⁻⁴⁶ For the sake of clarity, hereafter, we will only use the ρ^{BCP} values to characterize the strength of these interactions within the QTAIM approach. The range of the ρ^{BCP}

values agrees with that obtained for other IL ion pairs of similar nature like EmimB(CN)₄⁴⁷ and EmimBF₃R.⁴⁸

As it was noted before, BmimTFSI reveals the broadest interatomic NCI surface. This is naturally reflected in the higher number of BCPs revealed. We also note that it exhibits the shortest ($\approx 2.1 \text{ \AA}$) and strongest ($\rho^{\text{BCP}} \approx 0.019 \text{ a.u.}$) hydrogen bond within the studied set of ILs. It is established between the C²-H² hydrogen atom of the cation and the O¹ oxygen atom of the anion and can be noted as the most blueish zone in the corresponding NCI isosurface. Nevertheless, we consider the occurrence of this BCP rather as an artifact than a strong persistent interaction, if one takes into account the mentioned above lability of the structure of this ion pair.

3.2.3 The effect of implicit solvation

In order to model the nonspecific solvation effects which always accompany the dilution in polar molecular solvents we have performed the same analysis for the ion pair structures optimized within the PCM solvation. With respect to the mixtures of ILs with molecular solvents, this effect can be thought of as a general dilution of the IL network in a dielectric continuum that leads to the screening of the Coulomb interionic interactions.

The structures of the ion pairs obtained within the PCM approach with different values of the relative static dielectric permittivities of the solvents employed in this study are shown in Figure 3.9. The corresponding vacuum structures are shown as well for the sake of comparison. It is apparent that inclusion of the implicit solvation effects does not markedly distort the structures obtained in vacuum. A general effect of slight stretching, *i.e.*, interionic separation, is observed, which is typical for polar and ionic solutes when immersed in a polar medium. We also note that there is no apparent difference between the structures calculated in different solvent environments.

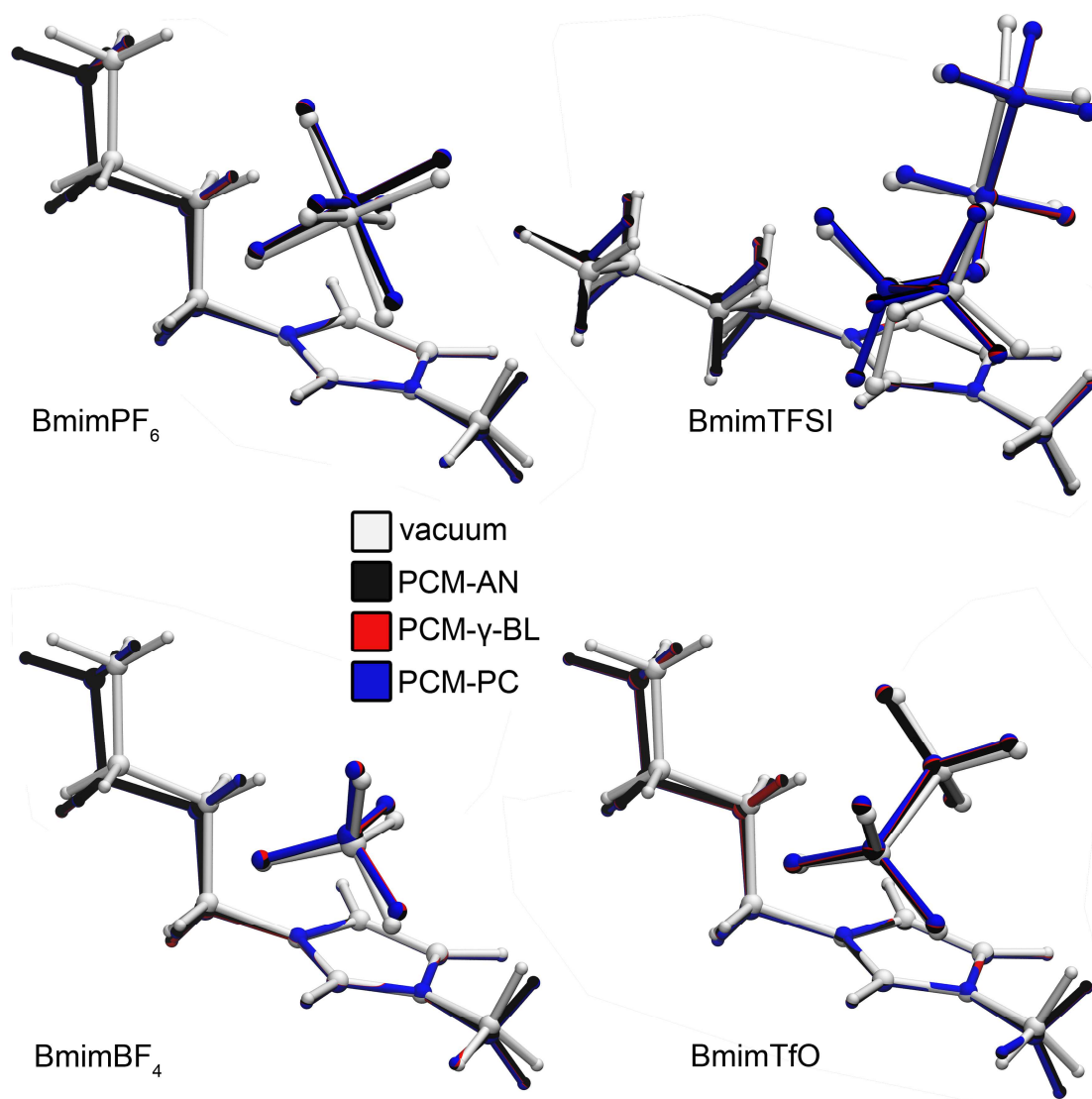


Figure 3.9. Structures of the studied ion pairs optimized in vacuum and in polar media within the PCM approach, superimposed by the imidazolium ring carbon atoms.

The relative stability of the ion pairs in the polar medium can be assessed in several ways. First, the conventional electronic ion pair binding energies calculated on the basis of PCM results for the ion pairs and the isolated counterions. These values are compared in the negative part of the left panel in Figure 3.10

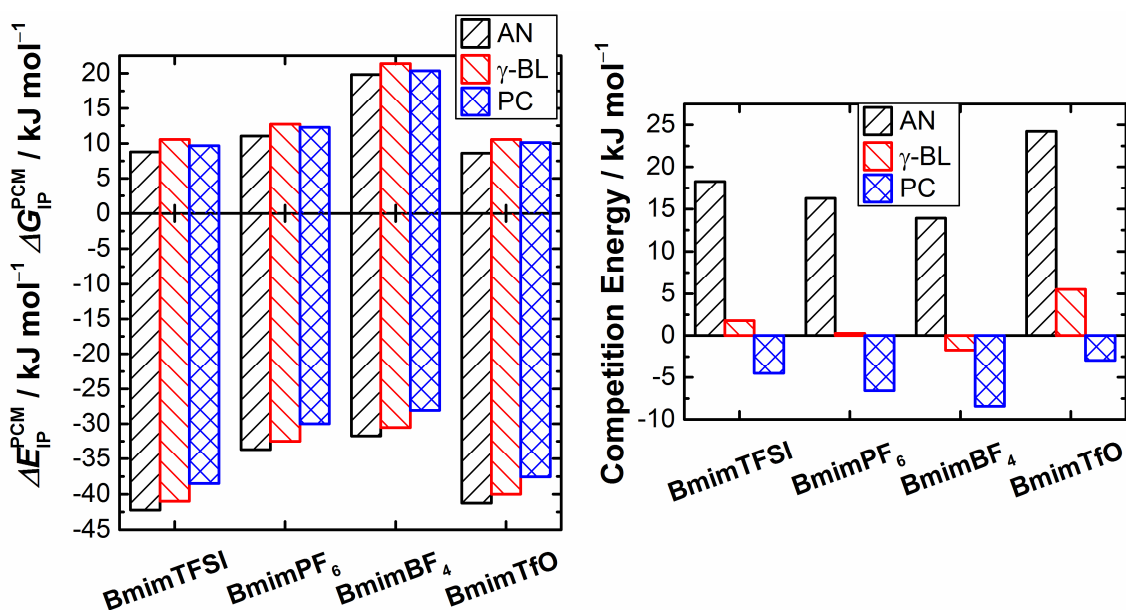


Figure 3.10. Electronic binding energy (*negative part of the left panel*) and free energy of ion pair formation (*positive part of the left panel*) of the studied IL ion pairs obtained by calculation in polar media within the PCM approach Competition energy, as defined by Hu *et al.*¹⁸, calculated within the PCM approach (*right panel*).

The ion pair binding energies, estimated in this manner, are an order of magnitude lower than the corresponding gas phase values estimated in vacuum calculations (Figure 3.3). For a given IL ion pair, the more polar the solvent the less it favors the ion pair formation. This result is in accordance with the calculations on MmimPF₆⁵ and EmimBF₄/CF₃CO₂/OAc¹⁸ ion pairs in various polar media.

As a second way to assess the tendency to ion pairing in polar media, Palomar *et al.*⁵ also proposed to use the Gibbs free energies of ion pair formation estimated via standard statistical mechanics relations.⁴⁹ The corresponding values are shown in the positive part of the left panel in Figure 3.10. The positive sign of the Gibbs free energies of ion pair formation in the polar media implies that the association equilibrium is shifted towards dissociated ions for all the presented systems. This conclusion is in contradiction with experimental results on conductivity measurements of dilute solutions of imidazolium ILs in AN and other polar molecular solvents.⁵⁰⁻⁵¹ The standard Gibbs free energies of association

calculated from the thermodynamic association constants are around $-5-10 \text{ kJ mol}^{-1}$. Moreover, both ion pair binding energies and the Gibbs free energies of ion pairing predict the following order of ion pairing tendency: $\text{BmimTfO} \approx \text{BmimTFSI} > \text{BmimPF}_6 > \text{BmimBF}_4$. This is also strikingly different from the gas-phase results (Figure 3.3) and from the experimental order of the association constants.⁵⁰⁻⁵¹ We note, however, that the differences in the calculated ion pair binding energies and Gibbs free energies are rather low ($< 10 \text{ kJ mol}^{-1}$) between the ion pairs and can be considered as negligible.

The third way to assess the ion pair stability in a polar medium, which was proposed by Hu *et al.*¹⁸, uses a combination of implicit and explicit solvation models. Competition energy was defined by the authors as the difference between, from one side, the sum of binding energies of an isolated cation and anion with a solvent molecule and the binding energy of the ion pair, from the other side, all being calculated within the PCM framework. The positive values of the competition energy indicate higher stability of the ion pair while the negative ones imply that the stabilizing effect of solvation of the individual ions outweighs that of the ion pair formation. Competition energies calculated for the studied systems are shown in the right panel in Figure 3.10. The results suggest a clear tendency towards ion pairing in AN (positive values above 15 kJ mol^{-1}) and an effective competition between the two ion solvation and association in the case of γ -BL and PC (the values are in the range $\pm 5 \text{ kJ mol}^{-1}$).

The mentioned above increase of the interionic separation, when going from the gas phase ion pair structures to those calculated within the PCM approach, leads to the rupture of the weakest and the most unstable noncovalent interionic interactions and to the weakening of the major ones. This can be tracked in Figure 3.11 when comparing the results for vacuum and PCM-calculated structures by the disappearance of the BCPs at low values of the electron density and by the shift of the rest of the BCPs to larger distances (by *ca.* $0.1-0.2 \text{ \AA}$) and lower ρ^{BCP} values (by

ca. 0.003-0.005 a.u.). The largest shifts are observed in the case of BmimTFSI which agrees with its high liability to structural perturbations mentioned before.

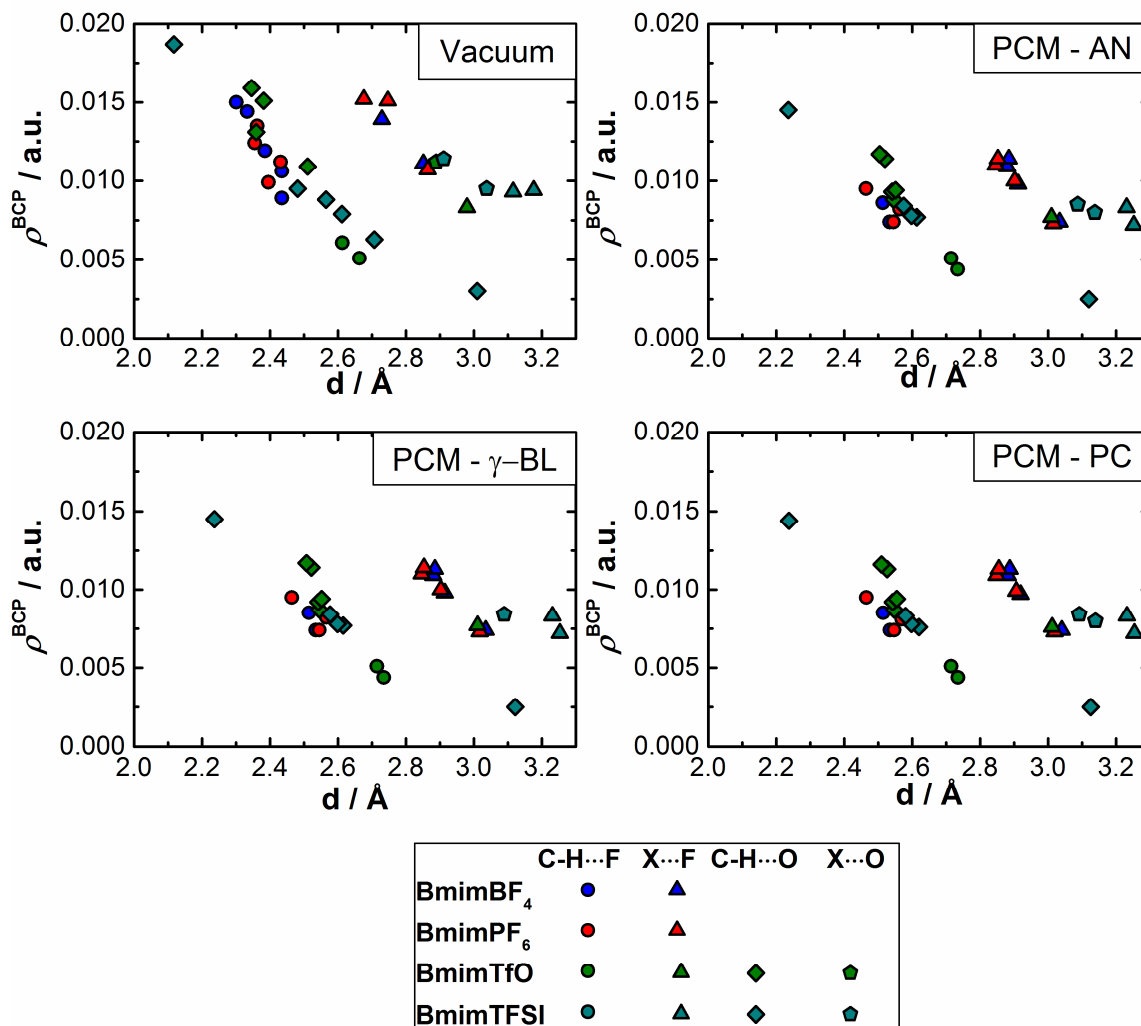


Figure 3.11. The BCP electron density values for the weak noncovalent interactions as a function of distance between the interacting atoms, as revealed by means of QTAIM analysis in the structures of the studied ion pairs obtained in vacuum and in polar media within the PCM approach.

Similar conclusions may be drawn from analysis of the results given in Figure 3.12, where the corresponding NCI plots are shown. In the region of bonding interactions ($\text{sign}(\lambda_2)\rho < 0$) the spikes shift to lower values of the electron density. These regions become narrower, *i.e.*, the corresponding NCI surfaces (not shown) would enclose smaller volume of space. The number of spikes and the

general density of points is also apparently reduced in the region of very weak dispersive interactions ($\rho < 0.01$ a.u.).

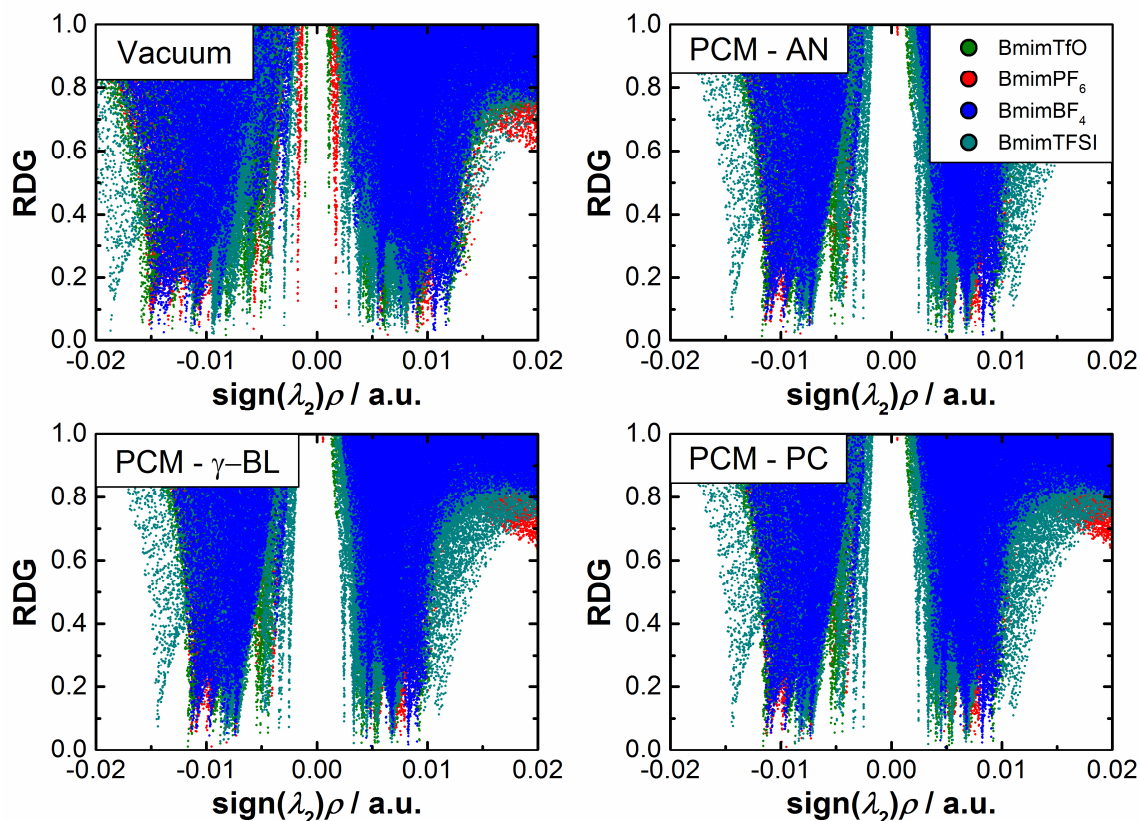


Figure 3.12. The NCI plots for the structures of the studied ion pairs obtained in vacuum and in polar media within the PCM approach.

3.2.4 Ion pair dimers

In several theoretical studies,^{15-16,31-32,35-36,52-53} it has been claimed that the smallest unit capable to represent the main structural features of neat ILs is not the ion pair but rather its dimer. Taking these considerations into account, we have also undertaken a study on the ion pair dimers in order to model IL network structures and to understand the possible changes in the electronic structure when the size of ion aggregates is decreased upon dilution.⁵⁴ Given that the possible number of stable ion pair dimer structures is rather high and their extensive search is rather computationally expensive and, in fact, out of scope of this study, we took

advantage of the results of Matthews *et al.*^{32,36} who performed a systematic study on the ion pair dimers of MmimCl/BF₄/NO₃/CH₃SO₄/TfO at the B3LYP-D3/6-311+g(d,p) level of theory. The most stable structures were found to be with imidazolium cations in a stacked antiparallel arrangement and each anion interacting with the C²-H² site of one cation and C⁴⁻⁵-H⁴⁻⁵ of the other one. Cations can be offset from the perfect stacked antiparallel arrangement rather easily depending on anion.

We have constructed the initial configurations of the ion pair dimers in accordance with the results of Matthews *et al.*^{32,36} The optimized structures are shown in Figure 3.13 along with the corresponding NCI surfaces. The structures of the ion pair dimers revealed in our calculations at the M06-2X/6-311++g(d,p) level of theory are in good agreement with the results of Danten *et al.*^{15,31,52} obtained for the same set of ion pair dimers at the B3LYP/6-31+g(d) level of theory.

Upon inspection of the NCI surfaces depicted in Figure 3.13 several features become apparent. In addition to the obvious increase of area of weak nonvocalent interactions between the ions, there are some areas of contact between the cations. Particularly, in the case of BmimTfO cations are the least displaced from the stacked arrangement and the corresponding NCI surface of weak dispersion interaction extends over the whole space between the imidazolium rings. We also note the increased number and strength of the cation-anion bonding contacts and hydrogen bonds seen as blueish regions. This is a result of expelling of the anions from the on top of C² arrangement, compared to ion pair structures, towards more in-plane like positions where the hydrogen bond like directional arrangements are more favored. These contacts are also observed at the C⁴⁻⁵-H⁴⁻⁵ sites.

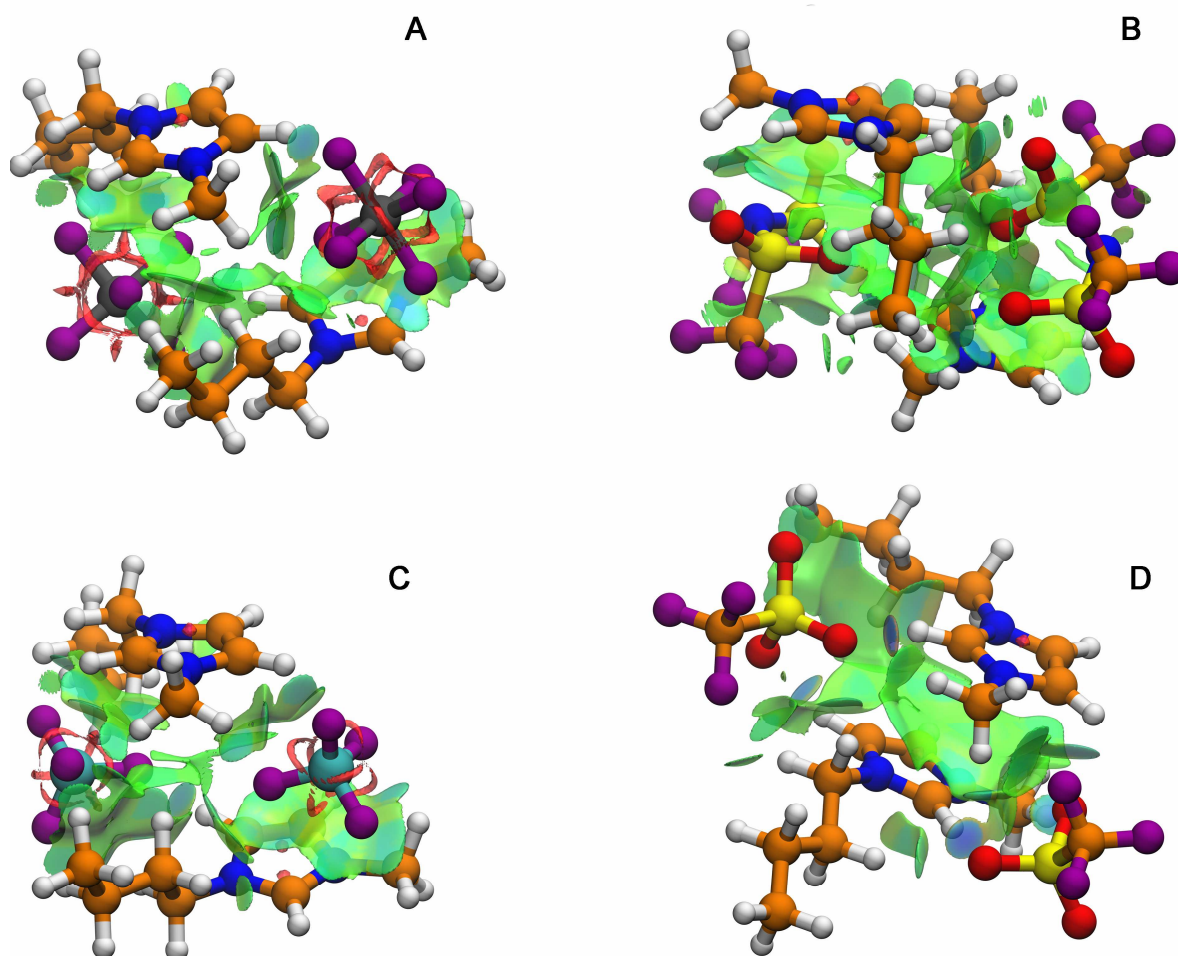


Figure 3.13. NCI isosurfaces for the BmimPF₆ (A), BmimTFSI (B), BmimBF₄ (C), and BmimTfO (D) ion pair dimer structures obtained at the M06-2X/6-311++g(d,p) level of theory in vacuum. The RDG isovalue is 0.6. The $\text{sign}(\lambda_2)\rho$ value is colormapped onto the isosurfaces in the region from -0.03 a.u. to $+0.03$ a.u. in the blue-green-red palette. Color coding of the elements: white – H, orange – C, blue – N, purple – F, cyan – B, gray – P, yellow – S.

The electron density values of the BCPs revealed by the QTAIM analysis of the ion pair dimer structures are plotted as function of the distance between the interacting atoms in Figure 3.14. The most important interactions with the imidazolium ring atoms are marked. The noted above increase of the number of bonding contacts is reflected in the higher number of BCPs found. This is particularly apparent for the weak contacts of low electron density ($\rho < 0.01$ a.u.) for all the investigated ILs.

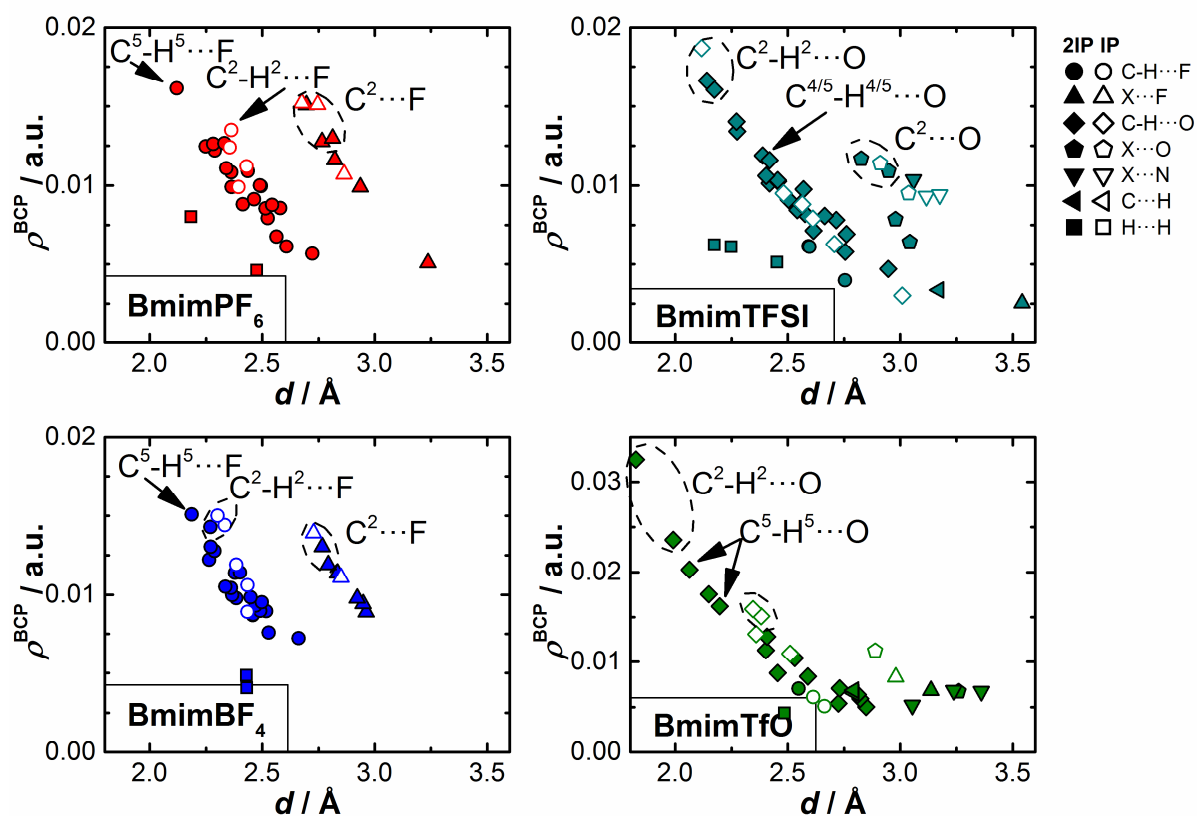


Figure 3.14. The BCP electron density values for the weak noncovalent interactions as a function of distance between the interacting atoms, as revealed by means of QTAIM analysis in the structures of the studied ion pairs (open symbols) and ion pair dimers (filled symbols). X indicates any nonhydrogen atom of the cation, *i.e.*, carbon or nitrogen.

As for the BCPs involving the imidazolium ring sites, we note that for BmimBF₄ and BmimPF₆ ion pair dimers the BCPs with the C²-H² fragment are insignificantly influenced in terms of the corresponding distances and the electron density values, whereas the newly revealed bonding contacts with the C⁵-H⁵ site are of comparable or even slightly higher strength. In contrast, in the case of BmimTfO and BmimTFSI ion pair dimers a remarkable number of BCPs are revealed at significantly higher ρ^{BCP} values compared to the corresponding ion pairs. This enhancement of the strength of hydrogen bonding is particularly prominent for the C²-H² hydrogen while the hydrogen bonds with the C⁴⁻⁵-H⁴⁻⁵ sites are only slightly stronger than the hydrogen bonds in the parent ion pairs.

All the bonding contacts between the counterions in the ion pair dimer structures fall on the same trend lines that were established for the corresponding ion pairs (Figure 3.14). The BCPs that do not obey these trends are related to the very weak contacts like H-H between the cations (squares in Figure 3.14) and to the stacking interactions in the case of BmimTfO (down triangles in Figure 3.14). Figure 3.15 presents the NCI plots of the ion pairs and the corresponding ion pair dimers. Main conclusions correspond to the results of the QTAIM analysis.

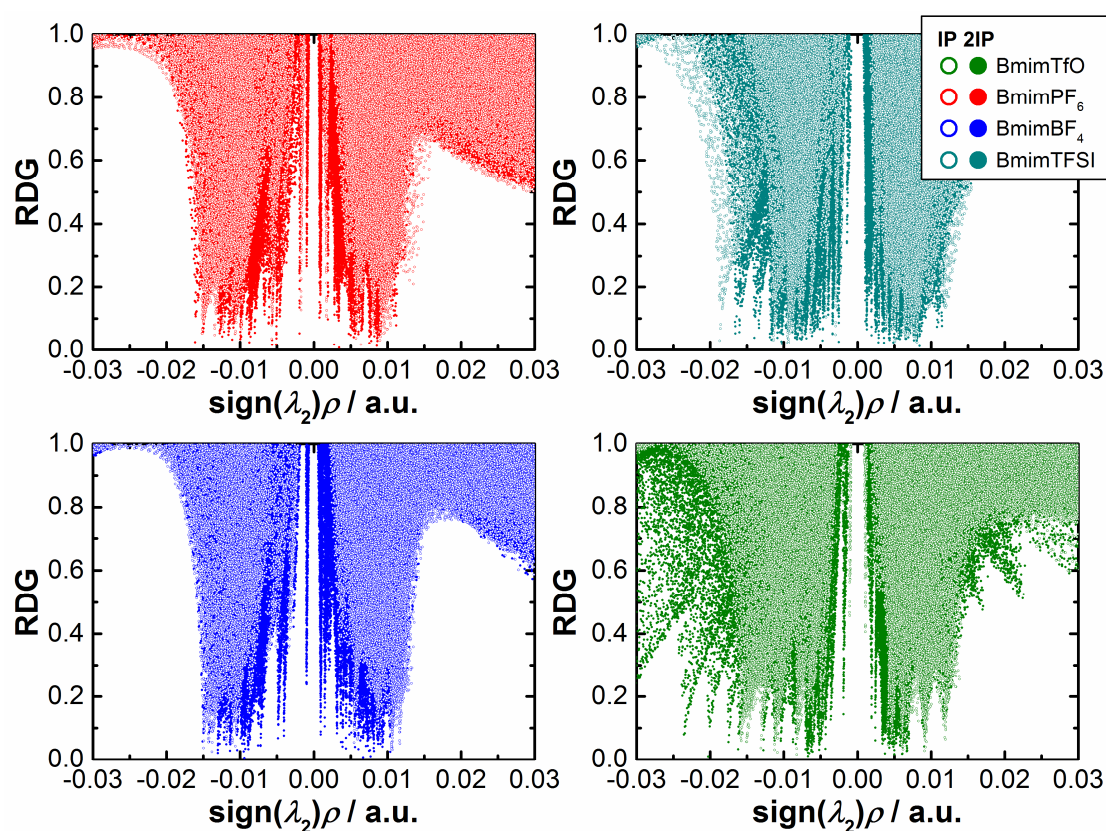


Figure 3.15. The NCI plots for the structures of the studied ion pairs (open symbols) and ion pair dimers (filled symbols).

The higher number of spikes and data points in the region of weak nonbonding interactions ($\rho < 0.01$ a.u.) observed for the ion pair dimers is the reflection of the broader extent of the corresponding NCI surfaces. The strongest bonding interactions are of comparable strength between the ion pairs and ion pair dimers in the case of BmimBF₄ and BmimPF₆. A significant increase of the

strength is observed for BmimTfO. For BmimTFSI, given that the spike at *ca.* -0.019 a.u. stems from the allegedly unstable hydrogen bond at the C^2-H^2 site in the ion pair structure and should be thus neglected, the enhancement of the strength of the bonding interactions is also noticed.

As it was mentioned in Chapter 2 when the QTAIM approach was outlined, it can also produce atomic charges. In particular, the charges on the hydrogen atoms can be used to additionally characterize hydrogen bonding as it is usually accompanied with the increase of charge on the hydrogen atoms involved. The results are presented in Figure 3.16

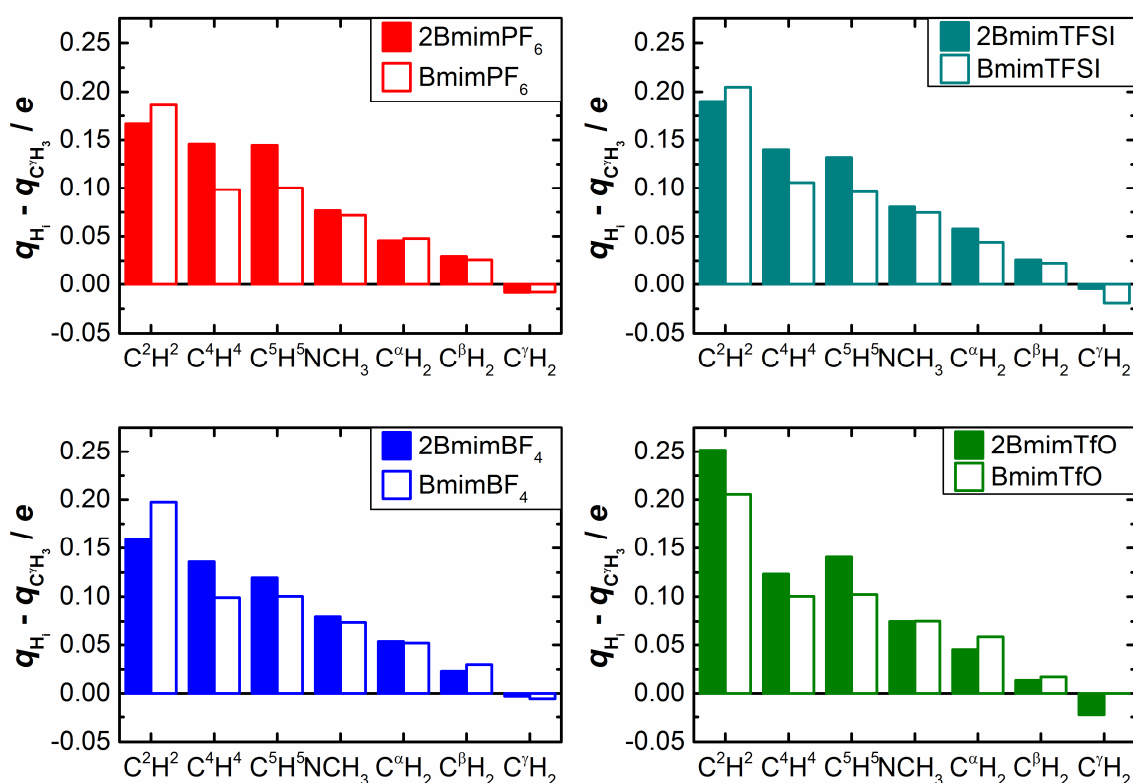


Figure 3.16. QTAIM charges of the hydrogen atoms of Bmim⁺ cations for the studied ion pairs and ion pair dimers referenced to the charge of the hydrogen atoms of the terminal methyl group of the butyl chain. Charges of the chemically equivalent hydrogen atoms of CH₂ and CH₃ groups are averaged.

We note that in view of the analysis of NMR chemical shifts which is presented in Chapter 4, the atomic charges are referenced to the atomic charges of the corresponding atoms of the terminal methyl group of butyl chain. In fact, the

absolute QTAIM atomic charges of this group are essentially zero (less than 0.02 e for hydrogen atoms on average and less than 0.025 e for the carbon atoms).

As can be seen from Figure 3.16, for all the ionic liquids the charges of the C⁴⁻⁵-H⁴⁻⁵ hydrogen atoms significantly increase of when going from ion pairs to the corresponding ion pair dimers. This is a direct consequence of the hydrogen formation at these sites. For the C²-H² hydrogen a slight decrease of the atomic charge is observed for BmimBF₄ and BmimPF₆. This is rather a result of electron density redistribution when the strength of the hydrogen bond at the C²-H² is not altered but the new ones are formed at the C⁴⁻⁵-H⁴⁻⁵ sites.

BmimTfO constitutes another case. The QTAIM atomic charge of the C²-H² hydrogen is also significantly increased in the ion pair dimer compared to the ion pair. This means that the hydrogen bonds at this site is particularly sensitive to ion aggregation. Atomic charges in BmimTFSI are difficult to interpret given the mentioned above concerns.

The charges on the alkyl hydrogen atoms adjacent to the imidazolium ring also increase when going from ion pairs to the corresponding ion pair dimers but to a much lesser extent compared to the imidazolium ring hydrogen atoms. This can be rationalized as a result of both the formation of new interionic hydrogen bonds involving these hydrogen atoms and the electron density redistribution due to hydrogen bonding at the imidazolium ring.

3.3. IL-solvent complexes

In order to establish the effects of explicit solvation on the structure and the electron density distribution in mixtures ILs-molecular solvents, we performed the calculations on the complexes of IL ions and ion pairs with solvent molecules. Given the fact that implicit solvation effects modeled within the PCM framework do not bring about any significant changes in the structures and in the overall pattern of weak intermolecular interactions, as it was established for the IL ion

pairs in section 3.2.3, here we will discuss the results for the gas phase optimized structures. As for the results of the analysis of electron density distribution, we will concentrate here only on those relevant for the IL cations as these are highly relevant for interpretation of the NMR chemical shift data in the following chapter.

Several studies report on quantum-chemical calculations of the complexes of imidazolium ILs with different solvent molecules.^{14-16,18,31,55-58} It was established that in the most stable structures of the complexes of ion pairs with aprotic polar molecular solvents, *e.g.*, AN^{16,18} or DMSO¹⁴, the solvent molecule is found at the C²-H² site of the cation where it establishes a directional interaction between its donor atom and the C²H² hydrogen atom of the cation. Weaker interaction of the solvent molecule with anion, which is located on top of the C²-H² fragment, was also noted.^{16,18}

3.3.1 Explicit solvation in AN

In a recent study on the BmimBF₄-AN system, Zheng *et al.*¹⁶ claimed that cation-solvent complex was irrelevant to interpret the observed variations in ¹H-NMR chemical shifts and IR spectra in the region of the imidazolium ring stretching vibrations as a function of mixture composition. Keeping this in mind, we still included the cation-solvent complexes in our calculations as model of a limiting case of infinitely dilute solutions.

The structures of the complexes of AN with the Bmim⁺ cation and with all the investigated ion pairs are shown in Figure 3.17 along with the corresponding NCI surfaces and CPs.

The cation-solvent complex (Figure 3.17, A) shows almost a linear hydrogen bond of considerable strength between the nitrogen atom of AN and the C²-H² hydrogen of the Bmim⁺ cation. A weaker bonding contact is observed with one of the alkyl hydrogen atoms of the NCH₃ group.

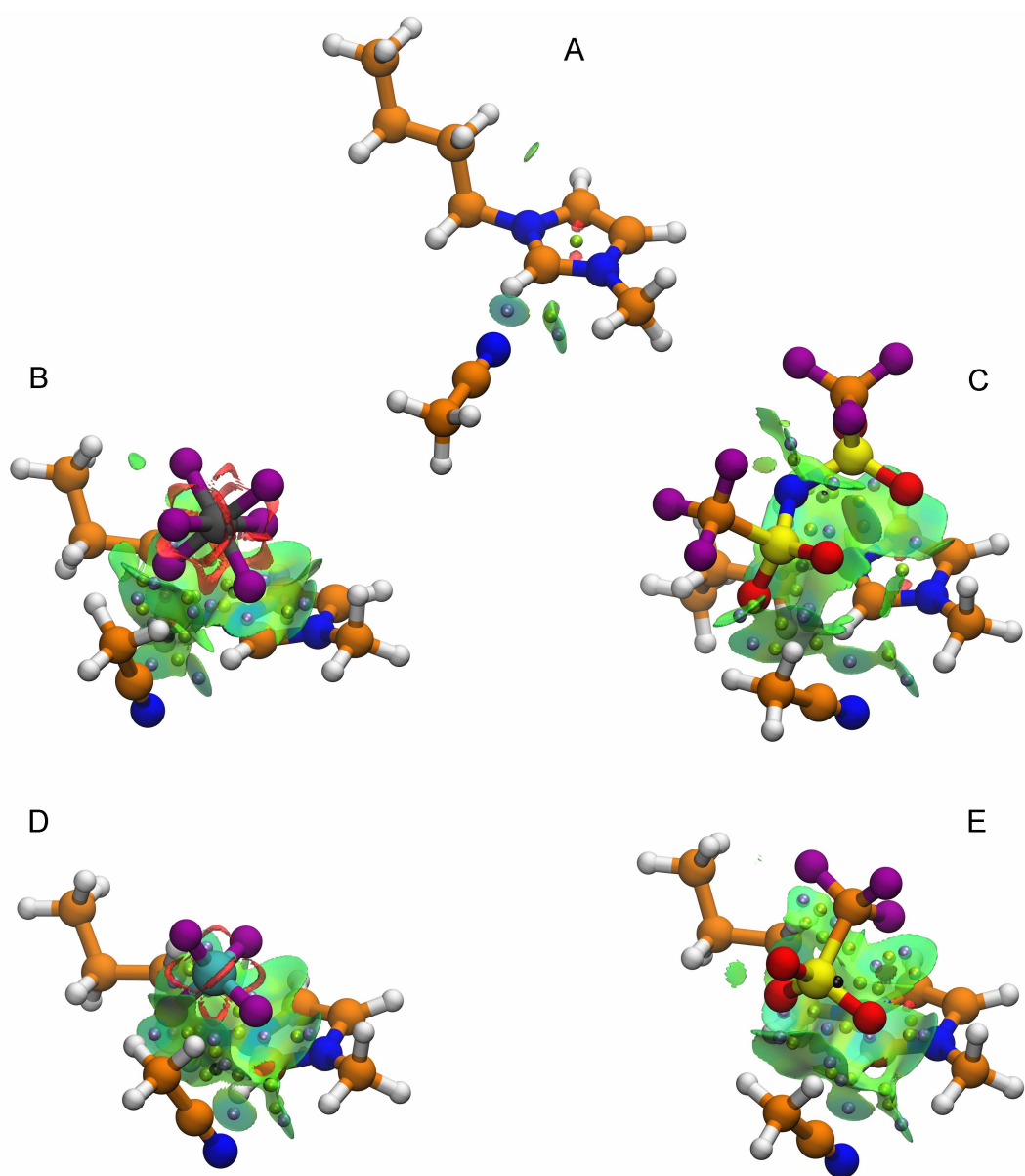


Figure 3.17. NCI isosurfaces for the complexes of Bmim^+ (A), BmimPF_6 (B), BmimTFSI (C), BmimBF_4 (D), and BmimTfO (E) with AN molecule obtained at the M06-2X/6-311++g(d,p) level of theory in vacuum. The RDG isovalue is 0.6. The $\text{sign}(\lambda_2)\rho$ value is colormapped onto the isosurfaces in the region from -0.03 a.u. to $+0.03$ a.u. in the blue-green-red palette. QTAIM revealed CPs are depicted as light blue (BCPs), green (RCPs), and black (CCPs) spheres. Color coding of the elements: white – H, orange – C, blue – N, purple – F, cyan – B, gray – P, yellow – S.

In the structures of the complexes between the ion pairs and AN molecule (Figure 3.17, B-E), the solvent molecule is aligned parallel to the line connecting the C^2 atom of the cation and the central atom X of the anion. The nitrogen atom of

the AN molecule is located in front of the C²-H² fragment of the anion and the hydrogen bond is established similar to what was observed for the Bmim⁺...AN complex, but of lower strength. There is a broad continuous NCI surface between the methyl group of the AN molecule and the anion with blue zones corresponding to the weak bonding interactions of the methyl hydrogen atoms of AN and the electronegative atoms of the anion.

We note that, in comparison with the unperturbed geometries of the ion pairs (Figure 3.1), addition of the AN molecule moves the anion to more on-top-of-C² like configuration. As a result, the strength of the weak noncovalent interactions between the counterions in the structure of complexes of the ion pairs with the AN molecule is reduced. BmimPF₆ and BmimTFSI are particularly prone to this effect which is a consequence of their lower ion pair binding energies (Figure 3.3). Another result of such shift of the anions towards the on-top arrangement is that the QTAIM analysis does not reveal the interionic BCPs with the C²-H² hydrogen since they are turned into interactions with the C² carbon atom.

In a more quantitative manner, these interactions can be analyzed in the corresponding plots of the ρ^{BCP} values (Figure 3.14) and the NCI plots (Figure 3.15). One can see from Figure 3.14 that the hydrogen bond C²-H²...N which is formed in the solvated ion pairs (depicted as a black star) is weaker than the one found in the cation-solvent complex (blue star). This hydrogen bond in the solvated ion pairs is weaker than the interionic one in the native ion pair structures, marked with arrows in Figure 3.14, for BmimTfO and BmimBF₄. It is somewhat stronger for BmimPF₆, while for BmimTFSI its strength is comparable with that of C-H...O hydrogen bonds with the alkyl hydrogen atoms. The hydrogen bonds between the AN molecule and the ILs fall on the same trend line with the interionic hydrogen bonds found in the IL ion pairs.

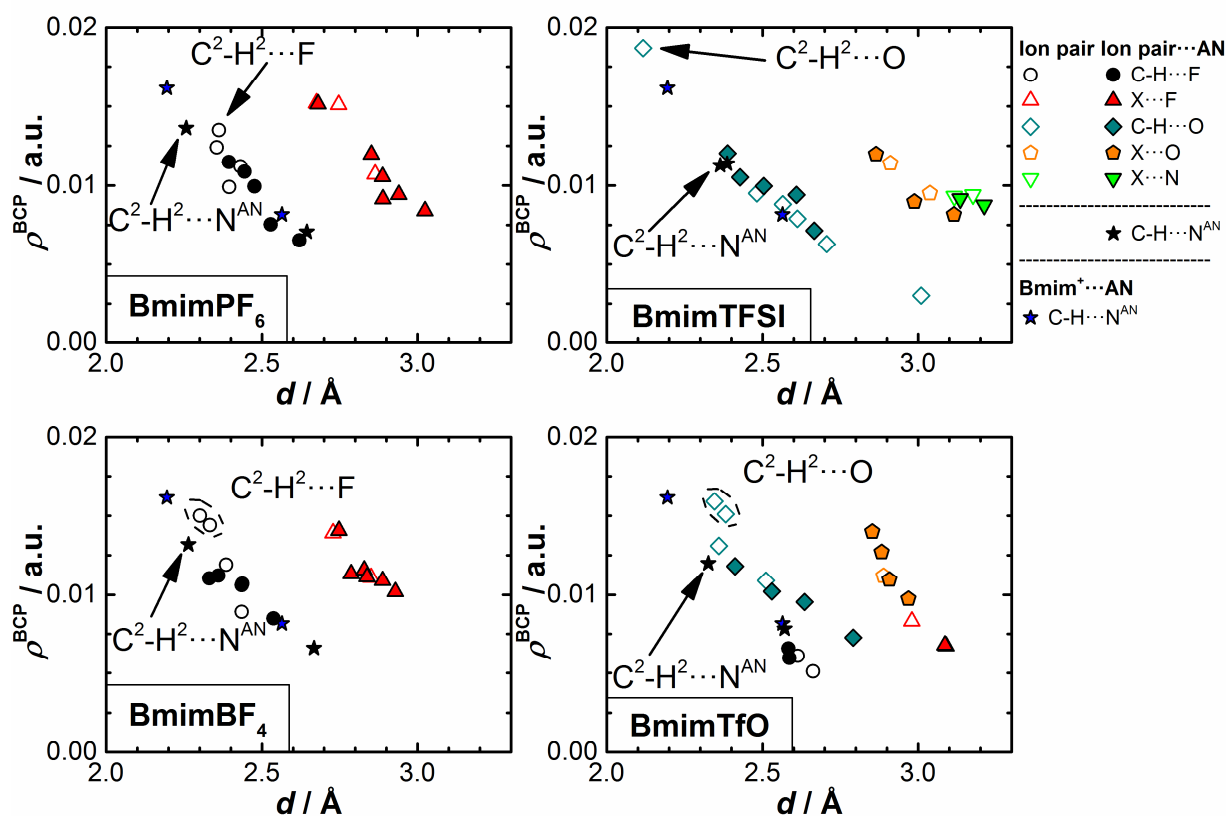


Figure 3.18. The BCP electron density values for the weak noncovalent interactions as a function of distance between the interacting atoms, as revealed by means of QTAIM analysis in the structures of the studied ion pairs, their complexes with AN molecule and the cation...AN complex. X indicates any nonhydrogen atom of the cation, *i.e.*, carbon or nitrogen.

From the NCI plots presented in Figure 3.19 similar conclusions on the relative strength of the strongest hydrogen bonding interactions occurring at the C²-H² site can be drawn. Indeed, in the case of BmimTfO and BmimBF₄, the spikes for the ion pairs are found at more negative $\text{sign}(\lambda_2)\rho$ values than for the ion pair solvates. For BmimPF₆ and BmimTFSI (apart from the mentioned before spike at -0.019 a.u.) the spikes corresponding to the bonding interactions ($\text{sign}(\lambda_2)\rho < 0.01$ a.u.) are very similar for both ion pairs and ion pair solvates.

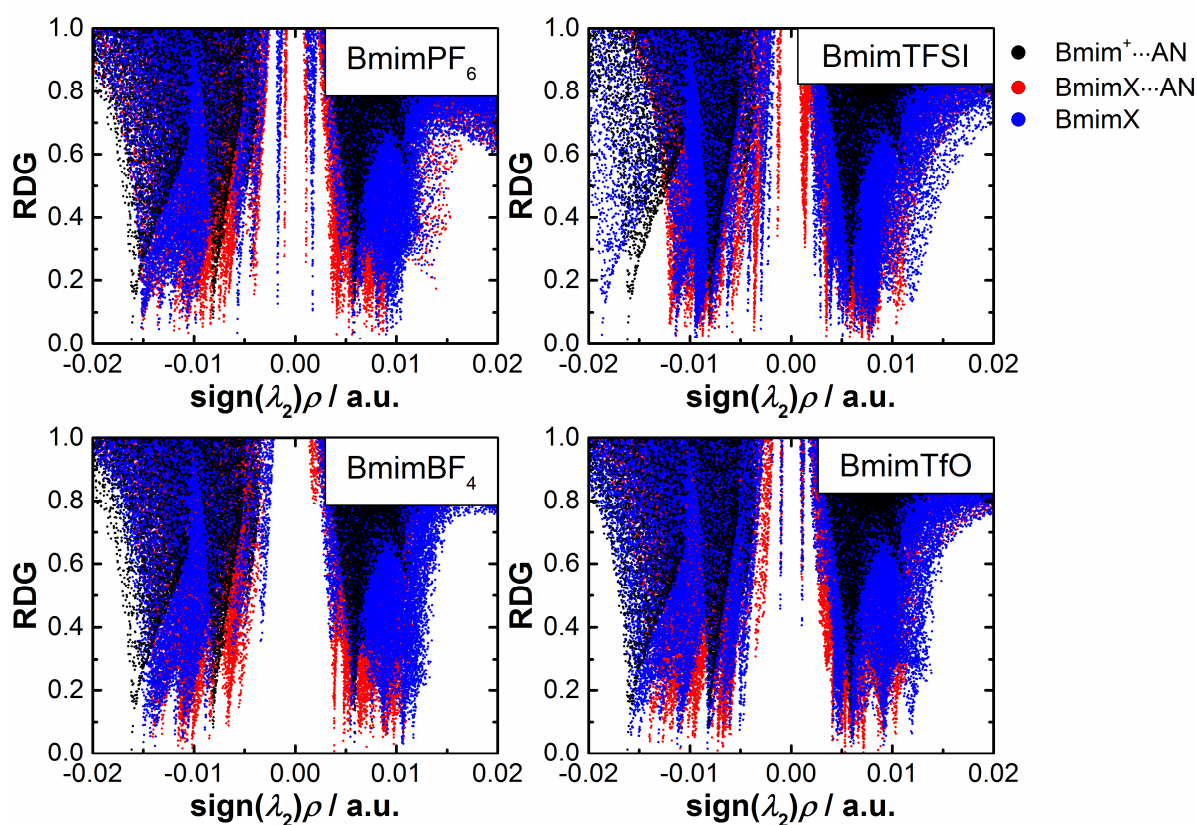


Figure 3.19. The NCI plots for the structures of the studied ion pairs, their complexes with AN molecule and the cation \cdots AN complex.

Additional spikes found in the region of very weak interactions ($\rho \approx 0.005$ - 0.010 a.u.) for the ion pair solvates correspond to the NCI surfaces of anion-solvent contact.

Figure 3.21 shows the QTAIM charges for the hydrogen atoms in the studied ion pairs and the corresponding complexes with the AN molecule. In general, the differences in charges between the different types of structures are rather negligible. For all the studied ILs, an increase of charge is observed for the C²-H² hydrogen atom when going from ion pairs to ion pair solvates due to additional hydrogen bonding. The corresponding charge in cation-solvent complex is lower than in the ion pair solvate, but higher than in the ion pairs. This is an indication of higher strength of the C²-H² \cdots N hydrogen bond compared to the C²-H² \cdots F/O hydrogen bonds in the ion pairs.

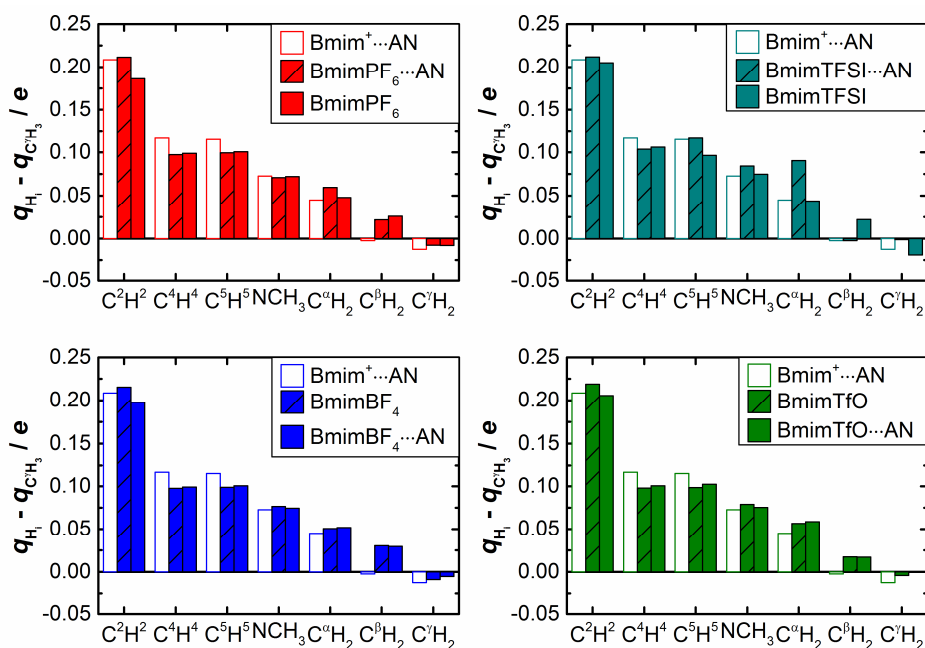


Figure 3.20. QAIM charges of the hydrogen atoms of Bmim⁺ cations for the studied ion pairs, their complexes with AN molecule and the cation...AN complex referenced to the charge of the hydrogen atoms of the terminal methyl group of the butyl chain. Charges of the chemically equivalent hydrogen atoms of CH₂ and CH₃ groups are averaged.

Similarly, for the QAIM charges of cation's carbon atoms, which are shown in Figure 3.21, the only appreciable difference is observed for the C² carbon which gains electron density when going to the cation-AN complex.

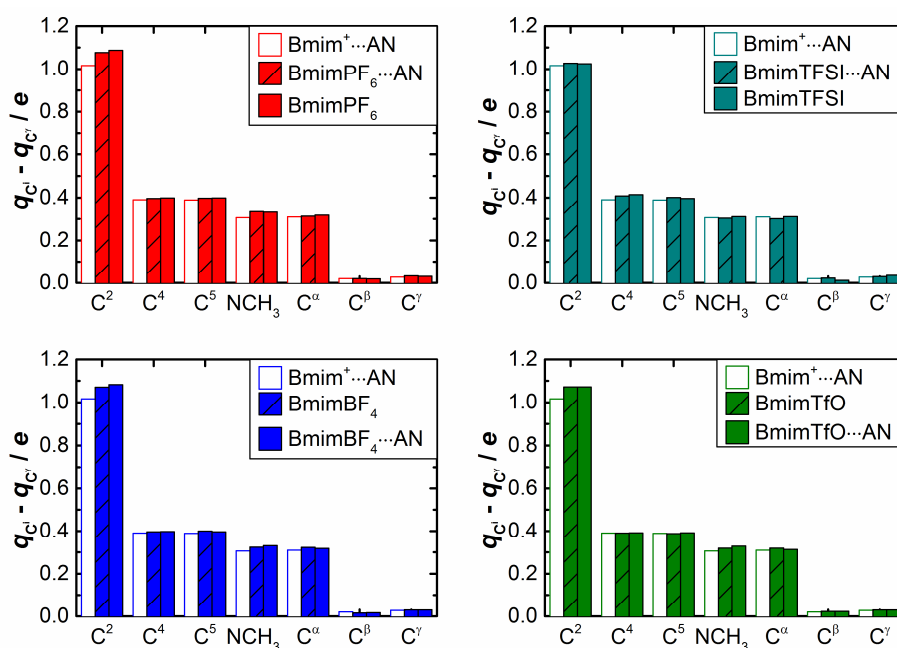


Figure 3.21. QTAIM charges of the carbon atoms of Bmim^+ cations for the studied ion pairs, their complexes with AN molecule and the cation \cdots AN complex referenced to the charge of the carbon atom of the terminal methyl group of the butyl chain.

3.3.2 Explicit solvation in γ -BL

As in the case of the complexes with AN, we explored the properties of the complexes of the Bmim^+ cation and of the IL ion pairs with the γ -BL molecule located at the $\text{C}^2\text{-H}^2$ site of the cation. The corresponding optimized structures are shown in Figure 3.22 along with the NCI surfaces and CPs.

As can be seen, the γ -BL molecule is arranged in the structure of solvates so that its carbonyl oxygen atom is in front of the $\text{C}^2\text{-H}^2$ fragment and establishes rather strong hydrogen bond. Weaker, but still noticeable as blueish regions on the NCI surfaces, interactions are established with the adjacent alkyl hydrogen atoms. The ester oxygen also participates in the latter type interactions with the hydrogen atoms of the butyl chain.

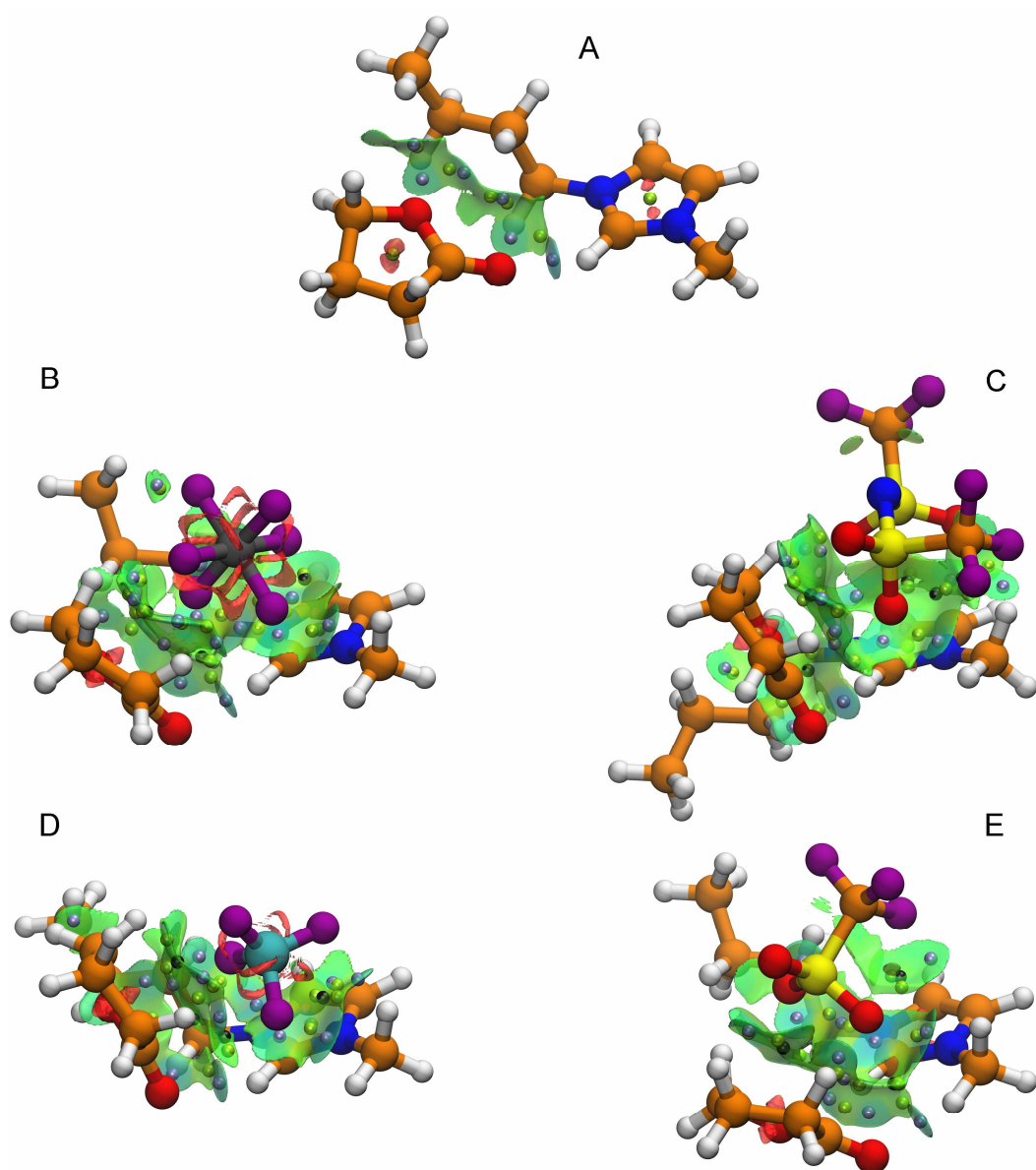


Figure 3.22. NCI isosurfaces for the complexes of Bmim^+ (A), BmimPF_6 (B), BmimTFSI (C), BmimBF_4 (D), and BmimTfO (E) with $\gamma\text{-BL}$ molecule obtained at the M06-2X/6-311++g(d,p) level of theory in vacuum. The RDG isovalue is 0.6. The $\text{sign}(\lambda_2)\rho$ value is colormapped onto the isosurfaces in the region from -0.03 a.u. to $+0.03$ a.u. in the blue-green-red palette. QTAIM revealed CPs are depicted as light blue (BCPs), green (RCPs), and black (CCPs) spheres. Color coding of the elements: white – H, orange – C, blue – N, purple – F, cyan – B, gray – P, yellow – S.

In the structure of the ion pair solvates, apart from the mentioned above weak noncovalent interactions between the $\gamma\text{-BL}$ molecule and the cation, the $\gamma\text{-BL}$ molecule also interacts with the anions via its methylene hydrogen atoms.

Addition of the γ -BL molecule to the IL ion pairs leads to more pronounced distortions of the parent ion pair structures than it was observed in the case of AN. For example, for BmimBF₄ and BmimPF₆ solvates with γ -BL, this can be noted by the fact that the interionic NCI surfaces extend further away towards the C⁴⁻⁵ site, compared to the analogous structure with the AN molecule, and even several RCPs and CCPs are observed in this region. As a result, the γ -BL molecule in the solvates with these ILs can more efficiently compete with the anions for the interaction with the C²-H² hydrogen and the corresponding NCI zones are more blueish compared to the solvates of BmimTfO and BmimBF₄.

The electron density values at the BCPs for the solvates with the γ -BL are shown in Figure 3.23 while the corresponding NCI plots are presented in Figure 3.24. We note that the hydrogen bond formed between the Bmim⁺ cation and the γ -BL molecule is significantly stronger than the one in the case of AN. This is true both for the cation-solvent complex and for the ion pair-solvent complexes. As a result, the higher strength of the C²-H²...O ^{γ -BL} hydrogen bonds in the complexes of BmimPF₆ and BmimTFSI with the γ -BL molecules compared to the hydrogen bonds with the C²-H² hydrogen atom in the corresponding ion pairs is even more evident. For the cases of BmimBF₄ and BmimTfO, the corresponding hydrogen bonds at the C²-H² site in the ion pairs and the ion pair-solvent complexes are of comparable strength. Between the four complexes ion pair-solvent, the hydrogen bond C²-H²...O ^{γ -BL} is stronger in the case of the BmimTfO and BmimTFSI ILs than in the case of BmimBF₄ and BmimPF₆.

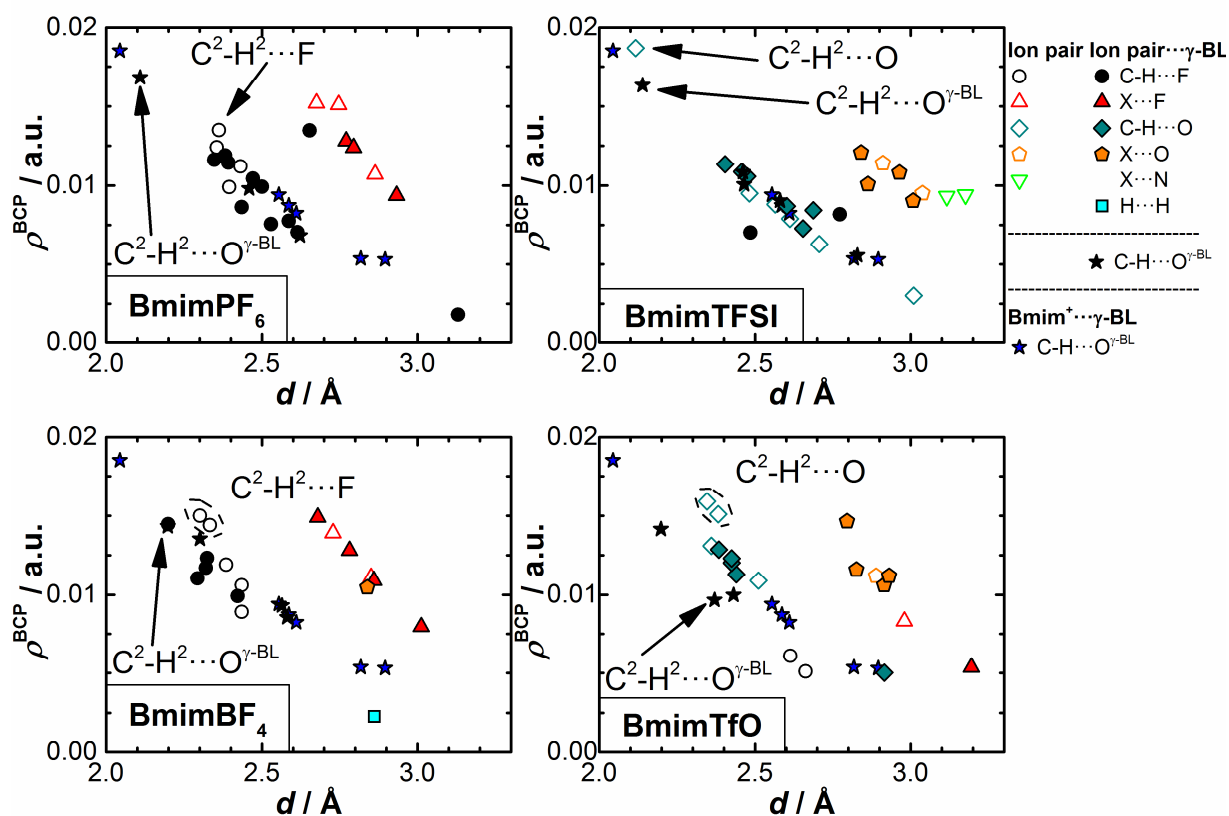


Figure 3.23. The BCP electron density values for the weak noncovalent interactions as a function of distance between the interacting atoms, as revealed by means of QTAIM analysis in the structures of the studied ion pairs, their complexes with $\gamma\text{-BL}$ molecule and the cation... $\gamma\text{-BL}$ complex. X indicates any nonhydrogen atom of the cation, *i.e.*, carbon or nitrogen.

Similarly, from Figure 3.24, we note that for BmimTfO and BmimBF₄ the spikes corresponding to the strongest bonding noncovalent interactions in the ion pairs and their complexes with the $\gamma\text{-BL}$ molecule almost coincide. At the same time, for BmimTFSI and BmimPF₆ the corresponding spikes in the solvates correspond to distinctly stronger interactions than in the ion pairs.

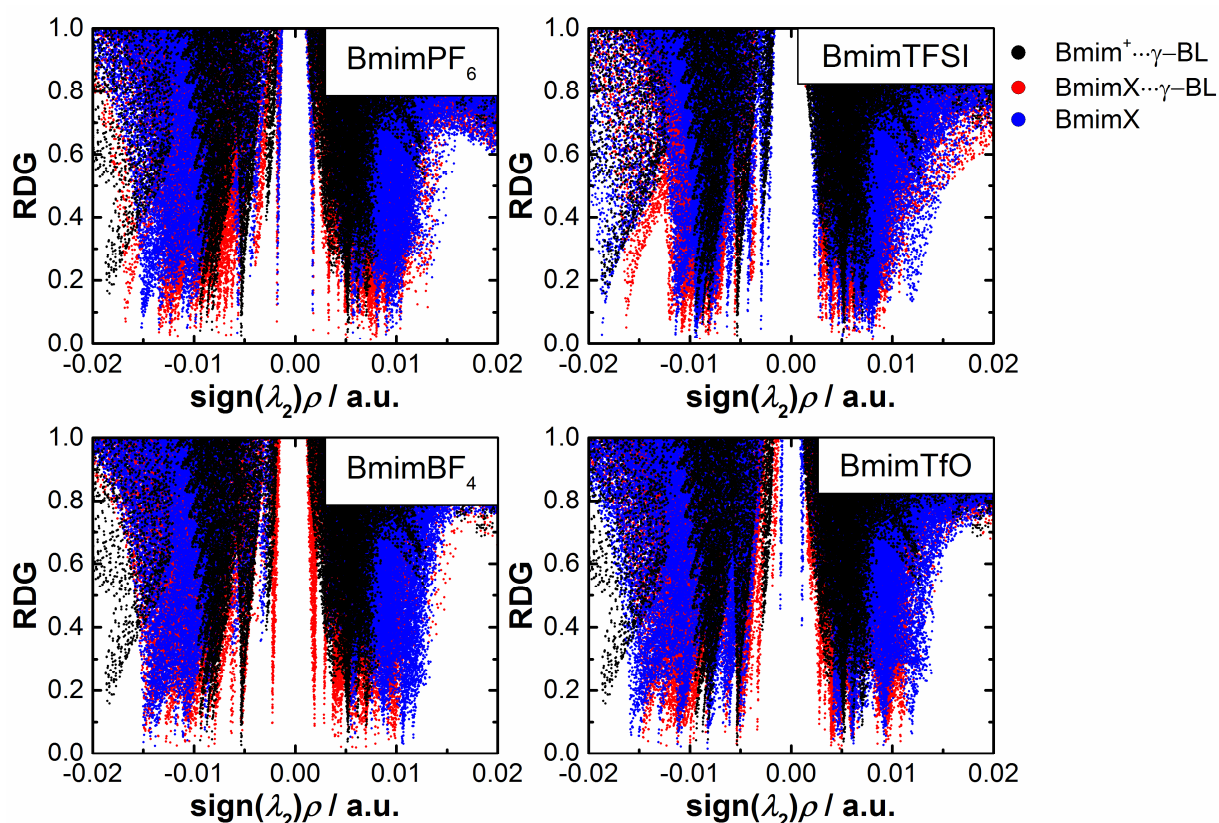


Figure 3.24. The NCI plots for the structures of the studied ion pairs, their complexes with γ -BL molecule and the cation... γ -BL complex.

The QTAIM atomic charges of hydrogen and carbon atoms of the cation in the complexes with the γ -BL molecules are presented in Figure 3.25 and Figure 3.26, respectively. The C²-H² hydrogen atom charge for the cation-solvent complex is very close to its value in the ion-pair solvent complex. However, the QTAIM atomic charge of the corresponding C² carbon atom in the cation-solvent complex is lower than in the ion pair-solvent complex, which, in turn, is lower or close to the charge in the ion pair. The high atomic charge of the C²-H² hydrogen atom in the complexes with the γ -BL molecule definitely points to enhanced hydrogen bonding at this site. The variations of charges at other sites, particularly, the C² carbon, are subject to much more complex effects of charge redistribution. Moreover, the shape and volume of the atomic basins which are used for integration of the atomic charge can be significantly different for different representative structures.

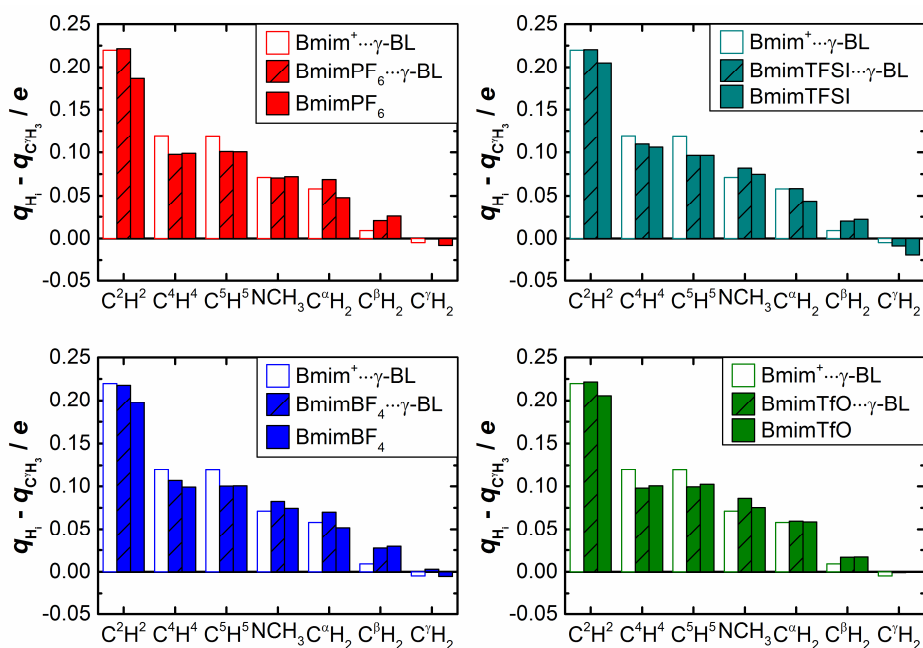


Figure 3.25. QTAIM charges of the hydrogen atoms of Bmim^+ cations for the studied ion pairs, their complexes with $\gamma\text{-BL}$ molecule and the cation $\cdots\gamma\text{-BL}$ complex referenced to the charge of the hydrogen atoms of the terminal methyl group of the butyl chain. Charges of the chemically equivalent hydrogen atoms of CH_2 and CH_3 groups are averaged.

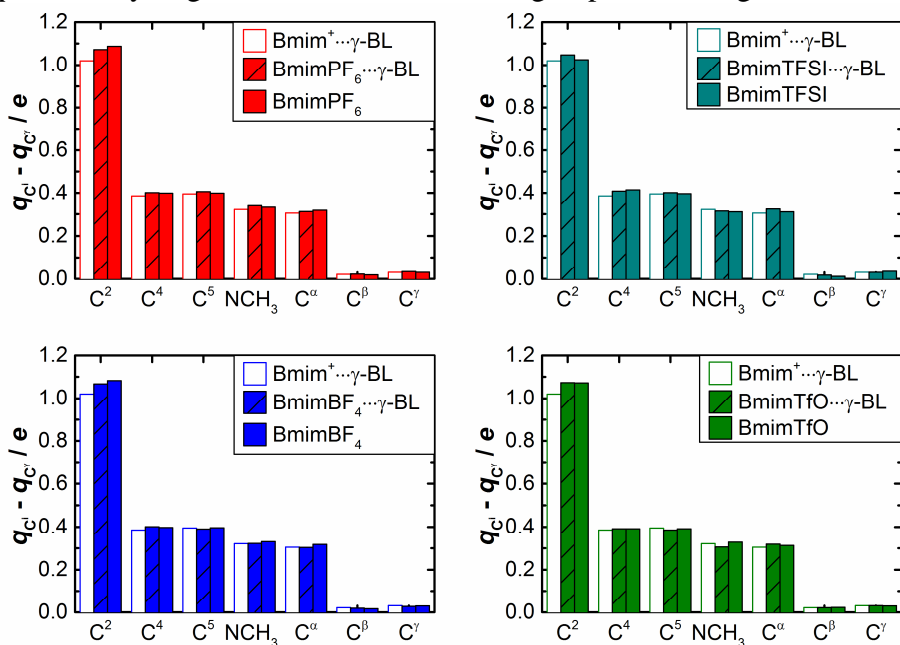


Figure 3.26. QTAIM charges of the carbon atoms of Bmim^+ cations for the studied ion pairs, their complexes with $\gamma\text{-BL}$ molecule and the cation $\cdots\gamma\text{-BL}$ complex referenced to the charge of the carbon atom of the terminal methyl group of the butyl chain.

3.3.3 Explicit solvation in PC

The complexes with the PC molecule mostly resemble those with γ -BL which were discussed above. Hence, here we will mark only the main features and peculiarities.

The structures of the cation-solvent and ion pair-solvent complexes are shown in Figure 3.27 along with the corresponding NCI surfaces and CPs. The presence of two ester oxygen atoms next to the carbonyl fragment of the PC molecule leads to increased repulsion between the ester fragment and the negatively charged group of the anion. This results in slightly larger distances between the solvent molecule and cations and, hence, longer and weaker hydrogen bonds compared to the case of γ -BL. The perturbing effect of the solvent molecule on the ion pair structure and the corresponding pattern of weak noncovalent interactions between the ions are less pronounced in the case of ion pair complexes with the PC molecule than with the γ -BL. It is still much more evident though than in the case of complexes with AN.

The electron density values at the BCPs corresponding to the weak noncovalent interactions in the studied systems are plotted as a function of distance between the interacting atoms in Figure 3.28. The NCI plots for the complexes with the PC molecule are shown in Figure 3.29.

The results suggest that, similarly to the complexes with the γ -BL molecule, for the BmimTFSI and BmimPF₆ ILs, addition of the PC molecule enhances hydrogen bonding at the C²-H² site compared to the ion pairs, while for BmimTfO and BmimBF₄ the hydrogen bonds cation-solvent are comparable in strength with the interionic hydrogen bonds.

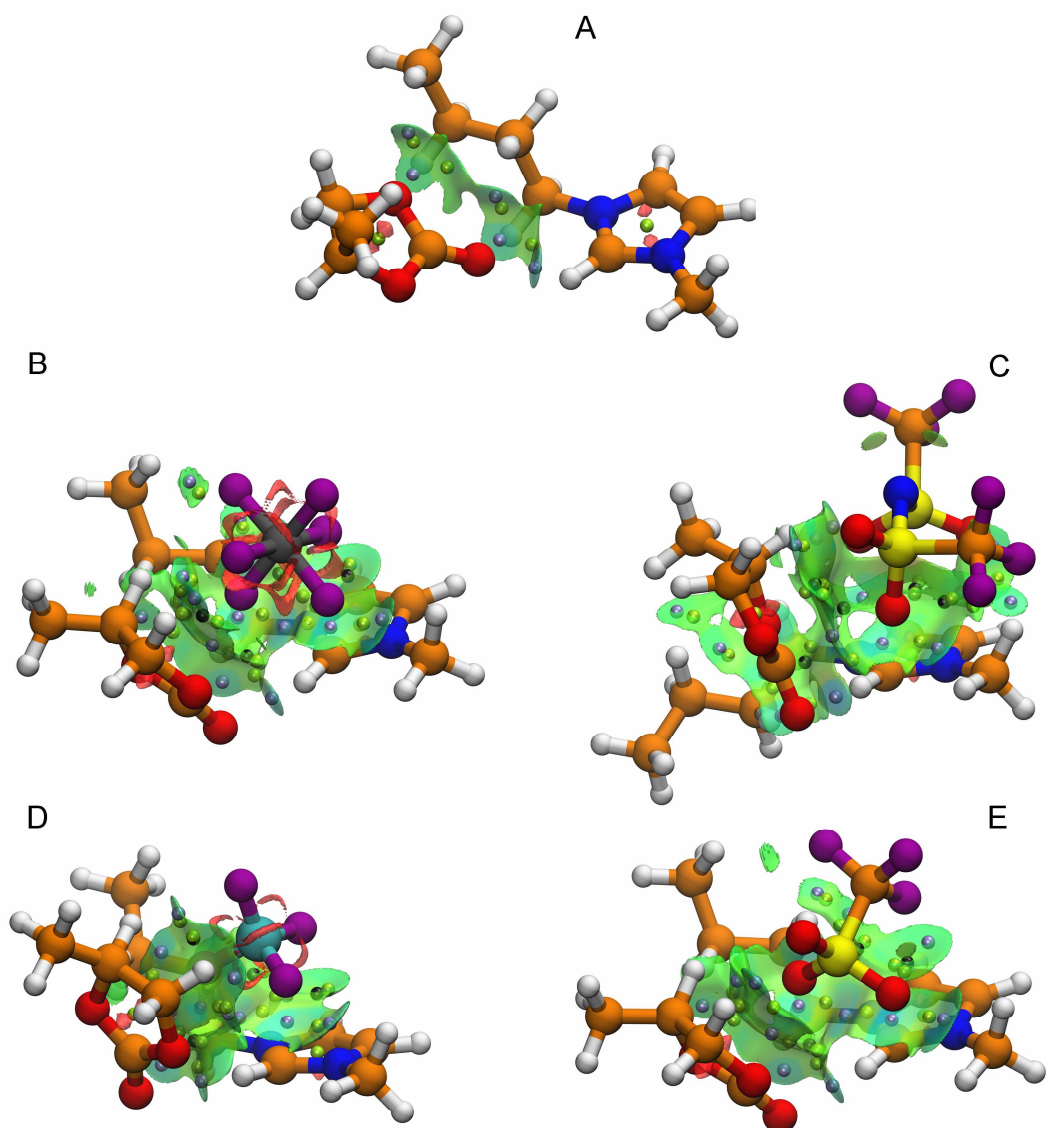


Figure 3.27. NCI isosurfaces for the complexes of Bmim^+ (A), BmimPF_6 (B), BmimTFSI (C), BmimBF_4 (D), and BmimTfO (E) with PC molecule obtained at the M06-2X/6-311++g(d,p) level of theory in vacuum. The RDG isovalue is 0.6. The $\text{sign}(\lambda_2)\rho$ value is colormapped onto the isosurfaces in the region from -0.03 a.u. to $+0.03$ a.u. in the blue-green-red palette. QTAIM revealed CPs are depicted as light blue (BCPs), green (RCPs), and black (CCPs) spheres. Color coding of the elements: white – H, orange – C, blue – N, purple – F, cyan – B, gray – P, yellow – S.

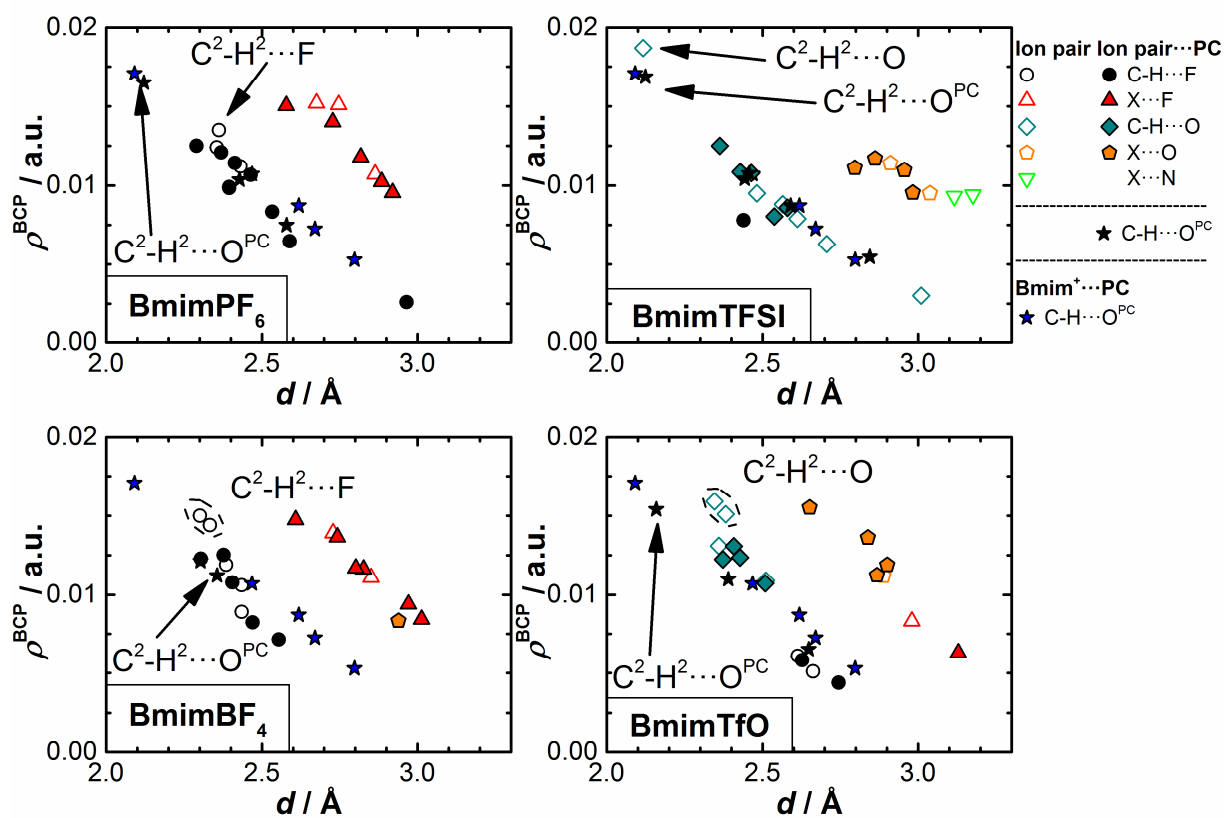


Figure 3.28. The BCP electron density values for the weak noncovalent interactions as a function of distance between the interacting atoms, as revealed by means of QTAIM analysis in the structures of the studied ion pairs, their complexes with PC molecule and the cation...PC complex. X indicates any nonhydrogen atom of the cation, *i.e.*, carbon or nitrogen.

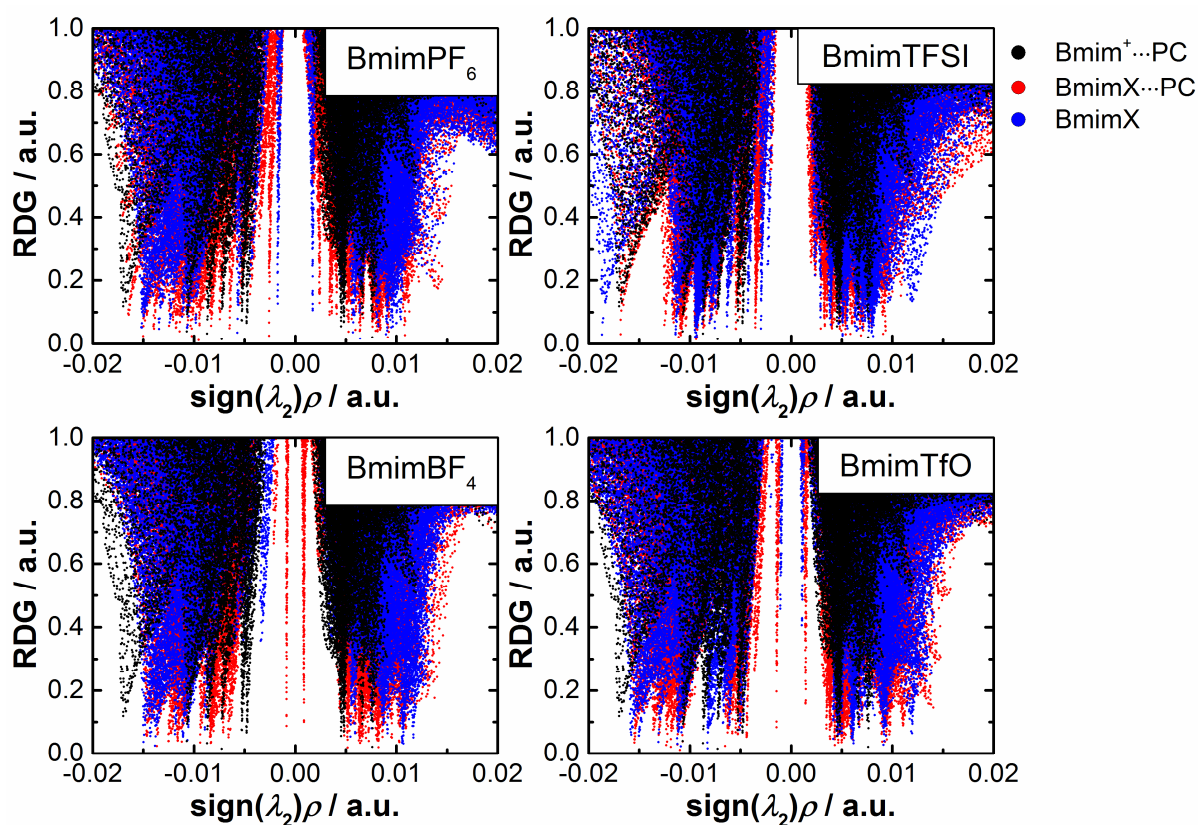


Figure 3.29. The NCI plots for the structures of the studied ion pairs, their complexes with PC molecule and the cation...PC complex.

The QTAIM atomic charges of the hydrogen and carbon atoms of the Bmim⁺ cation in the studied systems are shown in Figure 3.30 and Figure 3.31, respectively. The increase of charge of the C²-H² hydrogen atom when going from the ion pair to the corresponding complex with the PC molecule is similar to what is observed for the solvates with γ -BL and reflects enhanced hydrogen bonding at this site. The lower value of the charge of the C²-H² hydrogen atom in the cation-PC complex compared to the case of γ -BL can be related to the relative strengths of the corresponding hydrogen bonds.

The QTAIM charges of the carbon atom C² slightly decreases and no effective change is observed for the others when going from the ion pair to the complexes with the PC molecule. This result is also very similar to the case of the complexes with γ -BL.

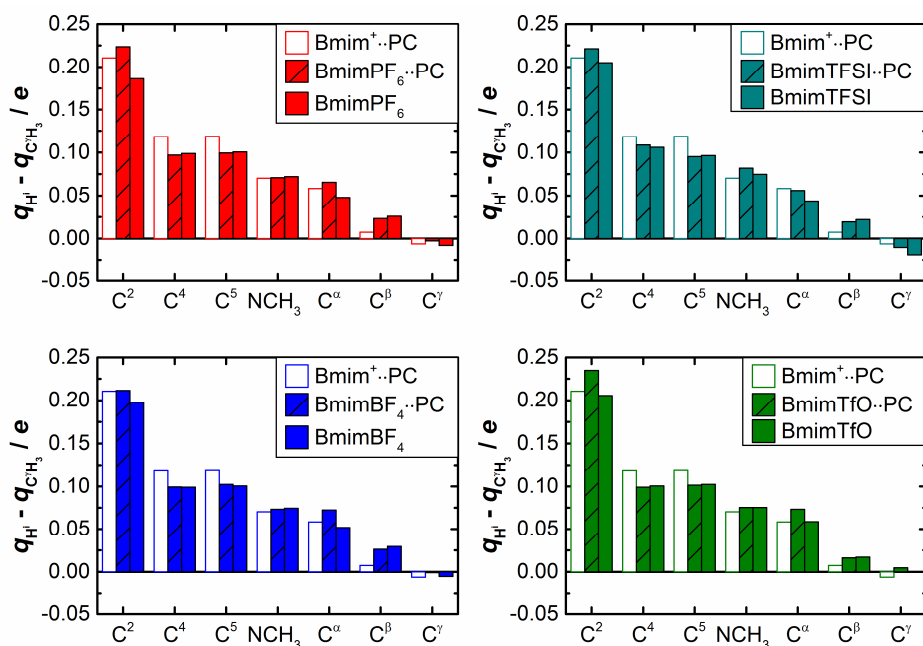


Figure 3.30. QTAIM charges of the hydrogen atoms of Bmim⁺ cations for the studied ion pairs, their complexes with γ -BL molecule and the cation $\cdots\gamma$ -BL complex referenced to the charge of the hydrogen atoms of the terminal methyl group of the butyl chain. Charges of the chemically equivalent hydrogen atoms of CH₂ and CH₃ groups are averaged.

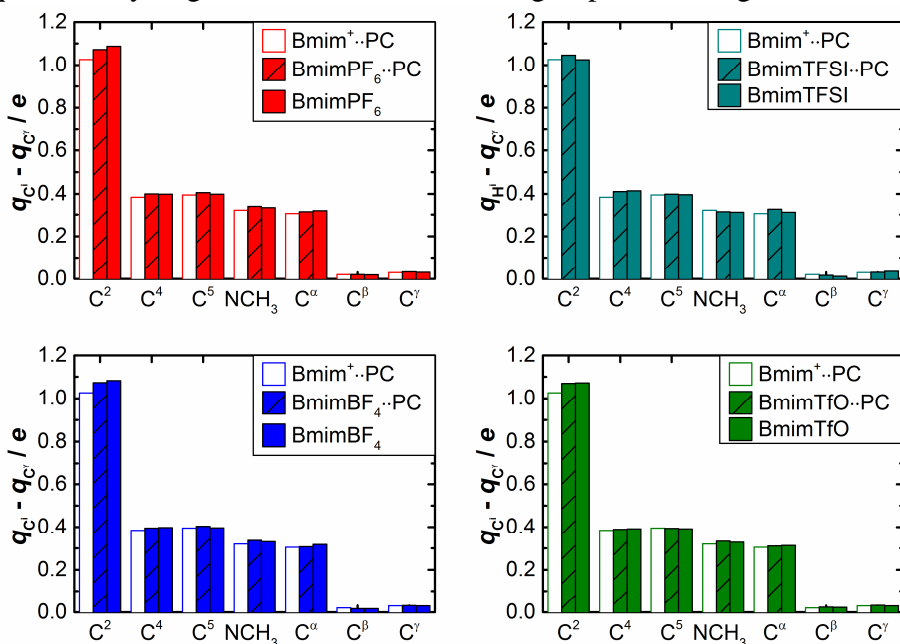


Figure 3.31. QTAIM charges of the carbon atoms of Bmim⁺ cations for the studied ion pairs, their complexes with γ -BL molecule and the cation $\cdots\gamma$ -BL complex referenced to the charge of the carbon atom of the terminal methyl group of the butyl chain.

3.4. Conclusions

Quantum chemical calculations of the representative structures of model clusters of ILs and their complexes with the solvent molecules have been used to analyze the main structural features and interactions. These systems are considered as model ones which, despite limited size, can help to gather the most relevant information for subsequent interpretation of spectroscopic data on IL-molecular solvent mixtures.

Advanced methods of analysis of the electron density distribution and of the weak noncovalent interactions have been employed to capture the details and relative strength of hydrogen bonds and other types of weak interactions in the studied systems.

All the studied ILs reveal the ion pair configuration with anion positioned on top of the C²-H² fragment as the most stable one. In this configuration anions form weak interionic electrostatic hydrogen bonds with the C²-H² imidazolium ring hydrogen atom. Slightly weaker hydrogen bonds are also established with the hydrogen atoms of the adjacent alkyl groups. In larger aggregates, hydrogen bonding at the C⁴⁻⁵-H⁴⁻⁵ sites is observed. In BmimTfO and BmimTFSI, the higher strength of the hydrogen bond at the C²-H² site is more apparent than in the case of BmimBF₄ and BmimPF₆. Apart from the localized hydrogen bonding interactions, there are multiple delocalized weak noncovalent interactions between the counterions.

Upon addition of a solvent molecule the native ion pair structure becomes distorted. The interionic interactions with the C²-H² fragment of the cation are weakened and the new hydrogen bonds with the solvent molecule are established. Solvent molecules also interact with the alkyl hydrogen atoms adjacent to the imidazolium ring. Among the selected solvents, the magnitude of this effect

follows the order AN < PC < γ -BL. BmimPF₆ and BmimTFSI ILs are found to be more sensitive compared to BmimBF₄ and BmimTfO.

Strengthening of hydrogen bonding at a given site leads to the increase of the charge of the corresponding hydrogen atom. A complex pattern of redistribution of the electron density on the adjacent groups can also be observed. Particularly, the charge of the C² carbon atom decreases when hydrogen bond is formed at the C²-H² site.

3.5. References for Chapter 3

- (1) Kirchner, B., Ionic liquids from theoretical investigations. In *Ionic Liquids*, Kirchner, B., Ed. Springer-Verlag: Berlin/Heidelberg, 2010; Vol. 290, pp 213-262.
- (2) Zahn, S.; Brehm, M.; Brüssel, M.; Hollóczki, O.; Kohagen, M.; Lehmann, S.; Malberg, F.; Pensado, A. S.; Schöppke, M.; Weber, H.; Kirchner, B., Understanding ionic liquids from theoretical methods. *J. Mol. Liq.* **2014**, *192*, 71-76.
- (3) Chaban, V. V.; Prezhdo, O. V., Ionic and Molecular Liquids: Working Together for Robust Engineering. *J. Phys. Chem. Lett.* **2013**, *4*, 1423-1431.
- (4) Koßmann, S.; Thar, J.; Kirchner, B.; Hunt, P. A.; Welton, T., Cooperativity in ionic liquids. *J. Chem. Phys.* **2006**, *124*, 174506.
- (5) Palomar, J.; Ferro, V. R.; Gilarranz, M. A.; Rodriguez, J. J., Computational Approach to Nuclear Magnetic Resonance in 1-Alkyl-3-methylimidazolium Ionic Liquids. *J. Phys. Chem. B* **2007**, *111*, 168-180.
- (6) Chen, S.; Vijayaraghavan, R.; MacFarlane, D. R.; Izgorodina, E. I., Ab Initio Prediction of Proton NMR Chemical Shifts in Imidazolium Ionic Liquids. *J. Phys. Chem. B* **2013**, *117*, 3186-3197.
- (7) Dong, K.; Song, Y.; Liu, X.; Cheng, W.; Yao, X.; Zhang, S., Understanding Structures and Hydrogen Bonds of Ionic Liquids at the Electronic Level. *J. Phys. Chem. B* **2012**, *116*, 1007-1017.
- (8) Katsyuba, S. A.; Zvereva, E. E.; Vidiš, A.; Dyson, P. J., Application of Density Functional Theory and Vibrational Spectroscopy Toward the Rational Design of Ionic Liquids. *J. Phys. Chem. A* **2006**, *111*, 352-370.
- (9) Heimer, N. E.; Del Sesto, R. E.; Meng, Z.; Wilkes, J. S.; Carper, W. R., Vibrational spectra of imidazolium tetrafluoroborate ionic liquids. *J. Mol. Liq.* **2006**, *124*, 84-95.
- (10) Tsuzuki, S.; Tokuda, H.; Hayamizu, K.; Watanabe, M., Magnitude and Directionality of Interaction in Ion Pairs of Ionic Liquids: Relationship with Ionic Conductivity. *J. Phys. Chem. B* **2005**, *109*, 16474-16481.
- (11) Hunt, P. A.; Gould, I. R.; Kirchner, B., The Structure of Imidazolium-Based Ionic Liquids: Insights From Ion-Pair Interactions. *Aust. J. Chem.* **2007**, *60*, 9-14.
- (12) Gao, Y.; Zhang, L.; Wang, Y.; Li, H., Probing Electron Density of H-Bonding between Cation–Anion of Imidazolium-Based Ionic Liquids with Different Anions by Vibrational Spectroscopy. *J. Phys. Chem. B* **2010**, *114*, 2828-2833.
- (13) Dong, K.; Zhang, S.; Wang, D.; Yao, X., Hydrogen Bonds in Imidazolium Ionic Liquids. *J. Phys. Chem. A* **2006**, *110*, 9775-9782.
- (14) Zhang, L.; Wang, Y.; Xu, Z.; Li, H., Comparison of the Blue-Shifted C–D Stretching Vibrations for DMSO-*d*₆ in Imidazolium-Based Room Temperature Ionic Liquids and in Water. *J. Phys. Chem. B* **2009**, *113*, 5978-5984.
- (15) Danten, Y.; Cabaço, M. I.; Besnard, M., Interaction of Water Highly Diluted in 1-Alkyl-3-methyl Imidazolium Ionic Liquids with the PF₆⁻ and BF₄⁻ Anions. *J. Phys. Chem. A* **2009**, *113*, 2873-2889.
- (16) Zheng, Y.-Z.; Wang, N.-N.; Luo, J.-J.; Zhou, Y.; Yu, Z.-W., Hydrogen-Bonding Interactions between [BMIM][BF₄] and Acetonitrile. *Phys. Chem. Chem. Phys.* **2013**, *15*, 18055-18064.
- (17) Cha, S.; Ao, M.; Sung, W.; Moon, B.; Ahlstrom, B.; Johansson, P.; Ouchi, Y.; Kim, D., Structures of ionic liquid-water mixtures investigated by IR and NMR spectroscopy. *Phys. Chem. Chem. Phys.* **2014**, *16*, 9591-9601.

- (18) Hu, X.; Lin, Q.; Gao, J.; Wu, Y.; Zhang, Z., Anion–cation and ion–solvent interaction of some typical ionic liquids in solvents with different dielectric constant. *Chem. Phys. Lett.* **2011**, *516*, 35-39.
- (19) Cremer, T.; Kolbeck, C.; Lovelock, K. R. J.; Paape, N.; Wölfel, R.; Schulz, P. S.; Wasserscheid, P.; Weber, H.; Thar, J.; Kirchner, B.; Maier, F.; Steinrück, H.-P., Towards a Molecular Understanding of Cation-Anion Interactions-Probing the Electronic Structure of Imidazolium Ionic Liquids by NMR Spectroscopy, X-ray Photoelectron Spectroscopy and Theoretical Calculations. *Chem. – Eur. J.* **2010**, *16*, 9018-9033.
- (20) Hardacre, C.; Holbrey, J. D.; Nieuwenhuyzen, M.; Youngs, T. G. A., Structure and Solvation in Ionic Liquids. *Acc. Chem. Res.* **2007**, *40*, 1146-1155.
- (21) Hardacre, C.; Holbrey, J. D.; Mullan, C. L.; Youngs, T. G. A.; Bowron, D. T., Small angle neutron scattering from 1-alkyl-3-methylimidazolium hexafluorophosphate ionic liquids ([C_nmim][PF₆], n=4, 6, and 8). *J. Chem. Phys.* **2010**, *133*, -.
- (22) Dhupal, N. R.; Noack, K.; Kiefer, J.; Kim, H. J., Molecular Structure and Interactions in the Ionic Liquid 1-Ethyl-3-methylimidazolium Bis(Trifluoromethylsulfonyl)imide. *J. Phys. Chem. A* **2014**, *118*, 2547-2557.
- (23) Köddermann, T.; Wertz, C.; Heintz, A.; Ludwig, R., Ion-Pair Formation in the Ionic Liquid 1-Ethyl-3-methylimidazolium Bis(triflyl)imide as a Function of Temperature and Concentration. *ChemPhysChem* **2006**, *7*, 1944-1949.
- (24) Housaindokht, M. R.; Hosseini, H. E.; Sadeghi Googheri, M. S.; Monhemi, H.; Najafabadi, R. I.; Ashraf, N.; Gholizadeh, M., Hydrogen bonding investigation in 1-ethyl-3-methylimidazolium based ionic liquids from density functional theory and atoms-in-molecules methods. *J. Mol. Liq.* **2013**, *177*, 94-101.
- (25) Obi, E. I.; Leavitt, C. M.; Raston, P. L.; Moradi, C. P.; Flynn, S. D.; Vaghjiani, G. L.; Boatz, J. A.; Chambreau, S. D.; Douberly, G. E., Helium Nanodroplet Isolation and Infrared Spectroscopy of the Isolated Ion-Pair 1-Ethyl-3-methylimidazolium bis(trifluoromethylsulfonyl)imide. *J. Phys. Chem. A* **2013**, *117*, 9047-9056.
- (26) Cooper, R.; Zolot, A. M.; Boatz, J. A.; Sporleder, D. P.; Stearns, J. A., IR and UV Spectroscopy of Vapor-Phase Jet-Cooled Ionic Liquid [emim]⁺[Tf₂N]⁻: Ion Pair Structure and Photodissociation Dynamics. *J. Phys. Chem. A* **2013**, *117*, 12419-12428.
- (27) Martinelli, A.; Matic, A.; Johansson, P.; Jacobsson, P.; Börjesson, L.; Fericola, A.; Panero, S.; Scrosati, B.; Ohno, H., Conformational evolution of TFSI⁻ in protic and aprotic ionic liquids. *J. Raman. Spectrosc.* **2011**, *42*, 522-528.
- (28) Fujii, K.; Fujimori, T.; Takamuku, T.; Kanzaki, R.; Umebayashi, Y.; Ishiguro, S.-i., Conformational Equilibrium of Bis(trifluoromethanesulfonyl) Imide Anion of a Room-Temperature Ionic Liquid: Raman Spectroscopic Study and DFT Calculations. *J. Phys. Chem. B* **2006**, *110*, 8179-8183.
- (29) Deetlefs, M.; Hardacre, C.; Nieuwenhuyzen, M.; Padua, A. A. H.; Sheppard, O.; Soper, A. K., Liquid Structure of the Ionic Liquid 1,3-Dimethylimidazolium Bis{(trifluoromethyl)sulfonyl}amide. *J. Phys. Chem. B* **2006**, *110*, 12055-12061.
- (30) Akai, N.; Kawai, A.; Shibuya, K., Ion-Pair Structure of Vaporized Ionic Liquid Studied by Matrix-Isolation FTIR Spectroscopy with DFT Calculations: A Case of 1-Ethyl-3-methylimidazolium Trifluoromethanesulfonate. *J. Phys. Chem. A* **2010**, *114*, 12662-12666.
- (31) Danten, Y.; Cabaço, M. I.; Besnard, M., Interaction of water diluted in 1-butyl-3-methylimidazolium ionic liquids by vibrational spectroscopy modeling. *J. Mol. Liq.* **2010**, *153*, 57-66.
- (32) Matthews, R. P.; Ashworth, C.; Tom, W.; Patricia, A. H., The impact of anion electronic structure: similarities and differences in imidazolium based ionic liquids. *J. Phys.: Condens. Matter* **2014**, *26*, 284112.

- (33) Hunt, P. A.; Kirchner, B.; Welton, T., Characterising the electronic structure of ionic liquids: an examination of the 1-butyl-3-methylimidazolium chloride ion pair. *Chem. – Eur. J.* **2006**, *12*, 6762-6775.
- (34) Hunt, P. A.; Gould, I. R., Structural characterization of the 1-butyl-3-methylimidazolium chloride ion pair using ab initio methods. *J. Phys. Chem. A* **2006**, *110*, 2269-2282.
- (35) Krekeler, C.; Schmidt, J.; Zhao, Y. Y.; Qiao, B.; Berger, R.; Holm, C.; Delle Site, L., Study of 1,3-dimethylimidazolium chloride with electronic structure methods and force field approaches. *J. Chem. Phys.* **2008**, *129*, -.
- (36) Matthews, R. P.; Welton, T.; Hunt, P. A., Competitive pi interactions and hydrogen bonding within imidazolium ionic liquids. *Phys. Chem. Chem. Phys.* **2014**, *16*, 3238-3253.
- (37) Tsuzuki, S.; Arai, A. A.; Nishikawa, K., Conformational Analysis of 1-Butyl-3-methylimidazolium by CCSD(T) Level Ab Initio Calculations: Effects of Neighboring Anions. *J. Phys. Chem. B* **2008**, *112*, 7739-7747.
- (38) Canongia Lopes, J. N. A.; Pádua, A. A. H., Using Spectroscopic Data on Imidazolium Cation Conformations To Test a Molecular Force Field for Ionic Liquids. *J. Phys. Chem. B* **2006**, *110*, 7485-7489.
- (39) Emel'yanenko, V. N.; Verevkin, S. P.; Heintz, A., The Gaseous Enthalpy of Formation of the Ionic Liquid 1-Butyl-3-methylimidazolium Dicyanamide from Combustion Calorimetry, Vapor Pressure Measurements, and Ab Initio Calculations. *J. Am. Chem. Soc.* **2007**, *129*, 3930-3937.
- (40) Ozawa, R.; Hayashi, S.; Saha, S.; Kobayashi, A.; Hamaguchi, H.-o., Rotational Isomerism and Structure of the 1-Butyl-3-methylimidazolium Cation in the Ionic Liquid State. *Chemistry Letters* **2003**, *32*, 948-949.
- (41) Hayashi, S.; Ozawa, R.; Hamaguchi, H.-o., Raman Spectra, Crystal Polymorphism, and Structure of a Prototype Ionic-liquid [bmim]Cl. *Chemistry Letters* **2003**, *32*, 498-499.
- (42) Umabayashi, Y.; Hamano, H.; Tsuzuki, S.; Canongia Lopes, J. N.; Pádua, A. A. H.; Kameda, Y.; Kohara, S.; Yamaguchi, T.; Fujii, K.; Ishiguro, S.-i., Dependence of the Conformational Isomerism in 1-n-Butyl-3-methylimidazolium Ionic Liquids on the Nature of the Halide Anion. *J. Phys. Chem. B* **2010**, *114*, 11715-11724.
- (43) Katayanagi, H.; Hayashi, S.; Hamaguchi, H.-o.; Nishikawa, K., Structure of an ionic liquid, 1-n-butyl-3-methylimidazolium iodide, studied by wide-angle X-ray scattering and Raman spectroscopy. *Chem. Phys. Lett.* **2004**, *392*, 460-464.
- (44) Hatano, N.; Takekiyo, T.; Abe, H.; Yoshimura, Y., Effect of Counteranions on the Conformational Equilibrium of 1-Butyl-3-methylimidazolium-Based Ionic Liquids. *Int. J. Spectrosc.* **2011**, *2011*.
- (45) Koch, U.; Popelier, P. L. A., Characterization of C-H-O hydrogen bonds on the basis of the charge density. *J. Phys. Chem.* **1995**, *99*, 9747-9754.
- (46) Grabowski, S. J., What Is the Covalency of Hydrogen Bonding? *Chem. Rev.* **2011**, *111*, 2597-2625.
- (47) Mao, J. X.; Lee, A. S.; Kitchin, J. R.; Nulwala, H. B.; Luebke, D. R.; Damodaran, K., Interactions in 1-ethyl-3-methyl imidazolium tetracyanoborate ion pair: Spectroscopic and density functional study. *J. Mol. Struct.* **2013**, *1038*, 12-18.
- (48) Shakourian-Fard, M.; Jamshidi, Z.; Bayat, A.; Fattahi, A., Structural and electronic properties of alkyl-trifluoroborate based ionic liquids: A theoretical study. *J. Fluorine Chem.* **2013**, *153*, 96-100.
- (49) Ochterski, J. W., Thermochemistry in gaussian. **2000**.
- (50) Kalugin, O. N.; Voroshylova, I. V.; Riabchunova, A. V.; Lukinova, E. V.; Chaban, V. V., Conductometric Study of Binary Systems Based on Ionic Liquids and Acetonitrile in a wide Concentration Range. *Electrochim. Acta* **2013**, *105*, 188-199.

- (51) Bešter-Rogač, M.; Stoppa, A.; Buchner, R., Ion Association of Imidazolium Ionic Liquids in Acetonitrile. *J. Phys. Chem. B* **2014**, *118*, 1426-1435.
- (52) Cabaço, M. I.; Besnard, M.; Danten, Y.; Coutinho, J. A. P., Solubility of CO₂ in 1-Butyl-3-methyl-imidazolium-trifluoro Acetate Ionic Liquid Studied by Raman Spectroscopy and DFT Investigations. *J. Phys. Chem. B* **2011**, *115*, 3538-3550.
- (53) Izgorodina, E. I.; Rigby, J.; MacFarlane, D. R., Large-scale ab initio calculations of archetypical ionic liquids. *Chem. Commun.* **2012**, *48*, 1493-1495.
- (54) Dupont, J., On the solid, liquid and solution structural organization of imidazolium ionic liquids. *J. Braz. Chem. Soc.* **2004**, *15*, 341-350.
- (55) Zhang, Q.-G.; Wang, N.-N.; Yu, Z.-W., The Hydrogen Bonding Interactions between the Ionic Liquid 1-Ethyl-3-Methylimidazolium Ethyl Sulfate and Water. *J. Phys. Chem. B* **2010**, *114*, 4747-4754.
- (56) Zhang, Q.-G.; Wang, N.-N.; Wang, S.-L.; Yu, Z.-W., Hydrogen Bonding Behaviors of Binary Systems Containing the Ionic Liquid 1-Butyl-3-methylimidazolium Trifluoroacetate and Water/Methanol. *J. Phys. Chem. B* **2011**, *115*, 11127-11136.
- (57) He, H.; Chen, H.; Zheng, Y.; Zhang, X.; Yao, X.; Yu, Z.; Zhang, S., The Hydrogen-Bonding Interactions between 1-Ethyl-3-Methylimidazolium Lactate Ionic Liquid and Methanol. *Aust. J. Chem.* **2013**, *66*, 50-59.
- (58) Chang, H.-C.; Jiang, J.-C.; Chang, C.-Y.; Su, J.-C.; Hung, C.-H.; Liou, Y.-C.; Lin, S. H., Structural Organization in Aqueous Solutions of 1-Butyl-3-methylimidazolium Halides: A High-Pressure Infrared Spectroscopic Study on Ionic Liquids. *J. Phys. Chem. B* **2008**, *112*, 4351-4356.

3.6. Chapter 3 appendix

Table A 3.1. The main parameters of weak noncovalent interactions as obtained by means of QTAIM analysis of the optimized in vacuum ion pair structures of the studied ILs

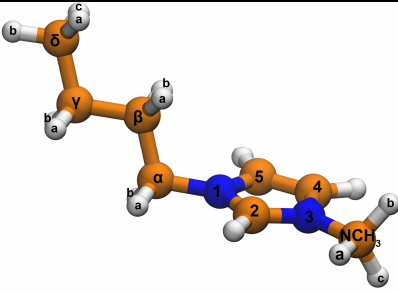
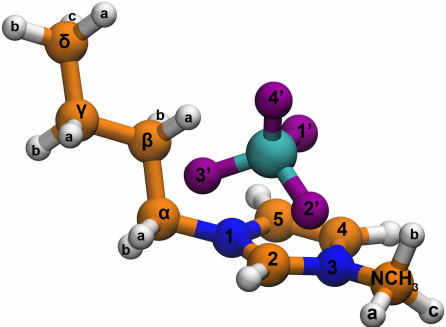
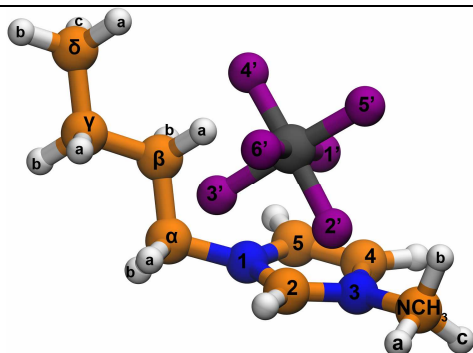
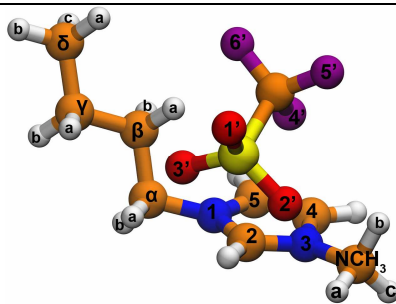
Interacting atoms	Interatomic distance / Å	Angle (C-H...X) / deg	ρ / a.u.	$\Delta\rho$ / a.u.	H / a.u.	ε
						
RCP N ¹ -C ² -N ³ -C ⁴ -C ⁵	1.079		0.2878			
			0.0567	0.4175	0.0063	
						
Interacting atoms	Interatomic distance / Å	Angle (C-H...X) / deg	ρ / a.u.	$\Delta\rho$ / a.u.	H / a.u.	ε
BCPs						
C ^β -H ^a ...F ^{1'}	2.435	144.279	0.0089	0.0325	0.0010	0.0203
C ^β -H ^a ...F ^{3'}	2.435	112.897	0.0106	0.0411	0.0012	0.3467
NCH ₃ ...F ^{2'}	2.851	-	0.0111	0.0486	0.0015	1.3671
C ^α -H ^a ...F ^{3'}	2.385	108.679	0.0119	0.0478	0.0013	0.3231
C ² ...F ^{1'}	2.729	-	0.0139	0.0552	0.0011	0.4213
C ² -H ² ...F ^{3'}	2.333	103.181	0.0144	0.0597	0.0018	0.4261
C ² -H ² ...F ^{2'}	2.301	104.268	0.0150	0.0622	0.0018	0.4382
RCPs						
F ^{1'} -C ² -N ¹ -C ^α -C ^β -C ^β H ^a			0.0059	0.02424	0.0009	
F ^{3'} -C ^β H ^a -F ^{1'} -B			0.0076	0.0340	0.0013	
F ^{3'} -C ^α H ^a -C ^α -N ¹ -C ² -H ²			0.0087	0.0417	0.0017	
F ^{2'} -NCH ₃ -N ³ -C ² -H ²			0.0087	0.0425	0.0018	
F ^{3'} -C ^β H ^a -C ^β -C ^α -C ^α H ^a			0.0091	0.0432	0.0017	
F ^{3'} -H ² -C ² -F ^{1'} -B			0.0106	0.0516	0.0019	
F ^{2'} -H ² -C ² -F ^{1'} -B			0.0107	0.0517	0.0018	
F ^{2'} -H ² -C ³ -F ^{3'} -B			0.0117	0.0571	0.0020	
N ¹ -C ² -N ³ -C ⁴ -C ⁵			0.0570	0.4191	0.0063	
CCPs						
H ² -C ² -N ¹ -C ^α -C ^α H ^a -C ^β -C ^β H ^a			0.0055	0.0260	0.0012	
F ^{1'} -F ^{3'} -B						
H ² -C ² -F ^{1'} -F ^{2'} -F ^{3'} -B			0.0106	0.0528	0.0020	

Table A 3.1 continued.



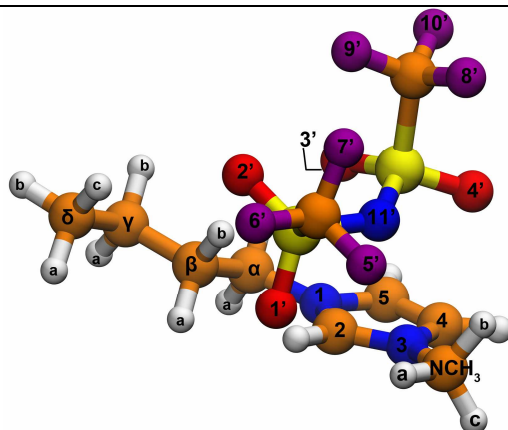
Interacting atoms	Interatomic distance / Å	Angle (C-H...X) / deg	ρ / a.u.	$\Delta\rho$ / a.u.	H / a.u.	ϵ
BCPs						
C ^β -H ^a ...F ^{1'}	2.395	131.466	0.0099	0.0359	0.0010	0.0203
NCH ₃ ...F ^{2'}	2.864	-	0.0107	0.0476	0.0016	0.3467
C ^β -H ^a ...F ^{3'}	2.431	121.928	0.0112	0.0440	0.0012	1.3671
C ^α H ^a ...F ^{3'}	2.355	104.894	0.0124	0.0521	0.0015	0.3231
C ² -H ² ...F ^{2'}	2.362	95.826	0.0135	0.0548	0.0015	0.4213
C ² ...F ^{3'}	2.747	-	0.0151	0.0617	0.0016	0.4261
C ² ...F ^{1'}	2.676	-	0.0152	0.0616	0.0010	0.4382
RCPs						
C ² -N ¹ -C ^α -C ^β -C ^β H ^a -F ^{1'}			0.0064	0.0271	0.0010	
C ^β H ^a -F ^{1'} -P-F ^{3'}			0.0081	0.0355	0.0011	
C ² -C ² H ² -F ^{2'} -NCH ₃ -N ³			0.0082	0.0408	0.0017	
C ² -N ¹ -C ^α -C ^α H ^a -F ^{3'}			0.0091	0.0454	0.0018	
C ² -C ² H ² -F ^{2'} -P-F ^{1'}			0.0095	0.0457	0.0014	
C ^α H ^a -C ^α -C ^β -C ^β H ^a -F ^{3'}			0.0096	0.0472	0.0018	
C ² -F ^{1'} -P-F ^{3'}			0.0100	0.0475	0.0014	
C ² -C ² H ² -F ^{2'} -P-F ^{3'}			0.0104	0.0506	0.0016	
N ¹ -C ² -N ³ -C ⁴ -C ⁵			0.0570	0.4191	0.0063	
CCPs						
C ² -N ¹ -C ^α -C ^β -C ^α H ^a -C ^β H ^b -P-F ^{1'} -F ^{3'}			0.0059	0.0284	0.0012	
C ² -C ² H ² -P-F ^{1'} -F ^{2'} -F ^{3'}			0.0090	0.0482	0.0019	

Table A 3.1 continued.



Interacting atoms	Interatomic distance / Å	Angle (C-H...X) / deg	ρ / a.u.	$\Delta\rho$ / a.u.	H / a.u.	ϵ
BCPs						
C ^{β} H ^a ...F ^{6'}	2.663	168.107	0.0051	0.0197	0.0008	0.2697
C ^{β} H ^a ...F ^{4'}	2.613	143.468	0.0061	0.0228	0.0008	0.0643
N ³ ...F ^{4'}	2.980	-	0.0083	0.0360	0.0012	7.4919
C ^{β} H ^a ...O ^{3'}	2.511	110.432	0.0109	0.0384	0.0012	0.3117
NCH ₃ ...O ^{2'}	2.889	-	0.0112	0.0486	0.0018	1.5216
C ^{α} H ^a ...O ^{3'}	2.360	111.419	0.0131	0.0515	0.0018	0.3185
C ² H ^a ...O ^{3'}	2.382	104.222	0.0151	0.0564	0.0016	0.6318
C ² H ^a ...O ^{2'}	2.346	105.354	0.0159	0.0595	0.0017	0.6176
RCPs						
N ¹ -C ^{α} -C ^{β} -C ^{β} H ^a			0.0045	0.0185	0.0008	
F ^{4'} -C ^{β} H ^a -F ^{6'} -C			0.0048	0.0211	0.0010	
O ^{2'} -C ^{β} H ^a -O ^{3'} -S-C			0.0050	0.0207	0.0009	
N ³ -C ² -C ² H ² -O ^{2'} -S-C-F ^{4'}			0.0062	0.0256	0.0010	
C ^{α} H ^a -C ² -C ² H ² -O ^{2'} -NCH ₃			0.0091	0.0420	0.0017	
C ² -N ¹ -C ^{α} -C ^{α} H ^a -O ^{3'} -C ² H ²			0.0092	0.0421	0.0016	
F ^{4'} -C ^{α} -C ^{β} -C ^{β} H ^a -O ^{3'}			0.0094	0.0427	0.0017	
N ³ -C ² H ² -O ^{3'} -S			0.0120	0.0522	0.0016	
N ¹ -C ² -N ³ -C ⁴ -C ⁵			0.0569	0.4182	0.0062	
CCPs						
C ² -N ¹ -C ² H ² -C ^{α} -C ^{β} -C ^{α} H ^a -C ^{β} H ^a -N ³ -C-S-O ^{3'} -O ^{2'} -F ^{4'}			0.0042	0.0180	0.0008	

Table A 3.1 continued.



Interacting atoms	Interatomic distance / Å	Angle (C-H...X) / deg	ρ / a.u.	$\Delta\rho$ / a.u.	H / a.u.	ϵ
BCPs						
C ^δ H ^c ...O ^{2'}	3.010	141.817	0.0030	0.0115	0.0006	0.9248
NCH ₃ ^a ...O ^{1'}	2.707	136.817	0.0063	0.0209	0.0006	0.0994
NCH ₃ ^b ...O ^{4'}	2.612	122.244	0.0079	0.0274	0.0008	0.3453
C ^β H ^b ...O ^{3'}	2.565	122.829	0.0088	0.0296	0.0009	0.2085
NCH ₃ ...N ^{11'}	3.116	-	0.0093	0.0350	0.0013	1.1857
C ² ...N ^{11'}	3.176	-	0.0094	0.0280	0.0007	0.9552
C ⁴ ...O ^{4'}	3.038	-	0.0095	0.0319	0.0008	3.1725
C ^β H ^b ...O ^{2'}	2.482	162.811	0.0095	0.0291	0.0008	0.1036
N ¹ ...O ^{3'}	2.911	-	0.0114	0.0405	0.0010	0.6375
C ² H ² ...O ^{1'}	2.117	142.100	0.0187	0.0709	0.0024	0.0261
RCPs						
C ^β -C ^β H ^b -O ^{2'} -C ^δ H ^c -C ^δ -C ^γ			0.0029	0.0117	0.0006	
N ^{11'} -S-C-F ^{7'} -F ^{9'} -C-S			0.0038	0.0190	0.0010	
N ¹ -C ⁵ -C ⁵ H ⁵ -O ^{1'} -S-O ^{2'} -C ^β H ^b -C ^β -C ^α			0.0051	0.0171	0.0006	
NCH ₃ -NCH ₃ ^a -O ^{1'} -S-N ^{11'}			0.0055	0.0212	0.0007	
C ² -N ³ -NCH ₃ -NCH ₃ ^a -O ^{1'} -C ² H ²			0.0056	0.0218	0.0009	
C ^β H ^b -O ^{2'} -S-N ^{11'} -S-O ^{3'}			0.0056	0.0200	0.0007	
NCH ₃ -NCH ₃ ^b -O ^{4'} -S-N ^{11'}			0.0065	0.0265	0.0010	
N ^{11'} -S-O ^{2'} -F ^{9'} -C-S			0.0066	0.0286	0.0009	
N ¹ -C ^α -C ^β -C ^β H ^b -O ^{3'}			0.0070	0.0324	0.0013	
N ³ -C ⁴ -O ^{4'} -NCH ₃ ^b -NCH ₃			0.0073	0.0289	0.0009	
C ² -N ³ -C ⁴ -O ^{4'} -S-N ^{11'}			0.0077	0.0286	0.0010	
C ² -C ² H ² -O ^{1'} -S-N ^{11'}			0.0080	0.0300	0.0010	
N ¹ -C ² -N ^{11'} -S-O ^{3'}			0.0080	0.0293	0.0011	
C ² -N ³ -NCH ₃ -N ^{11'}			0.0081	0.0315	0.0011	
N ¹ -C ² -N ³ -C ⁴ -C ⁵			0.0571	0.4191	0.0061	
CCPs						
N ¹ -C ² -C ^α -C ^β -C ² H ² -C ^β H ^b -N ^{11'} -S-S-O ^{2'} -O ^{1'} -O ^{3'}			0.0039	0.0136	0.0006	
C ² -N ³ -NCH ₃ -C ² H ² -NCH ₃ ^a -N ^{11'} -S-O ^{1'}			0.0051	0.0216	0.0009	
C ² -N ³ -C ⁴ -NCH ₃ -NCH ₃ ^b -N ^{11'} -S-O ^{4'}			0.0063	0.0277	0.0011	

Chapter 4. Chemical Shift Variation in IL-Molecular Solvent Mixtures

In order to address the intermolecular interactions the chemical shift variation of ^1H and ^{13}C nuclei was followed in mixtures of imidazolium ILs 1-*n*-butyl-3-methylimidazolium tetrafluoroborate (BmimBF_4), 1-*n*-butyl-3-methylimidazolium hexafluorophosphate (BmimPF_6), 1-*n*-butyl-3-methylimidazolium trifluoromethanesulfonate (BmimTfO) and 1-*n*-butyl-3-methylimidazolium bis(trifluoromethylsulfonyl)imide (BmimTFSI) with acetonitrile (AN), γ -butyrolactone (γ -BL), and propylene carbonate (PC) molecular solvents over the entire composition range at 300 K. The concept of relative chemical shift variation is proposed to assess on a unified and unbiased scale the observed effects of electron density redistribution at different atomic sites of ILs with changing mixture composition.

It was established that hydrogen bonds between the imidazolium ring hydrogen atoms and electronegative atoms of anions are stronger for BmimBF_4 and BmimTfO ILs than those in BmimTFSI and BmimPF_6 . Hydrogen at position 2 of the imidazolium ring is particularly more sensitive to interionic hydrogen bonding than those at positions 4-5 in the case of BmimTFSI and BmimTfO ILs. These hydrogen bonds are disrupted upon dilution in molecular solvents due to ionic dissociation which is more pronounced at high dilutions.

Solvation in γ -BL and PC leads to the formation of hydrogen bonds between the solvent molecules and the imidazolium ring hydrogen atoms which are of comparable strength with the interionic ones. Hydrogen at position 2 of the imidazolium ring is more sensitive to the solvation effects for all the studied ILs. Solvation of the cations of ILs in AN is poorly manifested.

Relative tendencies for ion-pairing and hydrogen bond strengths between the ILs as well as solvating capabilities of the solvents are interpreted with the help of quantum chemical calculations and literature data.

4.1. Introduction

From the very beginning of extensive research on the first generation of chloroaluminate ionic liquids in 1980s¹⁻³ composition dependent chemical shift variation has been used to address various specific interactions (mainly hydrogen bonding, but also stacking and C-H $\cdots\pi$ interactions). Wilkes *et al.* studied mixtures of 1-ethyl-3-methylimidazolium chloride (EmimCl) with varying amounts of AlCl₃ by following the evolution of ¹H-NMR chemical shifts,¹ as well as ²⁷Al and ¹³C chemical shifts.² The observed significant decrease of the chemical shifts of the imidazolium ring atoms, specifically at the position 2, was assigned to the drastic changes in interionic interactions when going from ‘hard’ Cl⁻ anion to ‘soft’, weakly coordinating AlCl₄⁻ and Al₂Cl₇⁻ anions upon addition of AlCl₃.

The same authors also studied this system in the presence of LiCl, N-butylpyridinium chloride and of various molecular solvents.³ They rationalized the observed diminution of chemical shifts of the imidazolium ring protons and to a lesser extent of the adjacent alkyl protons upon addition of a third component as a result of binding of Cl⁻ (in case of LiCl) or due to the screening effect of molecular solvent.

The first thorough investigation of variation of chemical shifts in mixtures of imidazolium ILs with molecular solvents was done by Avent *et al.*⁴ They studied Emim⁺ halides in deuterated acetonitrile (AN-*d*₃) and dichloromethane (CD₂Cl₂) over a wide range of concentrations, as well as solutions in deuterated chloroform (CDCl₃) at a fixed concentration of 2 mol dm⁻³. It was found that for CDCl₃ solutions that the H² signal and the corresponding carbon signal were the most sensitive to the nature of anion, whereas the variations for the other ring sites (hydrogen atoms at positions 4 and 5) were also significant but of lower magnitude.

Concentration studies on AN-*d*₃ solutions revealed for all the halides a maximum of chemical shift with a drastic decrease at very high dilutions. The

effect was more pronounced for the ring hydrogen atoms, specifically for the H² site, but it was still noticeable for the adjacent alkyl protons (C^αH₂ and NCH₃). The largest variation was observed in the case of the chloride anion. In contrast to cation signals, ³⁵Cl and ¹²⁷I chemical shifts revealed monotonic decrease upon dilution at all studied concentrations. The observed variations were interpreted in terms of disruption of interionic hydrogen bonds, especially at high dilutions.

Chemical shift variation in a low-polar CD₂Cl₂ revealed distinctly different trends. H² and H⁴⁻⁵ signals showed the opposite direction of chemical shift drift upon dilution: a decrease for H⁴⁻⁵ and an increase for H². These observations were interpreted in terms of the model of strong aggregation of ion pairs implying anti-parallel stacking of cations, where intermolecular effects of the aromatic ring shielding cone play the main role.

Another important study to mention was conducted by Bonhôte and colleagues⁵ on a series of Emim⁺ salts with anions of different basicity in deuterated acetone (Ac-*d*₆) over a wide range of concentrations. They discovered that for anions of high basicity (containing carboxylic group COO⁻) dilution leads to a slight increase of the H² chemical shift at high concentrations followed by a drastic decrease at high dilutions while H⁴⁻⁵ chemical shifts monotonically decrease over the whole course of dilution. Solutions of ILs containing weakly coordinating anions, in contrast, showed slight monotonic increase of chemical shifts of the imidazolium ring hydrogen atoms upon dilution with Ac-*d*₆. At the same time, the alkyl protons' signals were found to move to higher chemical shift values with decreasing IL concentration independent on the nature of anion.

The observations were rationalized by a model where alkyl hydrogen atoms are only prone to the general dilution effects leading to effective deshielding. Anions of low basicity are considered not to form hydrogen bonds, thus the corresponding imidazolium ring protons follow the same non-specific trend which is observed for the alkyl protons. In contrast, the ring protons of ILs with basic

anions exhibit specific pattern of hydrogen bonding and ionic association which is reflected in the slight shielding of H² proton upon at low dilution due to aromatic stacking effects and strong deshielding at low concentrations due to ionic dissociation effects. The latter are the only one leading to the decrease of the chemical shifts for H⁴⁻⁵.

In the mentioned above studies where the chemical shift variations in IL-solvent mixture was interpreted as a reflection of ionic association equilibria, there was typically a single observed signal that was treated as a population averaged one between the associated and 'free' species. This seems logical since tentative ion-pair lifetimes are considered to be in the (sub)nanosecond range,⁶ while a signal separation of 0.1 ppm in ¹H-NMR spectrum recorded on a 400 MHz instrument would require the corresponding species lifetime to be not less than *ca.* 6 ms.⁷ Nevertheless, Tubbs and Hoffmann⁸ observed two sets of signals in ¹H-NMR spectrum of EmimTFSI dissolved at a fixed concentration in a mixed solvent CDCl₃-CCl₄ or CDCl₃-Ac-*d*₆ with variable composition. Effective static relative dielectric permittivity of solution was changed from 4.3 to 5.62 by varying the composition of the mixed solvent which led to redistribution of intensities between the two sets of signals. The authors considered the two sets of signals to originate from 'free' and ion paired species. Subsequent study by the same group on RmimTFSI in CDCl₃ by means of calorimetric and NMR diffusion measurements⁹ revealed that the two kinds of species distinguished in the NMR spectrum are rather ion pairs and larger aggregates than ion pairs and 'free' ions as it was initially assumed. Two-sets of signal were also observed for solutions of BmimBF₄ in low polar solvent dioxane ($\epsilon = 2.22$).¹⁰

Most of the mentioned above studies (as well as other studies revealed during the literature survey) dealing with concentration dependence of chemical shifts in mixtures 'imidazolium IL-molecular solvent' did not cover wide range of systems in a systematic manner. Among the most remarkable investigations on the

influence of IL (imidazolium cation alkyl chain length and/or nature of anion) on the concentration trends of the chemical shifts of cations over the whole range of compositions it is worthy to mention studies on RmimBF₄/PF₆ with thiophene,¹¹ RmimPF₆ in Ac-*d*₆,¹² RmimBF₄/Cl in H₂O,¹³ RmimTFSI in MeOH-*d*₄,¹⁴ RmimBF₄/MeSO₄/OctSO₄/Cl in D₂O,¹⁵ RmimMeSO₄/MeSO₃/Cl in H₂O,¹⁶ RmimBF₄/OctSO₃/MeSO₄/Cl in ethylene glycol,¹⁷⁻¹⁸ BmimHal/BF₄ in D₂O.¹⁹ Main studies concerning the effect of the nature of solvent on the same issue were conducted on mixtures of RmimTFSI with aromatic solvents,²⁰⁻²² BmimBF₄ with alcohols and amines,²³ BmimPF₆ in a set of polar aprotic solvents.²⁴ As a result, there is still no clear and comprehensive understanding of the influence of the nature of constituents of IL-solvent mixtures on the concentration trends in chemical shifts and, subsequently, on the underlying intermolecular interactions. This applies, particularly, for the mixtures selected for the present study (imidazolium IL with perfluorinated anions + polar molecular solvents).

4.2. Problems of chemical shift referencing

The lack of a unified model, mentioned in the previous paragraph, stems not only from rather scattered and poorly systematized literature data but also from different chemical shift referencing techniques employed. The latter issue causes significant problems in comparing different results if one wishes to rationalize them in a single framework.

Even though ¹H-NMR chemical shift measuring has become a common technique to assess interactions in IL based systems, their accuracy has rarely been discussed. The main issue concerns chemical shift referencing. Since the concentration studies on mixtures of ILs with molecular solvents usually imply rather high concentrations, neither signal of a solvent nor of a reference compound, tetramethylsilane (TMS) or any other, cannot be regarded as non-influenced by intermolecular interactions in the system and hence they cannot serve as an

absolute reference in the so-called internal referencing procedure. Despite this obvious limitation there is an appreciable amount of studies based on interpreting the concentration induced variation of chemical shifts with internal referencing approach. Among the employed internal reference compounds and studied systems to mention there are chlorotrimethylsilane in EmimCl-AlCl₃,¹ TMS in RmimBF₄-Ac-d₆,²⁵ RmimPF₆/HexmimBF₄-Ac-d₆,¹² HexmimBr-Ac-d₆,²⁶ RmimPF₆/HexmimBr/HexmimBF₄-Ac-d₆,²⁷ EmimEtSO₄-D₂O (*though solubility of TMS in D₂O is highly questionable*),²⁸ BmimCF₃CO₂-D₂O/CD₃OD,²⁹ RmimTFSI-Ac-d₆,³⁰ residual protonated solvent in BmimX-CD₂Cl₂,³¹ RmimCl/RmimOAc-DMSO-d₆/D₂O/CD₃OD/CDCl₃,³² BmimX-CD₂Cl₂,³³ and water-soluble analogues of TMS in BmimTFSI-D₂O,³⁴ BmimBF₄-D₂O.³⁵ In order to avoid the problems of internal referencing and also when a researcher wishes to avoid using deuterated solvents, but the experiment requires it for the so-called lock (a special procedure to maintain the constant magnetic field strength during measurements), an external referencing technique is the most frequently used one. In this technique, a coaxial capillary containing the reference compound and lock-solvent is inserted into the NMR tube containing the sample itself (see Figure 4.1). Just as in internal referencing, the deuterated solvent can serve as both lock-compound and chemical shift reference (due to residual protonated solvent molecules for ¹H-NMR).

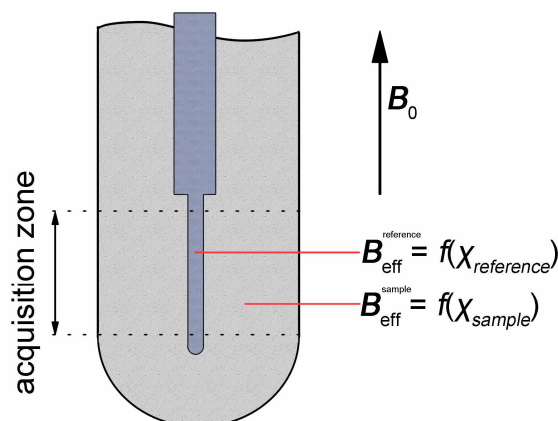


Figure 4.1. Schematic representation of the external referencing setup with a coaxial capillary containing a reference compound/lock-solvent inserted into the NMR tube. The external magnetic field created by spectrometer, characterized by its induction vector B_0 , is aligned with the central axis of the acquisition zone.

However, chemical shifts referenced in this way are inaccurate due to differences in bulk magnetic properties of the sample (see Figure 4.1) and of the contents of the capillary.³⁶⁻³⁷ The observed chemical shift, δ^{obs} , can be presented as following:

$$\delta^{obs} = \delta^{real} + k(\chi_{sample} - \chi_{reference}) \quad (4.1)$$

One can see that correction that connects δ^{obs} with the real value of chemical shift, δ^{real} , which reflects only the differences in shielding between the sample and reference nuclei, depends on geometrical properties of the insert, expressed as a geometrical factor, k , and on the difference in volume magnetic susceptibilities, χ , of the sample and reference media. In general, both geometrical factor and magnetic susceptibility differences are sample-specific. Indeed, the value of k is known *a priori* only for ideal geometrical shapes (sphere, infinite cylinder *etc.*) and in practice it is unique for each capillary and can be estimated in a separate experiment. At the same time, sample's magnetic susceptibility is a function of the

composition and it may vary significantly.* Unfortunately, to the best of our knowledge, at present no systematic data can be found in the literature on magnetic susceptibilities of any ILs except for a narrow class of magnetic ionic liquids, where χ is one of the main characteristics,³⁸ and for EmimTFSI where it was estimated on purpose to correct for the magnetic susceptibility effects.³⁹

As a result, one should be very cautious when interpreting concentration induced drifts of chemical shifts obtained in external referencing approach as they contain also contribution due to variation of the magnetic susceptibility correction. For the studies of ILs with molecular solvents, to the best of our knowledge, the magnetic susceptibility correction has been explicitly taken into account only in studies done by Takamuku *et al.*^{14,21-22,39-41} They employed so-called ‘external double reference’ method⁴²⁻⁴⁴ in which a special capillary insert with a sphere blown out at its bottom is used. Reference compound gives two signals coming from molecules contained in the spherical and cylindrical parts of the capillary.⁴⁵ If the geometrical factor k of a given capillary has been calibrated in advance, then the separation between the two reference signals can be used to correct for the sample’s magnetic susceptibility.^{14,21-22,39-41}

An approach which is free of magnetic susceptibility correction is based on referencing the chemical shifts to one of the signals from the sample without addition of internal reference compound. In this framework the observed chemical shift variation will reflect the relative concentration drift of the shielding of a given nucleus (*i.e.*, the real chemical shift) with respect to the reference one. Hoffmann and co-workers^{16,46-48} used the terminal CH₃ of alkyl chain of Rmim⁺ cation to reference proton chemical shifts in various mixtures of imidazolium IL with

*In private communications with Professor T. Takamuku it was mentioned that for certain mixtures IL+solvent the observed concentration trend of chemical shifts changes its direction after correction for bulk magnetic susceptibility. It is thus evident that the magnitude of the correction can be at least on the order of tens of ppm.

molecular solvents. They assumed on the basis of several conventional external referencing studies that the terminal methyl hydrogen atoms are the least polarizable and do not experience significant changes in microenvironment upon dilution (less than 0.1 ppm), as a result, the observed chemical shifts of the rest of the signals can be considered as close to the real ones when referenced to the terminal methyl group signal. In another work NCH₃ hydrogen atoms of Emim⁺ cation were considered as unperturbed with addition of solvent and the corresponding signal was taken as reference.⁴⁹

Indeed, the real chemical shifts of terminal CH₃ and of NCH₃ hydrogen atoms that were measured by Takamuku and his colleagues vary by 0.3 ppm and 1.0 ppm, respectively, in DodecmimTFSI-C₆H₆ mixture,²¹⁻²² by less than 0.05 ppm each in DodecmimNO₃-D₂O/C₆D₆⁴¹ and in EmimTFSI-H₂O,³⁹ by 0.05 ppm and 0.15 ppm in EmimCl-AN and by 0.07 ppm each in EmimTFSI-MeOH mixtures.⁴⁰ The corresponding ¹³C real chemical shifts, where they were reported,²¹⁻²² exhibited variations of similar magnitude. Thus we may conclude that the choice of terminal methyl hydrogen atoms of Rmim⁺ cations as internal ¹H and ¹³C references is credible for a broad set of combinations ‘imidazolium IL-molecular solvent’. Nevertheless, it is only better than conventional internal referencing approach in the sense that the studied system is not perturbed by addition of a reference compound.

With respect to interpretation of such an internally referenced chemical shift variations with changing concentration, it is noteworthy to mention work of Li *et al.*⁵⁰ who clearly introduced and illustrated for EmimBF₄-H₂O system the concept of ‘relative chemical shift’ as the difference in chemical shifts between two different signals originating from the same compound at a given concentration. The corresponding concentration dependence of the relative chemical shift shows whether the nuclei of interest and reference ones experience the same changes in shielding when concentration is varied or there is some asynchronicity in the

occurring changes of microenvironment of various nuclei. The same strategy was also used by Lyčka *et al.*⁵¹ to follow the relative changes of ¹⁵N chemical shifts of the imidazolium ring nitrogens for several neat RmimX ILs and for BmimBF₄ in several molecular solvents.

This approach is free of doubts and does not require the reference to be an absolute one (*i.e.*, to be unaffected by changes in concentration). In contrast, the concentration trend in the relative chemical shift changes is in essence interpreted as a signature of discrepancy in behavior of nuclear shieldings of a given signal and the reference one as a function of concentration.

However, if one needs to address the concentration induced chemical shift variation for the entire set of signals of particular molecule this approach is impractical since the relative chemical shifts span over a broad range of values (1-10 ppm for ¹H and 10-150 ppm for ¹³C for representative imidazolium IL-based systems) whereas the variations rarely exceed 1 ppm. In order to compare variations of all the signals, *i.e.*, to put them on the same scale, it is proposed to present chemical shifts (either relative or absolute) after subtraction of the corresponding values of chemical shifts at some reference concentration. The reference concentration can be chosen arbitrarily, so far the following options were proposed in the literature: a virtually intermediate concentration,⁵ the lowest employed concentration,⁵²⁻⁵³ or the highest one.^{12,24,26,49,54} However, from the point of view of interpretation, the most relevant reference concentration is that of the corresponding neat compound, and it was the most used whenever a reference concentration approach was employed to address chemical shift variation upon changes in concentration.^{10-11,23,28-29,55-59}

Summarizing the proposed methodologies of analysis of concentration induced chemical shift variations in mixtures of imidazolium ILs with molecular solvents, we come up to the following recommendations:

(i) If possible, one should use the external double reference method to determine concentration dependent chemical shifts of each non-equivalent nuclei i with respect to the corresponding reference compound which are corrected for sample's magnetic susceptibility $\delta_i^{corr}(x)$. In order to carefully examine these chemical shift variations, a reference (subtraction) should also be made with respect to chemical shifts of the neat substance $\Delta\delta_i^{corr}(x) = \delta_i^{corr}(x) - \delta_i^{corr}(x=1)$. This value expresses the concentration dependent variation of the real chemical shift, *i.e.*, direct measure of shielding.

The main disadvantage of this method apart from the high cost and fragility of the special capillary insert is that due to the complex shape of the insert magnetic field homogeneity in the acquisition zone is significantly reduced which leads to strong distortion of the signal shapes and, hence, makes it difficult to determine the actual peak positions.[†]

(ii) If the double external reference capillary insert is not available, then a simple cylindrical capillary (Figure 4.1) with a deuterated solvent should be used to provide for deuterium field-lock. To avoid magnetic susceptibility issues, initial referencing should be done to one of the sample molecule's signal, terminal CH₃ for Rmim⁺ cation and the most shielded group for a solvent (*e.g.*, CH₃ in AN, MeOH)

$$\Delta\delta_i^{\text{CH}_3}(x) = \delta_i^{\text{obs}}(x) - \delta_{\text{CH}_3}^{\text{obs}}(x) = \delta_i^{\text{real}}(x) - \delta_{\text{CH}_3}^{\text{real}}(x) \quad (4.2)$$

We note that our raw experimental data, which was initially externally referenced to the residual HDO in D₂O contained in the capillary insert, showed monotonic increase of ¹H and ¹³C NMR chemical shifts of the terminal methyl

[†]At the end of this experimental stage Professor Takamuku generously provided us with the special capillary inserts for the external-double reference method. In our trial experiments in addition to the mentioned in the text significant signal distortion we could not capture the deuterium lock signal from the insert due to very low volume of the lock/reference-compound contained in the insert inside the acquisition zone of spectrometer.

group upon dilution in all the 12 studied systems by *ca.* 0.3-0.6 ppm. However, the magnitude of magnetic susceptibility correction contributing to this value is unknown.

In mixtures of imidazolium ionic liquids with molecular solvent, upon varying the concentration, it is the ion-ion and the ion-solvent interactions that mainly govern changes in electron density redistribution at molecular level. It is rather well established that these interactions are preferentially located at the imidazolium ring of cations while terminal methyl hydrogen atoms are hardly influenced. An additional indirect proof of inertness of the terminal methyl group of the alkyl chain in Rmim⁺ is given by results of Cremer *et al.*⁶⁰ whose calculations of natural population analysis (NPA) charges for a family of 1-octyl-3-methylimidazolium salts with different anions revealed a rapid exponential decay of the charges of methylene group down to zero when going away from the imidazolium ring.

As it was mentioned above, thus referenced difference in the observed chemical shifts equals to the difference in real chemical shifts. These relative chemical shifts are then put on the same scale by subtracting the corresponding values of the neat substances:

$$\Delta\Delta\delta_i(x) = \Delta\delta_i^{\text{CH}_3}(x) - \Delta\delta_i^{\text{CH}_3}(x=1) \quad (4.3)$$

Thus obtained values reflect how the real chemical shift difference between a given signal and the reference one (originating from the same molecule) changes with concentration. In fact, the relative order of referencing procedures does not matter. Indeed, one can rewrite the expression for $\Delta\Delta\delta_i(x)$ in the following way:

$$\begin{aligned} \Delta\Delta\delta_i(x) &= \Delta\delta_i^{\text{CH}_3}(x) - \Delta\delta_i^{\text{CH}_3}(x=1) = \\ &= \{\delta_i^{\text{obs}}(x) - \delta_{\text{CH}_3}^{\text{obs}}(x)\} - \{\delta_i^{\text{obs}}(x=1) - \delta_{\text{CH}_3}^{\text{obs}}(x=1)\} = \\ &= \{\delta_i^{\text{obs}}(x) - \delta_i^{\text{obs}}(x=1)\} - \{\delta_{\text{CH}_3}^{\text{obs}}(x) - \delta_{\text{CH}_3}^{\text{obs}}(x=1)\} = \\ &= \Delta\delta_i^{\text{obs}}(x) - \Delta\delta_{\text{CH}_3}^{\text{obs}}(x) = \Delta\delta_i^{\text{real}}(x) - \Delta\delta_{\text{CH}_3}^{\text{real}}(x) \end{aligned} \quad (4.4)$$

From this expression it is clear that the value of $\Delta\Delta\delta_i(x)$ can be obtained by initial subtraction of the observed chemical shift values for the corresponding signal of neat component followed by the calculation of difference between the obtained values for a given signal and the reference one (*e.g.*, terminal CH₃). It is worth mentioning again that such treatment of the observed chemical shifts, which are normally referenced to residual protonated species of the lock compound contained in the external capillary, lead to results which are free of magnetic susceptibility correction.

The second representation of the $\Delta\Delta\delta_i(x)$ values shows that they can be regarded as the chemical shift drift of a given signal relative to the drift of a reference signal originating from the same molecule and we propose to stick to this style of interpretation.

Within the proposed approach of looking at the chemical shift changes we have summarized the literature observations on ‘imidazolium IL-molecular solvent’ systems which can be analyzed in this way (*i.e.*, where the observed absolute chemical shifts of the signals of interest, like those of the imidazolium ring hydrogen atoms, are published along with the terminal methyl group chemical shifts). The relative chemical shift variations $\Delta\Delta\delta_i(x)$ of the imidazolium ring hydrogen atoms were found to be negative in most of the studies which concern the following systems: RmimHal-H₂O,^{13,16,19,54,58} BmimCF₃CO₂-MeOH/H₂O,²⁹ EmimOAc-H₂O,⁴⁹ RmimMeSO₃-H₂O,^{16,46,48} EmimEtSO₄-H₂O,²⁸ BmimBF₄-H₂O,^{35,53,61} HexmimBr-Ac-*d*₆,²⁶ EmimTfO-Ac-*d*₆,⁵ BmimBF₄-MeOH,²³ BmimOctSO₄-ethylene glycol,¹⁷ BmimBF₄-AN,⁵⁹ EmimHal-AN,^{4,40} RmimBF₄/PF₆-thiophene,¹¹ DodecmimTFSI/NO₃-C₆H₆.^{22,41} Nevertheless, there are as well reports where the imidazolium ring hydrogen atoms exhibit more significant deshielding than the terminal methyl ones, *i.e.*, positive relative chemical shift variations are observed: EmimTFSI-Ac-*d*₆,⁵ RmimPF₆/BF₄-Ac-*d*₆,¹² EmimTFSI-MeOH,⁴⁰ EmimTFSI-H₂O.³⁹ For some systems, however, there was no appreciable difference

in chemical shift variation for the ring hydrogen atoms and the terminal methyl which resulted in roughly zero values of the relative chemical shift variations like in BmimBF₄-H₂O (note that there is a number of reports for this system concerning negative values of the relative chemical shift variation),^{13,19} and RmimBF₄-ethylene glycol.¹⁷ There are several examples of rather peculiar behavior when H² and H⁴⁻⁵ show opposite trends in their relative chemical shift variations. For HexmimTFSI in CDCl₃, H² was found to exhibit high positive values of $\Delta\Delta\delta_i(x)$ and moderate negative values for H⁴⁻⁵,⁴⁷ similar observations were reported for EmimBF₄ in CD₂Cl₂,⁶² while for BmimCl in DMSO the situation was inverse in signs.⁵⁴

One can see, that negative values of the relative chemical shift variation for the imidazolium ring hydrogen atoms are typically observed for ILs with rather basic anions which tend to form strong directional hydrogen bonds, like *e.g.*, halides Hal⁻, substituted sulfonates RSO₃⁻ and sulfates RSO₄⁻, carboxylates RCO₂⁻ in various molecular solvents and for tetrafluoroborate BF₄⁻ based ILs. A separate class of systems which falls into this category deals with imidazolium ILs mixed with aromatic solvents where the negative relative chemical shift variations stem from significant shielding of the imidazolium hydrogen atoms interacting with aromatic π -electron density of the solvents.^{11,22,41} Positive values are, in turn, observed for ILs with rather ‘soft’ large anions which have delocalized charge distribution like bis(trifluoromethylsulfonyl)imide TFSI⁻, or hexafluorophosphate PF₆⁻ mixed with highly polar and donating solvents like MeOH, Ac or H₂O.

A common observation for all of the mentioned above studies on chemical shift variation in IL-solvent mixtures is that the most significant changes occur at low IL content (typically at $x_{\text{IL}} < 0.1-0.2$). Even more drastic changes were observed at higher dilutions ($x_{\text{IL}} < 0.05-0.01$) where the corresponding concentration range was studied.^{16,21,41,46-47,50,54} As it was already mentioned by Dupont⁶³ under such high dilution regime the inherent IL-like ionic network is disrupted to ion pairs and other small aggregates and full dissociation into

individual ions is occurring at the infinite dilution limit. In other words, under such conditions IL switch to conventional electrolyte-like behavior that is governed by the interplay between ion-ion and ion-molecular interactions.

Speculating about chemical shift variation in mixtures of imidazolium ILs with molecular solvents, particularly with polar aprotic ones, three main effects may be put forward in order to explain the observed chemical shift variations which may be linked to distinct underlying intermolecular interactions. Firstly, general dilution effect, when a solvent is regarded as a structureless medium which 'lubricates' the IL native network structure and then dilutes it producing progressively smaller aggregate units up to full dissociation limit.^{5,63} This effect is non-specific and it is equally applicable to all the atoms of IL over the entire concentration range. In terms of electronic effects, the increase of effective separation between IL ions caused by dilution should result in a general deshielding of the hydrogen atoms, *i.e.*, an increase of chemical shifts. However, as can be judged from the results of Takamuku *et. al.*^{21-22,39-41} this effect rarely exceeds 0.05 ppm. Secondly, the effect associated with the specific interionic interactions. Indeed, for ILs these interactions are hydrogen bonds between the imidazolium ring hydrogen atoms, and to a lesser extent between the adjacent alkyl hydrogen atoms, from one side and electronegative atoms of anions from the other side.⁶⁴⁻⁶⁵ When these interactions are progressively disrupted by dilution, this leads to shielding of the hydrogen atoms involved. The magnitude of this effect correlates with the strength of the hydrogen bond.⁶⁶ Thirdly, solvation of IL cations in polar molecular solvents can be mediated via formation of hydrogen bonds with donor atoms of the solvent molecules (*e.g.*, oxygen in alcohols, DMSO, Ac *etc.*; nitrogen in AN, amines *etc.*) in addition to non-specific ion-dipole interactions. Formation of such cation-solvent hydrogen bonds upon dilution of IL would contribute to deshielding of the imidazolium ring and of the adjacent alkyl hydrogen atoms.

Apparently, the third and second effects are opposing each other and they are localized at the imidazolium ring and the adjacent hydrogen atoms. Hence, when referencing to the terminal methyl hydrogen atoms which are only prone to the first effect, the net observation on the relative chemical shift variation of the hydrogen atoms of interest should reflect the balance between the second and third effects. In particular, when $\Delta\Delta\delta_i(x_{\text{IL}}) > 0$ is observed for the imidazolium ring hydrogen atoms, *i.e.*, effective deshielding, this can be interpreted as that hydrogen bonds established with solvent molecules are stronger than those broken down between the IL counterions. If the relative chemical shift values are close to zero (as a tentative threshold we propose to use ± 0.05 ppm as estimated for the real chemical shift drift of terminal methyl group of Rmim⁺ by Takamuku et al.^{21-22,39-41}), then the hydrogen bonds of cations with solvent molecules and with anions are of comparable strength. A situation in which neither the cation-solvent hydrogen bonds are formed nor the cation-anion ones are disrupted is hardly plausible for mixtures of imidazolium ILs with polar aprotic solvents. Last but not the least, negative relative chemical shift variation values $\Delta\Delta\delta_i(x_{\text{IL}}) < 0$ suggest that the interionic hydrogen bonds are stronger than cation-solvent ones. We stress, that this conclusion has nothing to do with ‘absolute’ strength of the corresponding hydrogen bonds. Indeed, this conclusion can be drawn, for example, when a strong interionic bond is disrupted and an intermediate one is established with solvent and, equally, when a moderate hydrogen bond between the counterions is replaced with a very weak one with solvent. There is a particular case of large negative values $\Delta\Delta\delta_i(x_{\text{IL}}) \ll 0$ which can be attributed to the very strong interionic hydrogen bonds and rather weak ones between cation and solvent molecules. This is exactly the case of many systems with ILs with highly basic anions which form rather strong hydrogen bonds mentioned above.

In this study we apply this framework to study the interplay of interionic interactions in mixtures of imidazolium IL with polar aprotic solvents as a function

of composition over the entire concentration range. The selection of the systems is aimed at establishing the effect of IL anion structure and basicity (BF_4^- , PF_6^- , TfO^- , TFSI^-) and of polarity and donicity of the molecular solvent (AN, γ -BL, PC).

4.3. Results and discussion

4.3.1 Relative chemical shift variation in AN

The relative chemical shift variations in ^1H -NMR spectra of mixtures of Bmim BF_4 , Bmim PF_6 , BmimTfO, BmimTFSI with AN referenced to the chemical shift of terminal methyl group of cation's butyl chain as a function of IL mole fraction x_{IL} are shown in Figure 4.2. Our data on Bmim BF_4 -AN system agrees very well with the recently published results of Zheng *et. al.*⁵⁹

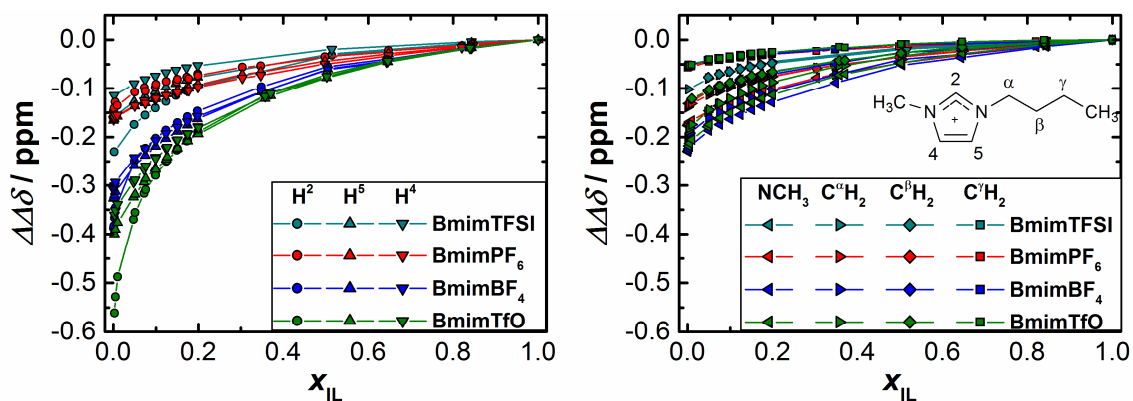


Figure 4.2. Relative ^1H chemical shift variation in mixtures of imidazolium IL with AN. Left panel shows the values for the imidazolium ring hydrogen atoms $\text{H}^{2/4/5}$ and the values for the alkyl hydrogen atoms are presented on the right panel.

In AN all the relative chemical shift variations of the hydrogen atoms in the studied set of systems are negative. This implies that the effect of ionic dissociation accompanied with the rupture of interionic hydrogen bonds overwhelms the specific solvation effects. This is not surprising since AN is only moderately polar donating.

The most significant effects are observed for the imidazolium ring hydrogen atoms, particularly at high dilutions. As discussed in the previous chapter, this

finding can be connected to the fact that interionic hydrogen bonds with the alkyl hydrogen atoms are rather weak compared to that with the imidazolium ring hydrogen atoms. BmimBF₄ and BmimTfO show the largest negative values, that is a clear indication of the interionic hydrogen bond rupture in these systems.

For a given IL, H² hydrogen revealed to be the most sensitive one among the imidazolium ring hydrogen atoms (this is especially well pronounced for BmimTFSI and BmimTfO). Particular sensitivity of the H² site was noticed in most of the mentioned above studies and was related to the higher positive charge and acidity of the C²-H² fragment compared to the C⁴-H⁴ and C⁵-H⁵ fragments and, hence, to the higher strength of the corresponding hydrogen bonds.^{40,58} The fact that this enhanced sensitivity of the H² chemical shift is much less pronounced for BmimBF₄ and BmimPF₆ also agrees with the literature data on systems containing these ILs. The difference in relative chemical shifts between H² and H⁴⁻⁵ signals did not exceed 0.1 ppm at highest dilution.^{11-13,15,17,23,35,50,59,61} At the same time, for mixtures containing imidazolium ILs with anions of low symmetry (TFSI⁻, TfO⁻, RSO₃⁻, RCO₂⁻) H² was found to be exceptionally sensitive just as in the present study.^{5,14,16,29-30,40,46,48-49} This can be related to differences in strengths of the hydrogen bonds present in ionic aggregates at H² and H⁴⁻⁵ sites as it was noted in the previous chapter.

A notable effect is also observed for C^αH₂ and NCH₃ protons (which are adjacent to the imidazolium ring) and even for C^βH₂. This agrees well with the results of our model calculations that in the most stable arrangement of the ion pairs and ionic aggregates the multiatomic anions are located above the C²-H² fragment which allows them to form hydrogen bonds with the adjacent alkyl hydrogen atoms of the Bmim⁺ cation. These hydrogen bonds are considerably weaker than those with the imidazolium ring hydrogen atoms.

In the studied set of ILs for the case of mixtures with AN the magnitude of relative chemical shift variations of the imidazolium ring hydrogen atoms

follows $\text{TfO}^- \geq \text{BF}_4^- > \text{PF}_6^- \sim \text{TFSI}^-$. The difference between the ILs for the relative chemical shift variations of the alkyl hydrogen atoms is much more difficult to be discerned but also agrees with the proposed trend. This sequence correlates rather with the relative hydrogen bond strengths revealed by our quantum chemical calculations shown in Chapter 3 than with the estimated in vacuum interaction energies.⁶⁷ Relative tendency to ion-pairing as estimated with the help of thermodynamic constants of ionic association derived from accurate conductivity measurements of the corresponding dilute solutions of BmimX ILs in AN⁶⁸⁻⁶⁹ fits the trend much better. The values of K_A ^{298.15} in $\text{dm}^3 \text{mol}^{-1}$ are 24.0⁶⁹ for BmimTfO, 18.15⁶⁹ or 15.7⁶⁸ for BmimBF₄, 15.6⁶⁸ for BmimPF₆, 12.67⁶⁸ for HexmimTFSI (for BmimTFSI there is no literature data but it is expected to be higher by *ca.* 0.1-0.2 $\text{dm}^3 \text{mol}^{-1}$). Other reported values of the association constant of these ILs in AN seem to be much both less accurate and credible: 27.0 $\text{dm}^3 \text{mol}^{-1}$ for BmimPF₆,⁷⁰ *ca.* 700 $\text{dm}^3 \text{mol}^{-1}$ for BmimBF₄ and BmimPF₆,⁷¹ 205±20 $\text{dm}^3 \text{mol}^{-1}$ for BmimTFSI and 46±7 $\text{dm}^3 \text{mol}^{-1}$ for BmimTfO.⁷²

Another observation that the difference between the ILs becomes more pronounced with dilution and even shows some enhancement at the lowest employed concentrations ($x_{\text{IL}} < 0.05$) serves as additional hint that is in this concentration range where the ultimate disruption of ionic associates down to the individual ions takes place.

In contrast to ¹H-NMR discussed above, studies on the concentration induced variations of ¹³C-NMR chemical shifts in mixtures of imidazolium ILs with molecular solvents are rather scarce.^{12,14,21-22,26} Since ¹³C-NMR goes as a supplement to more elaborated ¹H-NMR investigation, the comments are usually limited to general statements that carbon shifts roughly follow the trends established for hydrogen atoms, which is not always true though.^{12,26} Indeed, interpretation of the variations in ¹³C chemical shifts is not that straight forward since they are not involved explicitly into the intermolecular interactions even

though the observed variations are close in magnitude to those found for ^1H chemical shifts.^{12,14,21-22,26} Another difficulty in interpretation of the chemical shift variations for carbons is that apart from the effects established for the adjacent hydrogen atoms they are also liable to the effects of electron density redistribution along the skeleton of Rmim^+ cation. As the observed chemical shift change reflects only the net effect of electron density gain/loss at a given atom, it is rather challenging to track all the pathways of electron density redistribution and to assign it to distinct intermolecular interactions.

Figure 4.3 shows the relative ^{13}C chemical shift variations in mixtures of the studied ILs with AN. Apparently, they do not follow the patterns observed for the corresponding ^1H relative chemical shift variations. One can see from Figure 4.3 that most of the carbon atoms show positive or essentially zero values, whereas C^2 carbon for all the studied ILs and C^4 , C^α , C^β , C^γ of BmimTFSI show negative values. Between the alkyl carbons of a given IL the effect is most pronounced for the ones adjacent to the imidazolium ring (NCH_3 and C^α).

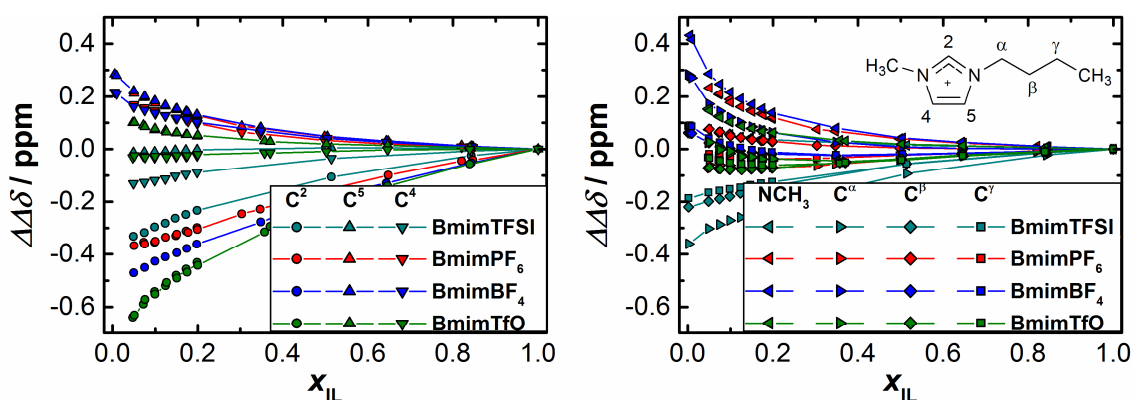


Figure 4.3. Relative ^{13}C chemical shift variation in mixtures of imidazolium IL with AN. Left panel shows the values for the imidazolium ring carbons $\text{C}^{2/4/5}$ and the values for the alkyl carbons are presented on the right panel.

The observed effective deshielding of most of the carbon atoms (as referenced to the terminal methyl one, $\Delta\Delta\delta_i(x_{\text{IL}}) > 0$) is essentially opposite to what has been established for the corresponding hydrogen atoms. At the same time C^2

carbon behaves in accordance with H² hydrogen (Figure 4.2) and reveals almost the same trend in the magnitudes of the relative chemical shift variation (TfO⁻ > BF₄⁻ > PF₆⁻ ~ TFSI⁻).

Keeping in mind the mentioned above complexity in interpretation of the ¹³C relative chemical shift variations, here we will only mention that significant shielding of C² carbon upon dilution in AN agrees well with the results of partial charge assessment described in the previous chapter. Particular behavior of the relative chemical shift of this carbon atom can be also related to another fact revealed by accurate analysis of electron density distribution in model representative structures. In contrast to other carbon atoms, C² explicitly interacts with anion which is located on top of the C²-H² fragment and the strength of this interaction is quite similar to that with the H² hydrogen atom. As for the other imidazolium ring carbons and the alkyl ones, these relative chemical shift changes presumably result from rather complex effects of electron density redistribution.

4.3.2 Relative chemical shift variation in γ -BL and PC

Polar molecular solvents γ -BL and PC are different from AN in term of their solvating abilities due to different nature of the polar donating group. The carbonyl group C=O present in γ -BL and PC is more polar and donating than the cyano group C \equiv N of AN. This is reflected in their polarity and, hence, the capacity to establish specific interactions with the cations.

¹H-NMR relative chemical shift variations in mixtures of the studied set of ILs with γ -BL and PC are shown in Figure 4.4. The most apparent change when comparing with similar representation for the mixtures with AN (Figure 4.2) is that all the data sets are shifted towards more positive values (by *ca.* 0.2-0.25 ppm in γ -BL and 0.1-0.15 ppm in PC at highest dilution). As a result, for the ILs which form weaker interionic hydrogen bonds (*i.e.*, BmimTFSI and BmimPF₆) the $\Delta\delta_i(x_{IL})$ values of the imidazolium ring hydrogen atoms are essentially neutral in PC and

positive in γ -BL. This clearly indicates (as it is mentioned in Chapter 3) the high capacity of these solvents to form hydrogen bonds with the imidazolium ring hydrogen atoms which are stronger (γ -BL) or of comparable strength (PC) than the inherent interionic ones in these ILs. For BmimBF₄ and BmimTfO, which were found to have stronger interionic hydrogen bonds, the relative chemical shift values for the imidazolium ring hydrogen atoms are still negative though less negative than it was observed in AN (they are less negative in PC than in γ -BL). Thus, we conclude that hydrogen bonds established between the γ -BL and PC solvent molecules and cations of BmimTfO and BmimBF₄ ILs are stronger than those existing in the native structure of these ILs.

Such trend of solvent capabilities for specific cation solvation, AN < PC < γ -BL, correlates not only with the results of model calculations but also with their Gutmann's donor numbers (see Table 2.2). The fact that the relative ¹H-NMR chemical shift variations are determined by solvating properties of the solvents towards cations but not by their polarity (in terms of static relative dielectric constant polarity varies as follows: PC > γ -BL > AN) corroborates that it is rather relative hydrogen bond strength which is probed than the tendency to ion-pairing.

Another feature to note is that H² is more sensitive than H⁴⁻⁵ to the shift to more positive values of the relative chemical shift variation when going from AN to γ -BL and PC. Indeed, while in AN the relative chemical shift variation of H² for BmimTfO was remarkably more negative than that of H⁴⁻⁵, in γ -BL and PC this effect is much more moderate. Similarly, but to a greater extent this is observed for BmimTFSI, where in PC H² shows almost the same neutral values of the relative chemical shift variation as for H⁴⁻⁵ and in γ -BL they are distinctly more positive than the corresponding values for the hydrogen atoms at positions 4-5. For ILs that did not reveal any specificity of the H² site under conditions of the interionic hydrogen bond rupture (*i.e.*, BmimBF₄ and BmimPF₆ in AN), solvation in γ -BL

and PC reveals H² to be particularly sensitive to establishing H-bonds with the solvent molecules which is reflected in its more positive values compared to H⁴⁻⁵.

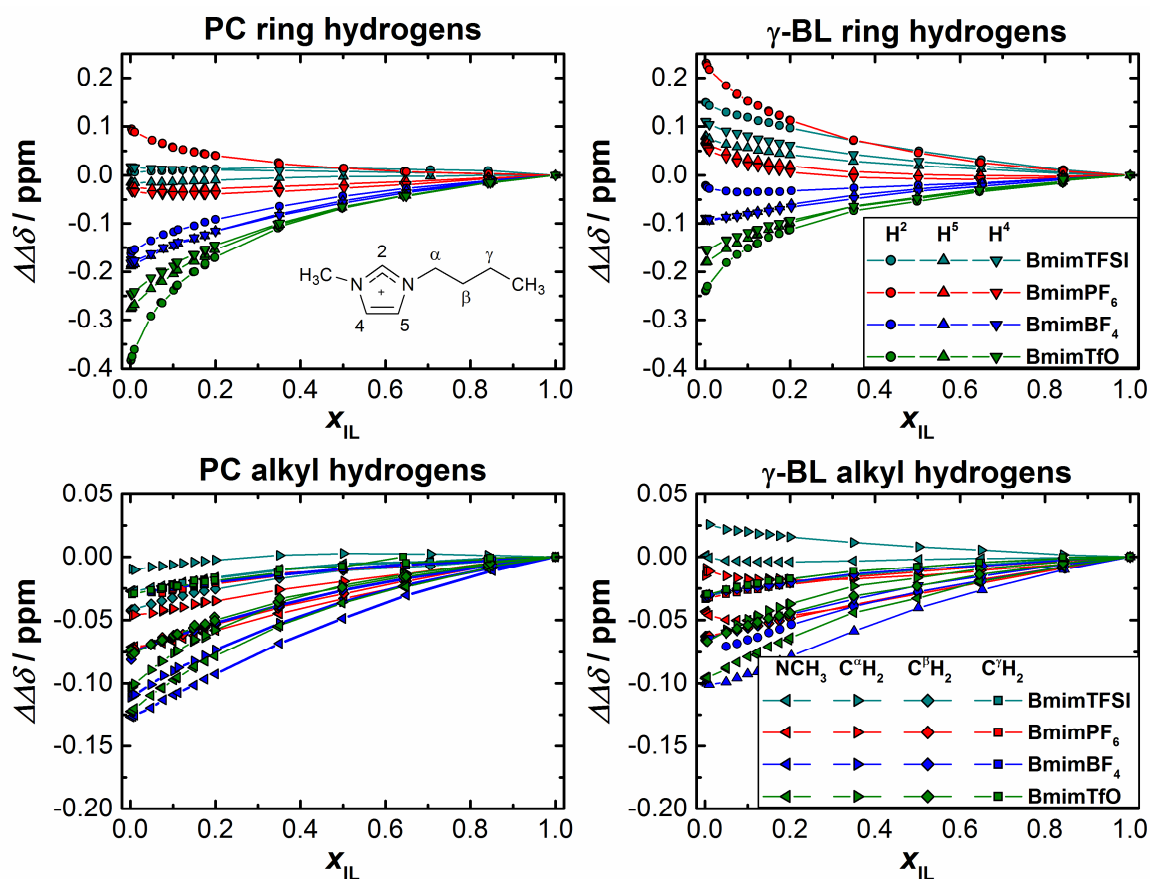


Figure 4.4. Relative ¹H chemical shift variation in mixtures of imidazolium ILs with γ -BL and PC.

For the alkyl hydrogen atoms, the observed in γ -BL and PC relative chemical shift variations follow the same trends as for the imidazolium ring ones but to a lesser degree. This finding is absolutely logical, since it is the ring hydrogen atoms which are the primary solvation sites, while the adjacent alkyl ones establish weaker hydrogen bonds, mainly, with the ester oxygen atoms of the γ -BL and PC molecules as revealed in our calculations on model representative structures (see Chapter 3).

Concerning the ^{13}C relative chemical shift variations in mixtures of the studied ILs with γ -BL and PC, which are shown in Figure 4.5, they are very similar to those observed for the corresponding mixtures with AN (Figure 4.3). An obvious difference is that for the carbons which show appreciable negative values of the relative chemical shift variations (namely, C^2 for all the ILs and the adjacent alkyl ones for BmimTFSI), they are even more negative in γ -BL and PC than what was observed in AN. This can be related to the stronger solvation effects anticipated in γ -BL and PC, particularly at C^2 site. However, there are still some discrepancies, such as why for ^{13}C chemical shifts the effect is more pronounced for PC than for γ -BL in contrast to the results of ^1H chemical shift analysis, while the calculations predict this effect to be of comparable strength for the solvated structures with all the solvent molecules.

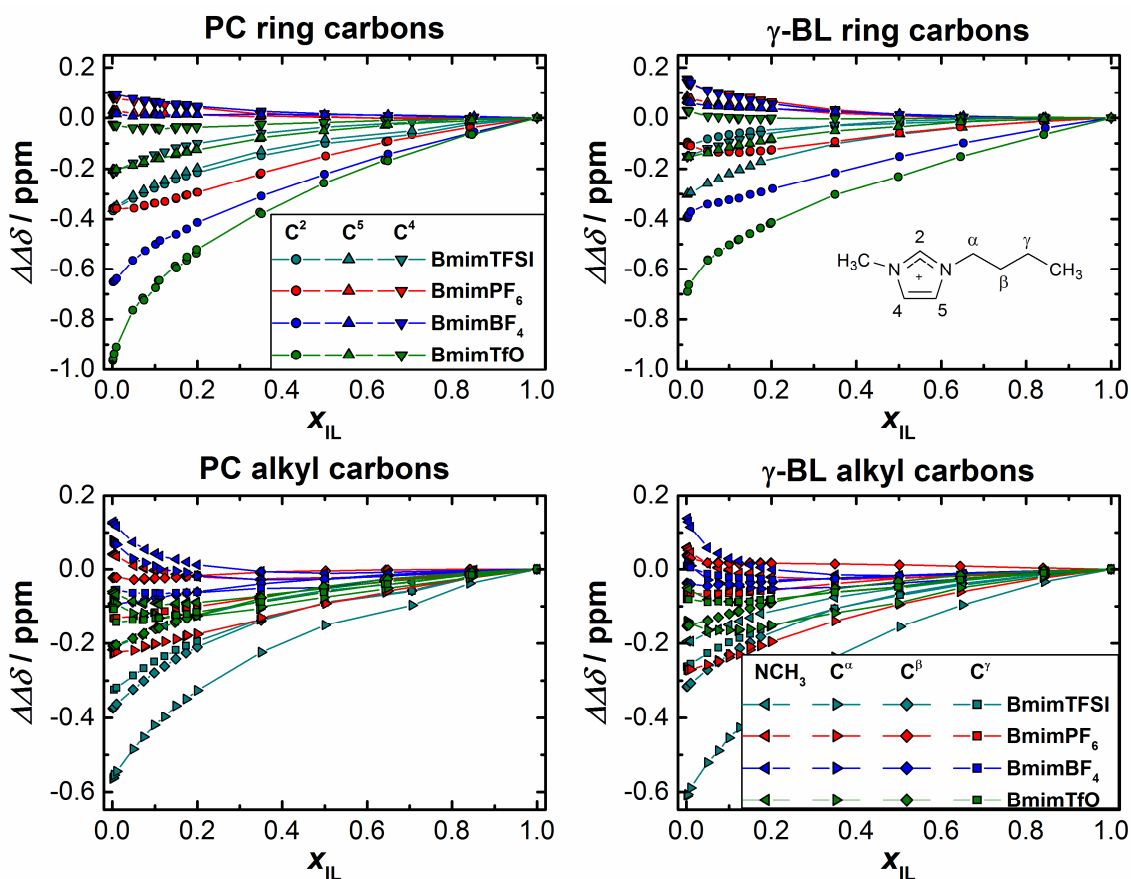


Figure 4.5. Relative ^{13}C chemical shift variation in mixtures of imidazolium ILs with γ -BL and PC.

4.3.3 ^{13}C relative chemical shift variations of anions in mixtures containing BmimTfO and BmimTFSI

Anions of BmimTfO and BmimTFSI ILs contain carbon atoms which allowed us to follow their ^{13}C chemical shifts in the framework of the relative chemical shift variations, *i.e.*, referenced to the terminal carbon of cation's butyl chain. Previously, an effective deshielding of the carbon atoms of the anions of RmimTFSI (when referenced to the terminal alkyl one) was observed for EmimTFSI upon heating⁷³ and for DodecmimTFSI upon dilution in C_6H_6 .²² In a recent study on EmimTFSI in DMSO and AN the relative chemical shift of TFSI⁻ carbons was found to be negative upon dilution, however, the real chemical shift variation of the reference terminal carbon was unusually highly positive and the

real chemical shift variation of TFSI⁻ carbons was indicative of its deshielding upon dilution.⁷⁴ This was attributed to the effect of electron density redistribution upon loosening of the interionic interactions. Nothing was found in the literature on ¹³C NMR chemical shift variations with concentration in RmimTfO-based systems.

Figure 4.6 shows the relative chemical shift variations of the carbon atoms of anions in mixtures of BmimTfO and BmimTFSI with AN, γ -BL, and PC. One can see that carbon atoms of the trifluoromethyl groups CF₃ behave differently in these ionic liquids: an apparent deshielding is observed for BmimTfO in all three solvents, while for BmimTFSI the relative chemical shift values are negative, which reflects effective shielding of the corresponding carbons upon dilution in three solvents.

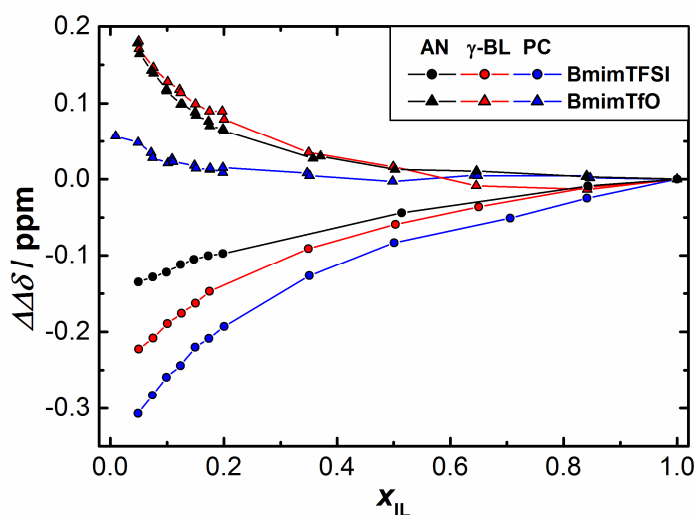


Figure 4.6. Relative ¹³C chemical shift variation for CF₃ carbons of anions in mixtures of BmimTfO and BmimTFSI with AN, γ -BL and PC.

This difference between the two anions can be rationalized as follows. As it was established in the previous chapter devoted to quantum-chemical calculations of the representative model molecular clusters, ion pair structure of BmimTfO is much more persistent than that of BmimTFSI when a solvent molecule is added. This is an indication of the relative stability of the ion pairs of these ILs. As a result, the main effect in solvation of BmimTFSI ion pair is the weakening of

interionic interactions due to structural distortion and increased separation (this reduces Coulomb attraction and weakens noncovalent interactions, *e.g.*, interionic hydrogen bonds). In BmimTfO, in contrast, the anion maintains its rather strong interactions with the cation upon addition of a solvent molecule and also establishes remarkable interactions with the solvent molecules via free sites of its SO₃ moiety. Generalizing these effects, one can suggest that upon solvation of BmimTfO the main effect experienced by the anion is the reinforcement of the intermolecular interactions in which it participates, while for BmimTFSI the net effect is the overall weakening of interactions involving the anion.

The effect of charge redistribution, which is, in fact, monitored by the relative chemical shift variation, is that for BmimTFSI electron density relaxes towards its unperturbed state which is accompanied with the decrease of charge of the corresponding carbon atoms, while for BmimTfO, strengthening of the interactions with the anion leads to its polarization enhancement which is manifested in the increase of the charge of the carbon atom. This idea agrees well with the results of the charge calculations in the QTAIM framework (see Chapters 2-3 for details) presented in Figure 4.7.

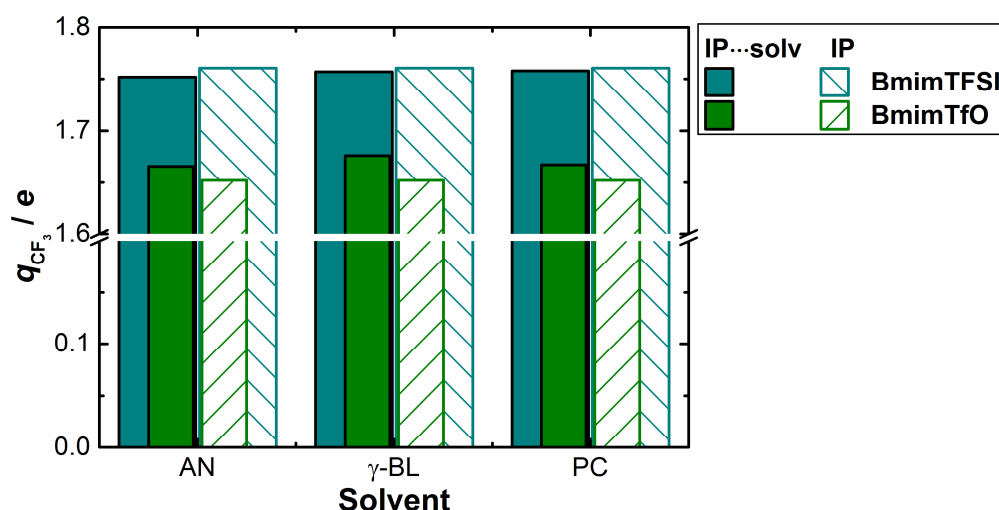


Figure 4.7. QTAIM-derived charges of CF₃ carbons of anions in BmimTfO and BmimTFSI ion pairs and their complexes with AN, γ-BL, and PC.

As for the effect of solvent on the ^{13}C relative chemical shift variation of anion's carbons, as seen from Figure 4.6, for BmimTFSI the magnitude of the shielding effect follows the sequence $\text{AN} < \gamma\text{-BL} < \text{PC}$, while for BmimTfO the deshielding magnitude is in the order $\text{PC} < \gamma\text{-BL} \approx \text{AN}$. These tendencies are not captured by the calculations, however, they can be interpreted implicating the previously mentioned general explanations of the phenomena. Indeed, if one assumes that in case of BmimTFSI it is only the overall weakening of interionic interactions which determines the observed relative chemical shift variations of anion's carbons, and then this effect should be modulate by polarity of the solvent medium. The extent of the shielding for TFSI $^-$ carbons upon dilution of the IL in different solvents agrees with their relative polarity expressed as static relative dielectric permittivity (Table 2.1). On the other hand, as it was stated above, for BmimTfO we assume the solvent-anion interaction in the structure of ion-pair solvates to play a role. This can be indirectly assessed via their electrophilic capabilities which are quantified by means of Gutmann's acceptor numbers.⁷⁵ From the corresponding values collected in Table 2.1 it is evident that is not the best descriptor for this effect (the corresponding values follow the order $\gamma\text{-BL} < \text{PC} < \text{AN}$). A more detailed investigation of this issue is needed.

4.4. Conclusions

Chemical shift variation in mixture of imidazolium ILs with polar molecular solvents can be used to follow the balance between interionic and ion-solvent interactions.

An approach based on referencing ^1H and ^{13}C NMR chemical shifts in the studied mixtures to the signal of terminal methyl of cation's butyl chain in the neat ILs is proposed. The variations in thus introduced relative chemical shifts as a function of mixture composition and depending on the nature of its constituents are interpreted in terms of specific and nonspecific intermolecular interactions.

BmimTfO and BmimBF₄ ILs are found to establish interionic hydrogen bonds involving the imidazolium ring hydrogen atoms and the hydrogen atoms of the adjacent alkyl groups, which are stronger than in the case of BmimPF₆ and BmimTFSI. Upon dilution in molecular solvents, these hydrogen bonds are progressively disrupted as a result of weakening of interionic interactions and ionic dissociation which is particularly pronounced at high dilutions ($x_{IL} < 0.1$). For BmimTfO and BmimTFSI ILs, the interionic hydrogen bond with the imidazolium ring hydrogen at position 2 (H²) is revealed to be stronger than with the hydrogen atoms at positions 4-5. The relative strengths of hydrogen bonding correlate well with the results established by quantum-chemical calculations set forth in the previous chapter.

Apart from the general dilution effect of the employed molecular solvents, they are also capable of establishing specific interactions with ILs, namely, hydrogen bonds with the imidazolium ring hydrogen atoms of cations. This is particularly prominent in PC and, to a greater extent, in γ -BL and H² shows enhanced sensitivity to this effect in all the studied ILs. Solvation in AN is not accompanied by formation of hydrogen bonds solvent-cation of an appreciable strength.

The solvation of anions was investigated for BmimTfO and BmimTFSI ILs by following the corresponding ¹³C relative chemical shifts. TFSI⁻ is considered to experience only the nonspecific effects of weakening of interionic interactions upon dilution in molecular solvents which is modulated by their polarity. In case of BmimTfO, due to its higher propensity to ionic association compared to BmimTFSI, solvent molecules interact not only with the cation but also with the anion and the strength of this interaction follows the order PC < γ -BL \approx AN.

4.5. References for Chapter 4

- (1) Wilkes, J. S.; Levisky, J. A.; Pflug, J. L.; Hussey, C. L.; Scheffler, T. B., Composition determinations of liquid chloroaluminate molten salts by nuclear magnetic resonance spectrometry. *Anal. Chem.* **1982**, *54*, 2378-2379.
- (2) Wilkes, J. S.; Frye, J. S.; Reynolds, G. F., Aluminum-27 and carbon-13 NMR studies of aluminum chloride-dialkylimidazolium chloride molten salts. *Inorg. Chem.* **1983**, *22*, 3870-3872.
- (3) Fannin, A. A.; King, L. A.; Levisky, J. A.; Wilkes, J. S., Properties of 1,3-dialkylimidazolium chloride-aluminum chloride ionic liquids. 1. Ion interactions by nuclear magnetic resonance spectroscopy. *J. Phys. Chem.* **1984**, *88*, 2609-2614.
- (4) Avent, A. G.; Chaloner, P. A.; Day, M. P.; Seddon, K. R.; Welton, T., Evidence for hydrogen bonding in solutions of 1-ethyl-3-methylimidazolium halides, and its implications for room-temperature halogenoaluminate(III) ionic liquids. *J. Chem. Soc., Dalton Trans.* **1994**, 3405-3413.
- (5) Bonhôte, P.; Dias, A.-P.; Papageorgiou, N.; Kalyanasundaram, K.; Grätzel, M., Hydrophobic, highly conductive ambient-temperature molten salts. *Inorg. Chem.* **1996**, *35*, 1168-1178.
- (6) Marcus, Y.; Hefter, G., Ion Pairing. *Chem. Rev.* **2006**, *106*, 4585-4621.
- (7) Bryant, R. G., The NMR time scale. *J. Chem. Educ.* **1983**, *60*, 933.
- (8) Tubbs, J. D.; Hoffmann, M. M., Ion-Pair Formation of the Ionic Liquid 1-Ethyl-3-methylimidazolium bis(triflyl)imide in Low Dielectric Media *J. Solution. Chem.* **2004**, *33*, 381-394.
- (9) Scharf, N.; Stark, A.; Hoffmann, M., Calorimetric Study on the Ion Pairing and Aggregation of 1-Ethyl-3-Methylimidazolium bis(trifluoromethylsulfonyl)amide ([C₂mim][NTf₂]) and Related Ionic Liquids in the Low-Dielectric Constant Solvent Chloroform. *J. Solution. Chem.* **2013**, *42*, 2034-2056.
- (10) D'Anna, F.; Frenna, V.; La Marca, S.; Noto, R.; Pace, V.; Spinelli, D., On the characterization of some [bmim][X]/co-solvent binary mixtures: a multidisciplinary approach by using kinetic, spectrophotometric and conductometric investigations. *Tetrahedron* **2008**, *64*, 672-680.
- (11) Su, B.-M.; Zhang, S.; Zhang, Z. C., Structural Elucidation of Thiophene Interaction with Ionic Liquids by Multinuclear NMR Spectroscopy. *J. Phys. Chem. B* **2004**, *108*, 19510-19517.
- (12) Zhai, C.; Wang, J.; Zhao, Y.; Tang, J.; Wang, H., A NMR Study on the Interactions of 1-Alkyl-3-Methylimidazolium Ionic Liquids with Acetone. *Z. Phys. Chem.* **2006**, *220*, 775-785.
- (13) Singh, T.; Kumar, A., Aggregation behavior of ionic liquids in aqueous solutions: effect of alkyl chain length, cations, and anions. *J. Phys. Chem. B* **2007**, *111*, 7843-7851.
- (14) Shimomura, T.; Fujii, K.; Takamuku, T., Effects of the alkyl-chain length on the mixing state of imidazolium-based ionic liquid-methanol solutions. *Phys. Chem. Chem. Phys.* **2010**, *12*, 12316-12324.
- (15) Singh, T.; Kumar, A., Cation-anion-water interactions in aqueous mixtures of imidazolium based ionic liquids. *Vib. Spectrosc.* **2011**, *55*, 119-125.
- (16) Russo, J. W.; Hoffmann, M. M., Measurements of Surface Tension and Chemical Shift on Several Binary Mixtures of Water and Ionic Liquids and Their Comparison for Assessing Aggregation. *J. Chem. Eng. Data.* **2011**, *56*, 3703-3710.
- (17) Singh, T.; Rao, K. S.; Kumar, A., Polarity Behaviour and Specific Interactions of Imidazolium-Based Ionic Liquids in Ethylene Glycol. *ChemPhysChem* **2011**, *12*, 836-845.

- (18) Kumar, B.; Singh, T.; Rao, K. S.; Pal, A.; Kumar, A., Thermodynamic and spectroscopic studies on binary mixtures of imidazolium ionic liquids in ethylene glycol. *J. Chem. Thermodyn.* **2012**, *44*, 121-127.
- (19) Cha, S.; Ao, M.; Sung, W.; Moon, B.; Ahlstrom, B.; Johansson, P.; Ouchi, Y.; Kim, D., Structures of ionic liquid-water mixtures investigated by IR and NMR spectroscopy. *Phys. Chem. Chem. Phys.* **2014**, *16*, 9591-9601.
- (20) Dias, N.; Shimizu, K.; Morgado, P.; Filipe, E. J. M.; Canongia Lopes, J. N.; Vaca Chávez, F., Charge Templates in Aromatic Plus Ionic Liquid Systems Revisited: NMR Experiments and Molecular Dynamics Simulations. *J. Phys. Chem. B* **2014**.
- (21) Shimomura, T.; Inoue, S.; Kadohata, S.; Umecky, T.; Takamuku, T., SANS, ATR-IR, and 1D- and 2D-NMR studies of mixing states of imidazolium-based ionic liquid and aryl solvents. *Phys. Chem. Chem. Phys.* **2013**, *15*, 20565-20576.
- (22) Shimomura, T.; Takamuku, T.; Yamaguchi, T., Clusters of Imidazolium-Based Ionic Liquid in Benzene Solutions. *J. Phys. Chem. B* **2011**, *115*, 8518-8527.
- (23) D'Anna, F.; Cascino, M.; Lo Meo, P.; Riela, S.; Noto, R., The effect of some amines and alcohols on the organized structure of [bmim][BF₄] investigated by ¹H NMR spectroscopy. *ARKIVOC* **2009**, *2009*, 30-46.
- (24) Hsu, W.-Y.; Tai, C.-C.; Su, W.-L.; Chang, C.-H.; Wang, S.-P.; Sun, I. W., A Criterion for Proper Cosolvents Used for Ionic Liquids: the Lewis Acidic and Basic Dual Nature of Propylene Carbonate. *Inorg. Chim. Acta* **2008**, *361*, 1281-1290.
- (25) Holbrey, J. D.; Seddon, K. R., The phase behaviour of 1-alkyl-3-methylimidazolium tetrafluoroborates; ionic liquids and ionic liquid crystals. *J. Chem. Soc., Dalton Trans.* **1999**, 2133-2140.
- (26) Cui-ping, Z.; Jian-ji, W.; Xiao-peng, X.; Han-qing, W.; Miao, C., Interactions of 1-hexyl-3-methylimidazolium Bromide with Acetone. *Chin. J. Chem. Phys.* **2006**, *19*, 447.
- (27) Zhai, C.; Wang, J.; Zhao, Y.; Tang, J., A NMR Relaxation Study for the Interactions of some 1-alkyl-3-methylimidazolium Ionic Liquids with Acetone. *Z. Anorg. Allg. Chem.* **2009**, *223*, 839-847.
- (28) Zhang, Q.-G.; Wang, N.-N.; Yu, Z.-W., The Hydrogen Bonding Interactions between the Ionic Liquid 1-Ethyl-3-Methylimidazolium Ethyl Sulfate and Water. *J. Phys. Chem. B* **2010**, *114*, 4747-4754.
- (29) Zhang, Q.-G.; Wang, N.-N.; Wang, S.-L.; Yu, Z.-W., Hydrogen Bonding Behaviors of Binary Systems Containing the Ionic Liquid 1-Butyl-3-methylimidazolium Trifluoroacetate and Water/Methanol. *J. Phys. Chem. B* **2011**, *115*, 11127-11136.
- (30) Ruiz, E.; Ferro, V. R.; Palomar, J.; Ortega, J.; Rodriguez, J. J., Interactions of Ionic Liquids and Acetone: Thermodynamic Properties, Quantum-Chemical Calculations, and NMR Analysis. *J. Phys. Chem. B* **2013**, *117*, 7388-7398.
- (31) Lungwitz, R.; Spange, S., A hydrogen bond accepting (HBA) scale for anions, including room temperature ionic liquids. *New J. Chem.* **2008**, *32*, 392-394.
- (32) Hesse-Ertelt, S.; Heinze, T.; Kosan, B.; Schwikal, K.; Meister, F., Solvent Effects on the NMR Chemical Shifts of Imidazolium-Based Ionic Liquids and Cellulose Therein. *Macromolecular Symposia* **2010**, *294*, 75-89.
- (33) Lungwitz, R.; Spange, S., Determination of Hydrogen-Bond-Accepting and -Donating Abilities of Ionic Liquids with Halogeno Complex Anions by Means of ¹H NMR Spectroscopy. *ChemPhysChem* **2012**, *13*, 1910-1916.
- (34) Freire, M. G.; Neves, C. M. S. S.; Silva, A. M. S.; Santos, L. s. M. N. B. F.; Marrucho, I. M.; Rebelo, L. s. P. N.; Shah, J. K.; Maginn, E. J.; Coutinho, J. o. A. P., ¹H NMR and Molecular Dynamics Evidence for an Unexpected Interaction on the Origin of Salting-In/Salting-Out Phenomena. *J. Phys. Chem. B* **2010**, *114*, 2004-2014.

- (35) Abe, H.; Hatano, N.; Ima, Y.; Ohta, S.; Shimizu, A.; Yoshimura, Y., Peculiar Concentration Dependence of H/D Exchange Reaction in 1-Butyl-3-methylimidazolium Tetrafluoroborate-D₂O Mixtures. *Open J. Phys. Chem.* **2011**, *1*, 70-76.
- (36) Harris, R. K.; Becker, E. D.; Cabral de Menezes, S. M.; Goodfellow, R.; Granger, P., NMR nomenclature. Nuclear spin properties and conventions for chemical shifts (IUPAC Recommendations 2001). *Pure Appl. Chem.* **2001**, *73*, 1795-1818.
- (37) Harris, R. K.; Becker, E. D.; Cabral de Menezes, S. M.; Granger, P.; Hoffmann, R. E.; Zilm, K. W., Further conventions for NMR shielding and chemical shifts (IUPAC Recommendations 2008). *Pure Appl. Chem.* **2008**, *80*, 59-84.
- (38) Wang, J.; Yao, H.; Nie, Y.; Zhang, X.; Li, J., Synthesis and characterization of the iron-containing magnetic ionic liquids. *J. Mol. Liq.* **2012**, *169*, 152-155.
- (39) Umecky, T.; Takamuku, T.; Matsumoto, T.; Kawai, E.; Takagi, M.; Funazukuri, T., Effects of Dissolved Water on Li⁺ Solvation in 1-Ethyl-3-methylimidazolium Bis(trifluoromethanesulfonyl)amide Ionic Liquid Studied by NMR. *J. Phys. Chem. B* **2013**, *117*, 16219-16226.
- (40) Takamuku, T.; Honda, Y.; Fujii, K.; Kittaka, S., Aggregation of imidazolium ionic liquids in molecular liquids studied by small-angle neutron scattering and NMR. *Anal. Sci.* **2008**, *24*, 1285-1290.
- (41) Takamuku, T.; Shimomura, T.; Sadakane, K.; Koga, M.; Seto, H., Aggregation of 1-dodecyl-3-methylimidazolium nitrate in water and benzene studied by SANS and ¹H NMR. *Phys. Chem. Chem. Phys.* **2012**, *14*, 11070-11080.
- (42) Mizuno, K.; Tamiya, Y.; Mekata, M., External double reference method to study concentration and temperature dependences of chemical shifts determined on a unified scale. *Pure Appl. Chem.* **2004**, *76*, 105-114.
- (43) Momoki, K.; Fukazawa, Y., Bulbed capillary external referencing method for proton nuclear magnetic resonance spectroscopy. *Anal. Chem.* **1990**, *62*, 1665-1671.
- (44) Momoki, K.; Fukazawa, Y., Bulbed Capillary External Referencing Method Using a Superconducting Magnet NMR Instrument. *Anal. Sci.* **1994**, *10*, 53-58.
- (45) Mulay, L. N.; Haverbusch, M., Modified Shape Factor NMR Method for Measuring Magnetic Susceptibility. *Review of Scientific Instruments* **1964**, *35*, 756-757.
- (46) Stark, A.; Zidell, A. W.; Hoffmann, M. M., Is the Ionic Liquid 1-Ethyl-3-Methylimidazolium Methanesulfonate [emim][MeSO₃] Capable Of Rigidly Binding Water? *J. Mol. Liq.* **2011**, *160*, 166-179.
- (47) Scharf, N. T.; Stark, A.; Hoffmann, M. M., Ion Pairing and Dynamics of the Ionic Liquid 1-Hexyl-3-methylimidazolium Bis(irifluoromethylsulfonyl)amide ([C₆mim][NTf₂]) in the Low Dielectric Solvent Chloroform. *J. Phys. Chem. B* **2012**, *116*, 11488-11497.
- (48) Stark, A.; Zidell, A. W.; Russo, J. W.; Hoffmann, M. M., Composition Dependent Physicochemical Property Data for the Binary System Water and the Ionic Liquid 1-Butyl-3-methylimidazolium Methanesulfonate ([C₄mim][MeSO₃]). *J. Chem. Eng. Data.* **2012**, *57*, 3330-3339.
- (49) Hall, C. A.; Le, K. A.; Rudaz, C.; Radhi, A.; Lovell, C. S.; Damion, R. A.; Budtova, T.; Ries, M. E., Macroscopic and Microscopic Study of 1-Ethyl-3-methyl-imidazolium Acetate-Water Mixtures. *J. Phys. Chem. B* **2012**, *116*, 12810-12818.
- (50) Xu, Y.; Gao, Y.; Zhang, L.; Yao, J.; Wang, C.; Li, H., Microscopic structures of ionic liquids 1-ethyl-3-methylimidazolium tetrafluoroborate in water probed by the relative chemical shift. *Sci. China Chem.* **2010**, *53*, 1561-1565.
- (51) Lyčka, A.; Doleček, R.; Šimůnek, P.; Macháček, V., ¹⁵N NMR spectra of some ionic liquids based on 1,3-disubstituted imidazolium cations. *Magn. Reson. Chem.* **2006**, *44*, 521-523.

- (52) Blesic, M.; Marques, M. H.; Plechkova, N. V.; Seddon, K. R.; Rebelo, L. P. N.; Lopes, A., Self-aggregation of ionic liquids: micelle formation in aqueous solution. *Green Chem.* **2007**, *9*, 481-490.
- (53) Zhai, C.-P.; Liu, X.-J.; Zhao, Y.; Wang, J.-J., NMR Study on the Aggregation of [C₄mim][BF₄] in D₂O and CDCl₃. *Acta Phys.-Chim. Sin.* **2009**, *25*, 1185-1189.
- (54) Remsing, R. C.; Liu, Z.; Sergeev, I.; Moyna, G., Solvation and Aggregation of N,N'-Dialkylimidazolium Ionic Liquids: A Multinuclear NMR Spectroscopy and Molecular Dynamics Simulation Study. *J. Phys. Chem. B* **2008**, *112*, 7363-7369.
- (55) Gutel, T.; Santini, C. C.; Pádua, A. I. A. H.; Fenet, B.; Chauvin, Y.; Canongia Lopes, J. N.; Bayard, F. o.; Costa Gomes, M. F.; Pensado, A. S., Interaction between the π -System of Toluene and the Imidazolium Ring of Ionic Liquids: A Combined NMR and Molecular Simulation Study. *J. Phys. Chem. B* **2009**, *113*, 170-177.
- (56) Vreekamp, R.; Castellano, D.; Palomar, J.; Ortega, J.; Espiau, F.; Fernández, L. s.; Penco, E., Thermodynamic Behavior of the Binaries 1-Butylpyridinium Tetrafluoroborate with Water and Alkanols: Their Interpretation Using ¹H NMR Spectroscopy and Quantum-Chemistry Calculations. *J. Phys. Chem. B* **2011**, *115*, 8763-8774.
- (57) D'Anna, F.; Marullo, S.; Vitale, P.; Noto, R., Binary Mixtures of Ionic Liquids: A Joint Approach to Investigate their Properties and Catalytic Ability. *ChemPhysChem* **2012**, *13*, 1877-1884.
- (58) Cesare Marincola, F.; Piras, C.; Russina, O.; Gontrani, L.; Saba, G.; Lai, A., NMR Investigation of Imidazolium-Based Ionic Liquids and Their Aqueous Mixtures. *ChemPhysChem* **2012**, *13*, 1339-1346.
- (59) Zheng, Y.-Z.; Wang, N.-N.; Luo, J.-J.; Zhou, Y.; Yu, Z.-W., Hydrogen-Bonding Interactions between [BMIM][BF₄] and Acetonitrile. *Phys. Chem. Chem. Phys.* **2013**, *15*, 18055-18064.
- (60) Cremer, T.; Kolbeck, C.; Lovelock, K. R. J.; Paape, N.; Wölfel, R.; Schulz, P. S.; Wasserscheid, P.; Weber, H.; Thar, J.; Kirchner, B.; Maier, F.; Steinrück, H.-P., Towards a Molecular Understanding of Cation-Anion Interactions-Probing the Electronic Structure of Imidazolium Ionic Liquids by NMR Spectroscopy, X-ray Photoelectron Spectroscopy and Theoretical Calculations. *Chem. – Eur. J.* **2010**, *16*, 9018-9033.
- (61) Moreno, M.; Castiglione, F.; Mele, A.; Pasqui, C.; Raos, G., Interaction of Water with the Model Ionic Liquid [bmim][BF₄]: Molecular Dynamics Simulations and Comparison with NMR Data. *J. Phys. Chem. B* **2008**, *112*, 7826-7836.
- (62) Katsyuba, S. A.; Griaznova, T. P.; Vidiš, A.; Dyson, P. J., Structural Studies of the Ionic Liquid 1-Ethyl-3-methylimidazolium Tetrafluoroborate in Dichloromethane Using a Combined DFT-NMR Spectroscopic Approach. *J. Phys. Chem. B* **2009**, *113*, 5046-5051.
- (63) Dupont, J., On the solid, liquid and solution structural organization of imidazolium ionic liquids. *J. Braz. Chem. Soc.* **2004**, *15*, 341-350.
- (64) Tsuzuki, S.; Tokuda, H.; Mikami, M., Theoretical analysis of the hydrogen bond of imidazolium C2–H with anions. *Phys. Chem. Chem. Phys.* **2007**, *9*, 4780.
- (65) Dong, K.; Song, Y.; Liu, X.; Cheng, W.; Yao, X.; Zhang, S., Understanding Structures and Hydrogen Bonds of Ionic Liquids at the Electronic Level. *J. Phys. Chem. B* **2012**, *116*, 1007-1017.
- (66) Gilli, G.; Gilli, P. *The nature of the hydrogen bond: outline of a comprehensive hydrogen bond theory*; Oxford University Press: 2009; 317 p.
- (67) Tsuzuki, S.; Tokuda, H.; Hayamizu, K.; Watanabe, M., Magnitude and Directionality of Interaction in Ion Pairs of Ionic Liquids: Relationship with Ionic Conductivity. *J. Phys. Chem. B* **2005**, *109*, 16474-16481.

- (68) Bešter-Rogač, M.; Stoppa, A.; Buchner, R., Ion Association of Imidazolium Ionic Liquids in Acetonitrile. *J. Phys. Chem. B* **2014**, *118*, 1426-1435.
- (69) Kalugin, O. N.; Voroshylova, I. V.; Riabchunova, A. V.; Lukinova, E. V.; Chaban, V. V., Conductometric Study of Binary Systems Based on Ionic Liquids and Acetonitrile in a wide Concentration Range. *Electrochim. Acta* **2013**, *105*, 188-199.
- (70) Jan, R.; Rather, G.; Bhat, M., Association of Ionic Liquids in Solution: Conductivity Studies of [BMIM][Cl] and [BMIM][PF₆] in Binary Mixtures of Acetonitrile + Methanol. *J. Solution. Chem.* **2013**, *42*, 738-745.
- (71) Wang, H.; Wang, J.; Zhang, S.; Pei, Y.; Zhuo, K., Ionic Association of the Ionic Liquids [C₄mim][BF₄], [C₄mim][PF₆], and [C_nmim]Br in Molecular Solvents. *ChemPhysChem* **2009**, *10*, 2516-2523.
- (72) Belov, A. V.; Solov'ev, S. N., Thermochemistry of the dissolution and association of ionic liquids in aqueous and acetonitrile solutions. *Russ. J. Phys. Chem.* **2014**, *88*, 1351-1356.
- (73) Fujii, K.; Soejima, Y.; Kyoshoin, Y.; Fukuda, S.; Kanzaki, R.; Umebayashi, Y.; Yamaguchi, T.; Ishiguro, S.-i.; Takamuku, T., Liquid Structure of Room-Temperature Ionic Liquid, 1-Ethyl-3-methylimidazolium Bis-(trifluoromethanesulfonyl) Imide. *J. Phys. Chem. B* **2008**, *112*, 4329-4336.
- (74) Takamuku, T.; Hoke, H.; Idrissi, A.; Marekha, B.; Moreau, M.; Honda, Y.; Umecky, T.; Shimomura, T., Microscopic interactions of the imidazolium-based ionic liquid with molecular liquids depending on their electron-donicity *Phys. Chem. Chem. Phys.* **2014**, submitted.
- (75) Reichardt, C.; Welton, T. *Solvents and Solvent Effects in Organic Chemistry*; Fourth, Updated and Enlarged Edition ed.; Wiley-VCH Verlag GmbH & Co. KGaA: Weinheim, 2011; 718 p.

Chapter 5. Translational Diffusion in IL-Molecular

Solvent Mixtures

The material presented in this chapter forms the basis of publication

Marekha, B. A.; Kalugin, O. N.; Bria, M.; Buchner, R.; Idrissi, A. *Translational Diffusion in Mixtures of Imidazolium ILs with Polar Aprotic Molecular Solvents*. **J. Phys. Chem. B**, 2014, 118, 5509–5517.

Self-diffusion coefficients of cations and solvent molecules were determined with $^1\text{H-NMR}$ in mixtures of 1-*n*-butyl-3-methylimidazolium (Bmim^+) tetrafluoroborate (BF_4^-), hexafluorophosphate (PF_6^-), trifluoromethanesulfonate (TfO^-) and bis(trifluoromethylsulfonyl)imide (TFSI^-) with acetonitrile (AN), γ -butyrolactone (γ -BL), and propylene carbonate (PC) over the entire composition range at 300 K. The relative diffusivities of solvent molecules to cations as a function of concentration were found to depend on the solvent but not on the anion (*i.e.*, IL). In all cases the values exhibit a plateau at low IL content ($x_{\text{IL}} < 0.2$) and then increase steeply (AN), moderately (γ -BL), or negligibly (PC) at higher IL concentrations. This behavior was related to the different solvation patterns in the employed solvents. In BmimPF_6 -based systems, anionic diffusivities were followed via ^{31}P nuclei and found to be higher than the corresponding cation values in IL-poor systems and lower in the IL-rich region. The inversion point of relative ionic diffusivities was found around equimolar composition and does not depend on the solvent. At this point, a distinct change in the ion-diffusion mechanism appears to take place.

5.1. Introduction

In contrast to conventional nonaqueous electrolyte solutions, where salt concentrations rarely exceed 0.2-0.3 in mole fraction units, imidazolium ILs are fully miscible with most nonaqueous polar solvents. This gives an opportunity to follow the variation of many physicochemical properties, diffusivity in particular, over a much broader range of compositions: from very dilute solutions of ILs through concentrated ones (which roughly corresponds to ‘conventional electrolyte solution’ regime) up to IL-rich mixtures where the molecular component is dispersed in the supramolecular ionic network.

Diffusion is a decisive factor not only for electrochemical applications but also for chemical reactions as well. Moreover, modern NMR methods allow observation of self-diffusion coefficients, D_i , for chemically nonequivalent species i .¹ Such data can serve as a basis for developing a comprehensive picture of dynamics in such systems.

Since much attention in the field of IL-solvent mixtures has been paid to aqueous systems²⁻⁸ experimental diffusion-related studies on mixtures of ILs with nonaqueous molecular solvents are rather scarce.

At present, there is still lack of microscopic information not only on the structure but also on the dynamics of ionic subsystem in mixtures of ILs with nonaqueous (mid)polar aprotic solvents. This chapter presents the results of a NMR-diffusometrical study on mixtures of 1-*n*-butyl-3-methylimidazolium (Bmim⁺) based ILs, namely 1-*n*-butyl-3-methylimidazolium trifluoromethanesulfonate (triflate) BmimTfO, 1-*n*-butyl-3-methylimidazolium bis(trifluoromethanesulfonyl)imide BmimTFSI, 1-*n*-butyl-3-methylimidazolium hexafluorophosphate BmimPF₆, and 1-*n*-butyl-3-methylimidazolium tetrafluoroborate BmimBF₄, with AN, PC and γ -BL (see Figure 1.1 for chemical structures) over the entire composition range. The rest of the chapter is organized

as follows: general trends in experimental data are given a brief overview in Section 5.2.1; the data is rationalized in terms of relative diffusion coefficients in Section 5.2.2; Section 5.2.3 is devoted to the discussion of counterion diffusion in BmimPF₆-based mixtures and the conclusions are outlined in the section 5.3.

5.2. Results and Discussion

5.2.1 Absolute self-diffusion coefficients as a function of mixture composition

The composition dependence of diffusion coefficients for liquid mixtures, including electrolyte solutions, can be interpreted with various approaches.⁹ Currently, no strict theoretical framework is available that would predict and explain diffusivities of the constituents in ion-molecular systems over a broad range of concentration. As a result, most studies concerning diffusion in conventional electrolyte solutions and mixtures of ILs with molecular solvents almost exclusively operate with general considerations and/or employ very simplistic models that hardly represent all the complexity and peculiarities of such systems.

For all 12 mixtures studied, the self-diffusion coefficients of all species (cations, anions, and solvent molecules) roughly follow a linear behavior in a semilogarithmic representation at the molar fraction scale (see sample data sets for BmimPF₆-AN, BmimPF₆-PC, and BmimBF₄-AN systems in Figure 5.1, all data are collected in Table A 5.1 of the Appendix for this chapter), *i.e.*, diffusivities exponentially decrease with increasing IL mole fraction. Over the entire composition range solvent molecules move several times faster than the ionic species. On the other hand, cations and anions exhibit comparable mobilities. The latter observation is usually considered as a manifestation of strong correlation in ionic motion due to high density of charged species.^{5,10} It should also be pointed out

that the diffusion coefficients of all particles vary over 1.5–2 orders of magnitude with concentration.

For comparison, data of Hsu *et al.*¹¹ and the very recent results from Liang *et al.*¹² are included in Figure 5.1. Absolute values of our diffusion coefficients for cations and solvent molecules compare very well with the literature, and this agreement becomes excellent when relative diffusion coefficients are considered (see Figure 5.2 and discussion in Section 5.2.2).

For an empirical description of the concentration dependence experimental logarithmic diffusion coefficients were fitted to a third-order polynomial in accordance with eq (5.1):

$$\log D = \sum_{i=0}^3 a_i x_{IL}^i \quad (5.1)$$

Fitted parameters along with raw experimental data are collected in Table A 5.2 of the Appendix for this chapter.

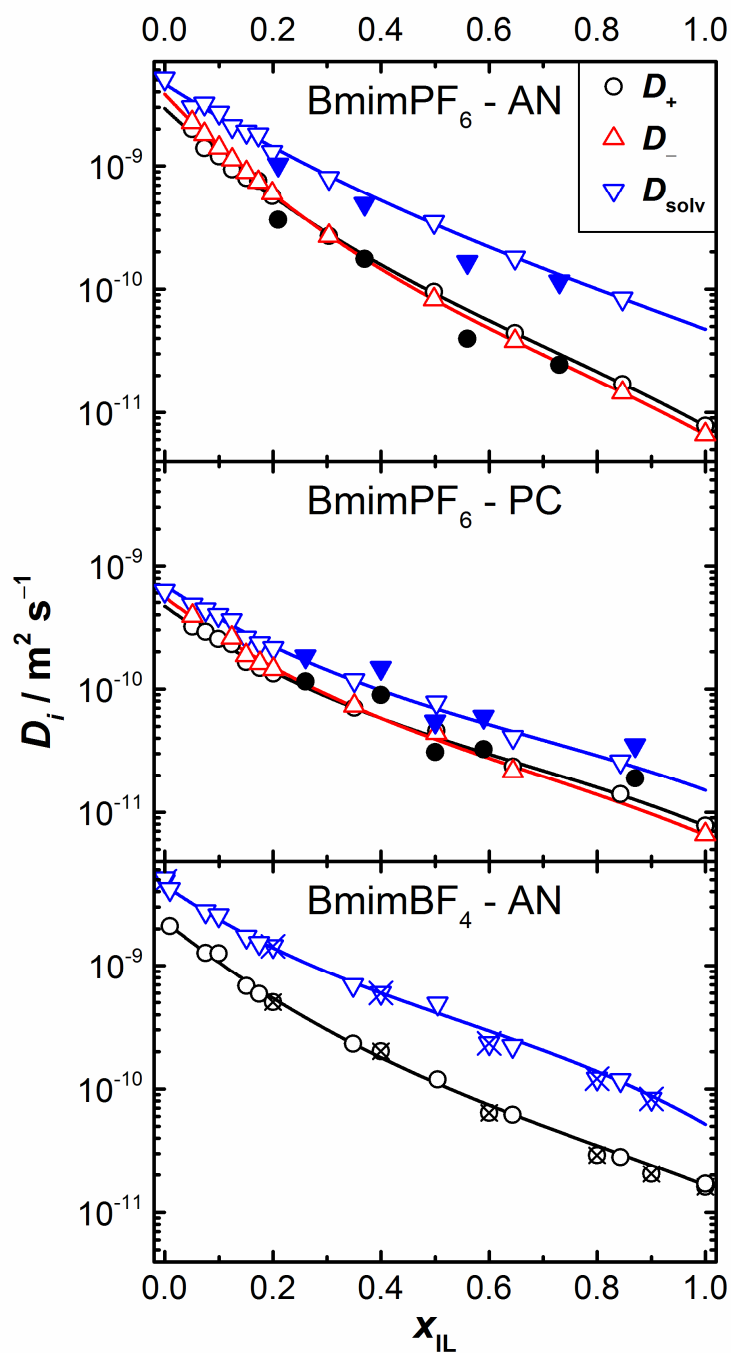


Figure 5.1. Experimental self-diffusion coefficients of the solvent molecules D_{solv} , cations D_+ and anions D_- as a function of IL molar fraction in mixtures BmimPF₆-AN (*top*), BmimPF₆-PC (*middle*), and BmimBF₄-AN (*bottom*). Lines represent cubic fits of experimental data to eq (5.1). Solid symbols show data from Hsu *et al.*,¹¹ while the crossed ones are from Liang *et al.*¹² for comparison. Note logarithmic scaling in diffusion dimension.

At first glance, the observed trend, decreasing self-diffusion coefficients with increasing IL concentration, is a consequence of the exponential viscosity increase

upon IL addition.¹³⁻¹⁴ Scharf and co-workers¹⁰ studied HexmimTFSI in the low-polarity and thus strongly ion-pairing solvent CDCl_3 and in moderately polar $\text{DMSO-}d_6$ at rather high dilutions ($x_{\text{IL}} < 0.1$) by following the self-diffusion coefficients of the constituting ions, D_+ and D_- , over a broad temperature range (288–318 K). In $\text{DMSO-}d_6$, the ions were found to diffuse independently, with the respective diffusion coefficients being practically insensitive to changes in temperature and/or concentration. In contrast, motions of cations and anions in CDCl_3 revealed to be highly correlated. The values of D_+ and D_- were very close and exhibited a simultaneous rapid increase at very high dilutions opposite to the monotonous decrease of viscosity. These observations not only imply strong ion-pairing but significant ionic aggregation towards even bigger clusters.

5.2.2 Relative self-diffusion coefficients solvent-cation as a function of mixture composition

In their numerous studies on NMR-diffusometry of nonaqueous aprotic electrolyte (mainly Li^+ -based) solutions,¹⁵⁻²⁰ Hayamizu and colleagues used the concept of proportionality between ionic and solvent diffusion coefficients as an indication for the validity of the Stokes-Einstein relation (*i.e.*, that particle diffusion is only modulated by macroscopic viscosity changes). This idea is based on the generally observed proportionality between the diffusion coefficients of neat solvents and their fluidity ($= \eta^{-1}$). Viscosity, in turn, is considered to increase with concentration due to enhanced ion-molecular interactions. Any deviations from such proportionality were attributed to ionic association phenomena without detailed discussion. For the visual inspection of such details they proposed to plot the ratio of the diffusion coefficient of solvent molecules to that of ions as a function of concentration. It was anticipated that specific changes in ion-molecular and interionic interactions, if present, would cause an offset from a constant value.

In accordance with the Stokes-Einstein relation, the ratio should be defined by the inverse ratio of the hydrodynamic radii of the diffusing species.

This methodology of using the ratio of diffusion coefficients, introduced by Hayamizu *et al.*,¹⁵⁻²⁰ has been used for several diffusion studies of aqueous mixtures of ILs^{3,6} over a broad range of concentrations. In their study of BmimPF₆ mixed with various nonaqueous solvents, Hsu *et al.*¹¹ pushed this approach further by proposing the so-called ‘aggregation index’, defined as the diffusion ratio solvent-ion divided by the reciprocal of the corresponding radii ratio. The latter was estimated on the basis of quantum-mechanical calculations. They discovered that on dilution and/or heating, the aggregation index decreases but never reaches the limiting value of unity. The highest extent of screening of the interionic interactions (*i.e.*, the smallest aggregation index) was observed for PC and DMSO, while AN was found to weaken ionic association only poorly. On the other hand, from the slope of the corresponding concentration trends an opposite conclusion can be reached: The steepest change in aggregation index was found for AN, whereas for PC it varied only slightly. This suggests that AN-based systems experience more pronounced changes when their composition is changed than those containing PC.

In order to avoid using poorly proven approaches, namely the highly questionable applicability of the Stokes-Einstein relation to IL-based systems²¹⁻²³ (*vide infra*) and the concept of hydrodynamic radius for such nonspherical particles as IL ions, which can also bear some degree of conformational flexibility, we will stick here to the diffusion ratios of Hayamizu and disregard the aggregation index of Hsu.

Figure 5.2 depicts the solvent-cation diffusion ratios as a function of mixture composition. Several clear observations should be pointed out. First, within experimental certainty, the ratio is practically independent of the anion for all three employed solvents. Despite the anticipated significant anion influence on the studied dynamical properties due to substantial diversity of anion sizes, shapes,

symmetries and charge distribution, it is not confirmed in the present study. This can be an indication of either negligible or less probable, non-negligible but indistinguishable influence of different anions on the solvation pattern of the cations which is indirectly probed by the ratio of corresponding diffusion coefficients. This finding, however, does not rule out probable differences in ion-pairing tendencies of the studied ILs that could be probed by other more accurate techniques. Second, in all three employed solvents, the ratio scatters around some solvent-specific constant value at low IL content ($x_{\text{IL}} < 0.2$) before rising with increasing IL concentration. Following Hayamizu, such concentration dependence is a sign of strong interionic interactions leading to ionic aggregation at higher concentrations. The low concentration plateau regime, in turn, corresponds to a state where the major factors determining particle diffusivities, namely their hydrodynamic size, mode of interaction with the microenvironment and microviscosity of the surrounding medium, either do not change or change simultaneously for cations and solvent molecules. This can be treated as a range of compositions, where dilute solution-like solvation pattern is maintained, which is modulated only by the general viscosity increase with increasing IL content. Third, the rise at high IL concentrations is most pronounced for AN (at $x_{\text{IL}} \approx 0.85$, solvent molecules diffuse 4–5 times faster than cations compared to $D_{\text{solv}}/D_{+} = 2.5$ at $x_{\text{IL}} < 0.2$), whereas it is less significant in γ -BL and almost negligible in PC. The same order is observed for the magnitude of the low-concentration plateau value. This can be rationalized when comparing relative sizes of the solvent molecules and neat solvent properties. AN has the smallest molecule which results in higher value of the corresponding plateau value at $x_{\text{IL}} < 0.2$, as it is mainly determined by the relative sizes of the cation-solvent pair. γ -BL and PC have somewhat bigger molecules (see the Appendix for this chapter) and, hence, lower D_{solv}/D_{+} plateau values. Also AN is the least polar and least donating solvent among the studied set, which suggests that its interaction with ILs is more easily weakened with

increasing IL concentration when compared to the cases of γ -BL and PC. This could be the reason for the steeper slope of the high concentration part of the relative diffusion coefficient dependence AN-cation as it implies more significant changes in the diffusion-determining factors with concentration. Thus, our observations are perfectly in line with those of Hsu *et al.* for BmimPF₆-based systems.¹¹ The fact that relative diffusion coefficients from different investigations agree better than the corresponding absolute values probably stems from probe calibration errors.²⁴

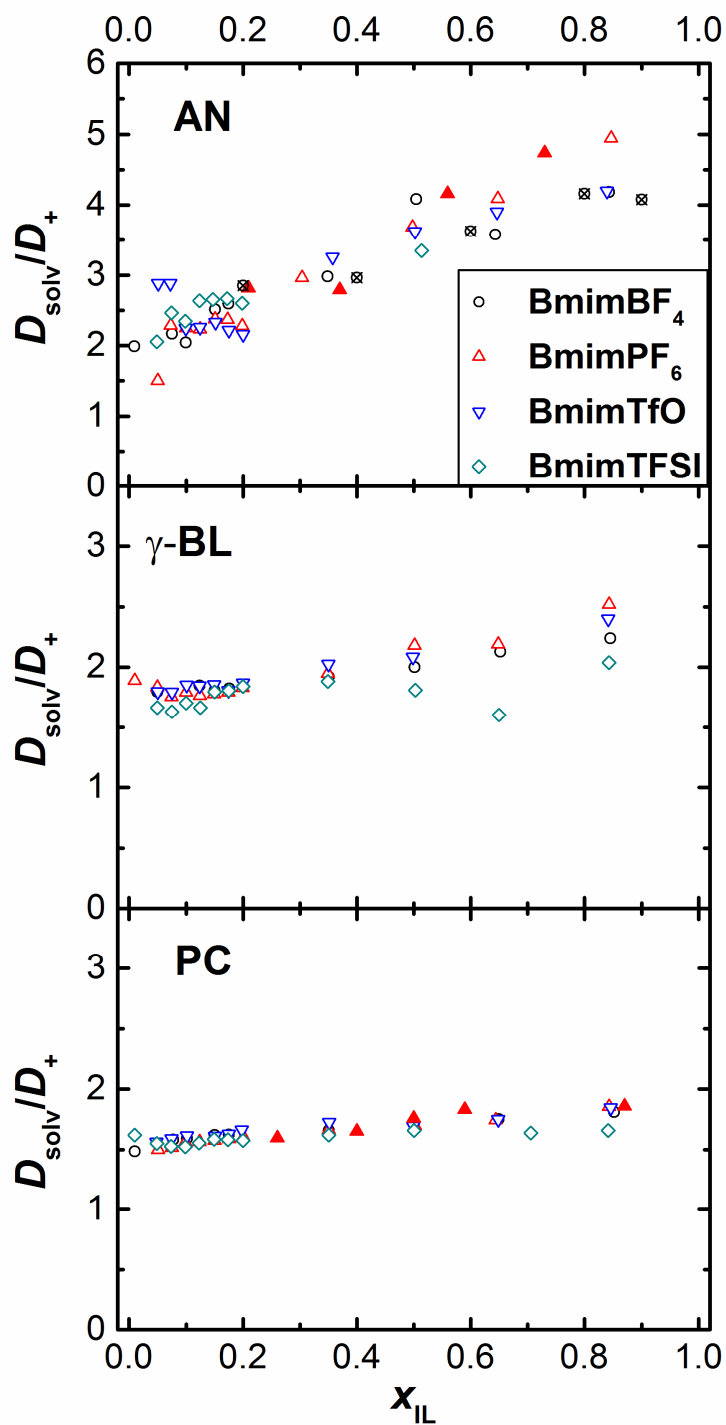


Figure 5.2. Ratio of self-diffusion coefficients for solvent molecules and cations as a function of IL molar fraction (open symbols). Solid symbols show results of Hsu *et al.*⁵⁸, while the crossed ones are from Liang *et al.*⁴⁴ for comparison.

When considering diffusion models, the Stokes-Einstein (SE) relation (eq (5.2)) is probably the most popular. It relates the self-diffusion coefficient, D , of a

particle to its hydrodynamic radius, r , a factor, A , determining the hydrodynamic boundary conditions (stick, slip or intermediate) and the medium viscosity, η .

$$D = \frac{kT}{A\pi\eta r} \quad (5.2)$$

Accurate absolute values of the hydrodynamic radii of diffusing species can be estimated from data obtained by NMR experiments only if the gradient calibration of the probe was properly performed and the SE relation holds its relevance.²⁵ Originally, the SE relation was derived under the assumption of a large sphere moving in a structureless continuum whose molecules are negligible in size with respect to the diffusing particle. In mixtures of molecular solvents with ILs the representative diffusing species are of comparable sizes, so one has to expect that generally the SE relation would not be satisfied. Indeed, usually unrealistically low values of the hydrodynamic radii of individual ions are found no matter how the boundary condition is set.^{12,21-23}

In an attempt to check the applicability of eq (5.2) to the studied systems we plot in Figure 5.3 for selected systems the effective Stokes radius $(Ar)_i = kT(D_i\eta\pi)^{-1}$ for cations and solvent molecules as a function of IL mole fraction. Viscosities were interpolated from experimental data by fitting logarithmic excess viscosities to a Riedlich-Kister type polynomial (see the Appendix for this chapter for details). This representation, based on experimentally accessible quantities only, was chosen since there is no a priori knowledge of the hydrodynamic factor, A , for these systems. Moreover, it cannot be excluded that A varies with composition due to possible changes of diffusion mechanism, solution structure, and/or boundary condition. Figure 5.3 provides strong evidence that for the studied mixtures viscosity grows faster than particle diffusivities decrease when the IL concentration is increased. According to theory, the A factor in eq (5.2) equals four for slip²⁶ and six²⁷ for stick hydrodynamic boundary conditions. Taking this into account, reasonable values of the hydrodynamic radii of cations and solvent molecules

(3.65 Å for Bmim⁺ cation and 2.52, 2.95, and 3.06 Å for AN, γ -BL, and PC molecules, respectively, as estimated from quantum-chemical calculations of molecular volumes, see Appendix for this chapter for details) can only be expected at very low IL content. Moreover, predicted effective radii of the ion pairs range from *ca.* 4.0 to 4.5 Å (see Table A 5.4) suggesting that it is rather individual cations than the ion pairs which are the representative diffusing entities containing cation at these mole fractions. At higher concentrations, the apparent hydrodynamic sizes progressively decrease down to unphysical values <2 Å. We consider this as strong evidence for the inadequacy of the SE relation in concentrated mixtures of ILs with molecular solvents and a clear indication of severe changes in solution microstructure and associated dynamics.

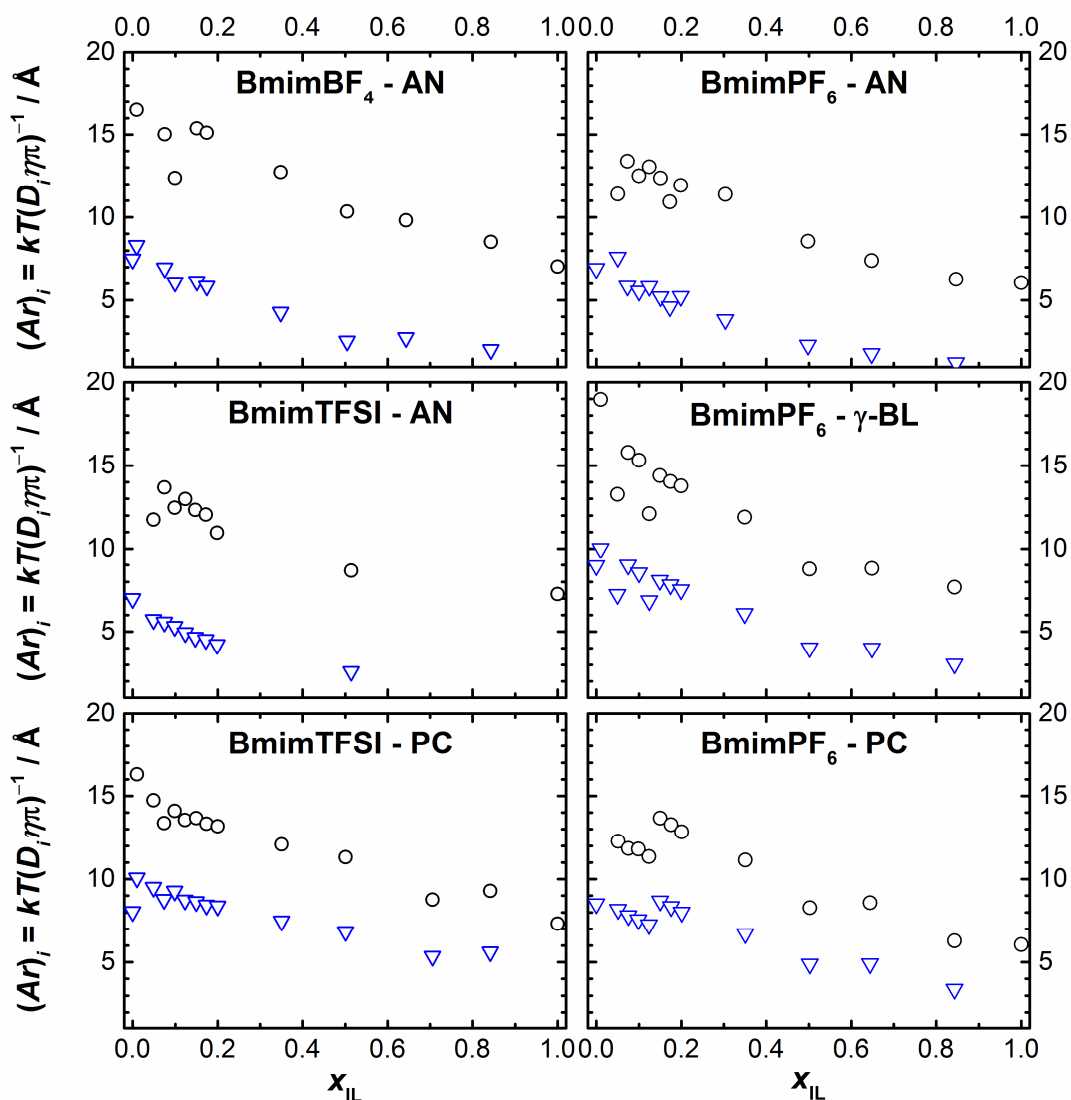


Figure 5.3. Estimated effective Stokes radii, A_r , for cations (black circles) and solvent molecules (blue down-triangles) in selected mixtures as a function of the IL mole fraction.

Such a monotonic decrease of effective radii with IL concentration was also observed in $\text{BmimBF}_4/\text{PF}_6\text{-PEG}^{28}$ and in $\text{RmimMeSO}_3\text{-H}_2\text{O}$ mixtures.^{4,7} In the latter case, this was interpreted as an increase in the size of non-polar domains formed by cation aggregates induced by the added solvent. In another recent study by Scharf *et al.*²⁹ on EmimTFSI dissolved in organic solvents of different polarity at very high dilutions ($x_{\text{IL}} < 0.005$) the results of a Stokes-Einstein analysis of the observed ionic diffusivities were interpreted in terms of weighted averages of dissociated and ion-paired species. For the least polar employed solvent (CDCl_3)

the authors even detected a second set of resonances that was attributed to large ionic aggregates with aggregation numbers reaching 10–20.²⁹

5.2.3 Relative self-diffusion coefficients as a function of mixture composition

In case of BmimPF₆-based systems we were also able to follow anion diffusion by means of ³¹P nuclei. The so obtained D_- values allowed us to calculate corresponding diffusivity ratios of solvent/anion and anion/cation which are plotted together with already discussed solvent/cation ratios in Figure 5.4.

In contrast to the latter, solvent/anion ratios do not show a plateau at low concentrations (though more points are needed to prove this) and rise more steeply. This results in an inversion of ionic diffusivities, *i.e.*, at $x_{IL} < 0.3-0.4$ anions diffuse faster than cations, whereas in concentrated solutions and in neat ILs the opposite is observed. Interestingly, the inversion trend is very similar for all the three solvents.

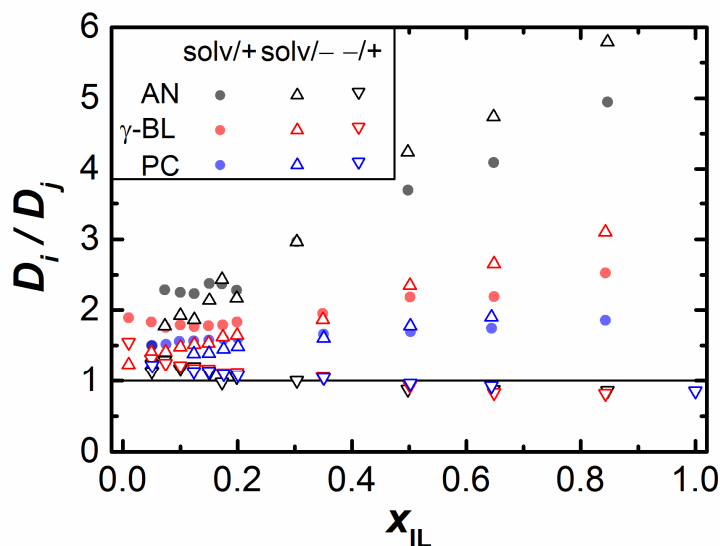


Figure 5.4. Ratio of diffusion coefficients for solvent molecules, cations and anions in BmimPF₆-based mixtures vs IL mole fraction.

To the best of our knowledge, Hsu *et al.*^{11,30} were the first to pay attention to the observation that the unexpectedly low diffusivity of the smaller anions in pure

ILs can be enhanced more efficiently than that of the bigger cations by heating and/or dilution with molecular solvent. In other words, at a certain degree of dilution/heating an inversion is expected. On the basis of their various observations, mainly on BmimPF₆-based systems,¹¹ Hsu *et al.* proposed and later³⁰ claimed the hypothesis of hyper-anion prevalence. The hypothesis implies that in pure ILs and in concentrated solutions along with neutral ion aggregates, there are also (predominantly singly) charged associates. In accordance with this hypothesis, these charged aggregates are preferably enriched with anions. In other words, positively charged aggregates should be generally smaller in size than those with negative excess charge. Since NMR-diffusometry operates at a timescale of tens to hundreds of milliseconds, the observed self-diffusion coefficient is an apparent value averaged over all diffusing species. Thus, if one follows the hypothesis, anions are mainly localized in larger aggregates, which diffuse slower than the smaller cation-enriched aggregates. As a result, in pure ILs and in concentrated solutions (where the native supramolecular network structure of the neat ILs is maintained) $D_+ > D_-$, despite the opposite prediction from ion size. Upon dilution and/or heating, the aggregates get smaller and smaller until complete dissociation is reached and individual ions are the representative diffusing species. At this stage, the anticipated relative order of diffusion coefficients is found. This approach has also been used to explain similar observations on aqueous systems.³

There are other explanations of the anomaly of ionic diffusion coefficients in pure ILs in the literature. Stark *et al.*, in their studies on RmimMeSO₃-H₂O mixtures,^{4,10} employed ideas of fast fluctuating nonpolar domains existing in neat ILs and in concentrated solutions. The domains are considered to be composed of the alkyl moieties of the cations and to have a pseudomicellar structure. It was claimed that at the same hopping rate for counterions, cations have to pass longer distances between different aggregates than the anions which diffuse in between the aggregates. This should result in higher values for cation self-diffusion coefficients.

We believe that any speculation on details of ionic motions in such complex systems as ILs and their mixtures with molecular components of different compositions should be based on some strong knowledge of diffusion mechanism. This can be achieved by means of complementary use of rather sophisticated experimental, *e.g.*, quasi-elastic scattering techniques, and simulation, *e.g.*, well-parametrized molecular dynamics (MD), methodologies which is still likely a ‘tabula rasa’ in the field of ILs. Urahata and Ribeiro³¹ used equilibrium MD with nonpolarizable force-field for singly charged ILs of RmimHal and RmimPF₆ type to elucidate that cation diffusion is strongly anisotropic: compared to anion diffusion it is significantly enhanced in the direction perpendicular to the line connecting the imidazolium-ring nitrogen atoms in the ring plane. However, these results should be considered with caution as it has been frequently shown that significant polarization phenomena have to be taken into account to accurately capture dynamical properties of IL-based systems by means of MD simulations.³²⁻³³ Similar, but somewhat different results concerning the anisotropy of cation diffusion were obtained by Liu and Maginn³⁴ from MD simulations of BmimTFSI where ionic charges were downscaled by 20%. We stress the urgent need of such studies to shed light on the diffusion mechanism and on the nature of the diffusing particles. Our results prove that the inversion of diffusion coefficients is a kind of universal behavior in mixtures of ILs with molecular solvents.

5.3. Conclusions

In the present study, mixtures of BmimBF₄, BmimPF₆, BmimTfO, and BmimTFSI with AN, γ -BL, and PC were studied over the entire composition range by means of NMR-diffusometry at 300 K. Diffusion coefficients of the solvent molecules, cations, and anions progressively decrease with IL addition, roughly following the exponential viscosity increase. In a given solvent, the relative diffusion coefficients of solvent/cation (D_{solv}/D_+) are independent of the anion.

Data scatter around a constant value at $x_{\text{IL}} < 0.2$ and increase at higher concentrations. This increase is most pronounced for AN, less significant in γ -BL, and almost negligible in PC and may be an indication of rather strong cation solvation (both individual and/or in ionic aggregates) in γ -BL and PC over the entire composition range employed in this study.

From the observed variation of the effective hydrodynamic radius with composition, a significant change in solution structure and dynamics is expected for the mixtures of all three studied solvents. For the BmimPF₆-based system, a solvent-independent inversion of ionic diffusivities is observed around $x_{\text{IL}} \approx 0.3$ -0.4. At low IL content anions diffuse faster than cations as anticipated from their relative sizes, whereas at high concentrations and in neat ILs anion diffusion is slower. A separate study on the diffusion mechanism is needed to explain this rather universal behavior for IL-solvent mixtures.

5.4. References for Chapter 5

- (1) Price, W. S., NMR Diffusometry. *Mod. Magn. Reson.* **2006**, Part 1, 109-115.
- (2) Menjoge, A.; Dixon, J.; Brennecke, J. F.; Maginn, E. J.; Vasenkov, S., Influence of Water on Diffusion in Imidazolium-Based Ionic Liquids: A Pulsed Field Gradient NMR study. *J. Phys. Chem. B* **2009**, *113*, 6353-6359.
- (3) Hou, J.; Zhang, Z.; Madsen, L. A., Cation/Anion Associations in Ionic Liquids Modulated by Hydration and Ionic Medium. *J. Phys. Chem. B* **2011**, *115*, 4576-4582.
- (4) Stark, A.; Zidell, A. W.; Hoffmann, M. M., Is the Ionic Liquid 1-Ethyl-3-Methylimidazolium Methanesulfonate [emim][MeSO₃] Capable Of Rigidly Binding Water? *J. Mol. Liq.* **2011**, *160*, 166-179.
- (5) Rollet, A.-L.; Porion, P.; Vaultier, M.; Billard, I.; Deschamps, M.; Bessada, C.; Jouvensal, L., Anomalous Diffusion of Water in [BMIM][TFSI] Room-Temperature Ionic Liquid. *J. Phys. Chem. B* **2007**, *111*, 11888-11891.
- (6) Hall, C. A.; Le, K. A.; Rudaz, C.; Radhi, A.; Lovell, C. S.; Damion, R. A.; Budtova, T.; Ries, M. E., Macroscopic and Microscopic Study of 1-Ethyl-3-methyl-imidazolium Acetate–Water Mixtures. *J. Phys. Chem. B* **2012**, *116*, 12810-12818.
- (7) Stark, A.; Zidell, A. W.; Russo, J. W.; Hoffmann, M. M., Composition Dependent Physicochemical Property Data for the Binary System Water and the Ionic Liquid 1-Butyl-3-methylimidazolium Methanesulfonate ([C₄mim][MeSO₃]). *J. Chem. Eng. Data.* **2012**, *57*, 3330-3339.
- (8) Cornellias, A.; Perez, L.; Comelles, F.; Ribosa, I.; Manresa, A.; Garcia, M. T., Self-Aggregation and Antimicrobial Activity of Imidazolium and Pyridinium Based Ionic Liquids in Aqueous Solution. *J. Colloid Interface Sci.* **2011**, *355*, 164-171.
- (9) Hawlicka, E., Self-Diffusion in Multicomponent Liquid Systems. *Chem. Soc. Rev.* **1995**, *24*, 367-377.
- (10) Scharf, N. T.; Stark, A.; Hoffmann, M. M., Ion Pairing and Dynamics of the Ionic Liquid 1-Hexyl-3-methylimidazolium Bis(irifluoromethylsulfonyl)amide ([C₆mim][NTf₂]) in the Low Dielectric Solvent Chloroform. *J. Phys. Chem. B* **2012**, *116*, 11488-11497.
- (11) Hsu, W.-Y.; Tai, C.-C.; Su, W.-L.; Chang, C.-H.; Wang, S.-P.; Sun, I. W., A Criterion for Proper Cosolvents Used for Ionic Liquids: the Lewis Acidic and Basic Dual Nature of Propylene Carbonate. *Inorg. Chim. Acta* **2008**, *361*, 1281-1290.
- (12) Liang, M.; Zhang, X.-X.; Kaintz, A.; Ernsting, N. P.; Maroncelli, M., Solvation Dynamics in a Prototypical Ionic Liquid + Dipolar Aprotic Liquid Mixture: 1-Butyl-3-methylimidazolium Tetrafluoroborate + Acetonitrile. *J. Phys. Chem. B* **2014**, *118*, 1340–1352.
- (13) Wang, J.; Tian, Y.; Zhao, Y.; Zhuo, K., A volumetric and viscosity study for the mixtures of 1-n-butyl-3-methylimidazolium tetrafluoroborate ionic liquid with acetonitrile, dichloromethane, 2-butanone and N, N - dimethylformamide. *Green Chem.* **2003**, *5*, 618-622.
- (14) Seddon, K. R.; Stark, A.; Torres, M.-J., Influence of Chloride, Water, and Organic Solvents on the Physical Properties of Ionic Liquids. *Pure Appl. Chem.* **2000**, *72*, 2275-2287.
- (15) Hayamizu, K.; Aihara, Y.; Arai, S.; Garcia, Pulse-Gradient Spin-Echo ¹H, ⁷Li, and ¹⁹F NMR Diffusion and Ionic Conductivity Measurements of 14 Organic Electrolytes Containing LiN(SO₂CF₃)₂. *J. Phys. Chem. B* **1999**, *103*, 519-524.
- (16) Aihara, Y.; Sugimoto, K.; Price, W. S.; Hayamizu, K., Ionic Conduction and Self-Diffusion Near Infinitesimal Concentration in Lithium Salt-Organic Solvent Electrolytes. *J. Chem. Phys.* **2000**, *113*, 1981-1991.

- (17) Hayamizu, K., Temperature Dependence of Self-Diffusion Coefficients of Ions and Solvents in Ethylene Carbonate, Propylene Carbonate, and Diethyl Carbonate Single Solutions and Ethylene Carbonate + Diethyl Carbonate Binary Solutions of LiPF₆ Studied by NMR. *J. Chem. Eng. Data.* **2012**, *57*, 2012-2017.
- (18) Hayamizu, K.; Matsuo, A.; Arai, J., A Divalent Lithium Salt Li₂B₁₂F₁₂ Dissolved in Propylene Carbonate Studied by NMR Methods. *J. Electrochem. Soc.* **2009**, *156*, A744-A750.
- (19) Hayamizu, K.; Aihara, Y., Ion and Solvent Diffusion and Ion Conduction of PC-DEC and PC-DME Binary Solvent Electrolytes Of LiN(SO₂CF₃)₂. *Electrochim. Acta* **2004**, *49*, 3397-3402.
- (20) Aihara, Y.; Bando, T.; Nakagawa, H.; Yoshida, H.; Hayamizu, K.; Akiba, E.; Price, W. S., Ion Transport Properties of Six Lithium Salts Dissolved in γ -Butyrolactone Studied by Self-Diffusion and Ionic Conductivity Measurements. *J. Electrochem. Soc.* **2004**, *151*, A119-A122.
- (21) Alam, T. M.; Dreyer, D. R.; Bielawski, C. W.; Ruoff, R. S., Combined Measurement of Translational and Rotational Diffusion in Quaternary Acyclic Ammonium and Cyclic Pyrrolidinium Ionic Liquids. *J. Phys. Chem. B* **2013**, *117*, 1967-1977.
- (22) Hayamizu, K.; Tsuzuki, S.; Seki, S.; Umebayashi, Y., Multinuclear NMR Studies on Translational and Rotational Motion for Two Ionic Liquids Composed of BF₄ Anion. *J. Phys. Chem. B* **2012**, *116*, 11284-11291.
- (23) Taylor, A. W.; Licence, P.; Abbott, A. P., Non-classical diffusion in ionic liquids. *Phys. Chem. Chem. Phys.* **2011**, *13*, 10147-10154.
- (24) Durand, J.; Fernández, F.; Barrière, C.; Teuma, E.; Gómez, K.; González, G.; Gómez, M., DOSY Technique Applied to Palladium Nanoparticles in Ionic Liquids. *Magn. Reson. Chem.* **2008**, *46*, 739-743.
- (25) Macchioni, A.; Ciancaleoni, G.; Zuccaccia, C.; Zuccaccia, D., Determining Accurate Molecular Sizes in Solution Through NMR Diffusion Spectroscopy. *Chem. Soc. Rev.* **2008**, *37*, 479.
- (26) McLaughlin, E., Viscosity and self-diffusion in liquids. *Trans. Faraday Soc.* **1959**, *55*, 28-38.
- (27) Einstein, A. *Investigations on the Theory of the Brownian Movement*; Dover Publications: New York, 1956; 144 p.
- (28) Wu, T.-Y.; Wang, H.-C.; Su, S.-G.; Gung, S.-T.; Lin, M.-W.; Lin, C.-b., Characterization of Ionic Conductivity, Viscosity, Density, and Self-Diffusion Coefficient for Binary Mixtures of Polyethyleneglycol (or Polyethyleneimine) Organic Solvent with Room Temperature Ionic Liquid BMIBF₄ (or BMIPF₆). *Journal of the Taiwan Institute of Chemical Engineers* **2010**, *41*, 315-325.
- (29) Scharf, N.; Stark, A.; Hoffmann, M., Calorimetric Study on the Ion Pairing and Aggregation of 1-Ethyl-3-Methylimidazolium bis(trifluoromethylsulfonyl)amide ([C₂mim][NTf₂]) and Related Ionic Liquids in the Low-Dielectric Constant Solvent Chloroform. *J. Solution. Chem.* **2013**, *42*, 2034-2056.
- (30) Chen, W.-T.; Hsu, W.-Y.; Lin, M.-Y.; Tai, C.-C.; Wang, S.-P.; Sun, I. W., Isolated BMI⁺ Cations Are More than Isolated PF₆⁻ Anions in the Room Temperature 1-Butyl-3-Methylimidazolium Hexafluorophosphate (BMI-PF₆) Ionic Liquid. *Journal of the Chinese Chemical Society* **2010**, *57*, 1293-1298.
- (31) Urahata, S. M.; Ribeiro, M. C. C., Single Particle Dynamics in Ionic Liquids of 1-Alkyl-3-Methylimidazolium Cations. *J. Chem. Phys.* **2005**, *122*, 024511.
- (32) Chaban, V., Polarizability versus mobility: atomistic force field for ionic liquids. *Phys. Chem. Chem. Phys.* **2011**, *13*, 16055-16062.
- (33) Chaban, V. V.; Voroshylova, I. V.; Kalugin, O. N.; Prezhdo, O. V., Acetonitrile boosts conductivity of imidazolium ionic liquids. *J. Phys. Chem. B* **2012**, *116*, 7719-7727.

(34) Liu, H.; Maginn, E., A molecular dynamics investigation of the structural and dynamic properties of the ionic liquid 1-n-butyl-3-methylimidazolium bis(trifluoromethanesulfonyl)imide. *J. Chem. Phys.* **2011**, *135*, 124507.

5.5. Chapter 5 Appendix

Table A 5.1 Experimental self-diffusion coefficients of molecules and ions D_i ($10^{-10} \text{ m}^2 \text{ s}^{-1}$) in mixtures of imidazolium ILs with polar molecular solvent as a function of IL mole fraction

x_{IL}								
x_{IL}	D_{solv}	D_+	x_{IL}	D_{solv}	D_+	x_{IL}	D_{solv}	D_+
BmimTfO – AN			BmimTfO – γ -BL			BmimTfO – PC		
0.0514	36.0	12.5	0.0502	7.9	4.4	0.0486	5.15	3.3
0.0725	36.0	12.5	0.0756	7.0	3.9	0.0747	3.89	2.45
0.0996	26.9	12.0	0.1010	6.3	3.4	0.1019	3.5	2.17
0.1244	23.9	10.6	0.1241	5.9	3.2	0.1510	2.9	1.8
0.1514	21.4	9.2	0.1499	5.2	2.8	0.1755	2.7	1.66
0.1753	18.8	8.5	0.1746	4.7	2.6	0.1982	2.51	1.51
0.2004	16.6	7.7	0.2005	4.3	2.3	0.3512	1.57	0.91
0.3574	6.5	2.0	0.3500	2.53	1.25	0.4995	1.15	0.68
0.5029	3.8	1.05	0.4992	1.75	0.84	0.6487	0.7	0.4
0.6465	2.3	0.59	0.8419	0.72	0.3	0.8464	0.48	0.26
0.8392	1.3	0.31						
BmimTFSI – AN			BmimTFSI – γ -BL			BmimTFSI – PC		
0.0492	39.0	19.0	0.0500	5.5	3.3	0.0100	4.7	2.9
0.0746	32.0	13.0	0.0754	4.89	3.0	0.0489	4.11	2.65
0.0991	27.2	11.6	0.1005	4.6	2.7	0.0738	3.97	2.6
0.1237	24.0	9.1	0.1253	4.73	2.84	0.0990	3.35	2.2
0.1475	21.1	7.95	0.1500	4.1	2.28	0.1234	3.2	2.06
0.1724	18.0	6.75	0.1749	3.81	2.11	0.1495	2.9	1.83
0.1986	16.0	6.15	0.2000	3.26	1.77	0.1739	2.69	1.7
0.5144	4.62	1.38	0.3492	2.13	1.13	0.2004	2.44	1.55
			0.5033	1.51	0.834	0.3506	1.62	1.0
			0.6504	1.25	0.78	0.5013	1.14	0.688
			0.8433	0.76	0.373	0.7056	0.88	0.537
						0.8414	0.63	0.38

Table A 5.1 continued

x_{IL}	D_{solv}	D_+	x_{IL}	D_{solv}	D_+	x_{IL}	D_{solv}	D_+
BmimBF ₄ – AN			BmimBF ₄ – γ -BL			BmimBF ₄ – PC		
0.0095	41.8	21.0	0.0497	7.9	4.4	0.0099	4.97	3.35
0.0751	27.5	12.7	0.1240	6.1	3.3	0.0778	3.8	2.4
0.0997	25.7	12.6	0.1505	4.37	2.42	0.1019	3.5	2.2
0.1512	17.2	6.85	0.1757	4.01	2.2	0.1501	3.0	1.85
0.1745	15.3	5.9	0.3503	2.19	1.14	0.1751	2.76	1.7
0.3486	6.94	2.33	0.5020	1.39	0.695	0.3503	1.51	0.91
0.5047	4.9	1.2	0.6525	0.888	0.417	0.6491	0.66	0.377
0.6434	2.22	0.62	0.8454	0.571	0.255	0.8517	0.395	0.218
0.8434	1.18	0.282						

x_{IL}	D_{solv}	D_+	D_-	x_{IL}	D_{solv}	D_+	D_-	x_{IL}	D_{solv}	D_+	D_-
BmimPF ₆ – AN				BmimPF ₆ – γ -BL				BmimPF ₆ – PC			
0.0504	30.0	20.0	22.6	0.0100	7.0	3.7	5.7	0.0514	4.8	3.2	3.9
0.0735	32.0	14.0	18.05	0.0496	7.7	4.2	5.5	0.0751	4.4	2.9	-
0.1002	27.0	12.0	14.05	0.0750	5.35	3.05	3.8	0.0991	3.97	2.54	-
0.1247	21.0	9.4	11.26	0.1003	4.88	2.72	3.3	0.1240	3.6	2.3	2.6
0.1511	19.0	8.0	8.9	0.1243	5.3	3.0	3.5	0.1506	2.6	1.65	1.87
0.1733	18.0	7.6	7.4	0.1495	3.9	2.19	2.55	0.1761	2.35	1.48	1.62
0.1987	13.0	5.7	6.0	0.1745	3.5	1.95	2.16	0.2007	2.15	1.34	1.45
0.3040	8.0	2.7	2.7	0.1996	3.17	1.73	1.93	0.3505	1.18	0.71	0.736
0.4985	3.5	0.95	0.826	0.3491	1.74	0.892	0.935	0.5025	0.78	0.46	0.44
0.6479	1.8	0.44	0.38	0.5018	1.2	0.55	0.51	0.6443	0.41	0.235	0.216
0.8469	0.84	0.17	0.145	0.6483	0.583	0.266	0.22	0.8428	0.26	0.14	
				0.8431	0.31	0.123	0.1				

Table A 5.2 Third order polynomial fitting coefficients a_i and standard deviations σ for logarithmic diffusion coefficients ($\log(D_i / \text{m}^2 \text{s}^{-1})$) as a function of IL mole fraction (x_{IL})

system	a_0	a_1	a_2	a_3	σ
BmimTfO – AN					
solv	–8.28	–2.8	1.1	0	0.026
cation	–8.71	–2.3	–1.0	1	0.068
BmimTfO – γ-BL					
solv	–8.99	–2.18	1.7	–0.9	0.008
cation	–9.25	–2.25	1.5	–0.8	0.011
BmimTfO – PC					
solv	–9.22	–2.3	2.2	–1.2	0.031
cation	–9.42	–2.3	1.9	–0.9	0.032
BmimTFSI – AN					
solv	–8.24	–3.7	6	–5	0.006
cation	–8.56	–4.2	4.3	–2.0	0.028
BmimTFSI – γ-BL					
solv	–9.16	–1.8	1.5	–0.8	0.027
cation	–9.37	–2.0	1.6	0	0.051
BmimTFSI – PC					
solv	–9.29	–1.9	1.7	–0.8	0.017
cation	–9.50	–1.7	0.8	–0.8	0.023
BmimBF₄ – AN					
solv	–8.35	–3.0	2.7	–1.6	0.047
cation	–8.64	–3.6	2.4	–0.9	0.040
BmimBF₄ – γ-BL					
solv	–8.97	–2.7	2.3	0	0.036
cation	–9.23	–2.6	1.7	–0.7	0.029
BmimBF₄ – PC					
solv	–9.29	–1.68	5	0	0.006
cation	–9.47	–1.83	5	0	0.012
BmimPF₆ – AN					
solv	–8.33	–2.8	0	0	0.036
cation	–8.53	–4.1	2.8	–1.3	0.026
anion	–8.417	–4.68	3.43	–1.52	0.002
BmimPF₆ – γ-BL					
solv	–9.09	–2.2	0	0	0.049
cation	–9.36	–1.8	0	0	0.046
anion	–9.21	–2.5	0	0	0.044
BmimPF₆ – PC					
solv	–9.16	–2.9	2.4	–1.1	0.037
cation	–9.33	–3.1	2.7	–1.3	0.034
anion	–9.26	–3.3	2.6	–1.3	0.041

Details of viscosity calculations

The mixture viscosities that were taken to calculate the effective hydrodynamic radii of the diffusing particles (Figure 5.3) were interpolated from published experimental data (for BmimBF₄ – AN^{A5.1}, BmimTFSI – AN^{A5.2}, and BmimTFSI – PC^{A5.3}) or from our own measurements (for BmimPF₆ – *solv* systems), both obtained at 298.15 K. The latter were carried out at Regensburg University with an Anton Paar AMVn rolling-ball microviscometer. Results of eight repetitive measurements at two tilt angles of the capillary were averaged for each sample. Every employed set ‘capillary – rolling ball’ was preliminary calibrated with degassed Millipore water and suitable calibration oils (supplied by Cannon Instrument Company) at exactly the same experimental conditions. Densities of the mixtures needed to convert rolling time to dynamic viscosity were measured with an Anton Paar DMA 5000 M vibrating-tube densimeter. We estimate that errors due to temperature mismatch (our diffusion measurements were performed at 300 K) are comparable or smaller than those due to interpolation errors and the well-known scattering of pure-IL viscosities in the literature.

Viscosity values at desired mixture compositions, $\eta_{mix}(x_{IL})$, were calculated following the methodology described by Canongia Lopez *et al.*^{A5.2} who used an extended empirical Grunberg-Nissan equation A5.1

$$\eta_{mix}(x_{IL}) = \eta_{solv}^{1-x_{IL}} \eta_{IL}^{x_{IL}} \eta^{ex} \quad (\text{A5.1})$$

where η_{solv} and η_{IL} correspond to the viscosities of pure solvent and IL, respectively, while an excess term, η^{ex} , was estimated via a third-order Redlich-Kister type interpolation polynomial (A5.2).

$$\ln(\eta^{\text{ex}}(x_{\text{IL}})) = x_{\text{IL}}(1-x_{\text{IL}}) \sum_{i=0}^2 A_i (2x_{\text{IL}}-1)^i \quad (\text{A5.2})$$

The fit parameters A_i of eq A5.2 are collected in Table A 5.3.

Table A 5.3. Redlich-Kister polynomial fitting coefficients A_i for the logarithmic excess dynamic viscosities ($\ln(\eta / \text{mPa s})$) as a function of IL mole fraction (x_{IL}) for selected mixtures and the standard deviations of the fits σ

system	A_0	A_1	A_2	σ
BmimPF ₆ – AN	1.89	-0.40	-0.13	0.03
BmimPF ₆ – γ -BL	0.79	-0.03	0.00	0.006
BmimPF ₆ – PC	1.04	-0.13	-0.07	0.008
BmimBF ₄ – AN	2.05	-1.05	0.76	0.015
BmimTFSI – AN	3.50	-1.18	0.32	0.008
BmimTFSI – PC	1.53	-0.47	0.19	0.008

Estimation of radii of particles

Effective radii of the solvent molecules, cations and selected ion pairs were recalculated in terms of spherical approximation from molecular volumes. The latter were estimated as the amount of space enclosed within the 0.001 a.u. electronic density isosurface obtained for the corresponding minimal energy geometries at the M06-2X/6-311++G(d,p) level of theory using GAUSSIAN 09 program suite^{A5.4}. In order to reduce errors in the estimation of molecular volume an increased density of integration points was employed (keyword `Volume=Tight`) along with averaging over 15 values. The anticipated uncertainty in thus calculated effective radii is assumed to be within 0.05 Å.

Table A 5.4. Effective radii of the solvent molecules, cation and selected ion pairs as estimated from quantum-chemical calculations

Particle	Effective radius, Å
AN	2.52
γ -BL	2.95
PC	3.06
Bmim ⁺	3.65
BmimBF ₄	3.97
BmimPF ₆	4.08
BmimTFSI	4.53

References for Chapter 5 Appendix

(A5.1) Zhu, A.; Wang, J.; Han, L.; Fan, M., Measurements and Correlation of Viscosities and Conductivities for the Mixtures of Imidazolium Ionic Liquids with Molecular Solutes. *Chem. Eng. J.* **2009**, *147*, 27-35.

(A5.2) Canongia Lopes, J. N.; Costa Gomes, M. F.; Husson, P.; Pádua, A. I. A. H.; Rebelo, L. P. N.; Sarraute, S.; Tariq, M., Polarity, Viscosity, and Ionic Conductivity of Liquid Mixtures Containing [C₄C₁im][Ntf₂] and a Molecular Component. *J. Phys. Chem. B* **2011**, *115*, 6088-6099.

(A5.3) Vraneš, M.; Zec, N.; Tot, A.; Papović, S.; Dožić, S.; Gadžurić, S., Density, Electrical Conductivity, Viscosity and Excess Properties of 1-Butyl-3-Methylimidazolium Bis(trifluoromethylsulfonyl)imide + Propylene Carbonate Binary Mixtures. *J. Chem. Thermodyn.* **2014**, *68*, 98-108.

(A5.4) Frisch, M. J.; Trucks, G. W.; Schlegel, H. B.; Scuseria, G. E.; Robb, M. A.; Cheeseman, J. R.; Scalmani, G.; Barone, V.; Mennucci, B.; Petersson, G. A.; Nakatsuji, H.; Caricato, M.; Li, X.; Hratchian, H. P.; Izmaylov, A. F.; Bloino, J.; Zheng, G.; Sonnenberg, J. L.; Hada, M.; Ehara, M.; Toyota, K.; Fukuda, R.; Hasegawa, J.; Ishida, M.; Nakajima, T.; Honda, Y.; Kitao, O.; Nakai, H.; Vreven, T.; Montgomery, J. A. J.; Peralta, J. E.; Ogliaro, F.; Bearpark, M.; Heyd, J. J.; Brothers, E.; Kudin, K. N.; Staroverov, V. N.; Keith, T.; Kobayashi, R.; Normand, J.; Raghavachari, K.; Rendell, A.; Burant, J. C.; Iyengar, S. S.; Tomasi, J.; Cossi, M.; Rega, N.; Millam, J. M.; Klene, M.; Knox, J. E.; Cross, J. B.; Bakken, V.; Adamo, C.; Jaramillo, J.; Gomperts, R.; Stratmann, R. E.; Yazyev, O.; Austin, A. J.; Cammi, R.; Pomelli, C.; Ochterski, J. W.; Martin, R. L.; Morokuma, K.; Zakrzewski, V. G.; Voth, G. A.; Salvador, P.; Dannenberg, J. J.; Dapprich, S.; Daniels, A. D.; Farkas, O.; Foresman, J. B.; Ortiz, J. V.; Cioslowski, J.; Fox, D. J. *Gaussian 09, Revision D.01*, Gaussian, Inc.: Wallingford CT, 2013.

Chapter 6. Intermolecular Interactions in a Representative System IL-Molecular Solvent as Seen from Raman Spectroscopy

The material presented in this chapter forms the basis of publication

Marekha, B. A.; Koverga, V. A.; Moreau, M.; Kiselev, M.; Takamuku, T.; Kalugin, O. N.; Idrissi, A. *Intermolecular Interactions, Ion Solvation and Association in Mixtures of 1-n-Butyl-3-methylimidazolium Hexafluorophosphate and γ -Butyrolactone: Insights from Raman Spectroscopy*. Accepted for publication in **J. Raman Spectrosc.**

By means of Raman spectroscopy coupled with DFT calculations and Perturbation Correlation Moving Window two-dimensional correlation spectroscopy intermolecular interactions were assessed in mixtures of ionic liquid (IL) 1-*n*-butyl-3-methylimidazolium hexafluorophosphate (BmimPF₆) with polar aprotic solvent γ -butyrolactone (γ -BL) over the entire range of compositions. Symmetrical P-F stretching vibration of IL anion was found to be insensitive to changes in mixture concentration in contrast to C=O stretching vibration of γ -BL and imidazolium ring C-H stretching vibrations of IL cation. Each of these vibrational profiles was decomposed in various spectral contributions and their number was rationalized by the results of quantum-chemical calculations and/or by previous controversial published data. Progressive redshift of the ring C-H stretching wavenumbers was referred to pronounced solvation of cation at the imidazolium ring site accompanied with hydrogen bond formation. This is especially pronounced at $x_{\text{IL}} < 0.18$. Complicated variations in intensities of individual spectral contributions of the C=O profile were treated as a manifestation of the changing with concentration pattern of intermolecular interactions. Self-association of γ -BL molecules and distinct cation solvation as dominant intermolecular interactions at low IL content are replaced with weaker cation solvation and ion association at high concentrations of BmimPF₆. Possible representative molecular structures are proposed on the basis of DFT calculations.

6.1. Introduction

Vibrational spectroscopy techniques (ATR and transmission IR as well as Raman scattering) have been widely used to study intermolecular interactions in mixtures of imidazolium ILs with molecular solvents (hereafter we will generally refer to intermolecular interactions both in the sense of interactions between neutral solvent molecules and interactions involving molecular ions, *i.e.* ion-ion and ion-molecule).¹ Due to traditional interest and ubiquitous use of aqueous systems, the vast majority of published to date reports on IR or Raman studies on mixtures of ILs with molecular solvents concern those with H₂O or D₂O.²⁻¹³ The main topics covered by Raman spectroscopy are conformational isomerism along the C^α-C^β torsion (see Figure 6.1 for numbering) of the alkyl side chain of Rmim⁺ cation manifested in a set of bands in the region 500-700 cm⁻¹^{9-10,13-15} and hydrogen bonding at imidazolium ring reflected in the stretching region of C^(2,4,5)-H vibrations at 3000-3300 cm⁻¹.^{11,16} The latter issue was much more thoroughly studied by means of IR spectroscopy where the corresponding ring C-H stretching bands are significantly more intense and show higher sensitivity to variations in the microenvironment induced by the change in concentration.^{2-9,17-19}

Nevertheless, a number of studies (mainly using IR) have also dealt with mixtures of imidazolium ILs with such protic non-aqueous solvents as ethanol,²⁰ methanol,^{5,17,20-26} and ethylene glycol²⁷⁻²⁸ as well as with aprotic ones like DMSO,²⁹⁻³² AN,^{26,33-35} acetone³⁶ or chloroform.³⁷

Taking into account the complexity of the anticipated spectral changes as a function of mixture composition it has become a common practice to complement conventional spectra examination and band fitting steps with two-dimensional correlation spectroscopy (2DCoS)^{4,7-8,22,29,31} and/or quantum chemical calculations of some representative model systems.^{2,5,7-8,13,19,21-22,25,29,31-33,37-42} These techniques can significantly facilitate detailed analysis of spectral changes in the systems by

suggesting tentative number and approximate position of individual spectral contributions, their assignment and anticipated behavior with changing concentration.

It was reported for the mixture of BmimPF₆ with γ -BL that cooling produces crystal phase of the molecular solvent only at $x_{\text{IL}} < 0.18$ whereas at higher IL content only amorphous phase could be obtained.⁴³ This result was interpreted as the lack of free solvent molecules at high concentrations of IL and the critical number of γ -BL molecules solvating cation was thus estimated to be around 4.6. In the same study the authors observed similar behavior for BmimBF₄- γ -BL mixture and the lower value of solvation number of 3.6 was related to higher propensity of BmimPF₆ to dissociate and, hence, to accumulate higher number of solvent molecules in the cation's solvation shell compared to BmimBF₄.

In this chapter we tackle the BmimPF₆- γ -BL system (see Figure 6.1 for molecular structures), from the point of view of prevailing interactions via their manifestation in Raman spectra. This mixture is known to exhibit particular concentration behavior reflected in its thermophysical⁴³ and dynamical properties (as shown in Chapter 5) and here we are seeking for spectroscopic evidence to justify the previously proposed explanations of concentration regime crossover at $x_{\text{IL}} \sim 0.2$.

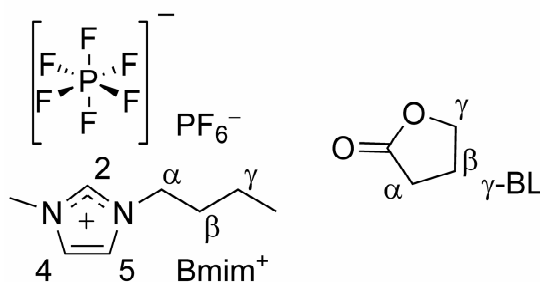


Figure 6.1. Molecular structures of BmimPF₆ and γ -BL. Nomenclature for carbon atoms of γ -BL as well as of the imidazolium ring and butyl chain of Bmim⁺ is also given.

We treat our results in terms of competition between solvation and ion association. Microscopic structural patterns deduced from the results presented here

will contribute to the general understanding of binary systems composed of ILs and polar aprotic molecular solvents. Quantum-chemical investigations and 2DCoS techniques were additionally used to help with data treatment and interpretation. The rest of the chapter is organized as follows: Section 6.2 presents details of two-dimensional correlation techniques used to help with analysis of the spectra; selection of bands for analysis is justified in section 6.3.1, the most important information relevant for the present analysis as derived from quantum-chemical calculations is presented in section 6.3.2, experimental results of each particular region selected for analysis are discussed in details in section 6.3.3. Conclusions are outlined in the last section of this chapter.

6.2. Advanced methods of Raman spectra analysis

General aspects of sample preparation and experimental procedure are outlined in Chapter 2. We will only reiterate here that we employed non-uniform concentration grid putting more concentrations in the range of IL mole fractions between 0.1 and 0.2 where we anticipated some significant changes in solution structure hinted by peculiar crystallization behavior,⁴³ by the occurrence of conductivity maximum in this range of compositions,⁴⁴⁻⁴⁶ and by the crossover of diffusion regimes (Chapter 5).

Apart from proper sampling of the concentration range of interest, the efficiency of spectral analysis by means of band fitting severely depends on a justified and unbiased selection of initial guess, *i.e.*, peak positions, widths, amplitudes. This is where advanced methods of spectra analysis, *e.g.*, 2DCoS and more elaborated ones come into play.

6.2.1 Two-dimensional correlation spectroscopy (2DCoS)

Generalized two-dimensional correlation spectroscopy (2DCoS) introduced by Noda⁴⁷ can enhance spectral resolution by probing spectral response to an

arbitrary external perturbation (temperature, sample composition etc.). This method is useful in discovering and assigning of hidden or strongly overlapping bands as it reveals correlations in perturbation induced variations between different spectral regions without *a priori* knowledge of the number of independent spectral contributions.

Calculation relies on some arbitrarily selected reference state and it is the variation of the dataset with respect to this reference which is plotted in synchronous and asynchronous spectra. For data that is unevenly spaced along the perturbation variable, which is our case since we used non-uniform concentration grid, the average reference spectrum $\bar{y}(\tilde{\nu})$ in a given data set of m spectra (where $m < n$, n being the total number of recorded spectra) was calculated as follows

$$\bar{y}(\tilde{\nu}) = \frac{\sum_{j=1}^m y_j(\tilde{\nu}, c_j) \cdot (c_{j+1} - c_{j-1})}{\sum_{j=1}^m (c_{j+1} - c_{j-1})} \quad (6.1)$$

where c_j stands for the corresponding concentrations. Two additional virtual concentrations outside the sampled region have to be defined as

$$c_0 = 2c_1 - c_2 \quad (6.2)$$

$$c_{m+1} = 2c_m - c_{m-1} \quad (6.3)$$

Thus obtained reference spectrum was then subtracted from original dataset $y(\tilde{\nu}, c_j)$ to obtain so-called dynamic spectrum $\tilde{y}(\tilde{\nu}, c_j)$:

$$\tilde{y}(\tilde{\nu}, c_j) = y(\tilde{\nu}, c_j) - \bar{y}(\tilde{\nu}) \quad (6.4)$$

Synchronous $\Phi(\tilde{\nu}_1, \tilde{\nu}_2)$ and asynchronous $\Psi(\tilde{\nu}_1, \tilde{\nu}_2)$ spectra were subsequently calculated as

$$\Phi(\tilde{\nu}_1, \tilde{\nu}_2) = \frac{\sum_{j=1}^m \tilde{y}_j(\tilde{\nu}_1, c_j) \cdot \tilde{y}_j(\tilde{\nu}_2, c_j) \cdot (c_{j+1} - c_{j-1})}{2(c_m - c_1)} \quad (6.5)$$

$$\Psi(\tilde{\nu}_1, \tilde{\nu}_2) = \frac{\sum_{j=1}^m \tilde{y}_j(\tilde{\nu}_1, c_j) \cdot \left(\frac{1}{2\pi} \sum_{k=1}^m \frac{\tilde{y}_k(\tilde{\nu}_2, c_k) \cdot (c_{k+1} - c_{k-1})}{c_k - c_j} \right) \cdot (c_{j+1} - c_{j-1})}{2(c_m - c_1)} \quad (6.6)$$

In synchronous spectra peaks at the same wavenumbers on both axes (diagonal or auto-peaks) show relative sensitivity of a given band to the applied perturbation. These peaks are always positive and their intensity reflects magnitude of the intensity variation. Symmetrical off-diagonal (also often called as cross-) peaks at a pair of wavenumbers $(\tilde{\nu}_1, \tilde{\nu}_2)$ indicate that in the corresponding spectral regions intensity changes are coherent and the higher the intensity of a cross-peak the higher the synchronicity between the two contributions. Positive and negative cross-peaks indicate same or opposite direction of intensity variation at a given pair of wavenumbers.

Asynchronous spectra have no peaks at diagonal, hence, only cross-peaks can be observed and they are antisymmetric with respect to it. An asynchronous peak at $(\tilde{\nu}_1, \tilde{\nu}_2)$ would mean that the corresponding spectral contributions vary out-of-phase when external application is applied. Typically, spectral contributions are neither purely synchronized nor asynchronous, *i.e.* they can show both synchronous and asynchronous peaks simultaneously. It is then possible to establish relative sequence of changes in accordance with Noda's rules⁴⁷: a positive asynchronous peak at $(\tilde{\nu}_1, \tilde{\nu}_2)$ indicates that the contribution at $\tilde{\nu}_1$ varies prior to that at $\tilde{\nu}_2$ if the corresponding synchronous cross-peak is positive and vice versa if it is negative.

2DCoS can help to reveal hidden peaks and shoulders which are not readily visible by inspection of 1D spectra. Moreover, some specific spectral changes such as wavenumber shift and bandwidth change can be recognized via characteristic patterns which are present in correlation spectra in such cases.⁴⁸⁻⁴⁹ When concentration is used as a perturbing factor and it is varied significantly, most of the observed spectral intensity variation would be caused mainly by the change of

the number of absorbing/emitting/scattering species. In order to reveal more details such as deviation from simple intensity scaling with concentration and other spectral effects, the spectra are normalized by concentration, by the area of internal reference band or by the total area of the spectrum. This allows one, in particular, to remove the general concentration effect.⁵⁰⁻⁵³ In our investigation prior to 2DCoS analysis baseline corrected spectra were normalized by the fitted area of a ring breathing vibration mode of γ -BL at 931 cm^{-1} as it was suggested in a Raman study on $\text{LiN}(\text{CF}_3\text{SO}_2)_2$ in γ -BL.⁵⁴ Our results show that peak position and full width at half height of this band vary by less than 0.5 cm^{-1} (see Chapter 6 Appendix) suggesting that this band is indeed hardly specifically affected by changing the concentration and, hence, can be reliably used for normalization.

6.2.2 Perturbation-correlation moving window 2DCoS

One of the drawbacks of conventional generalized two-dimensional correlation spectroscopy is that it probes the spectral response over the entire course of perturbation variable without giving any additional information if some spectral regions are particularly sensitive only at specific range of values of the perturbation variable. Moreover, if the same spectral region behaves strikingly different at various perturbation values a conclusion drawn from the correlation maps obtained for the entire dataset can be simply erroneous.⁵⁵⁻⁵⁶ It is possible though to split the entire dataset into smaller segments⁵⁶ and to apply classical 2DCoS for each segment with subsequent comparison of two-dimensional correlation maps between the data-segments. In order to overcome the ambiguity in proper selection of the segments, *e.g.*, the border between them, an approach called perturbation-correlation moving-window two-dimensional correlation spectroscopy (PCMW2DCoS) introduced by Morita *et al.*⁵⁷ is highly useful⁵⁶ and it has already been applied for such purpose for IL-based system.⁵⁸ Briefly, the algorithm scans the dataset by small portions ('moving windows') inside each of which the

correlation between spectral variation and the perturbation change is calculated in a manner similar to classical 2DCoS. As an output such analysis provides a synchronous and asynchronous correlation maps with spectral (wavenumber, frequency, wavelength etc.) and perturbation variables (temperature, concentration etc.) at the axes. Synchronous PCMW spectrum shows positive peaks in the regions where the spectral intensity varies in the same direction with the perturbation variable while the negative peaks represent regions with the opposite trends in changes of spectral intensity and perturbation variable. Simultaneously, signs of the peaks in corresponding asynchronous spectra show the convexity of these perturbation-induced variations. In a rough analogy, synchronous and asynchronous PCMW spectra correspond to derivative spectra with regard to perturbation variable of the first and second order, respectively.⁵⁷

In the present study we examined only synchronous PCMW spectra. In the total data set of n spectra for each moving window i which consists of $2l + 1$ spectra the calculation protocol requires to define the average \bar{c}_i and dynamic \tilde{c}_m concentrations as follows:

$$\bar{c}_i = \frac{1}{2l+1} \sum_{m=i-l}^{i+l} c_m \quad (6.7)$$

$$\tilde{c}_m = c_m - \bar{c}_i \quad (6.8)$$

where, for a given l value, m is the running index in each window and it changes from $i - l$ to $i + l$ while the number of windows is $n - 2l$ and the window index i takes integer values from $l + 1$ to $n - l$. Synchronous PCMW spectrum is then calculated for each window using the equation:

$$\Pi_{\Phi,i}(\bar{V}, c_i) = \frac{1}{2l} \sum_{m=i-l}^{i+l} \tilde{y}(\bar{V}, c_m) \cdot \tilde{c}_m \quad (6.9)$$

6.3. Results and Discussion

6.3.1 Selecting bands for analysis

Figure 6.2 shows Raman spectra of the neat components of the studied mixture. It is apparent that in the lower wavenumber region (below 1600 cm^{-1}) there is significant overlap between the spectral contributions of the IL and the solvent. This makes this spectral region not informative and difficult to study apart from a couple of strong spectral features: a contribution at around 741 cm^{-1} due to symmetrical P-F stretching vibration mode of the anion of BmimPF_6 ⁵⁹ (region III in Figure 6.2) and a ring breathing mode of $\gamma\text{-BL}$ ⁵⁴ / CH_2 rocking⁶⁰ at 931 cm^{-1} .

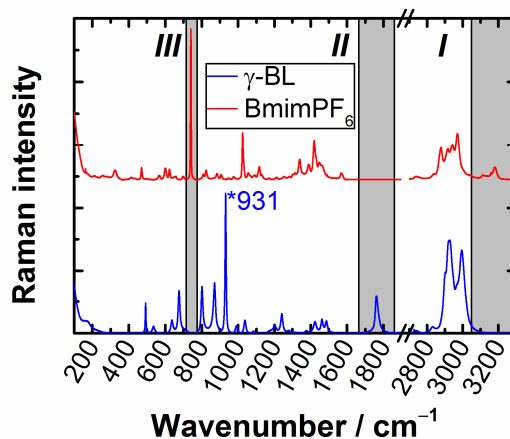


Figure 6.2. Raman spectra of BmimPF_6 (top) and $\gamma\text{-BL}$ (bottom). The band at 931 cm^{-1} which was used for normalization is marked with asterisk. Shaded areas indicate spectral regions of interest corresponding to III – P-F s. str. of BmimPF_6 , II – C=O str. of $\gamma\text{-BL}$, and I – ring C-H str. of BmimPF_6 .

The 741 cm^{-1} band was shown to be rather sensitive to interionic interactions both in IR⁵⁹ and in Raman⁶¹⁻⁶² and was thus selected for consideration in the present study, at the same time the latter is known to be insensitive to intermolecular interactions⁵⁴ and it was used in the normalization procedure. Figure 6.3 shows that the corresponding vibration mainly involves the methylene groups of the lactone ring but not the polar ester fragment and thus it should not be prone to intermolecular interactions.

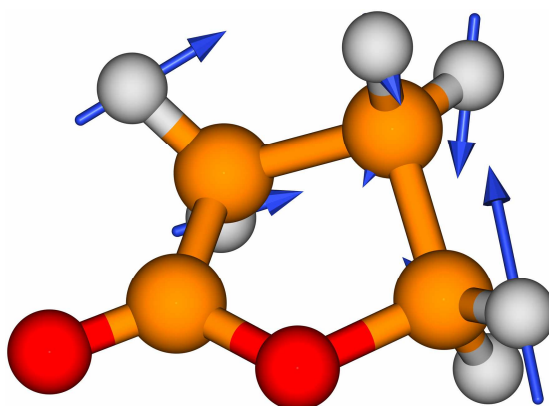


Figure 6.3. Scaled vectors of atomic displacements corresponding to ring breathing mode of γ -BL molecule. This band was used for the normalization procedure. Calculated wavenumber value at the M06-2X/6-311++G(d,p) level of theory is 952.5 cm^{-1} . Color coding of the elements: white – H, orange – C, red – O.

Region *II* in Figure 6.2 highlights the C=O stretching mode of γ -BL at *ca.* 1760 cm^{-1} .⁶³ This donating group is known to be quite sensitive IR and Raman probe for solvation interactions in different electrolyte solutions.⁶⁴⁻⁶⁶ Taken together with the fact that there are no interfering bands due to BmimPF₆ it makes this region interesting to follow.

In this investigation we used the imidazolium ring C-H stretching at $3050\text{-}3300 \text{ cm}^{-1}$ (highlighted as region *I* in Figure 6.2) as a probe of the interactions in BmimPF₆- γ -BL mixture though it is still not so well explored by Raman spectroscopy.^{11,62} Some IR studies suggest as well that alkyl C-H stretching region $2800\text{-}3050 \text{ cm}^{-1}$ could also be sensitive to modulation of interionic interactions induced by dilution with molecular solvent^{22,25,31,38-39,67} despite it often remains intact under such perturbation.^{4,21,30} However, due to severe overlap with broad and complex profile of C-H stretching vibrations of γ -BL (Figure 6.2) here we will abstain from analysis of this spectral region.

6.3.2 Model molecular clusters structures

Scaled vibrational frequencies of the studied vibrational modes as well as binding energies revealed by means of quantum-chemical calculations of the most

stable structures of the representative molecular clusters (ion pairs of IL, solvent dimers, and IL-solvent solvates) in vacuum and in polar medium are collected in Table 6.6.

6.2.3.1 γ -BL dimers

Due to high electric dipole moment of γ -BL molecule (4.19 Debye as estimated from dielectric studies upon dilution in benzene,⁶⁸ 4.9 and 6.3 Debye according to our calculations in vacuum and polar medium respectively) this solvent is prone to self-association similarly to other polar aprotic solvents.⁶⁹ Several experimental^{63,70-72} and theoretical^{60,70-72} investigations on γ -BL have claimed that its monomeric molecules tend to be in equilibrium with more than one type of dimeric forms and, presumably, even bigger aggregates. Remarkably strong tendency of γ -BL to self-association can be noted by occurrence of IR spectral bands associated with dimers on high dilution in CCl_4 ^{63,70-71} and in jet-cooled inert gas matrix.⁷²

Considering molecular structure of γ -BL dimers there have been proposed several types of arrangements. Perelygin and Itkulov tentatively suggested a cyclic in-plane dimer with antiparallel orientation of dipole moments and a chain-like linear structure with parallel arrangement of molecular dipoles.⁶³ More recent studies employing DFT and/or perturbation theory quantum-chemical calculations⁷⁰⁻⁷² have revealed a set of low-energy γ -BL dimers whose energy ordering depends on the used level of theory.⁷¹⁻⁷² All these computational studies discovered stacked antiparallel dipoles as one of the most stable structures. It is stabilized by both dipole-dipole interactions and symmetrical hydrogen bonding between carbonyl oxygen of one molecule and the methylene hydrogens of the neighbor. However, there are some discrepancies among other dimer structures revealed in previous computational studies on γ -BL. Aparicio and Alcalde⁷⁰ found cyclic in-plane structure to be 6 kJ mol^{-1} higher in energy than the antiparallel one

at B3LYP/6-311++G(d,p) level of theory whereas Hesse and Suhm⁷² using MP2 and B3LYP coupled with different basis sets reported a series of stacked configurations rotated from antiparallel arrangement with asymmetric hydrogen bonding pattern between the monomers involving both carbonyl and ester oxygen atoms. Vaz and Ribeiro-Carlo⁷¹ discovered both rotated stacked and cyclic in-plane configurations in addition to the antiparallel one at B3LYP/6-31G(d) and MP2/6-31G(d,p) levels of theory. Our studies only revealed rotated stacked configuration (referred to as ‘rotated’, see Figure 6.4) as minimum both in vacuum and polar medium. Implicit solvation does not bring about any significant structural distortions except for common slight intra- and intermolecular stretching of the structure. The stacked antiparallel dipoles structure was also obtained in our calculations both in vacuum and polar medium (depicted as ‘antiparallel’ in Figure 6.4). Introduction of polar medium leads to slight distortion of the antiparallel arrangement. As a result molecules are oriented to favor hydrogen bonding with C ^{α} H₂ hydrogen atoms and a non-zero dipole moment of 1.9 Debye is observed in contrast to non-polar vacuum structure.

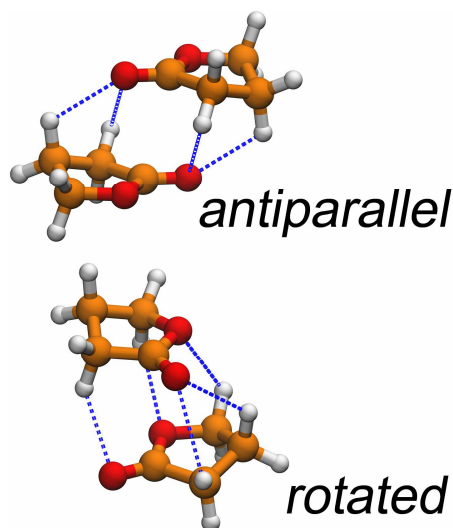


Figure 6.4. Optimized in vacuum geometries of γ -BL dimers. Notation reflects mutual orientation of carbonyl groups. Short stabilizing C-H \cdots O contacts are shown with blue dashed lines. Color coding of the elements: white – H, orange – C, red – O.

Furthermore, our result is in close agreement with reference⁷². We consider that discovery of the cyclic in-plane structure in previous studies is rather unreliable due to poor description of long-range dispersive interactions either due to selected functional⁷⁰ or because of modest basis set employed.⁷¹ Moreover, in the latter study the cyclic in-plane structure was found to be the least stable compared to antiparallel and rotated ones. Molecular dynamics simulations of neat γ -BL by Masia and Rey⁶⁰ also suggest that there is no preferential orientation of molecular dipoles since there were no maxima in the radial distribution functions between the atoms of carbonyl fragments. However, rather well pronounced maxima in the radial distributions between carbonyl oxygen and $C^{\alpha,\beta}H_2$ groups of hydrogen bond like character were noted.⁶⁰

From Table 6.6 one can see that both self-association and immersion into polar medium induce a remarkable redshift of the carbonyl stretching vibration. It is worth mentioning that once immersed into polar medium wavenumber shift due to dimerization is much less significant than in vacuum. Also polarized continuum favors the more polar rotated configuration of γ -BL dimer (dipole moment 3.5 and 5.7 Debye in vacuum and γ -BL medium, respectively) by $\sim 4 \text{ kJ mol}^{-1}$ while they were almost isoenergetic in vacuum.

Table 6.6. Calculated harmonic wavenumbers^a ($\tilde{\nu}$) of the selected vibrations and binding energies (E_{bind}) of representative model clusters

	$\tilde{\nu}$, cm ⁻¹										E_{bind} , kJ mol ⁻¹	
	P-F s. str.		C=O str.		C ² -H str.		C ⁽⁴⁻⁵⁾ -H as. str.		C ⁽⁴⁻⁵⁾ -H s. str.		vacuum	PCM
	vacuum	PCM	vacuum	PCM	vacuum	PCM	vacuum	PCM	vacuum	PCM		
γ-BL			1883	1814								
2γ-BL												
Rotated											-44.7	-22.6
Two-bonded ^b			1858	1811								
One-bonded ^b			1869	1816								
Antiparallel											-44.1	-18.5
In-phase			1833	1801								
Anti-phase (Raman forbidden ^c)			1859	1812								
Bmim⁺					3240	3250	3241	3246	3258	3264		
Bmim⁺...γ-BL												
at C ² -H/ C ^{α} H ₂ (Figure 6.6 B)			1830	1803	3213	3194	3243	3250	3261	3267	-76.4	-21.6
at C ² -H/NCH ₃ (Figure 6.6 C)			1832		3196		3243		3261		-73.3	
at C ⁽⁴⁻⁵⁾ -H (Figure 6.6 D)			1855		3241		3233		3263		-60.3	
PF₆⁻	721	725										
PF₆⁻...γ-BL	721	725	1843	1808							-59.2	-10.5
BmimPF₆...γ-BL												
at C ² -H	722	725	1822	1794	3213	3231	3252	3251	3272	3268	-438.3	-64.9
at C ⁽⁴⁻⁵⁾ -H	721		1830		3260		3255		3274		-433.0	
BmimPF₆	718	723			3257	3262	3249	3251	3268	3270	-359.9	-32.5
2BmimPF₆	722				3256		3246		3267		-826.7	
					3262		3253					

^aCalculated wavenumbers are scaled by a factor 0.983 corresponding to the selected level of theory.⁷³ ^bSee details in Figure 6.4. ^cIn PCM-optimized antiparallel structure due to slight distortion from perfect antiparallel arrangement the anti-phase vibration becomes allowed but its intensity is still negligible compared to the in-phase C=O stretching.

Despite experimental^{63,72} and computational⁷² predictions of possible existence of aggregates larger than dimers they are out of scope of our model calculations due to the large variety of possible configurations to explore. Nevertheless, it is expected that high-order aggregates would show even larger redshifts in the C=O stretching region compared to dimers.⁷²

6.2.3.2 BmimPF₆

It is a common approach in computational studies on ILs to take ion pair as the smallest representative structural unit even for condensed phase predictions.⁷⁴⁻⁷⁵ To the best of our knowledge all the published to date reports on computational studies of RmimPF₆ ion pairs have declared that configuration in which anion is located above imidazolium ring (*i.e.* at the same side with respect to imidazolium ring where the alkyl chain of Rmim⁺ cation points to) next to C²-H fragment is the dominating, if not the unique, low-energy structure.^{19,40-41,76-83} Within this structure PF₆⁻ is oriented with a face of its quasi-octahedron (*i.e.* with three fluorine atoms) towards the C²-H moiety. The latter serves as the main interaction site of Rmim⁺ cation due to localization of the highest positive charge.⁸⁴ Despite Coulomb interaction being the deciding one, our calculations show that there are multiple stabilizing short contacts C-H...F not only with C²-H hydrogen but also with adjacent alkyl hydrogen atoms NCH₃ and C^{α-β}H₂.^{78,81} Our calculations also reveal this configuration as the most stable one (see Figure 6.5). Moreover, initial configurations with anion located in-plane at C⁽⁴⁻⁵⁾-H site, in front of C²-H, between butyl chain and C⁵-H or between the methyl group and C⁴-H all converge to the on-top C²-H configuration. When PCM is applied the ion pair becomes slightly more on-top like: dihedral angle φ (see Chapter 3 for definition) changes from 74.3 to 77.7 degrees (perfect in-plane and on-top of C² arrangements of the anion would correspond to the φ dihedral values of 0 and 90 degrees, respectively). Polar

medium also induces slight increase of interionic separation: distance C²-P changes by 0.1 Å from 3.393 Å to 3.493 Å.

Since conformation isomerism along the butyl chain was found to have negligible effect on C-H stretching vibrations in ion pairs of BmimBF₄ on the basis of DFT calculations¹⁶ thus we have only considered all-anti conformation of the butyl chain in Bmim⁺ in our calculations.

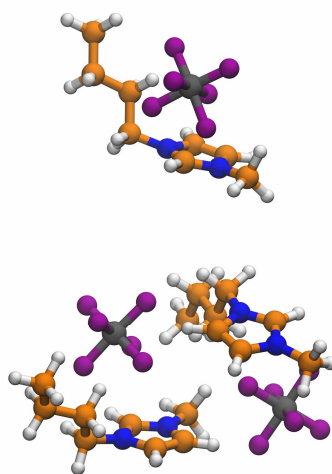


Figure 6.5. Optimized geometries of BmimPF₆ ion pair (*top*) and ion pair dimer 2BmimPF₆ (*bottom*). Color coding of the elements: white – H, orange – C, blue – N, purple – F, grey – P.

More recent computational studies share a common opinion that larger ionic clusters, at least dimers of ion pairs, are necessary to capture bulk-like structural pattern of neat ILs.^{33,38,40-41,85-87} Matthews *et al.*⁸⁷ have pointed out that in ion pair dimers of imidazolium ILs with multiatomic anions there is limited possibility for cation stacking due to preference of anions to occupy positions on top of the C²-H fragment. The most stable structure of BmimPF₆ ion pair dimer obtained in our investigation (see Figure 6.5) resembles some structures reported in the literature^{33,40-41,87} with offset stacked cations in almost antiparallel orientation and anions occupying positions on-top of one cation and at C^(4/5)-H sites of the second one. Multiple short contacts of fluorine atoms of anion with adjacent to

imidazolium ring alkyl hydrogen atoms are also evident from Figure 6.5. It is noteworthy to mention that already such ion pair dimer structure allowed us to capture the main structural details deduced from MD simulations of bulk RmimPF₆ ILs tested against neutron scattering experiments.⁸⁸⁻⁹⁰

Table 6.6 highlights that calculated in vacuum binding energy per single ion pair in dimer is ~50 kJ mol⁻¹ larger in absolute values than that in an isolated ion pair which proves importance many-body interactions in ionic clusters.⁸⁵ Apart from moving counterions further away in structure of ion pair polar medium also significantly screens interionic interactions. As a result, ion pair binding energy drastically drops from vacuum value of -359.9 kJ mol⁻¹ down to -32.5 kJ mol⁻¹ in PCM approach. This result is in accordance with previous computational studies^{77,82} which show that increasing solvent polarity progressively weakens ion pairing in terms of PCM-estimated ion pair binding energies.

Ion pairing and further clustering slightly blueshifts the ring C-H stretching wavenumbers which is in accordance with the literature data.^{8,33,38,74,91} Polar solvent effect as estimated by PCM calculation leads to almost negligible increase in the wavenumbers which also agrees well with results of Palomar *et al.*⁷⁷ but is in contradiction with some other reports.^{2,33} It is also to be noted that in ion pair and ion pair dimers calculated C²-H stretching wavenumber is found at slightly higher values than that of asymmetric C^(4,5)-H stretching. This result is in agreement with some IL cluster calculations.^{38,40} However, there are as well computational studies on BmimPF₆ ion pairs that claim C²-H stretching wavenumber to be lower than asymmetric C^(4,5)-H stretching^{79,83} which is more typical for much more basic anions which have in-plane arrangement of anion thus favoring strong directional hydrogen bond with C²-H hydrogen.¹⁹

6.2.3.3 IL-solvent complexes

In an attempt to describe molecular structure of representative structures in mixtures of BmimPF₆ with γ -BL we have calculated several complexes such as anion-solvent, cation-solvent, and ion pair-solvent. The optimized structures are shown in Figure 6.6.

Complex PF₆⁻... γ -BL (Figure 6.6, A) has anion at the positive side of molecular dipole of γ -BL molecule next to β,γ -CH₂ hydrogen atoms. This structure remains almost intact when transferred to polar medium. One can also note from Table 6.6 that complex formation does not alter significantly P-F symmetric stretching wavenumber of anion in contrast to carbonyl stretching of the solvent molecule which redshifts compared to isolated molecule similarly in magnitude with dimerization effect.

In the most stable structure of cation-solvent complex (Figure 6.6, B) γ -BL molecule is located in front of C²-H moiety where its carbonyl oxygen forms hydrogen bond with C²-H hydrogen atom (2.04 Å / 143.6 degrees) and ester oxygen is in close contact with alkyl hydrogen atoms of butyl chain of Bmim⁺ cation. In contrast to ion-cluster structures (Figure 6.5) such arrangement of the donor (C²-H) and acceptor (C=O) fragments is more favorable for hydrogen bond formation which results in significant redshift of the C²-H stretching wavenumber compared to both isolated cation and ion clusters (Table 6.6). In polar medium the solvent molecule gets slightly further away from the cation (not shown), however, geometrical arrangement of the hydrogen bond fragment becomes more linear (2.19 Å / 154.1 degrees) resulting in still remarkable redshift of the C²-H stretching vibration. One alternative arrangement of such solvate has γ -BL molecule bound with its carbonyl oxygen to C²-H while its ester oxygen is next to one of the NCH₃ hydrogens of cation (see Figure 6.6, C). This structure being 3 kJ mol⁻¹ less stable than the global minimum (Figure 6.6, B) has shorter, more directional and hence more redshifted hydrogen bond at C²-H site (2.02 Å / 151.7 degrees). Another

alternative being 16 kJ mol^{-1} less stable in vacuum structure with γ -BL molecule located at $\text{C}^{(4,5)}$ -H site (see Figure 6.6, *D* for molecular structure) shows appreciable redshift of asymmetric $\text{C}^{(4,5)}$ -H stretching vibration. Apparent hydrogen bonding between Bmim^+ cation and γ -BL molecule also manifests itself in the large redshift of the $\text{C}=\text{O}$ stretching which is especially pronounced in the structure bound at C^2 -H. This indicates that higher stability of this structure is at least partially due to stronger hydrogen bonding at C^2 -H site than at $\text{C}^{(4,5)}$ -H. It is also evident from Table 6.6 that γ -BL prefers to bind with cation rather than with anion both in vacuum and in polar medium, hence, it seems reasonable to attribute solvation effects mainly to interaction of γ -BL with Bmim^+ cation. This finding is similar to that established for BmimBF_4 -DMSO system³¹ suggesting that it is a common feature for systems with polar aprotic solvents in contrast to mixtures of protic solvents and ILs with basic anions.^{5,22}

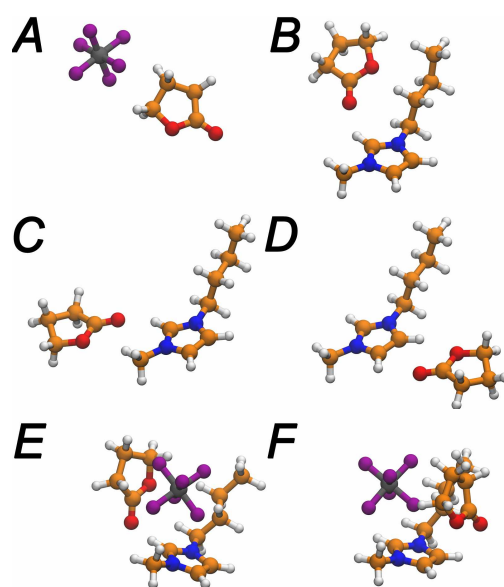


Figure 6.6. Optimized in vacuum geometries of the model solvated species: *A* – $\text{PF}_6^- \cdots \gamma$ -BL, *B* – $\text{Bmim}^+ \cdots \gamma$ -BL (at C^2 -H/ $\text{C}^\alpha\text{H}_2$), *C* – $\text{Bmim}^+ \cdots \gamma$ -BL (at C^2 -H/ NCH_3), *D* – $\text{Bmim}^+ \cdots \gamma$ -BL (at $\text{C}^{(4,5)}$ -H), *E* – $\text{BmimPF}_6 \cdots \gamma$ -BL (at C^2 -H), *F* – $\text{BmimPF}_6 \cdots \gamma$ -BL (at $\text{C}^{(4,5)}$ -H). Color coding of the elements: white – H, orange – C, blue – N, red – O, purple – F, grey – P.

Complexes ion pair-solvent were constructed in order to allow for the most favorable arrangements for intermolecular interactions (Figure 6.6, *C-D*), *i.e.* anion is on top of C²-H moiety of cation while γ -BL interacts with both cation and anion via its carbonyl oxygen and β,γ -CH₂ hydrogen atoms, respectively. Optimizations of configurations initially constructed as solvent-shared ion pairs, *i.e.* with solvent molecule physically separating the counterions, converged to one of the presented structures due to strong Coulomb attraction between the counterions. Careful inspection of values in Table 6.6 suggests that such mode of interaction still does not influence P-F symmetrical stretching wavenumbers in contrast to those of γ -BL C=O stretching and Bmim⁺ C²-H stretching vibrations. Polar medium effect induces the anticipated redshift of C=O stretching wavenumber of γ -BL and somewhat counterintuitive slight blueshift of symmetrical P-F and ring C-H stretching vibrations of IL. The latter is associated with the decrease of the interaction energy which can be rationalized in terms of overall larger intermolecular separation of the ions and molecules constituting the complex.

We also note that in terms of competition energy defined by Hu *et al.*⁸² from PCM calculations as the difference between the sum of cation-solvent and anion-solvent binding energies from one side and ion pair binding energy from another side one can expect a balanced competition between ion pairing and ion solvation. Indeed, such implicit calculation of competition energy gives value very close to zero ($-21.6 - 10.5 + 32.5 = 0.4 \text{ kJ mol}^{-1}$).

6.3.3 Experimental Raman spectra of BmimPF₆- γ -BL mixtures

Numerical fitting parameters of the studied vibrational bands in the regions *I-III* are collected in Tables A 6.1-6.3 (Chapter 6 Appendix), respectively.

6.3.3.1 Region *I*: imidazolium ring C-H stretching

As it was mentioned in the introduction section most of the research dealing with vibrational spectroscopy of mixtures of imidazolium ILs with molecular

solvents is focused on the ring C-H stretching region.¹ This spectral range turned out to be informative in our case as well. From Figure 6.7 an appreciable redshift of the entire profile at 3080-3250 cm⁻¹ is evident with decreasing IL concentration. Before going to detailed analysis we should note that three possible scenarios of behavior of imidazolium C-H stretching wavenumbers have been observed in mixtures of imidazolium ILs with molecular solvents. Upon dilution of neat IL with molecular solvent these scenarios include (i) redshift in such systems as BmimBF₄-MeOH,²⁵ BmimBF₄-DMSO,³⁰⁻³² EmimTFSI-PEO,⁶⁷ BmimPF₆/BF₄-PEO,⁹² (ii) blueshift in systems like EmimBF₄-H₂O,⁸ EmimLac-MeOH,²² RmimMeSO₄-H₂O,⁶⁻⁷ EmimEtSO₄-Acetone,³⁶ BmimCl/MeSO₄-EG,²⁷ BmimTFA-H₂O/MeOH,⁵ BmimHal-H₂O,^{2,10,39} or (iii) no apparent shift at all like in RmimBF₄-H₂O,^{2-3,9-11} EmimTFSI-MeOH,²¹ RmimBF₄-EG,²⁸ EmimTFSI-DiOx,⁶⁷ BmimBF₄/PF₆-AN³⁴ systems. This can be systematized as that redshift of the ring C-H-vibrations is induced by addition of donating solvents to weakly-associated ILs where solvent molecules can effectively compete with anions for the ring C-H sites in order to establish stronger hydrogen bonds. On the other hand, dilution of ILs with highly basic anions (*e.g.*, halides or those bearing carboxylic group) in solvents of different polarity typically leads to blueshifts interpreted as an indication of rupture of rather strong interionic hydrogen bonds which is not counterbalanced by solvation of the cation. The third group corresponds to the case when both anion basicity and solvent donicity are rather low and subsequently there is no persistent hydrogen bond network in neat ILs and solvent is not capable to disturb interionic interactions significantly.

As this scheme suggests and in accordance with our experimental observations the present BmimPF₆- γ -BL system falls into the first category. That is to say the redshift of imidazolium ring stretching vibrations of IL cation observed upon dilution with molecular solvent is a consequence of hydrogen bond like

interactions between the respective cation sites and polar donating group of γ -BL, *i.e.* the C=O group, and due to loosening of cation-anion interactions.

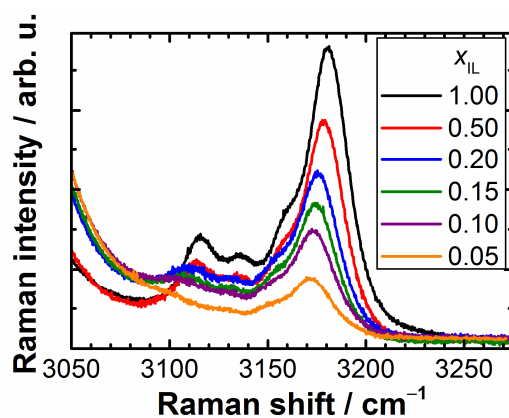


Figure 6.7. Raman spectra of selected BmimPF₆ - γ -BL mixtures in the region of imidazolium ring C-H str. vibrations.

In order to get more detailed picture of concentration induced wavenumber shift we have performed band fitting of the studied spectral region *I*. Spectral envelope in Figure 6.7 suggests at least four distinct contributions apart from interfering background below 3100 cm⁻¹ which comes from alkyl C-H stretching vibrational modes of both components. Russina *et al.*⁶² also used four peaks to fit this spectral region in their Raman study of BmimPF₆ at high pressures. A sample fit of the neat IL spectrum is shown in Figure 6.8.

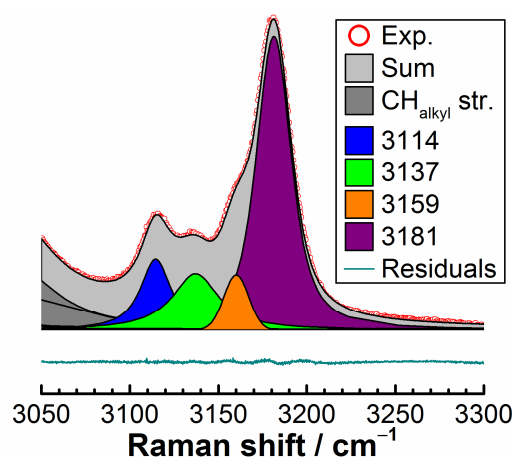


Figure 6.8. Sample deconvolution of the neat BmimPF₆ Raman spectrum in the region of ring C-H str. into four Voigt profiles. Numbers in the legend correspond to peak center positions. See Table A 6.1 for details.

Several studies did not observe an appreciable wavenumber shift of the ring C-H stretching vibrations over the course of dilution in molecular solvent but rather redistribution of intensities between the individual spectral contributions in favor of lower wavenumber shoulders/minor contributions.^{33,37} This is not the case here since we observe a remarkable redshift (Figure 6.9) for all the spectral contributions and no systematic redistribution of intensities between the bands (not shown).

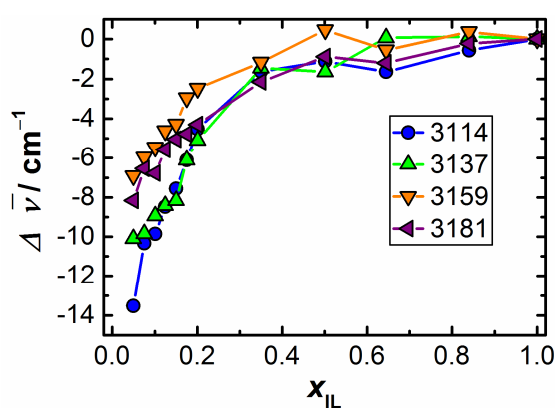


Figure 6.9. Peak wavenumber shifts with respect to the neat BmimPF₆ of the four components of ring C-H str. region. See Table A 6.1 for details.

Two main observations can be made upon inspection of Figure 6.9. First, the redshift trend is non-monotonic and remarkable offset is observed only at $x_{IL} < 0.2$ whereas at higher IL content the redshift is less than 2 cm^{-1} which is almost negligible on the scale of the total wavenumber shift. This was also noted for other systems of similar type^{25,31} and such behavior was explained as that the pronounced redshift is only observed when significant loosening of interionic interactions occurs allowing solvent molecules to approach the imidazolium ring C-H sites. Second, the magnitude of the redshift is higher in absolute value for the lower wavenumber couple of bands. The second observation brings us to the most controversial point of band assignment in this spectral region.

IR studies on deuterated EmimTFSI coupled with anharmonic calculations suggest that ring stretching overtones and combinations can interact via Fermi resonance with ring C-H stretching vibrations.⁹³ In accordance with the authors, hydrogen bonding effects are unnecessary to be invoked to interpret the spectral pattern. Further extension of the investigation over a broad selection of anions of different basicity also augmented with Raman spectroscopy confirmed rather complex coupling character and, hence, unclear spectral picture in the region of C²-H stretching.⁹⁴ It was found that increasing anion basicity leads to broadening, redshift and intensity enhancement of the C²-H stretching vibration which can hardly be separated from Fermi resonance effects. The authors proposed to use monodeuterated at position 2 analogues to simplify the spectral pattern and make it easier to study interionic interactions by means of vibrational spectroscopy.

Other spectroscopic studies on deuterated at C² RmimX ILs^{10,79,95} suggest that C²-H stretching should contribute to the lowest wavenumbers of the ring C-H stretching profile since it is the preferential site for hydrogen bonding and thus the most redshifted. Some minor contributions from hydrogen bonded with anion C^(4.5)-H vibrations are also expected in this low wavenumber part of the profile.⁷⁹ Johnson *et al.*,⁹⁵ in contrast, suggest that residual peaks in this region after deuteration of EmimBF₄ at C² could stem from combination of ring stretches at ~1570 cm⁻¹. Both groups admit though that the high-wavenumber component at 3170 cm⁻¹ remains unchanged upon deuteration and thus does not contain significant contributions from C²-H.^{79,95} *Ab initio* calculations and cryogenic IR spectra of small ionic clusters of EmimBF₄⁹⁵ show that significantly redshifted (*i.e.* strongly directionally hydrogen bonded) C²-H spectral patterns non-typical for bulk IL occur in small anionic clusters. However, cationic and larger anionic clusters are more appropriate to reproduce neat IL IR spectrum. It was noted that in these clusters C²-H spectral contribution inherently spans over a broader range of wavenumbers than what is expected from cluster-induced mild redshift. In another

recent study pair of bands at 3120 cm^{-1} (both in Raman and IR) is attributed to Fermi resonance between $\text{C}^2\text{-H}$ and an overtone of ring deformation on the basis of anharmonic calculations for RmimTFSI, whereas the high-wavenumber part of the ring C-H stretching profile (observed at 3160 and 3180 cm^{-1} in IR and Raman, respectively) is due to $\text{C}^{(4,5)\text{-H}}$ symmetric and anti-symmetric stretches.⁹⁶

An ongoing debate on hydrogen bonding/ion-pairing vs. Fermi resonance has not been reconciled yet. Nevertheless, the latest studies on this issue which use IR spectroscopy of EmimTFSI as single ion pairs in helium nanodroplets⁹⁷ or in jet-cooled IL vapor⁹⁸ suggest that both effects contribute to the complex broad low-wavenumber part of the ring C-H stretching profile which is attributed to $\text{C}^2\text{-H}$ stretching mode. *Ab initio* molecular dynamics using dispersion-corrected density functional⁹⁹⁻¹⁰⁰ showed that despite the fact that spectral contributions stemming from $\text{C}^2\text{-H}$ are revealed at somewhat lower wavenumbers they cover rather broad range strongly overlapping with $\text{C}^{(4,5)\text{-H}}$ contributions. Nevertheless, the lower wavenumber contributions of $\text{C}^2\text{-H}$ are dominated by strongly hydrogen bonded configurations. This is also confirmed by progressive redshift of the ring C-H contributions with increasing anion basicity.⁹⁹

Abstaining from ultimate assignment we suppose that both literature results and our calculations suggest that lower wavenumber contribution showing significant redshift is mainly due to hydrogen bonded at $\text{C}^2\text{-H}$ species whereas that at higher wavenumbers are due-to symmetrical and asymmetrical $\text{C}^{(4,5)\text{-H}}$ vibrations. Larger redshift of the former compared to the latter is an indication of stronger hydrogen bonding at $\text{C}^2\text{-H}$ site in conformity with current point of view on the issue and our calculations.

6.3.3.2 Region II: C=O stretching

As it was already mentioned above, both literature survey⁶⁴⁻⁶⁶ and DFT calculations presented here point to remarkable sensitivity of the C=O stretching

mode of γ -BL to intermolecular interactions and to solvation in particular. Due to inherent complexity of the spectral profile⁶³ and consequent need for advanced analysis we have normalized this spectral region by the fitted area of γ -BL ring stretching band at 931 cm^{-1} as it was noted in section 6.3.1. Indeed, this band maintains its position and width over the entire range of compositions studied (see Figure A 6.1) and thus can be reliably used for the purpose of normalization. The normalized Raman spectra in the region of C=O stretching vibration are shown in Figure 6.10. Initial inspection of the band evolution suggests that upon addition of ionic liquid to γ -BL slight blueshift is the main observed spectral change.

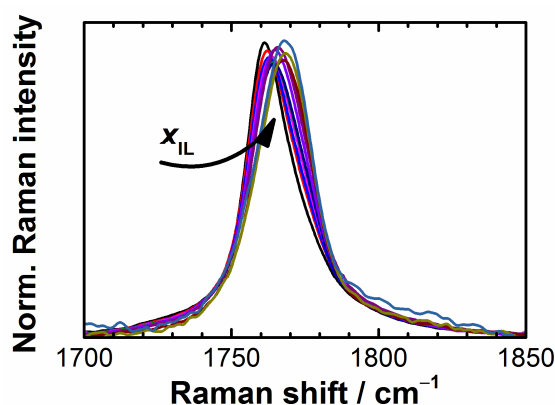


Figure 6.10. Normalized Raman profiles in the region of the C=O str. of γ -BL. Arrow indicates the direction of spectral changes induced by addition of BmimPF₆.

Indeed, if one examines the apparent peak position (Figure 6.11) it turns out to be monotonically blueshifting at $x_{\text{IL}} < 0.4$ by $\sim 7\text{ cm}^{-1}$ and keeping its position at higher IL concentrations. This is opposite to what was observed for solutions in γ -BL of various lithium salts⁶⁵⁻⁶⁶ and of EtNH₃NO₃ IL⁶⁴ where complex bandshape variation with an overall redshift of $\sim 20\text{ cm}^{-1}$ was related to strong interactions of cations with carbonyl oxygen of γ -BL molecules. The blueshift observed here could thus evidence that interactions of γ -BL with IL, in particular with its cation, are generally weaker than intermolecular interactions in the neat molecular solvent. Such interpretation is somehow in contradiction with our DFT calculations (see Section 6.2.3.3).

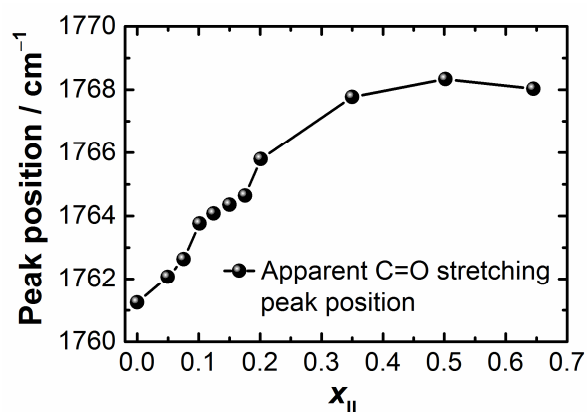


Figure 6.11. Apparent peak position of the C=O *str.* of γ -BL as a function of BmimPF₆ mole fraction

The non-monotonic concentration-induced blueshift of the apparent position of C=O stretching band prompted us to apply more advanced analysis. A simple 2DCoS analysis applied to the entire dataset (see Figure 6.12, A and B) shows pattern typical for conventional peak position shift⁴⁹ both in synchronous and asynchronous spectra and does not give any additional information.

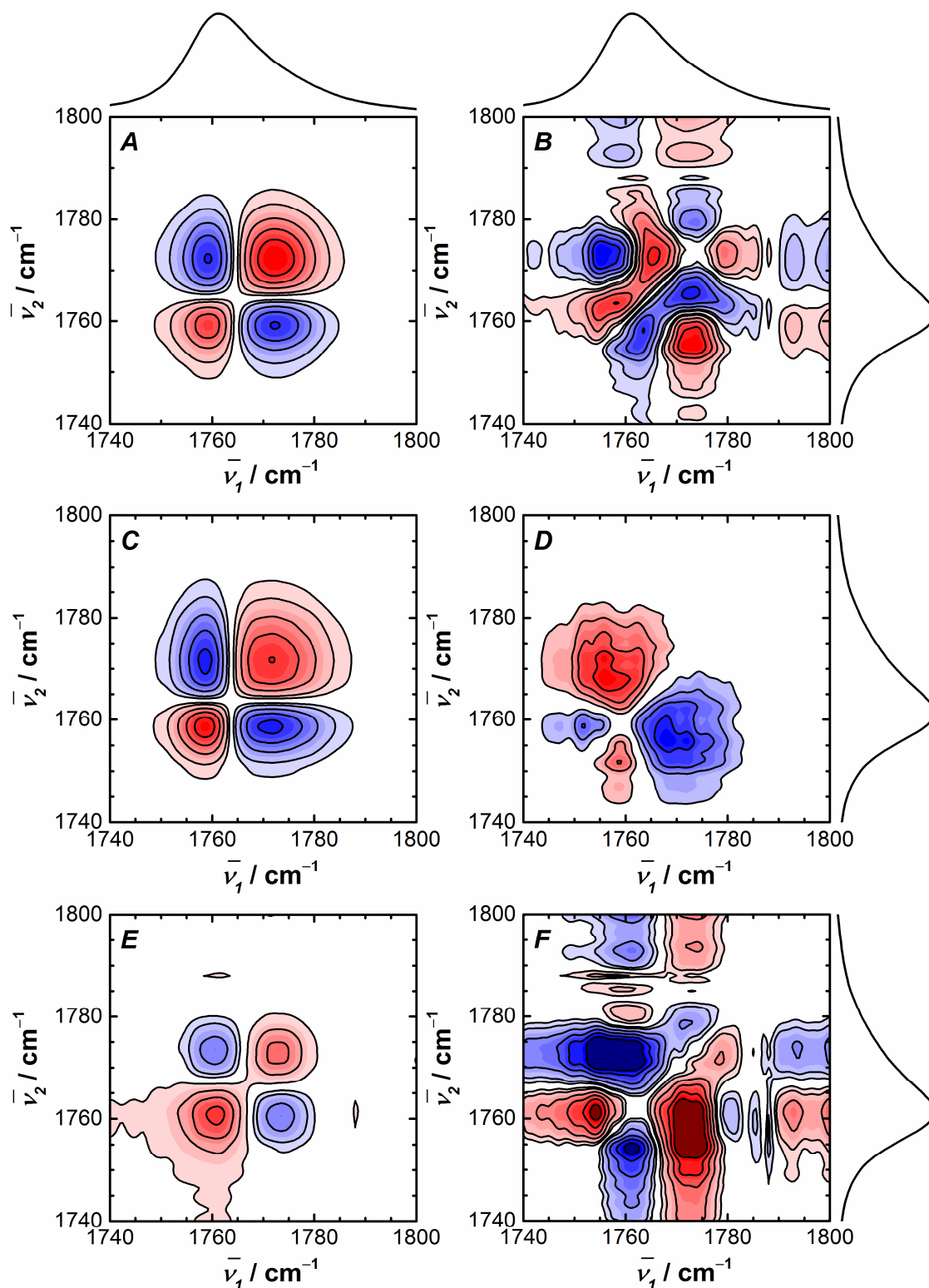


Figure 6.12. Generalized two-dimensional correlation maps (A, C, E – synchronous; B, D, F – asynchronous) for the entire dataset (A and B) and for segments of low (C and D) and high (E and F) concentrations of BmimPF₆. Red represents positive values and blue is for the negative values.

We then applied PCMW2DCoS to reveal particular concentration and wavenumber ranges which determine evolution of the total profile. The results are shown in Figure 6.13. It is apparent that there are two distinct concentration regimes. At low IL content ($x_{IL} < 0.15$) where contribution at $\sim 1755 \text{ cm}^{-1}$ loses intensity while that at $\sim 1775 \text{ cm}^{-1}$ gains it but to a lesser extent while at high IL content ($x_{IL} > 0.15$) the picture is reversed: high-wavenumber contribution is decreasing and the low-wavenumber one is increasing. Apart from opposite trends the two concentration ranges also differ by the extent of changes (at higher concentrations of IL the changes are more pronounced and more equal between the two contributions) and a slight blueshift of the low-wavenumber spot is observed in Figure 6.13 at higher IL concentrations towards $\sim 1760 \text{ cm}^{-1}$ compared to low concentration regime.

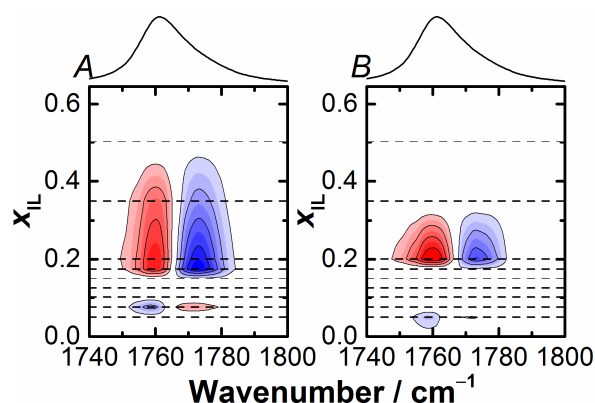


Figure 6.13. Perturbation-correlation moving window two dimensional synchronous correlation maps. Window sizes are 5 and 3 spectra in A and B respectively. Red represents positive values and blue is for the negative values. Dashed lines indicate experimental concentrations. Traces at the top and right sides of each panel correspond to spectrum of the neat γ -BL.

Such behavior with changing concentration is far more intricate than one could inspect from simple visual inspection of the peak-wavenumber shift. Having established two distinct concentration ranges we present in Figure 6.12 C-F 2D correlation maps for each of these ranges.

At low IL content synchronous map (Figure 6.12 C) suggests simple transfer of intensity between contributions at 1758 cm^{-1} and 1773 cm^{-1} . Following interpretations of PCMW2DCoS and the apparent blueshift of the peak position the intensity is transferred from the former to the latter. A negative cross-peak at (1768; 1757) in asynchronous spectrum taken together with a positive synchronous peak at approximately the same wavenumbers hints, in accordance with Noda's rules⁴⁷, that the low-wavenumber contribution reacts to internal perturbation (changing concentration) before than the high-wavenumber one. This can be related, but not necessarily, to the corresponding different intensities in PCMW2DCoS peaks at low IL concentrations. Weak and smeared asynchronous peak at (1759; 1752) points to possible existence of contribution below 1760 cm^{-1} .

At high IL content (Figure 6.12 E, F) two-dimensional correlation maps, particularly the asynchronous one, are much more complicated than at low IL content. Among the noticeable differences are inversed signs of the asynchronous peaks around (1773; 1758) and (1762; 1754) and low intensity traces (both synchronous and asynchronous) pointing to contributions at $1780\text{-}1795\text{ cm}^{-1}$.

In order to complement the undertaken approaches which tackle the observed spectral variance as a whole we also performed band fitting in an attempt to assign the band evolution to specific behavior of individual contributions. There is still no settled point of view on the number of contributions in the C=O stretching profile of neat γ -BL. Two recent studies employing temperature variation and dilution in inert solvent CCl_4 to resolve IR⁷⁰ and Raman⁷¹ C=O profiles end up at different conclusions. Aparicio and Alcalde⁷⁰ claim that there is equilibrium of monomer solvent molecules (1796 cm^{-1}) with cyclic in-plane dimer (1780 cm^{-1}) upon dilution with CCl_4 and with more stable stacked anti-parallel one upon heating, whereas Vaz and Ribeiro-Claro⁷¹ suggest that since there is no isosbestic point neither upon dilution nor upon heating (only gradual blueshift) a possible equilibrium should invoke more than two representative species. Perelygin and

Itkulov⁶³ on the basis of their studies on heating and dilution of γ -BL in CCl_4 also noted rather complex band shape variations both in Raman and IR and fitted their spectra with four contributions at 1760, 1765, 1775, and 1792 cm^{-1} tentatively attributed to chain dimers, in-phase vibration in cyclic dimers, anti-phase vibration in cyclic dimers, and monomers, respectively. It was noted that over the course of dilution/heating these contributions did not change their positions.

Despite questionable assignment we took Perelygin's four-component model⁶³ as initial approximation to fit our spectra. It turned out that even for the neat solvent we had to invoke a weak fifth contribution centered at around 1736 cm^{-1} in order to reproduce the profile (Figure 6.14). The four initial components perfectly agreed in wavenumbers and relative intensities/widths (upon visual comparison) with results of Perelygin and Itkulov.⁶³

The lowest wavenumber component was necessary only up to $x_{\text{IL}} \sim 0.2$. We also stress that, similarly to Perelygin's results,⁶³ peak wavenumbers of all the five (four) contributions are rather insensitive to increasing concentration of IL (Figure 6.14). Noticeable fluctuations of peak positions of the highest and lowest wavenumber contributions (1736 and 1792 cm^{-1}) are due to larger uncertainties of their determination stemming from their relatively low intensities.

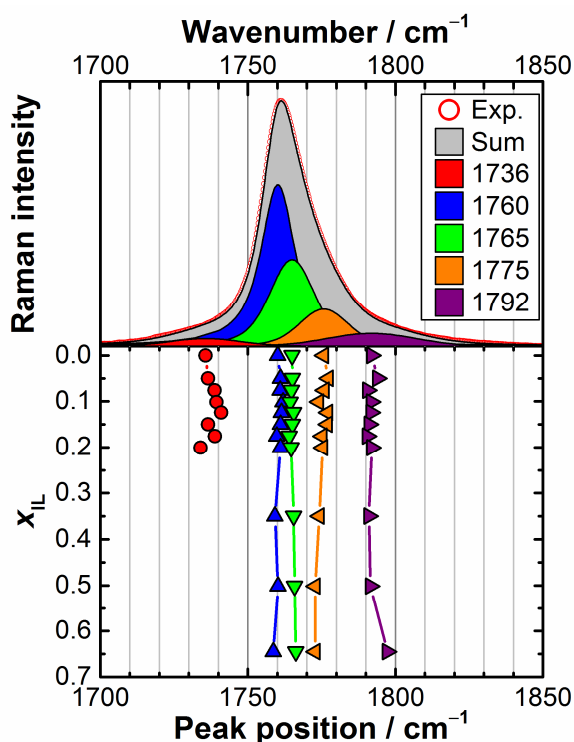


Figure 6.14. Sample deconvolution of the neat γ -BL Raman spectrum in the region of C=O str. into five Voigt profiles (top panel) and concentration dependences of the peak positions of the corresponding spectral contributions (bottom panel). See Table A 6.2 for details.

Fitted areas of discovered contributions to the C=O spectral profile are plotted as a function of BmimPF₆ mole fraction in Figure 6.15. It is apparent that at low IL content the main intensity variation is monotonic decrease of the 1760 cm⁻¹ contribution and slight increase of the 1775 cm⁻¹ contribution. At $x_{\text{IL}} > 0.18$ the latter starts to decrease while contributions at 1765 and 1792 cm⁻¹ gain intensity. These results are in line with conclusions drawn from PCMW and classical 2DCoS for segmented data analyses.

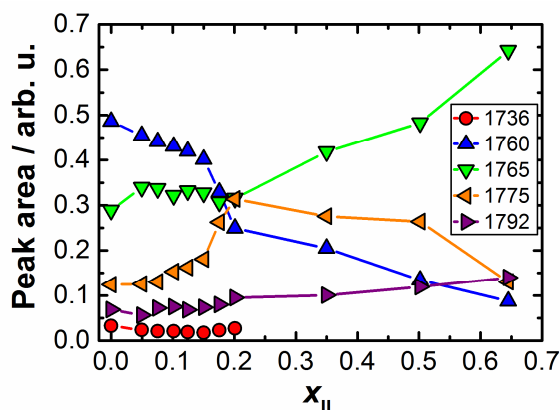


Figure 6.15. Relative peak areas of the components of the C=O str. profile of γ -BL as a function of BmimPF₆ mole fraction. See Table A 6.2 for details.

In order to rationalize the derived evolution of individual contributions and to reconcile it with quantum chemical DFT calculations presented in section 6.2.3.1 we propose the following assignment. The highest wavenumber mode at 1792 cm⁻¹ is inevitably assigned to monomer γ -BL molecules in accordance with Perelygin and Itkulov⁶³ and close to results of Aparicio and Alcalde⁷⁰ (1796 cm⁻¹ in IR). We note rather weak intensity and large broadness of this band which indicate significant degree of aggregation in the neat molecular solvent and a remarkable variety of microenvironments experienced in the mixture.

Our calculations suggest that the two revealed dimer structures should produce three bands in Raman spectra, since even if the anti-phase vibration of antiparallel dimer becomes slightly Raman active due to some symmetry distortions it will effectively overlap with contribution from the more bonded γ -BL molecule of rotated dimer. On this basis we assign the following three lower wavenumber contributions in the spectrum of neat γ -BL to vibrations of molecular dimers, namely 1775 cm⁻¹ contribution is due to less bound γ -BL molecules from rotated dimers, the mode at 1765 cm⁻¹ comes from more bound γ -BL molecules of rotated dimers and, maybe, from anti-phase vibration of distorted antiparallel dimers, and in-phase vibration of anti-parallel dimers contributes to the band at 1760 cm⁻¹. This assignment of bands stemming from dimers of γ -BL is also

supported by the smallest dimer shift of 16 cm^{-1} revealed by Hesse and Suhm in IR spectra of jet-expanded γ -BL.⁷²

The newly revealed weak and broad lowest wavenumber contribution centered at 1736 cm^{-1} can be tentatively assigned to higher order aggregates in the neat solvent. This is in line with experimental and computational results of Hesse and Suhm who predict higher aggregates to contribute at lower wavenumbers than the dimers.⁷²

Our calculations suggest that optimal structures of IL-solvent complexes show the most remarkable redshift of the C=O stretching wavenumber and thus can be expected to contribute to the lowest-wavenumber band at low IL content. One can assume that higher aggregates (1736 cm^{-1}) and less stable anti-parallel dimers (1760 cm^{-1}) are disrupted in favor of the solvated complexes and the less bound γ -BL molecules of the more stable rotated dimers. This gives one more point of agreement with Perelygin and Itkulov⁶³ who also noted the 1760 cm^{-1} contribution to be the least resistant to heating, *i.e.* to come from the least stable species.

At higher IL content at $x_{\text{IL}} > 0.18$ where effective molar ratio of the components is around 4:1 one can expect that there is no more high order solvent aggregates in the system and significant ionic aggregation due to lack of solvent is likely to occur. This is also corroborated by peculiar crystallization behavior of the mixture around this composition reported by Chagnes *et al.*⁴³ The intensity variations in this concentration range, namely vanishing of the lowest wavenumber contribution and decrease of the anti-parallel dimer (1760 cm^{-1}) and the less bound molecules of rotated dimer (1775 cm^{-1}) in favor of the contributions at 1792 and 1765 cm^{-1} , can be thought of as ultimate disruption of residual aggregate structures of γ -BL towards monomers (1792 cm^{-1}) and molecules bound to ionic clusters (1765 cm^{-1}). The latter assignment was not captured in our model calculations and requires more elaborate interpretation invoking larger scale simulations. Here, we stop at an assumption that in complexes of ionic aggregates with γ -BL anions of IL

would preferentially occupy all the favorable interaction sites at the imidazolium ring of cations which could result in less pronounced redshifts of C=O stretching mode of the bound γ -BL compared to solvated complexes with single cation or ion pair.

6.3.3.3 Region III: P-F symmetrical stretching

Literature data suggest that P-F symmetrical stretching vibration of PF_6^- anion is rather sensitive to changes in the symmetry of microenvironment upon changing polarity of solvent used to dilute IL⁵⁹ and to structural pattern of hydrogen bonding interactions whose changes may be induced by applying high pressure to neat IL.⁶¹⁻⁶² In mixtures of BmimBF₄ with water a slight blueshift in Raman spectra of a similar symmetric B-F stretching of anion was observed upon dilution of IL which was tentatively attributed to screening and weakening of interionic interactions.^{9,11} Despite the anticipated spectral variations in the present system apparent peak position of symmetrical P-F stretching does not deviate from the average value of 741 cm^{-1} by more than 0.5 cm^{-1} over the entire range of concentrations studied. This can be regarded as essentially zero shift. Nevertheless, a closer inspection of the spectral profile reveals its asymmetry with longer tail situated at low-wavenumber side. The band was fitted with two Voigt functions and the results are presented in Figure 6.16.

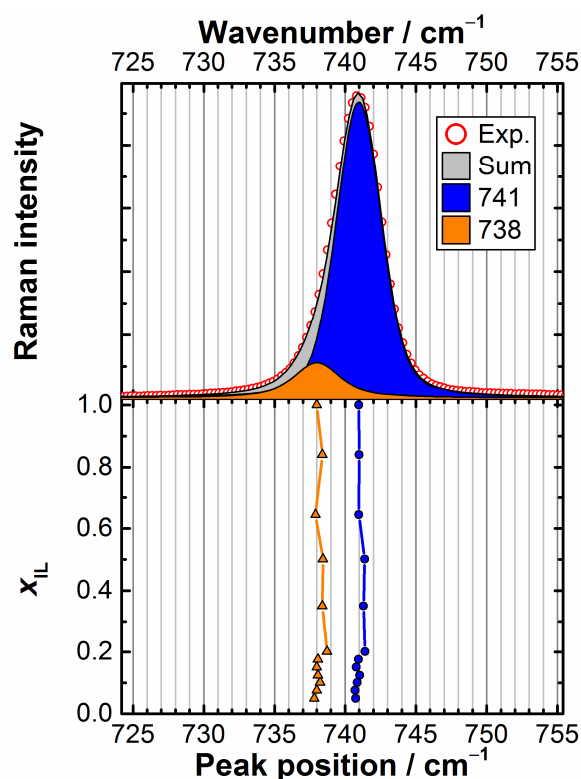


Figure 6.16. Sample deconvolution the neat BmimPF₆ Raman spectrum in the region of P-F s. str. into two Voigt profiles (*top panel*) and concentration dependences of the peak positions of the corresponding spectral contributions (*bottom panel*). See Table A 6.3 for details.

It is evident from Figure 6.16 that both dominant contribution at 741 cm⁻¹ and a minor one at 738 cm⁻¹ do not vary their positions by more than 1 cm⁻¹ over the course of dilution. Such insensitivity of P-F stretching band to the changes in concentration and to, presumably, variations in intermolecular interaction pattern is in accordance with our DFT calculations on model systems (Table 6.6). The minor low-wavenumber contribution whose fraction slightly increases at lower IL content (see Figure A 6.2) can be attributed to PF₆⁻ species bound in isolated ion pairs and/or at periphery of ionic clusters (Table 6.6). Such assignment is in line with the literature reports on blueshift of this vibration upon pressurizing the neat BmimPF₆, *i.e.* enhancing denser packing and interactions with larger number of neighboring cations.⁶¹⁻⁶² We note that there was no higher wavenumber minor contribution observed in contrast to results of Chaurasia *et al.*¹⁰¹ In their Raman study of BmimPF₆-PEO the contributions at 733, 741 (dominating), 747 cm⁻¹ were

tentatively assigned to PF_6^- in ionic aggregates of high order, in free state and in contact ion pairs respectively.

6.4. Conclusions

This chapter presents Raman spectroscopic study of mixtures of BmimPF_6 with $\gamma\text{-BL}$ over the entire range of compositions. Quantum-chemical DFT calculations as well as modern methods of two-dimensional correlation spectroscopy were employed in order to facilitate spectral analysis and assignment.

Imidazolium ring C-H stretching bands of cation ($3080\text{-}3250\text{ cm}^{-1}$) redshift upon dilution of neat IL which is more evident at higher dilutions ($x_{\text{IL}} < 0.18\text{-}0.20$). This is regarded as a remarkable manifestation of ionic solvation overwhelming ionic association in this concentration range. Higher propensity to intermolecular interactions at $\text{C}^2\text{-H}$ site is also noted.

Stretching mode of carbonyl group of the solvent at around 1760 cm^{-1} despite apparent blueshift upon addition of IL was found to have complex structure and intricate evolution of its revealed sub-components. A distinct change is observed at around $x_{\text{IL}} \approx 0.18\text{-}0.20$: at higher IL content main spectral contributions come from isolated molecules and from those which are weakly-bound to ionic clusters whereas at low concentrations of IL a sufficient amount of bulk-like species are in equilibrium with strongly solvated IL structures.

It was established that symmetrical stretching band of PF_6^- (located at 741 cm^{-1}) is insensitive to variations in concentration which does not preclude significance of anion in intermolecular interactions.

6.5. References for Chapter 6

- (1) Kiefer, J., Vibrational Spectroscopy for Studying Hydrogen Bonding in Imidazolium Ionic Liquids and their Mixtures with Cosolvents. In *Hydrogen Bonding and Transfer in the Excited State*, John Wiley & Sons, Ltd: 2010; pp 341-352.
- (2) Cha, S.; Ao, M.; Sung, W.; Moon, B.; Ahlstrom, B.; Johansson, P.; Ouchi, Y.; Kim, D., Structures of ionic liquid-water mixtures investigated by IR and NMR spectroscopy. *Phys. Chem. Chem. Phys.* **2014**, *16*, 9591-9601.
- (3) Takamuku, T.; Kyoshoin, Y.; Shimomura, T.; Kittaka, S.; Yamaguchi, T., Effect of Water on Structure of Hydrophilic Imidazolium-Based Ionic Liquid. *J. Phys. Chem. B* **2009**, *113*, 10817-10824.
- (4) Wang, H.; Wang, J.; Zhang, L., Temperature dependence of the microstructure of 1-butyl-3-methylimidazolium tetrafluoroborate in aqueous solution. *Vib. Spectrosc.* **2013**, *68*, 20-28.
- (5) Zhang, Q.-G.; Wang, N.-N.; Wang, S.-L.; Yu, Z.-W., Hydrogen Bonding Behaviors of Binary Systems Containing the Ionic Liquid 1-Butyl-3-methylimidazolium Trifluoroacetate and Water/Methanol. *J. Phys. Chem. B* **2011**, *115*, 11127-11136.
- (6) Andanson, J. M.; Traïkia, M.; Husson, P., Ionic association and interactions in aqueous methylsulfate alkyl-imidazolium-based ionic liquids. *J. Chem. Thermodyn.* **2014**.
- (7) Zhang, Q.-G.; Wang, N.-N.; Yu, Z.-W., The Hydrogen Bonding Interactions between the Ionic Liquid 1-Ethyl-3-Methylimidazolium Ethyl Sulfate and Water. *J. Phys. Chem. B* **2010**, *114*, 4747-4754.
- (8) Zhang, L.; Xu, Z.; Wang, Y.; Li, H., Prediction of the solvation and structural properties of ionic liquids in water by two-dimensional correlation spectroscopy. *J. Phys. Chem. B* **2008**, *112*, 6411-6419.
- (9) Jeon, Y.; Sung, J.; Kim, D.; Seo, C.; Cheong, H.; Ouchi, Y.; Ozawa, R.; Hamaguchi, H.-o., Structural Change of 1-Butyl-3-methylimidazolium Tetrafluoroborate + Water Mixtures Studied by Infrared Vibrational Spectroscopy. *J. Phys. Chem. B* **2008**, *112*, 923-928.
- (10) Jeon, Y.; Sung, J.; Seo, C.; Lim, H.; Cheong, H.; Kang, M.; Moon, B.; Ouchi, Y.; Kim, D., Structures of Ionic Liquids with Different Anions Studied by Infrared Vibration Spectroscopy. *J. Phys. Chem. B* **2008**, *112*, 4735-4740.
- (11) Fazio, B.; Triolo, A.; Di Marco, G., Local organization of water and its effect on the structural heterogeneities in room-temperature ionic liquid/H₂O mixtures. *J. Raman. Spectrosc.* **2008**, *39*, 233-237.
- (12) Holomb, R.; Martinelli, A.; Albinsson, I.; Lassègues, J. C.; Johansson, P.; Jacobsson, P., Ionic liquid structure: the conformational isomerism in 1-butyl-3-methyl-imidazolium tetrafluoroborate ([bmim][BF₄]). *J. Raman. Spectrosc.* **2008**, *39*, 793-805.
- (13) Hatano, N.; Watanabe, M.; Takekiyo, T.; Abe, H.; Yoshimura, Y., Anomalous Conformational Change in 1-Butyl-3-methylimidazolium Tetrafluoroborate-D₂O Mixtures. *J. Phys. Chem. A* **2012**, *116*, 1208-1212.
- (14) Klimavicius, V.; Gdaniec, Z.; Kausteklis, J.; Aleksa, V.; Aidas, K.; Balevicius, V., NMR and Raman Spectroscopy Monitoring of Proton/Deuteron Exchange in Aqueous Solutions of Ionic Liquids Forming Hydrogen Bond: A Role of Anions, Self-Aggregation, and Mesophase Formation. *J. Phys. Chem. B* **2013**, *117*, 10211-10220.
- (15) Berg, R. W., Raman Spectroscopy and Ab-Initio Model Calculations on Ionic Liquids. *Monatshefte für Chemie - Chemical Monthly* **2007**, *138*, 1045-1075.
- (16) Heimer, N. E.; Del Sesto, R. E.; Meng, Z.; Wilkes, J. S.; Carper, W. R., Vibrational spectra of imidazolium tetrafluoroborate ionic liquids. *J. Mol. Liq.* **2006**, *124*, 84-95.

- (17) Umebayashi, Y.; Jiang, J.-C.; Shan, Y.-L.; Lin, K.-H.; Fujii, K.; Seki, S.; Ishiguro, S.-I.; Lin, S. H.; Chang, H.-C., Structural change of ionic association in ionic liquid/water mixtures: A high-pressure infrared spectroscopic study. *J. Chem. Phys.* **2009**, *130*, -.
- (18) Cammarata, L.; Kazarian, S. G.; Salter, P. A.; Welton, T., Molecular states of water in room temperature ionic liquids. *Phys. Chem. Chem. Phys.* **2001**, *3*, 5192-5200.
- (19) Gao, Y.; Zhang, L.; Wang, Y.; Li, H., Probing Electron Density of H-Bonding between Cation–Anion of Imidazolium-Based Ionic Liquids with Different Anions by Vibrational Spectroscopy. *J. Phys. Chem. B* **2010**, *114*, 2828-2833.
- (20) Noack, K.; Leipertz, A.; Keifer, J., Molecular interactions and macroscopic effects in binary mixtures of an imidazolium ionic liquid with water, methanol, and ethanol. *J. Mol. Struct.* **2012**, *1018*, 45-53.
- (21) Roth, C.; Appelhagen, A.; Jobst, N.; Ludwig, R., Microheterogeneities in Ionic-Liquid–Methanol Solutions Studied by FTIR Spectroscopy, DFT Calculations and Molecular Dynamics Simulations. *ChemPhysChem* **2012**, *13*, 1708-1717.
- (22) He, H.; Chen, H.; Zheng, Y.; Zhang, X.; Yao, X.; Yu, Z.; Zhang, S., The Hydrogen-Bonding Interactions between 1-Ethyl-3-Methylimidazolium Lactate Ionic Liquid and Methanol. *Aust. J. Chem.* **2013**, *66*, 50-59.
- (23) Shimomura, T.; Fujii, K.; Takamuku, T., Effects of the alkyl-chain length on the mixing state of imidazolium-based ionic liquid-methanol solutions. *Phys. Chem. Chem. Phys.* **2010**, *12*, 12316-12324.
- (24) López-Pastor, M.; Ayora-Cañada, M. J.; Valcárcel, M.; Lendl, B., Association of methanol and water in ionic liquids elucidated by infrared spectroscopy using two-dimensional correlation and multivariate curve resolution. *J. Phys. Chem. B* **2006**, *110*, 10896-10902.
- (25) Chang, H.-C.; Jiang, J.-C.; Liou, Y.-C.; Hung, C.-H.; Lai, T.-Y.; Lin, S. H., Effects of water and methanol on the molecular organization of 1-butyl-3-methylimidazolium tetrafluoroborate as functions of pressure and concentration. *J. Chem. Phys.* **2008**, *129*, -.
- (26) Umebayashi, Y.; Jiang, J.-C.; Lin, K.-H.; Shan, Y.-L.; Fujii, K.; Seki, S.; Ishiguro, S.-I.; Lin, S. H.; Chang, H.-C., Solvation and microscopic properties of ionic liquid/acetonitrile mixtures probed by high-pressure infrared spectroscopy. *J. Chem. Phys.* **2009**, *131*, 234502.
- (27) Kumar, B.; Singh, T.; Rao, K. S.; Pal, A.; Kumar, A., Thermodynamic and spectroscopic studies on binary mixtures of imidazolium ionic liquids in ethylene glycol. *J. Chem. Thermodyn.* **2012**, *44*, 121-127.
- (28) Singh, T.; Rao, K. S.; Kumar, A., Polarity Behaviour and Specific Interactions of Imidazolium-Based Ionic Liquids in Ethylene Glycol. *ChemPhysChem* **2011**, *12*, 836-845.
- (29) Wang, N.-N.; Zhang, Q.-G.; Wu, F.-G.; Li, Q.-Z.; Yu, Z.-W., Hydrogen Bonding Interactions between a Representative Pyridinium-Based Ionic Liquid [BuPy][BF₄] and Water/Dimethyl Sulfoxide. *J. Phys. Chem. B* **2010**, *114*, 8689-8700.
- (30) Jiang, J.-C.; Lin, K.-H.; Li, S.-C.; Shih, P.-M.; Hung, K.-C.; Lin, S. H.; Chang, H.-C., Association structures of ionic liquid/DMSO mixtures studied by high-pressure infrared spectroscopy. *J. Chem. Phys.* **2011**, *134*, -.
- (31) Zheng, Y.-Z.; He, H.-Y.; Zhou, Y.; Yu, Z.-W., Hydrogen-bonding interactions between [BMIM][BF₄] and dimethyl sulfoxide. *J. Mol. Struct.* **2014**, *1069*, 140-146.
- (32) Zhang, L.; Wang, Y.; Xu, Z.; Li, H., Comparison of the Blue-Shifted C–D Stretching Vibrations for DMSO-*d*₆ in Imidazolium-Based Room Temperature Ionic Liquids and in Water. *J. Phys. Chem. B* **2009**, *113*, 5978-5984.
- (33) Zheng, Y.-Z.; Wang, N.-N.; Luo, J.-J.; Zhou, Y.; Yu, Z.-W., Hydrogen-Bonding Interactions between [BMIM][BF₄] and Acetonitrile. *Phys. Chem. Chem. Phys.* **2013**, *15*, 18055-18064.

- (34) Bhat, M. A.; Dutta, C. K.; Rather, G. M., Exploring physicochemical aspects of N-alkylimidazolium based ionic liquids. *J. Mol. Liq.* **2013**, *181*, 142-151.
- (35) Garcia, H. C.; de Oliveira, L. F. C.; Nicolau, B. G.; Ribeiro, M. C. C., Raman spectra of acetonitrile in imidazolium ionic liquids. *J. Raman. Spectrosc.* **2010**, *41*, 1720-1724.
- (36) Kiefer, J.; Molina, M. M.; Noack, K., The Peculiar Nature of Molecular Interactions between an Imidazolium Ionic Liquid and Acetone. *ChemPhysChem* **2012**, *13*, 1213-1220.
- (37) Köddermann, T.; Wertz, C.; Heintz, A.; Ludwig, R., Ion-Pair Formation in the Ionic Liquid 1-Ethyl-3-methylimidazolium Bis(triflyl)imide as a Function of Temperature and Concentration. *ChemPhysChem* **2006**, *7*, 1944-1949.
- (38) Chang, H.-C.; Jiang, J.-C.; Tsai, W.-C.; Chen, G.-C.; Lin, S. H., Hydrogen Bond Stabilization in 1,3-Dimethylimidazolium Methyl Sulfate and 1-Butyl-3-Methylimidazolium Hexafluorophosphate Probed by High Pressure: The Role of Charge-Enhanced C–H···O Interactions in the Room-Temperature Ionic Liquid. *J. Phys. Chem. B* **2006**, *110*, 3302-3307.
- (39) Chang, H.-C.; Jiang, J.-C.; Chang, C.-Y.; Su, J.-C.; Hung, C.-H.; Liou, Y.-C.; Lin, S. H., Structural Organization in Aqueous Solutions of 1-Butyl-3-methylimidazolium Halides: A High-Pressure Infrared Spectroscopic Study on Ionic Liquids. *J. Phys. Chem. B* **2008**, *112*, 4351-4356.
- (40) Danten, Y.; Cabaço, M. I.; Besnard, M., Interaction of Water Highly Diluted in 1-Alkyl-3-methyl Imidazolium Ionic Liquids with the PF₆⁻ and BF₄⁻ Anions. *J. Phys. Chem. A* **2009**, *113*, 2873-2889.
- (41) Danten, Y.; Cabaço, M. I.; Besnard, M., Interaction of water diluted in 1-butyl-3-methyl imidazolium ionic liquids by vibrational spectroscopy modeling. *J. Mol. Liq.* **2010**, *153*, 57-66.
- (42) Strauch, M.; Roth, C.; Kubatzki, F.; Ludwig, R., Formation of “Quasi” Contact or Solvent-separated Ion Pairs in the Local Environment of Probe Molecules Dissolved in Ionic Liquids. *ChemPhysChem* **2014**, *15*, 265-270.
- (43) Chagnes, A.; Allouchi, H.; Carre, B.; Lemordant, D., Thermal analysis of γ -butyrolactone+1 butyl-3-methyl-imidazolium ionic liquids mixtures. *Solid State Ionics* **2005**, *176*, 1419-1427.
- (44) Stoppa, A.; Hunger, J.; Buchner, R., Conductivities of binary mixtures of ionic liquids with polar solvents. *J. Chem. Eng. Data.* **2009**, *54*, 472-479.
- (45) Nishida, T.; Tashiro, Y.; Yamamoto, M., Physical and electrochemical properties of 1-alkyl-3-methylimidazolium tetrafluoroborate for electrolyte. *J. Fluorine Chem.* **2003**, *120*, 135-141.
- (46) Kalugin, O. N.; Voroshylova, I. V.; Riabchunova, A. V.; Lukinova, E. V.; Chaban, V. V., Conductometric Study of Binary Systems Based on Ionic Liquids and Acetonitrile in a wide Concentration Range. *Electrochim. Acta* **2013**, *105*, 188-199.
- (47) Noda, I.; Ozaki, Y. *Two-Dimensional Correlation Spectroscopy: Applications in Vibrational and Optical Spectroscopy*; Wiley: 2004;
- (48) Kim, H.; Jeon, S.-J., Simulations of Two-Dimensional Electronic Correlation Spectra. *Bull. Korean Chem. Soc.* **2001**, *22*, 807-815.
- (49) Gericke, A.; Gadaleta, S. J.; Brauner, J. W.; Mendelsohn, R., Characterization of biological samples by two-dimensional infrared spectroscopy: Simulation of frequency, bandwidth, and intensity changes. *Biospectroscopy* **1996**, *2*, 341-351.
- (50) Czarnecki, M. A., Two-Dimensional Correlation Spectroscopy: Effect of Normalization of the Dynamic Spectra. *Appl. Spectrosc.* **1999**, *53*, 1392-1397.
- (51) Šašić, S.; Muszynski, A.; Ozaki, Y., New Insight into the Mathematical Background of Generalized Two-Dimensional Correlation Spectroscopy and the Influence of Mean Normalization Pretreatment on Two-Dimensional Correlation Spectra. *Appl. Spectrosc.* **2001**, *55*, 343-349.

- (52) Czarnecki, M. A., Some Comments on the Application of Two-Dimensional Correlation Spectroscopy and Normalization of the Dynamic Spectra. *Appl. Spectrosc.* **2003**, *57*, 107-109.
- (53) Noda, I.; Ozaki, Y., Response to 'Some Comments on the Application of Two-Dimensional Correlation Spectroscopy and Normalization of the Dynamic Spectra' by Mirosław A. Czarnecki. *Appl. Spectrosc.* **2003**, *57*, 110-112.
- (54) Caillon-Caravanier, M.; Bossier, G.; Claude-Montigny, B.; Lemordant, D., Intermolecular Interactions in Lactone-Based Electrolytes. *J. Electrochem. Soc.* **2002**, *149*, E340-E347.
- (55) Huang, H.; Ding, X.; Zhu, C.; He, Z.; Yu, Y., 2D Correlation Analysis: Sequential Order Judging. *Anal. Chem.* **2013**, *85*, 2161-2168.
- (56) Noda, I., Frontiers of Two-Dimensional Correlation Spectroscopy. Part 1. New concepts and noteworthy developments. *J. Mol. Struct.* **2014**, *1069*, 3-22.
- (57) Morita, S.; Shinzawa, H.; Noda, I.; Ozaki, Y., Perturbation-Correlation Moving-Window Two-Dimensional Correlation Spectroscopy. *Appl. Spectrosc.* **2006**, *60*, 398-406.
- (58) Sun, B.; Wu, P., Trace of the Thermally Induced Evolution Mechanism of Interactions Between Water and Ionic Liquids. *J. Phys. Chem. B* **2010**, *114*, 9209-9219.
- (59) Buffeteau, T.; Grondin, J.; Lassègues, J.-C., Infrared Spectroscopy of Ionic Liquids: Quantitative Aspects and Determination of Optical Constants. *Appl. Spectrosc.* **2010**, *64*, 112-119.
- (60) Masia, M.; Rey, R., Computational Study of γ -Butyrolactone and Li^+ / γ -butyrolactone in Gas and Liquid Phases. *J. Phys. Chem. B* **2004**, *108*, 17992-18002.
- (61) Pison, L.; Costa Gomes, M. F.; Pádua, A. A. H.; Andrault, D.; Norman, S.; Hardacre, C.; Ribeiro, M. C. C., Pressure effect on vibrational frequency and dephasing of 1-alkyl-3-methylimidazolium hexafluorophosphate ionic liquids. *J. Chem. Phys.* **2013**, *139*, -.
- (62) Russina, O.; Fazio, B.; Schmidt, C.; Triolo, A., Structural organization and phase behaviour of 1-butyl-3-methylimidazolium hexafluorophosphate: an high pressure Raman spectroscopy study. *Phys. Chem. Chem. Phys.* **2011**, *13*, 12067-12074.
- (63) Perelygin, I. S.; Itkulov, I. G., Spontaneous raman spectroscopic study of the association of liquid γ -butyrolactone molecules. *J. Struct. Chem.* **1996**, *37*, 928-932.
- (64) Zarrougui, R.; Dhahbi, M.; Lemordant, D., Volumetric Properties of Ethylammonium Nitrate + γ -Butyrolactone Binary Systems: Solvation Phenomena from Density and Raman Spectroscopy. *J. Solution. Chem.* **2010**, *39*, 1531-1548.
- (65) Ikezawa, Y.; Atobe, K., In situ FTIR spectra at the Pt electrode/ γ -butyrolactone solution interface. *Electrochim. Acta* **2011**, *56*, 7078-7083.
- (66) Wang, J.; Xuan, X.; Lu, J.; Pei, N.; Mo, Y., A Vibrational Spectroscopic Study of Ion Solvation and Association in Lithium Perchlorate/ γ -Butyrolactone Electrolyte. *Z. Phys. Chem.* **2001**, *215*, 437-446.
- (67) Jiang, J.-C.; Li, S.-C.; Shih, P.-M.; Hung, T.-C.; Chang, S.-C.; Lin, S. H.; Chang, H.-C., A High-Pressure Infrared Spectroscopic Study on the Interaction of Ionic Liquids with PEO-PPO-PEO Block Copolymers and 1,4-Dioxane. *J. Phys. Chem. B* **2010**, *115*, 883-888.
- (68) Fornefeld-Schwarz, U. M.; Svejda, P., Refractive Indices and Relative Permittivities of Liquid Mixtures of γ -Butyrolactone, γ -Valerolactone, δ -Valerolactone, or ϵ -Caprolactone + Benzene, + Toluene, or + Ethylbenzene at 293.15 K and 313.15 K and Atmospheric Pressure. *J. Chem. Eng. Data.* **1999**, *44*, 597-604.
- (69) Reichardt, C.; Welton, T. *Solvents and Solvent Effects in Organic Chemistry*; Fourth, Updated and Enlarged Edition ed.; Wiley-VCH Verlag GmbH & Co. KGaA: Weinheim, 2011; 718 p.
- (70) Aparicio, S.; Alcalde, R., Characterization of two lactones in liquid phase: an experimental and computational approach. *Phys. Chem. Chem. Phys.* **2009**, *11*, 6455-6467.

- (71) Vaz, P.; Ribeiro-Claro, P. A., C-H ···O Hydrogen Bonds in Small Ring Carbonyl Compounds: Vibrational Spectroscopy and Ab initio Calculations. *Struct. Chem.* **2005**, *16*, 287-293.
- (72) Hesse, S.; Suhm, M. A., On the low volatility of cyclic esters: an infrared spectroscopy comparison between dimers of γ -butyrolactone and methyl propionate. *Phys. Chem. Chem. Phys.* **2009**, *11*, 11157-11170.
- (73) Zheng, J.; Alecu, I. M.; Lynch, B. J.; Zhao, Y.; Truhlar, D. G. Database of Frequency Scale Factors for Electronic Model Chemistries. Version 3 Beta 2. <http://comp.chem.umn.edu/freqscale/version3b2.htm> (accessed March 20, 2014).
- (74) Koßmann, S.; Thar, J.; Kirchner, B.; Hunt, P. A.; Welton, T., Cooperativity in ionic liquids. *J. Chem. Phys.* **2006**, *124*, 174506.
- (75) Kirchner, B., Ionic liquids from theoretical investigations. In *Ionic Liquids*, Kirchner, B., Ed. Springer-Verlag: Berlin/Heidelberg, 2010; Vol. 290, pp 213-262.
- (76) Chen, S.; Vijayaraghavan, R.; MacFarlane, D. R.; Izgorodina, E. I., Ab Initio Prediction of Proton NMR Chemical Shifts in Imidazolium Ionic Liquids. *J. Phys. Chem. B* **2013**, *117*, 3186-3197.
- (77) Palomar, J.; Ferro, V. R.; Gilarranz, M. A.; Rodriguez, J. J., Computational Approach to Nuclear Magnetic Resonance in 1-Alkyl-3-methylimidazolium Ionic Liquids. *J. Phys. Chem. B* **2007**, *111*, 168-180.
- (78) Dong, K.; Song, Y.; Liu, X.; Cheng, W.; Yao, X.; Zhang, S., Understanding Structures and Hydrogen Bonds of Ionic Liquids at the Electronic Level. *J. Phys. Chem. B* **2012**, *116*, 1007-1017.
- (79) Katsyuba, S. A.; Zvereva, E. E.; Vidiš, A.; Dyson, P. J., Application of Density Functional Theory and Vibrational Spectroscopy Toward the Rational Design of Ionic Liquids. *J. Phys. Chem. A* **2006**, *111*, 352-370.
- (80) Tsuzuki, S.; Tokuda, H.; Hayamizu, K.; Watanabe, M., Magnitude and Directionality of Interaction in Ion Pairs of Ionic Liquids: Relationship with Ionic Conductivity. *J. Phys. Chem. B* **2005**, *109*, 16474-16481.
- (81) Dong, K.; Zhang, S.; Wang, D.; Yao, X., Hydrogen Bonds in Imidazolium Ionic Liquids. *J. Phys. Chem. A* **2006**, *110*, 9775-9782.
- (82) Hu, X.; Lin, Q.; Gao, J.; Wu, Y.; Zhang, Z., Anion-cation and ion-solvent interaction of some typical ionic liquids in solvents with different dielectric constant. *Chem. Phys. Lett.* **2011**, *516*, 35-39.
- (83) Talaty, E. R.; Raja, S.; Storhaug, V. J.; Dölle, A.; Carper, W. R., Raman and Infrared Spectra and ab Initio Calculations of C2-4MIM Imidazolium Hexafluorophosphate Ionic Liquids. *J. Phys. Chem. B* **2004**, *108*, 13177-13184.
- (84) Hunt, P. A.; Kirchner, B.; Welton, T., Characterising the electronic structure of ionic liquids: an examination of the 1-butyl-3-methylimidazolium chloride ion pair. *Chem. – Eur. J.* **2006**, *12*, 6762-6775.
- (85) Izgorodina, E. I.; Rigby, J.; MacFarlane, D. R., Large-scale ab initio calculations of archetypical ionic liquids. *Chem. Commun.* **2012**, *48*, 1493-1495.
- (86) Matthews, R. P.; Welton, T.; Hunt, P. A., Competitive pi interactions and hydrogen bonding within imidazolium ionic liquids. *Phys. Chem. Chem. Phys.* **2014**, *16*, 3238-3253.
- (87) Matthews, R. P.; Ashworth, C.; Tom, W.; Patricia, A. H., The impact of anion electronic structure: similarities and differences in imidazolium based ionic liquids. *J. Phys.: Condens. Matter* **2014**, *26*, 284112.
- (88) Hardacre, C.; McMath, S. E. J.; Nieuwenhuyzen, M.; Bowron, D. T.; Soper, A. K., Liquid structure of 1, 3-dimethylimidazolium salts. *J. Phys.: Condens. Matter* **2003**, *15*, S159.

- (89) Hardacre, C.; Holbrey, J. D.; Mullan, C. L.; Youngs, T. G. A.; Bowron, D. T., Small angle neutron scattering from 1-alkyl-3-methylimidazolium hexafluorophosphate ionic liquids ([C_nmim][PF₆], n=4, 6, and 8). *J. Chem. Phys.* **2010**, *133*, -.
- (90) Macchiagodena, M.; Gontrani, L.; Ramondo, F.; Triolo, A.; Caminiti, R., Liquid structure of 1-alkyl-3-methylimidazolium-hexafluorophosphates by wide angle x-ray and neutron scattering and molecular dynamics. *J. Chem. Phys.* **2011**, *134*, 114521.
- (91) Katsyuba, S. A.; Griaznova, T. P.; Vidiš, A.; Dyson, P. J., Structural Studies of the Ionic Liquid 1-Ethyl-3-methylimidazolium Tetrafluoroborate in Dichloromethane Using a Combined DFT-NMR Spectroscopic Approach. *J. Phys. Chem. B* **2009**, *113*, 5046-5051.
- (92) Chang, H.-C.; Tsai, T.-T.; Kuo, M.-H., Using High-Pressure Infrared Spectroscopy to Study the Interactions between Triblock Copolymers and Ionic Liquids. *Macromolecules* **2014**, *47*, 3052-3058.
- (93) Lassègues, J.-C.; Grondin, J.; Cavagnat, D.; Johansson, P., New Interpretation of the CH Stretching Vibrations in Imidazolium-Based Ionic Liquids. *J. Phys. Chem. A* **2009**, *113*, 6419-6421.
- (94) Grondin, J.; Lassègues, J.-C.; Cavagnat, D.; Buffeteau, T.; Johansson, P.; Holomb, R., Revisited vibrational assignments of imidazolium-based ionic liquids. *J. Raman. Spectrosc.* **2011**, *42*, 733-743.
- (95) Johnson, C. J.; Fournier, J. A.; Wolke, C. T.; Johnson, M. A., Ionic liquids from the bottom up: Local assembly motifs in [EMIM][BF₄] through cryogenic ion spectroscopy. *J. Chem. Phys.* **2013**, *139*, -.
- (96) Roth, C.; Chatzipapadopoulos, S.; Kerlé, D.; Friedriszik, F.; Lütgens, M.; Lochbrunner, S.; Kühn, O.; Ludwig, R., Hydrogen bonding in ionic liquids probed by linear and nonlinear vibrational spectroscopy. *New J. Phys.* **2012**, *14*, 105026.
- (97) Obi, E. I.; Leavitt, C. M.; Raston, P. L.; Moradi, C. P.; Flynn, S. D.; Vaghjiani, G. L.; Boatz, J. A.; Chambreau, S. D.; Douberly, G. E., Helium Nanodroplet Isolation and Infrared Spectroscopy of the Isolated Ion-Pair 1-Ethyl-3-methylimidazolium bis(trifluoromethylsulfonyl)imide. *J. Phys. Chem. A* **2013**, *117*, 9047-9056.
- (98) Cooper, R.; Zolot, A. M.; Boatz, J. A.; Sporleder, D. P.; Stearns, J. A., IR and UV Spectroscopy of Vapor-Phase Jet-Cooled Ionic Liquid [emim]⁺[Tf₂N]⁻: Ion Pair Structure and Photodissociation Dynamics. *J. Phys. Chem. A* **2013**, *117*, 12419-12428.
- (99) Wendler, K.; Brehm, M.; Malberg, F.; Kirchner, B.; Delle Site, L., Short Time Dynamics of Ionic Liquids in AIMD-Based Power Spectra. *J. Chem. Theory Comput.* **2012**, *8*, 1570-1579.
- (100) Brehm, M.; Kirchner, B., TRAVIS - A Free Analyzer and Visualizer for Monte Carlo and Molecular Dynamics Trajectories. *Journal of Chemical Information and Modeling* **2011**, *51*, 2007-2023.
- (101) Chaurasia, S. K.; Singh, R. K.; Chandra, S., Ion-polymer and ion-ion interaction in PEO-based polymer electrolytes having complexing salt LiClO₄ and/or ionic liquid, [BMIM][PF₆]. *J. Raman. Spectrosc.* **2011**, *42*, 2168-2172.

6.6. Chapter 6 Appendix

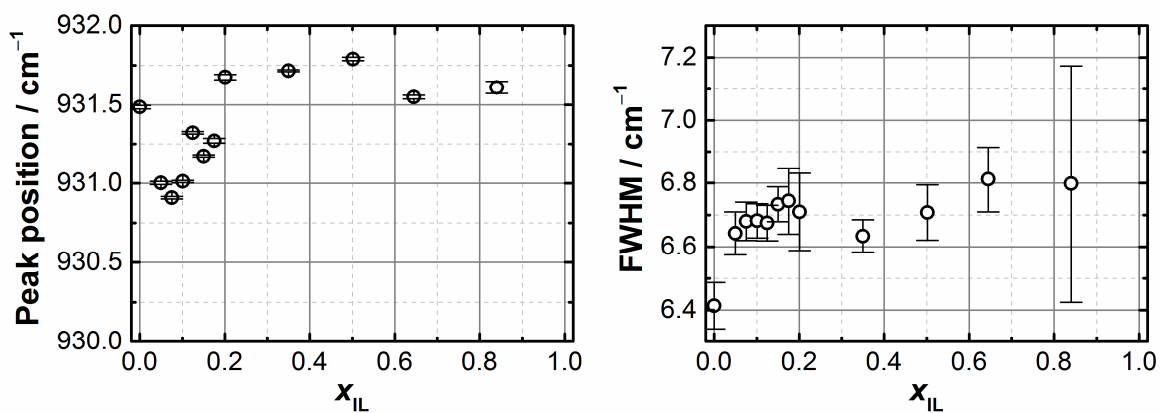


Figure A 6.1 Peak position (*left panel*) and full width and half maximum (*right panel*) of the fitted 931 cm^{-1} band as a function of BmimPF₆ mole fraction.

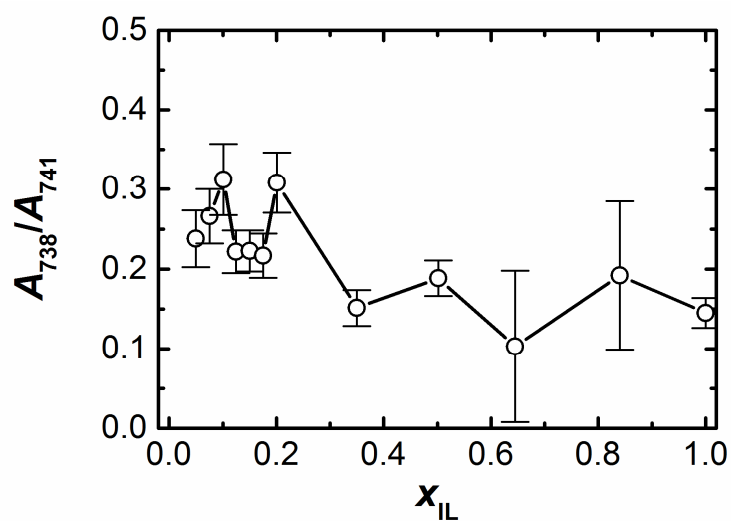


Figure A 6.2 Ratio of areas of contributions to the P-F symmetrical stretching profile fitted with two Voigt peaks as a function of BmimPF₆ mole fraction.

Table A 6.1 Peak fitting parameters for the bands in the spectral region I – C-H ring stretching of BmimPF₆

x_{iL}	0.0000	0.0496	0.0755	0.1012	0.1243	0.1503	0.1755	0.2011	0.3498	0.5018	0.6450	0.8405	1.0000
$\tilde{\nu}_1 / \text{cm}^{-1}$		3100.6±0.8	3104.2±0.2	3104.7±1.4	3106.0±0.8	3107.0±0.5	3108.4±0.5	3110.0±0.4	3112.9±0.3	3113.4±0.3	3112.9±0.3	3114.0±0.4	3114.5±0.2
A_1		930±80	2780±30	12900±700	14700±400	13000±300	16400±400	13800±300	10700±200	13800±300	13300±300	1600±100	14700±200
$\text{FWHM}_1 / \text{cm}^{-1}$		21±6	25.9±0.4	54±4	49±9	36±2	40±1	34±7	29.0±0.5	25±3	23±3	21.5±0.6	21±3
$\tilde{\nu}_2 / \text{cm}^{-1}$		3127.2±0.5	3126.8±0.4	3128.2±1.8	3129±3	3129±1	3131±1	3132±1	3135.6±0.6	3135.5±0.5	3127.2±0.4	3137.2±0.4	3137.1±0.3
A_2		1860±60	2660±70	3600±600	1240±180	2900±300	5500±400	3400±200	4700±300	6900±300	12100±400	1800±200	18300±300
$\text{FWHM}_2 / \text{cm}^{-1}$		28±3	21±5	43±11	23±5	23±4	32±5	24±3	21±5	23±6	29±4	32±2	31.8±1.2
$\tilde{\nu}_3 / \text{cm}^{-1}$		3153.2±0.2	3154.20±0.14	3155±1	3155.4±0.5	3155.8±0.4	3157.1±0.4	3157.6±0.3	3158.9±0.2	3160.5±0.2	3159.5±0.3	3160.4±0.4	3160.1±0.3
A_3		2800±50	7790±80	3521.6	11100±400	8300±300	13100±400	18800±300	12600±300	11100±150	9600±300	1300±100	6300±200
$\text{FWHM}_3 / \text{cm}^{-1}$		22±2	32±2	22±2	28±6	27±3	28.1±5	33.7±0.8	27±3	25.3±0.5	18±3	18.6±0.6	16.5±1.5
$\tilde{\nu}_4 / \text{cm}^{-1}$		3173.11±0.06	3174.74±0.06	3174.5±0.3	3175.7±0.2	3176.2±0.2	3176.5±0.2	3177.0±0.1	3179.1±0.1	3180.4±0.1	3180.1±0.1	3181.1±0.1	3181.3±0.1
A_4		10630±50	10900±30	19800±500	15140±180	20000±300	23800±300	24100±300	33400±300	3800±300	56800±300	10700±100	61700±200
$\text{FWHM}_4 / \text{cm}^{-1}$		23.8±0.6	23.6±0.1	24±3	22.5±0.4	22.9±1.5	22.4±1.5	22.1±1.2	22.5±0.9	22.2±0.7	23.1±0.7	23.2±0.7	23.6±0.5

Table A 6.2 Peak fitting parameters for the bands in the spectral region II – C=O stretching of γ -BL

x_{IL}	0.0000	0.0496	0.0755	0.1012	0.1243	0.1503	0.1755	0.2011	0.3498	0.5018	0.6450
$\tilde{\nu}_1 / \text{cm}^{-1}$	1735.62±2	1736.5±0.3	1738.8±0.3	1739.4±0.3	1741.0±0.3	1736.5±0.4	1738.8±0.2	1734.0±0.2			
A_1	0.025±0.005	0.0194±0.0004	0.0168±0.0003	0.0167±0.0003	0.0150±0.0004	0.0142±0.0004	0.0195±0.0003	0.0228±0.0002			
FWHM ₁ / cm^{-1}	28.0±1.5	23.6±0.6	25.5±0.7	27.1±0.7	20.2±0.7	20.2±0.8	31.3±0.5	27.6±0.4			
$\tilde{\nu}_2 / \text{cm}^{-1}$	1760.17±00.2	1761.11±0.02	1760.93±0.02	1761.91±0.01	1761.41±0.02	1761.15±0.03	1759.81±0.02	1761.08±0.02	1759.20±0.04	1760.20±0.07	1758.69±0.13
A_2	0.3836±0.0003	0.3639±0.0006	0.3517±0.0006	0.3499±0.0005	0.3373±0.0008	0.3188±0.0009	0.2787±0.0004	0.2121±0.0002	0.1674±0.0007	0.1104±0.0005	0.0854±0.0014
FWHM ₂ / cm^{-1}	13.9±1.4	15.4±0.3	16.4±0.2	16.4±0.2	19.3±0.3	22.6±0.3	27.3±0.3	28.6±0.1	31.9±0.7	30.9±0.3	24.7±1.8
$\tilde{\nu}_3 / \text{cm}^{-1}$	1764.98±0.02	1765.07±0.02	1764.82±0.02	1764.39±0.02	1765.56±0.02	1765.11±0.02	1764.09±0.01	1764.64±0.01	1765.55±0.01	1765.85±0.01	1766.21±0.02
A_3	0.2277±0.0004	0.2724±0.0007	0.2687±0.0006	0.2610±0.0005	0.2651±0.0007	0.2590±0.0007	0.2606±0.0003	0.2677±0.0003	0.3418±0.0005	0.3959±0.0007	0.6226±0.0014
FWHM ₃ / cm^{-1}	18.3±0.4	20.8±0.2	18.4±0.2	20.4±0.3	17.2±0.2	16.0±0.2	15.1±0.1	15.5±0.1	17.7±0.1	19.7±0.2	21.6±0.3
$\tilde{\nu}_4 / \text{cm}^{-1}$	1775.73±0.03	1777.28±0.06	1775.90±0.04	1773.99±0.02	1777.01±0.04	1776.91±0.04	1775.14±0.02	1775.35±0.02	1774.18±0.02	1772.87±0.02	1772.78±0.05
A_4	0.0982±0.0004	0.1010±0.0006	0.1049±0.0005	0.1252±0.0005	0.1296±0.0007	0.1443±0.0007	0.2234±0.0004	0.2665±0.04	0.2253±0.0005	0.2163±0.0007	0.1259±0.0011
FWHM ₄ / cm^{-1}	19.6±0.7	19.6±0.7	17.2±0.4	18.1±0.3	16.2±0.5	15.0±0.5	16.7±0.2	18.1±0.2	17.4±0.2	16.8±0.3	13.9±0.5
$\tilde{\nu}_5 / \text{cm}^{-1}$	1792.0±0.2	1794.0±0.2	1790.6±0.2	1791.8±0.2	1791.8±0.2	1791.2±0.2	1790.5±0.1	1791.9±0.1	1791.0±0.2	1791.5±0.2	1797.4±0.2
A_5	0.0539±0.0002	0.0452±0.0005	0.0575±0.0004	0.0608±0.0004	0.0542±0.0005	0.0588±0.0006	0.0677±0.0003	0.0805±0.0003	0.0821±0.0005	0.0980±0.0006	0.1357±0.0011
FWHM ₅ / cm^{-1}	35.1±0.2	32.9±0.4	35.7±0.3	35.7±0.3	36.1±0.4	38.0±0.4	41.0±0.2	46.9±0.2	53.4±0.4	54.0±0.4	55.8±0.5

Table A 6.3 Peak fitting parameters for the bands in the spectral region III – P-F symmetrical stretching of BmimPF₆

x_{IL}	0.0000	0.0496	0.0755	0.1012	0.1243	0.1503	0.1755	0.2011	0.3498	0.5018	0.6450	0.8405	1.0000
$\tilde{\nu}_1 / \text{cm}^{-1}$		737.8±0.2	738.0±0.2	738.2±0.2	738.1±0.2	738.0±0.2	738.1±0.2	738.74±0.19	738.4±0.3	738.4±0.2	738±2	738.4±1.2	738.0±0.2
A_1		4100±600	6600±800	10000±1300	8800±1000	10200±1100	11700±1500	16300±1900	11800±1400	15200±1800	19000±400	15000±7000	15100±1900
FWHM ₁ / cm^{-1}		3.55±0.12	3.53±0.09	3.61±0.09	3.71±0.10	3.68±0.10	3.75±0.12	3.76±0.10	3.69±0.12	3.96±0.11	6.5±0.8	9.0±1.2	3.91±0.11
$\tilde{\nu}_2 / \text{cm}^{-1}$		740.75±0.03	740.70±0.03	740.87±0.04	741.03±0.03	740.79±0.02	740.95±0.02	741.40±0.03	741.40±0.02	741.40±0.02	740.98±0.07	740.98±0.04	740.97±0.02
A_2		17500±700	25000±1000	30700±1500	39500±1100	45800±1300	53900±1600	53000±2000	80200±1500	81000±1900	104700±17000	79000±7000	104000±2000
FWHM ₂ / cm^{-1}		3.33±0.03	3.31±0.03	3.28±0.04	3.46±0.02	3.51±0.03	3.58±0.03	3.39±0.04	3.59±0.02	3.72±0.02	4.33±0.18	4.11±0.09	3.73±0.02

Conclusions and Perspectives

This thesis presents a multi-technique approach to the problem of microscopic description and interpretation of structure and dynamics in mixtures of imidazolium ionic liquids (ILs) with perfluorinated anions on one side and polar aprotic solvents on the other side. These mixtures possess a number of properties which are advantageous for electrochemical application (e.g., high ionic conductivity, thermal and electrochemical stability, low environmental hazardness) and they can be fine tuned due to the full miscibility of the components. Understanding the influence of the nature of the constituents and of the composition of these mixtures on the microscopic structure and dynamics is of crucial importance for their successful application.

Indeed, in this thesis, the mixtures of four imidazolium ILs with three polar aprotic molecular solvents have been investigated. The ILs contain a common cation 1-*n*-butyl-3-methylimidazolium (Bmim^+). It is combined with perfluorinated anions of different size, shape, symmetry, and electronic structure, namely, tetrafluoroborate (BF_4^-), hexafluorophosphate (PF_6^-), trifluoromethylsulfonate (TfO^-), and bis(trifluoromethanesulfonyl)imide (TFSI^-). Polar aprotic molecular solvents employed in this thesis are those common in electrochemistry of electrolyte solutions: acetonitrile (AN), γ -butyrolactone (γ -BL), and propylene carbonate (PC), which differ in terms of their polarity, donicity, viscosity, molecular shape and volume.

Quantum chemical calculations combined with advanced methods of analysis of the electron density distribution and of the weak noncovalent interactions have been used to analyze the main structural features and interactions of representative structures of model clusters of ILs and their complexes with the solvent molecules. These systems were considered as model ones which, despite limited size, can help to gather the most relevant information for subsequent interpretation of

spectroscopic data on IL-molecular solvent mixtures. All the studied ILs reveal the ion pair configuration with anion positioned on top of the C²-H² fragment as the most stable one. In this configuration, anions form weak interionic electrostatic hydrogen bonds with the C²-H² imidazolium ring hydrogen atom. Upon taking into account the effect of the solvent in these calculations, the native ion pair structure becomes distorted. The interionic interactions with the C²-H² fragment of the cation are weakened and the new hydrogen bonds with the solvent molecule are established. The magnitude of this effect follows the order AN < PC < γ -BL. BmimPF₆ and BmimTFSI ILs are found to be more sensitive compared to BmimBF₄ and BmimTfO. For all the established weak hydrogen bonds a linear correlation has been established between the electron density values at the bond critical points and the corresponding bond lengths.

In order to address the intermolecular interactions in mixtures of imidazolium ILs with molecular solvents, NMR and Raman spectroscopy were used. The chemical shift variation of ¹H and ¹³C nuclei was followed over the entire composition range at 300 K for all the 12 studied systems. The concept of relative chemical shift variation was proposed to assess, on a unified and unbiased scale, the observed effects of electron density redistribution at different atomic sites of ILs with changing mixture composition. With the help of the quantum chemical calculations results, it was established that hydrogen bonds between the imidazolium ring hydrogens and electronegative atoms of anions are stronger for BmimBF₄ and BmimTfO ILs than those in BmimTFSI and BmimPF₆. Hydrogen at position 2 of the imidazolium ring is particularly more sensitive to the interionic hydrogen bonding than those at positions 4-5 in the case of BmimTFSI and BmimTfO ILs. Solvation in γ -BL and PC leads to the formation of hydrogen bonds between the solvent molecules and the imidazolium ring hydrogens which are of comparable strength with the interionic ones. Hydrogen at position 2 of the

imidazolium ring is more sensitive to the solvation effects for all the studied ILs. Solvation of the cations of ILs in AN is poorly manifested.

By means of Raman spectroscopy coupled with DFT calculations and Perturbation Correlation Moving Window two-dimensional correlation spectroscopy intermolecular interactions were assessed in mixtures of a representative IL 1-*n*-butyl-3-methylimidazolium hexafluorophosphate (BmimPF₆) with polar aprotic solvent γ -BL over the entire range of compositions. Symmetrical P-F stretching vibration of IL anion was found to be insensitive to changes in mixture concentration in contrast to C=O stretching vibration of γ -BL and imidazolium ring C-H stretching vibrations of IL cation. Each of these vibrational profiles was decomposed in various spectral contributions and their number was rationalized by the results of quantum-chemical calculations and/or by previous controversial published data. Progressive redshift of the ring C-H stretching wavenumbers was referred to pronounced solvation of cation at the imidazolium ring site accompanied with H-bond formation. This is especially pronounced at $x_{\text{IL}} < 0.18$. Complicated variations in intensities of individual spectral contributions of the C=O profile were treated as a manifestation of the changing with concentration pattern of intermolecular interactions. Self-association of γ -BL molecules and distinct cation solvation as dominant intermolecular interactions at low IL content are replaced with weaker cation solvation and ion association at high concentrations of BmimPF₆. Possible representative molecular structures are proposed on the basis of DFT calculations.

Diffusion is a decisive factor for the electrochemical applications of these IL. Thus, self-diffusion coefficients of cations and solvent molecules were determined with ¹H-NMR in the IL/molecular solvent mixture over the entire composition range at 300 K. The relative diffusivities of solvent molecules to cations as a function of concentration were found to depend on the solvent but not on the anion (*i.e.*, IL). In all cases the values exhibit a plateau at low IL content ($x_{\text{IL}} < 0.2$) and

then increase steeply (AN), moderately (γ -BL), or negligibly (PC) at higher IL concentrations. This behavior was related to the different solvation patterns in the employed solvents. In BmimPF₆-based systems, anionic diffusivities were followed via ³¹P nuclei and found to be higher than the corresponding cation values in IL-poor systems and lower in the IL-rich region. The inversion point of relative ionic diffusivities was found around equimolar composition and does not depend on the solvent. At this point, a distinct change in the ion-diffusion mechanism appears to take place.

The general conclusions that may be drawn from the thesis work are as follows:

1. It was established that depending on the balance between ion association and solvation ionic liquids can exist at low concentrations ($x_{\text{IL}} < 0.2$) as predominantly ion paired or dissociated and well solvated. The balance is determined by both the nature of anion and solvent. Polar solvents with high donicity coupled with ILs with large anions with diffusive charge distribution promote ionic dissociation.

2. Multiple weak intermolecular interactions which cannot always be classified as conventional hydrogen bonds stand for the mechanism which determines spectral signatures (changes of the vibrational wavenumbers and NMR chemical shifts) of these phenomena.

3. Diffusion of molecules and ions does not depend strikingly on particular IL but rather on the solvent. An indication of universal behavior was noted for relative diffusion coefficients solvent-cation which show a plateau at low IL content and then start to increase at different slopes depending on the solvent.

Taken together, the results of the present thesis work contribute to the general idea of structure-composition-property relationship in mixtures of ionic liquids with molecular solvent and will serve a good comprehensive basis for the following further developments in the field:

- Selection of a proper combination IL-molecular solvent for particular application or for targeted search for new prospective systems. In the perspective of assessing the use of these IL-molecular solvent mixtures in electrochemical applications, the effect of temperature on the structure and dynamics in these mixtures should be analysed. A variable-temperature optical cell is currently under construction in order to perform such analysis. The results established in the present thesis work for the behavior of the studied systems at ambient temperature are invaluable in view of subsequent interpretation of the multitemperature data.
- Investigation of the structure and dynamics of these systems at different time and length scales. A dielectric relaxation experiment has been performed in Regensburg university for mixtures of BmimPF₆ with AN, γ -BL, and PC to study reorientational dynamics of dipolar species in the picosecond range (grant from the Centre de Coopération Universitaire Franco-Bavarois, not included in the present work, the results are under analysis). Quasi-elastic neutron scattering (trial experiments already performed at the Rutherford Appleton Laboratory) and X-ray diffraction (an experiment is planned using the facilities of Lille 1 University) will be used to study dynamics and structure at (sub)nanometer scale.
- Improvement of the force-fields for classical MD simulations of IL-molecular solvent mixtures. The information about the primary and secondary interaction sites, concentration trends of the diffusion coefficients, established in this work, will be used for thorough testing and fine tuning of the existing force-field models in order to reproduce all the structural and dynamic peculiarities of these systems. Thus refined force-field models could be used to study more complex phenomena and systems.
- Application of IL-molecular solvent mixtures in ternary systems containing photosensitive dye molecules as electrolytes for dye-sensitized solar cells.

The microscopic environment, in terms of its polarity, viscosity and possible specific intermolecular interactions, can significantly alter the photodynamics of the dye molecule which is, in turn, reflected in the performance of the entire device.